

Carbon and Water Dynamics in Modern and Ancient Plants and Soils

by

Rebekah A. Stein

A dissertation submitted in partial fulfillment
of the requirements for the degree of
Doctor of Philosophy
(Earth and Environmental Sciences)
in the University of Michigan
2020

Doctoral Committee:

Professor Nathan D. Sheldon, Co-Chair
Assistant Professor Selena Y. Smith, Co-Chair
Assistant Professor Gretchen Keppel-Aleks
Associate Professor Naomi E. Levin
Professor Christopher J. Poulsen

Rebekah A. Stein

restein@umich.edu

ORCID iD: 0000-0003-1505-8312

© Rebekah A. Stein 2020

DEDICATION

To Dr. Alvin Stein, PhD of Brooklyn, NY (November 24, 1925 – December 20, 2014).

ACKNOWLEDGMENTS

I would like to thank my advisors Nathan Sheldon and Selena Smith for their dedication and commitment to providing me excellent mentorship and advice. Their support, both in terms of my career but also my wellbeing, was instrumental throughout the pursuit of my PhD. This also could not have been done without the encouragement, feedback and mentorship from members of my committee: Chris Poulsen, Naomi Levin and Gretchen Keppel-Aleks. My time in the Michigan Earth department afforded me so many opportunities to be mentored by wonderful teachers: Nathan Sheldon, Gregg Crane, Kacey Lohmann, Greg Dick, Chris Poulsen, Jena Johnson, Naomi Levin, Selena Smith and instruct so many wonderful students, all of whom taught me so much. I thank my co-authors – Nathan, Selena, Becca Dzombak, Molly Ng, Michael Smith and Sarah Allen – for their expertise and helpful comments and considerations that made this dissertation possible.

Thank you to all members of the Sheldon, Smith and Hendy labs who have provided professional and personal advice over the years, including Ingrid Hendy, Katy Rico, Becca Dzombak, Melanie Shadix, Cecilia Howard, Kelly Matsunaga, Molly Ng, Zack Quirk, Xiaojing Du, Yi Wang, Madelyn Cook, Ashley Hamersma, Theresa Dowker, John Benedict and additional office mates – Derek Smith and Sarah Katz. Likewise, thank you to all of the amazing undergraduates who have worked with me in the lab over the year – Yvonne Wu, Sam Reasons, Aliah Wright-Johnson, Zoe Plonka, Fiona Fox and Sarah Sturtz.

I am deeply grateful for the field support from Becca Dzombak, Ashley Hamersma, Molly Ng, Nathan Sheldon, Nikolas Midttun, and Susana Fernandes, (University of Michigan School for Environment and Sustainability), all of whom were involved in collections of various leaves and soils. In addition, I thank Mike Blakeman (USFS: Rio Grande National Forest), Steve Baumann (NPS: El Malpais National Monument), Matthew Dubeau (NPS: Olympic National Park), Scott Esser (NPS: Rocky Mountain National Park), Matthew Klein (USFS: White River National Forest), Jayne Lebeda (USFS: Fishlake National Forest), Su Tao (Xishuangbanna Tropical Botanical Garden) and Jason Zayatz (USFS: Coconino National Forest) for their help in

Apache peoples of the North American Southwest. Furthermore, all lab work conducted on the University of Michigan's central campus and Stinchfield Woods site has origins in a land grant from the Anishinaabe (including Odawa, Ojibwe, Bodéwadmi (Potawatomi)) and Wyandot, wherein Governor Cass of Michigan persuaded these nations through manipulation, intimidation, and threats of violence to cede 3840 acres of land. Throughout my dissertation, I visited the greater Rock Springs area in Wyoming to sample Eocene sediments multiple times. The land on which I camped and conducted field work was taken from the Očhéthi Šakówiŋ, Arapaho, Cheyenne, Apsáalooke (Crow), Assiniboine, Arikara, Hidatsa and Mandan nations beginning with the dishonest Treaty of Fort Laramie (1851), and in the subsequent decades, during which the United States federal government rebuked on its promises made during this treaty. These acknowledgments do not undo the hundreds of years of violence and mistreatment conducted by the United States government and settlers, but pay homage to the importance of these traditional territories, and respect to members of these nations.

On a personal note, I thank my friends in the department of Earth and Environmental Sciences at the University of Michigan, especially members of the 2016 incoming class –Sha Chen, Alessio Capobianco, Becca Dzombak, Aaron Kurz, Sophie Macarewich, Juliana Mesa, Billy Medwedeff, Nikolas Midttun, Kierstin Rosenbach, James Saulsbury, Bian Wang, Alex Thompson and Kirk Townsend and my co-GSIs Sophie Macarewich, Mara Page and Mark Robbins. Thank you to my non-academic friends, and my Jiu-Jitsu community at Final Round Training Center. To my family for the love, support, compassion and confidence over the past five years – Mom, Dad, Joe, Sarah, Andrea, Pat, Luke, Anna and my honorary sister, Dr. Julia Blanchette. And finally, thank you to Conroy Baltzell: you are the most stable *rock* I know. Thank you for tolerating my terrible puns, and for your honesty, your patience, your advice, your groundedness and your amazing job as a father to Amadeus.

TABLE OF CONTENTS

DEDICATION.....	ii
ACKNOWLEDGMENTS.....	iii
LIST OF TABLES.....	viii
LIST OF FIGURES.....	ix
LIST OF TEXTBOXES.....	xii
LIST OF APPENDICES.....	xiii
ABSTRACT.....	xiv
CHAPTER I. Introduction.....	1
CHAPTER II. Rapid Response to Anthropogenic Climate Change by <i>Thuja occidentalis</i> : Implications for Past Climate Reconstructions and Future Climate Predictions.	23
2.1 Abstract.....	23
2.2 Introduction.....	24
2.3 Materials and Methods.....	30
2.4 Results.....	33
2.5 Discussion.....	36
2.6 Conclusions.....	42
2.7 Acknowledgments.....	43
2.8 References.....	43
CHAPTER III. C ₃ Plant Carbon Isotope Discrimination Does Not Respond to CO ₂ Concentration on Decadal to Centennial Timescales.....	51
3.1 Abstract.....	51
3.2 Introduction.....	52
3.3 Materials and Methods.....	58
3.4 Results.....	60
3.5 Discussion.....	64
3.6 Acknowledgments.....	69
3.7 References.....	69

CHAPTER IV. Soil Carbon Isotope Values and Paleo-Precipitation Reconstruction	75
4.1 Abstract.....	75
4.2 Introduction.....	75
4.3 Methods.....	80
4.4 Results.....	82
4.5 Discussion.....	86
4.6 Conclusions.....	96
4.7 Acknowledgments.....	96
4.8 References.....	97
CHAPTER V. Using Multiple Proxies to Characterize a Post-Early Eocene Climatic Optimum Ecosystem in the Rocky Mountain Interior.....	106
5.1 Abstract.....	106
5.2 Introduction.....	107
5.3 Methods.....	110
5.4 Results.....	121
5.5 Discussion.....	126
5.6 Conclusions.....	133
5.7 Acknowledgments.....	135
5.8 References.....	135
CHAPTER VI. Conclusions.....	144
APPENDICES.....	162

LIST OF TABLES

Table 4.1 Statistical results (p-value, significance test and R ² -value, coefficient of determination) for carbon isotope values ($\delta^{13}\text{C}_{\text{SOM}}$ and Δ_{SOM} values) compared to environmental and sampling location variables.....	84
Table 6.1 Taphonomic changes in $\Delta^{13}\text{C}_{\text{leaf}}$ for <i>Thuja occidentalis</i> samples over 32 weeks (sampled at 0, 2, 4, 8, 16 and 32 weeks).....	151
Table A1 Distribution of herbarium and botanical garden specimen data.....	167
Table A2 The range and mean values for measured climate variables in this study.....	167
Table A3 All collected data.....	168
Table B1 Isotope data measurements for specimens collected in the Earth Systems Science Lab (tab labeled <i>ESS Lab</i>) and from literature (tab labeled <i>Literature</i>).....	178
Table B2 Range of climate variables included in the historical portion of this study, as collected from PRISM Climate Group (2004), White et al. (2015), and Eggleston (2016).....	198
Table B3 Results from t-tests (assuming unequal variances) comparing the means and ranges of <i>Arabidopsis</i> (a) and <i>Raphanus</i> (b) and families highly sampled from the literature dataset.....	199
Table B4 Results showing the relationship between $\delta^{13}\text{C}_{\text{CO}_2}$ and $\delta^{13}\text{C}_{\text{plant}}$ for each species studied over Industrialization.....	200
Table B5 Sensitivity (S given as $\% \text{ ppm}^{-1}$) for eight species with long historical record.....	201
Table B6 Results showing the statistical relationship between carbon isotope discrimination and non-[CO ₂] climate variables for each species studied over Industrialization for each species studied over Industrialization.....	202
Table C1 Range of conditions for which soils are tested.....	211
Table C2 Multivariate relationships including coefficients of determination (R ²) and significance (p-value column).....	212
Table C3 All soil, paleosol, and reference data for modern and ancient samples included in this study.....	212
Table D1 Paleosol features, including color, evidence of disturbance, texture and depth.....	224
Table D2 All bulk geochemical and carbon isotope data from the Blue Rim escarpment.....	225

LIST OF FIGURES

Figure 1.1 Diagram of stomata on a leaf surface related to the water and carbon cycle.....	5
Figure 1.2 Cleared and stained stomata from <i>Thuja occidentalis</i> leaf surface, with arrows pointing to individual stomata.....	6
Figure 1.3 Diagram of carbon isotope discrimination during C ₃ photosynthesis.....	6
Figure 1.4 Isotopic compositions ($\delta^{13}\text{C}$) of natural sources and sinks of atmospheric CO ₂	9
Figure 1.5 Relationship between Δ_{leaf} values (‰) and mean annual precipitation (mm yr ⁻¹).....	10
Figure 1.6 Diagram of soil carbon isotope values in a soil profile including O- through B-horizons and major driving processes.....	14
Figure 2.1 Map of locations of <i>Thuja occidentalis</i> specimens.....	31
Figure 2.2 Δ_{leaf} vs. mean annual precipitation for <i>Thuja occidentalis</i> (black filled diamonds; $\Delta_{\text{leaf}} = -0.0003(\text{MAP}) + 18.75$, $R^2 < 0.01$).	33
Figure 2.3 C:N ratios of specimens vs. [CO ₂] (ppm) from 280–410 ppm	34
Figure 2.4 Δ_{leaf} vs. [CO ₂] for <i>Thuja</i> and dicots.	35
Figure 2.5 $\delta^{13}\text{C}_{\text{atm}}$ versus $\delta^{13}\text{C}_{\text{leaf}}$ values (‰) of <i>Thuja occidentalis</i>	36
Figure 3.1 Evolution of $\delta^{13}\text{C}_{\text{CO}_2}$ (‰) over time, including the Cenozoic, 12,000 years ago, the past 800 years, and the past 200 years including values reconstructed from $\delta^{13}\text{C}_{\text{leaf}}$ values.....	57
Figure 3.2 [CO ₂] values plotted against $\Delta^{13}\text{C}_{\text{plant}}$ for species with high-resolution records of the period of Industrialization.....	62
Figure 3.3 $\Delta^{13}\text{C}_{\text{plant}}$ values of plant growth forms, as collected from literature and this study.....	63
Figure 3.4 [CO ₂] values plotted against $\Delta^{13}\text{C}_{\text{plant}}$ for species with high-resolution records of the period of Industrialization.....	66
Figure 4.1 Modern soils from Wynn (2007) and a paleosol from Krull et al. (2002), displaying carbon isotope values ($\delta^{13}\text{C}_{\text{SOM}}$) with depth, demonstrating Rayleigh distillation processes.....	79
Figure 4.2 Map of modern soils.....	82
Figure 4.3 $\delta^{13}\text{C}_{\text{SOM}}$ values compared to mean annual precipitation (mm yr ⁻¹) for modern soils...	83

Figure 4.4 The relationship between $\delta^{13}\text{C}_{\text{SOM}}$, Δ_{SOM} and latitude (both absolute value of latitude, or degrees distance from the equator, and actual latitude).....	85
Figure 4.5 $\Delta^{13}\text{C}_{\text{SOM}}$ values compared to mean annual precipitation for modern soils.	93
Figure 4.6 Paleosol reconstructed mean annual precipitation values over time as compared to precipitation values reconstructed with different paleoprecipitation proxies.....	94
Figure 5.1 Map and Location of Blue Rim escarpment	108
Figure 5.2 Paleosol images and features.....	113
Figure 5.3 Stratigraphy with sedimentary geochemistry.....	114
Figure 5.4 Stratigraphy with parent material and provenance proxies.....	115
Figure 5.5 Stratigraphic column with climate proxies.....	116
Figure 5.6 Lateral extent of paleosols.....	117
Figure 5.7 $\delta^{13}\text{C}_{\text{atm}}$ as reconstructed from $\delta^{13}\text{C}_{\text{leaf}}$ of Blue Rim fossil flora.....	125
Figure 5.8 Paleosol-based (a) Floral Humidity Province and (b) Holdridge life zones (Holdridge 1967) in blue stars.....	132
Figure 6.1 Δ_{leaf} values compared to mean annual precipitation, with individual species collected for Sheldon, Smith, Stein & Ng (<i>Global Planetary Change</i> , 2020) overlaid on Diefendorf et al.'s (2010) meta-data set.....	146
Figure 6.2 Example of potential ecosystem level ^{13}C sampling (including gaseous CO_2 from the atmosphere, leaves, soil-respired CO_2 in gaseous form, and soil organic carbon) that could constrain isotope fluxes in an ecosystem.....	150
Figure 6.3 Power spectral analysis to determine strongest frequency, interpolated and regularly sampled on month (0.083 year) frequency, of <i>Thuja plicata</i> residual $\Delta^{13}\text{C}_{\text{leaf}}$ (‰) values over time.....	153
Figure 6.4 $\Delta^{13}\text{C}_{\text{leaf}}$ values (‰) vs (a) pore length (μm), (b) guard cell width (μm), (c) guard cell length (μm), (d) stomatal density (stomata mm^{-2}) and (e) guard cell volume (μm^3).....	155
Figure A1 Δ_{leaf} values versus mean annual temperature (-5 to 14°C) for collected specimens ($R^2 = 0.0001$).....	162
Figure A2 C:N ratios determined by wt. %C and wt. %N measured on a Costech Elemental Analyzer compared to a) time collected (year), b) $\delta^{13}\text{C}_{\text{atm}}$ values (‰), c) $\delta^{13}\text{C}_{\text{leaf}}$ values (‰)....	163
Figure A3 Linear regression between $\delta^{13}\text{C}_{\text{leaf}}$ values (‰) and $[\text{CO}_2]$ (283 to 407 ppm) for collected specimens ($R^2 = 0.61$).....	164
Figure A4 Linear regressions between Δ_{leaf} values and barometric measures.....	165
Figure A5 Box and whisker plots for Δ_{leaf} values of sampled months and seasons.....	166

Figure B1 [CO ₂] values plotted against $\Delta^{13}\text{C}_{\text{plant}}$ for species with medium-resolution records of the period of Industrialization.....	175
Figure B2 Comparison of $\Delta^{13}\text{C}_{\text{plant}}$ values of plants as sampled in this study, the Schubert & Jahren (2012) model, and from the literature and sorted by genera.....	176
Figure B3 Comparison of $\Delta^{13}\text{C}_{\text{plant}}$ values of plants as sampled in this study, the Schubert & Jahren (2012) model, and from the literature and sorted by family.....	177
Figure C1 $\delta^{13}\text{C}_{\text{SOM}}$ and Δ_{SOM} versus climate variables (a-b) elevation, (c-d) mean annual temperature, (e-f) Vapor Pressure Deficit Maximums, (g-h) VPD Minimums.....	217
Figure C2 (a) $\delta^{13}\text{C}_{\text{SOM}}$ values versus growing season precipitation for modern soils (mm yr ⁻¹).218	
Figure C3 Actual mean annual precipitation values (in mm yr ⁻¹) as collected from PRISM and extra-contiguous United States data sources as compared to reconstructed mean annual precipitation values (in mm yr ⁻¹) using Equation 4.1.....	219
Figure C4 (a) $\delta^{13}\text{C}_{\text{SOM}}$ values compared to mean annual precipitation (mm yr ⁻¹) for modern soils divided by soil order.....	220
Figure C5 Map of paleosol sites.....	221
Figure C6 Violin plots showing the distribution of $\delta^{13}\text{C}_{\text{SOM}}$ values in angiosperm- and gymnosperm- dominated ecosystems.....	222
Figure C7 Box plots showing the range of residual values between precipitation reconstructed using the $\delta^{13}\text{C}_{\text{SOM}}$ -paleoprecipitation proxy in this study, and other established proxies, divided by proxy.....	223
Figure D1 Geochemistry and features of a typical paleosol profile at Blue Rim escarpment....	231
Figure D2 Paleosol profile changes in mobile element transport calculations.....	232
Figure D3 Relationship between CIA-K and CIA for all paleosol bulk geochemistry data, measured by ALS laboratories.....	233
Figure D4 Comparison between organic content (%C) and leaching (Ba/Sr) in stratigraphic units.....	234
Figure D5 Common fossils found at Blue Rim escarpment (2019).....	235
Figure D6 Comparisons of climate reconstructed using multiple proxies.....	236
Figure D7 Current boundaries of Wyoming, USA with paleoenvironments plotted.....	237

LIST OF TEXTBOXES

Textbox 1.1 How to interpret isotope values.....	3
Textbox 1.2 Three photosynthetic pathways.....	12

LIST OF APPENDICES

Appendix A	Supplemental Figures and Tables for Chapter II.....	162
Appendix B	Supplemental Figures, Tables and References for Chapter III.....	175
Appendix C	Supplemental Figures, Tables and References for Chapter IV.....	211
Appendix D	Supplemental Figures, Tables and Methods for Chapter V.....	224

ABSTRACT

During modern times of unprecedented climate change, historical and geological records of past climate allow us to understand and project ancient patterns in the carbon and water cycle. Plants and soils are excellent records for climate because of the direct interaction between the terrestrial biosphere and the atmosphere and their preservation potential. Organic carbon isotope records in plants and soils have been linked to several environmental, evolutionary, and edaphic drivers, in addition to being used to measure ecosystem stress. Most of the works use organic carbon isotope values in ancient plant fossils with unconstrained and uncertain environments or in modern plant growth experiments with highly controlled environments that are not directly comparable to the natural world. The period of Industrialization provides a natural experiment with measurable, but not lab-controlled climate change, ideal for investigating the relationship between climate variability (particularly the carbon and water cycles) and C isotope values.

This dissertation includes several high-resolution spatiotemporal studies of several plant species through the pre-Industrial era. In **Chapter II**, leaf carbon isotope values from a single Great Lakes region species are compared to environmental variables involved in the water and carbon cycles (e.g. atmospheric CO₂ concentration and isotopic signature, temperature, precipitation, etc.) over the span of 200 years. Leaf isotope biogeochemistry of this species is unresponsive to every environmental variable except the isotopic composition of atmospheric CO₂. **Chapter III** expands on results from previous experiments, and investigates the

relationship between the carbon dioxide of the atmosphere and plant carbon isotope geochemistry with eight Northern Hemisphere focal species. These specimens are complemented by C₃ plant isotope analyses of aggregated from literature. Results from this work demonstrate that plants do not change biochemically as expected in response to CO₂ rise.

In **Chapter IV**, findings from previous chapters are re-examined from the context of aboveground carbon integrator: soils. The role of weathering in the development of soils provides incentive for investigating soils as potential water cycle records. As in **Chapter III**, this study includes soils collected across a climosequence, supplemented by aggregated carbon isotope values from prior publications. This work also tests the relationship between soil carbon isotopes and precipitation in ancient soils (paleosols). In both modern and ancient studies, carbon isotope values of soil correlate to precipitation.

Chapter V integrates the results and conclusions from early dissertation chapters with pre-established geochemical and physiognomic proxies to provide a comprehensive analysis of early Eocene hothouse sediments. Depositional basins from the Eocene are well-studied and contain opportunities for multi-proxy-based environmental reconstruction. Using organic and inorganic tools to constrain provenance, parent material, and other features of the depositional environment, an early Eocene fluvial-lacustrine subtropical forest deposit shows constant sedimentological and hydrological inputs and consistent climate during a time of expected cooling and tectonic activity.

In summary, this dissertation contains case studies relating soils and plants to the carbon and water cycle in modern, historical and deep time and demonstrates the recording power of the terrestrial biosphere. These findings can be used to contextualize and guide applications of organic isotope biogeochemistry in paleoclimate reconstructions. Related to modern climate

problems, results from this dissertation provide integral information about plants and soils as carbon and water distributors and mitigators of anthropogenic climate change.

CHAPTER I

Introduction

As Earth's climate changes due to anthropogenic forcing, it is imperative that we understand how terrestrial ecosystems respond such that we learn what changes to expect and how to mitigate these changes, as well as considering potential terrestrial carbon sinks (Cao & Woodward 1998). We look to ancient environmental records to elucidate what might happen in light of future climate change on individual species, and on regional and ecosystem scales. In particular, it is crucial that we understand how anthropogenic climate change will perturb the carbon and water cycle, as these cycles are vital for life on Earth. Examples of tools used to reconstruct paleoclimate include: microfossil records preserved in marine sediments (Hendy & Kennett 2000; Tipple et al. 2010), leaf fossil morphological traits (e.g. McElwain 1998; Peppe et al. 2011; Teodoridis et al. 2011; Peppe et al. 2018), the chemistry of leaf waxes (Tierney et al. 2017), paleosol elemental and isotopic geochemistry (e.g. carbonate paleobarometer; Chemical Index of Alteration; Paleosol Weathering Index; Cerling et al. 1991; Sheldon et al. 2002; Gallagher & Sheldon 2013), chemical sediments from lakes and caves (Scholz et al. 2007; Hopley et al. 2007; Conroy et al. 2008), and climate models (Zhu et al. 2019).

Land ecosystems provide a unique mechanism to reconstruct atmospheric events and parameters such as precipitation, concentration of carbon dioxide (CO₂), and changes in CO₂ fluxes due to the direct interaction between plants and the atmosphere (Cao & Woodward 1998; Stein et al. 2019). Furthermore, plants play irreplaceable roles in carbon and water cycles, acting as “giant straws” that funnel vast quantities of water from the ground via transpiration (Berner 1992; Pennisi 2008). In some ecosystems, this effect is greater than others (e.g. rainforest; Schlesinger & Jasechko 2014). Likewise, plants are important in the storage of carbon through photosynthesis (Bolin 1970) both in plant tissues (Hessen et al. 2004) and in soils (Ojima et al.

1993; Jobbágy & Jackson 2000). Due to the instrumental role that plants and soils have in these major global biogeochemical cycles, they are both (a) important to understand and protect, and (b) excellent potential records for perturbations within the carbon and water cycles (Sterling 2005). Carbon isotope values as recorded in plant tissues ($\delta^{13}\text{C}_{\text{leaf}}$) are relatively stable through time and can be excellent records for changes in the carbon and water cycles, as these values have been linked to environmental, edaphic, and phylogenetic factors (Sheldon et al. 2020). Carbon isotope values in soils ($\delta^{13}\text{C}_{\text{SOM}}$), originating from senescent plant material and soil microbial contributions (Wynn 2007), provide potential insight into environmental drivers on ecosystems. Soil carbon isotopes have additional fractionation processes complicating these signals, including microbial reduction and respiration and the formation of carbonates (Cruz-Martínez et al. 2012).

1.1 The mechanism of carbon isotope fractionation in terrestrial ecosystems: Incorporation of CO₂ into plants

The mechanism driving plant production of organic compounds from CO₂, and the role that this process plays in carbon isotope discrimination, has been well-constrained, and largely attributed to biochemical and physical factors (O'Leary 1981; Farquhar et al. 1989). The majority of carbon isotope discrimination in plants occurs due to the ribulose-1,5-bisphosphate carboxylase/oxygenase (RuBisCO) enzyme's selective preference for ¹²C. Diffusion, the second largest driving factor of fractionation, occurs as CO₂ gas encounters the leaf surface; CO₂ gas enters through the stomata (leaf pores; Fig. 1.1; O'Leary 1981). The different average velocities of ¹²C (faster) and ¹³C (slower) result in a carbon isotope fractionation of $\approx 4.4\%$ favoring entry of ¹²C at 1.0044 times the rate of ¹³C (Farquhar et al. 1989). Both biochemical reactions (e.g. RuBisCO) and physical fractionations related to plant morphology (e.g. diffusion) are sensitive to climate (O'Leary 1981; Farquhar et al. 1989; Arens et al. 2000). To facilitate photosynthesis, stomata must be open to let in CO₂. The stomatal aperture (diameter open) is important in this process, and when stomata are closed, photosynthesis stops. Due to the regulatory function stomata play in the inlet of CO₂ and outlet of leaf water (via transpiration), water availability and CO₂ availability play a large role in stomatal behavior (Haworth et al. 2011), which subsequently regulates isotopic fractionation via diffusion.

Stomatal parameters can be related to size (ultimately, the volume of gas that can be retained within the cell), including pore length, guard cell length, guard cell width, guard cell shape and the shape and/or presence of subsidiary cells (Franks et al. 2014; McElwain & Steinthorsdottir 2017); these are all taxonomically dependent parameters. Stomatal density is also very important in regulating atmosphere-biosphere interaction: this is a measure of the number of stomata per area, or can be measured as stomatal index (the number of stomata per total number of cells, Equation 1.1; Royer 2001).

$$\text{Stomatal Index} = \frac{\# \text{ stomata}}{\# \text{ epidermal cells} + \# \text{ stomata}} \quad (\text{Eq. 1.1})$$

Once CO₂ is inside the leaf surface, RuBisCO fixes the CO₂ contained within the leaf (e.g. Lorimer et al. 1976; Andersson & Backlund 2008). This process includes multiple steps — enolisation, carboxylation, hydration and protonation — before resulting in an unstable and ephemeral six-carbon chain that becomes two 3-phosphoglycerate molecules that make glucose (Andersson & Backlund 2008). RuBisCO's fixation alone has an isotope effect of 1.030, or ≈ 30‰ of additional fractionation, however, when including the effects of internal partial pressure of CO₂ within the leaf, this ends up resulting in a net isotope effect of 1.027 or ≈ 27‰ (Farquhar et al. 1989). Other isotope effects of steps in photosynthesis include boundary layer diffusion, diffusion of dissolved CO₂ in water, in C₄ plants: fixation by PEP carboxylase, and the poorly constrained process of photorespiration (Farquhar et al. 1989; Schubert & Jahren 2018). Most workers that focus on C₃ plants specifically address the roles of

Textbox 1.1: How to interpret isotope values

Alpha (α), or a fractionation factor, is one way to look at the fractionation of isotopes due to certain processes, and relates the absolute ratio of one isotope to the other. For example, the α value of RuBisCO is 1.030 (see text), which means that for each single ¹³C atom that is fixed by RuBisCO, 1.030 ¹²Cs are fixed. Delta notation (δ) helps us to measure and visualize the differences caused by isotope effects in more digestible numbers. δ relates the carbon isotope ratio of a substance as compared to a standard. Of note: δ is reported as units per one thousand (‰) (compared to percent (%) that is measured units per one hundred) (Eq. A).

$$\delta^{13}\text{C} = \left(\frac{\left(\frac{^{13}\text{C}}{^{12}\text{C}} \right)_{\text{sample}}}{\left(\frac{^{13}\text{C}}{^{12}\text{C}} \right)_{\text{standard}}} - 1 \right) * 1000 \quad (\text{Eq. A})$$

The standard used in this case is typically the Pee Dee Belemnite (PDB), a Cretaceous marine belemnite from the Pee Dee Formation in South Carolina, USA (Craig 1957). The PDB has an anomalously high ratio of ¹³C to ¹²C: 0.0112372, and was established as the $\delta^{13}\text{C} = 0$ value. Thus, any substance with a higher ¹³C:¹²C ratio than the PDB >0, while any substance with a lower ¹³C:¹²C ratio than the PDB is negative. 98% of all carbon on Earth is the more abundant and lighter ¹²C, while 1% is ¹³C, so most substances have a negative $\delta^{13}\text{C}$ value as compared to the PDB.

The absolute isotopic composition of a sample (α) is not easy to measure exactly due to tiny masses so this allows us to rely on tools like a mass spectrometer or cavity ring-down spectroscopy to calculate instead the deviation from the standard (Farquhar et al. 1989).

diffusion through the stomatal pore and fixation of gaseous CO₂ by RuBisCO in isotopic fractionation (disregarding the less impactful steps; Farquhar et al. 1989; Schubert & Jahren 2018).

$$\Delta_{leaf} (\text{‰}) = a + (b - a)\left(\frac{C_i}{C_a}\right) \quad (\text{Eq. 1.2})$$

Combined, these effects are summarized in Equation 1.2, where Δ_{leaf} denotes total carbon isotope discrimination of C₃ plants, “a” denotes fractionation due to diffusion of carbon in air (4.4‰), “b” denotes fractionation due to the process of carboxylation (mostly by RuBisCO (27‰), and “C_i/C_a” represents the relationship between internal leaf carbon dioxide (C_i) to atmospheric carbon dioxide (C_a), sometimes used to represent water use efficiency (Ponton et al. 2006). Equation 1.3 shows the relationship between Δ_{leaf} values and atmospheric source carbon isotope measurements (carbon isotope value of the atmosphere: $\delta^{13}\text{C}_{atm}$, and carbon isotope value of leaves: $\delta^{13}\text{C}_{leaf}$).

$$\Delta_{leaf} (\text{‰}) = \frac{\delta^{13}\text{C}_{atm} - \delta^{13}\text{C}_{leaf}}{1 + \left(\frac{\delta^{13}\text{C}_{leaf}}{1000}\right)} \quad (\text{Eq. 1.3})$$

RuBisCO’s enzymatic activity is very slow, with a catalytic rate of 0.03–0.60 s⁻¹ fixed each second per molecule of RuBisCO (Bar-On & Milo 2019). The rate of this activity is sensitive to temperature, to light, and to CO₂ (Crafts-Brandner & Salvucci 2000; Warren & Adams 2001; Bowes 1991), which introduces additional sensitivity of plants to environmental drivers in the context of their role in the carbon cycle.

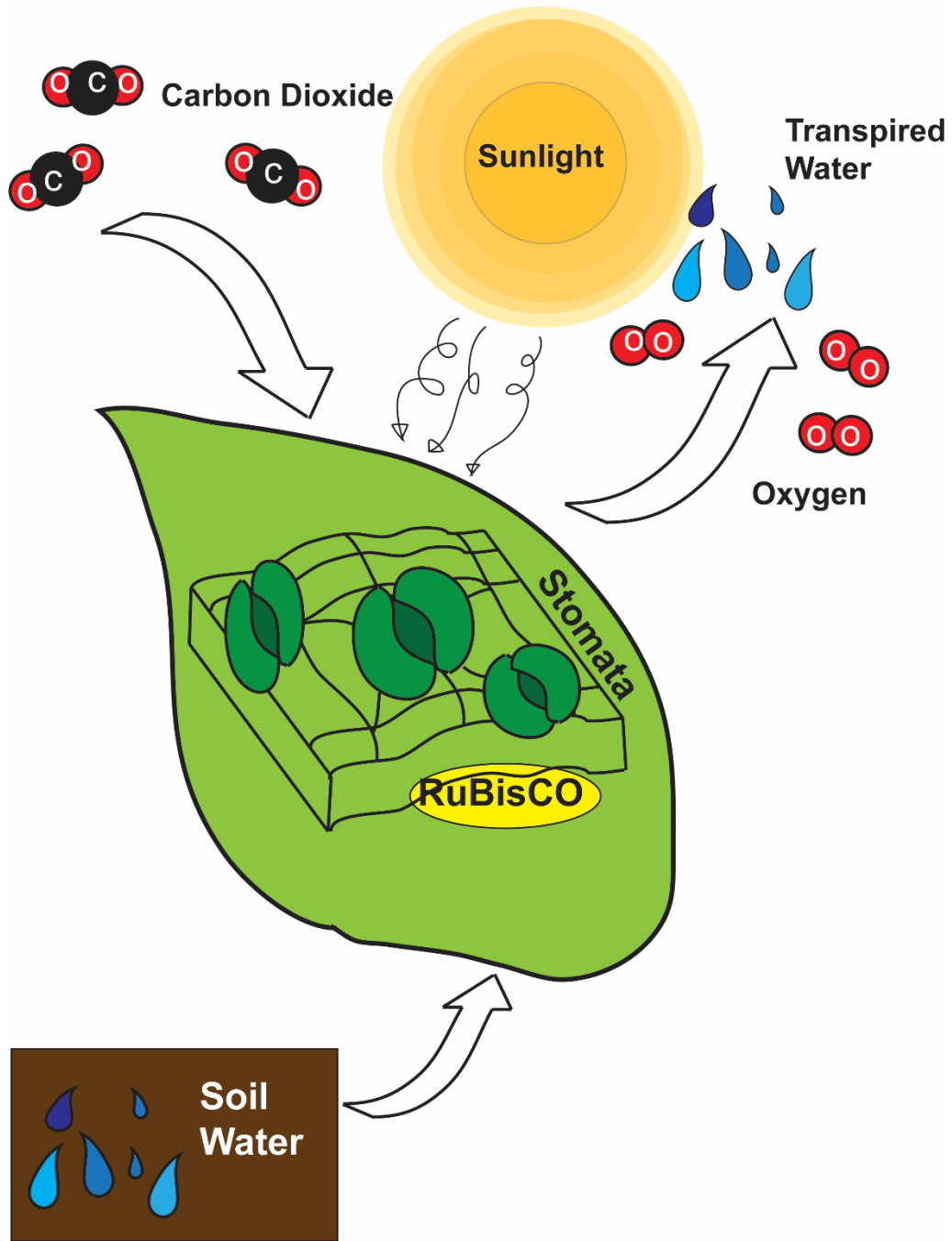


Figure 1.1 Diagram of a stoma on a leaf surface related to the role it plays in the carbon and water cycle.

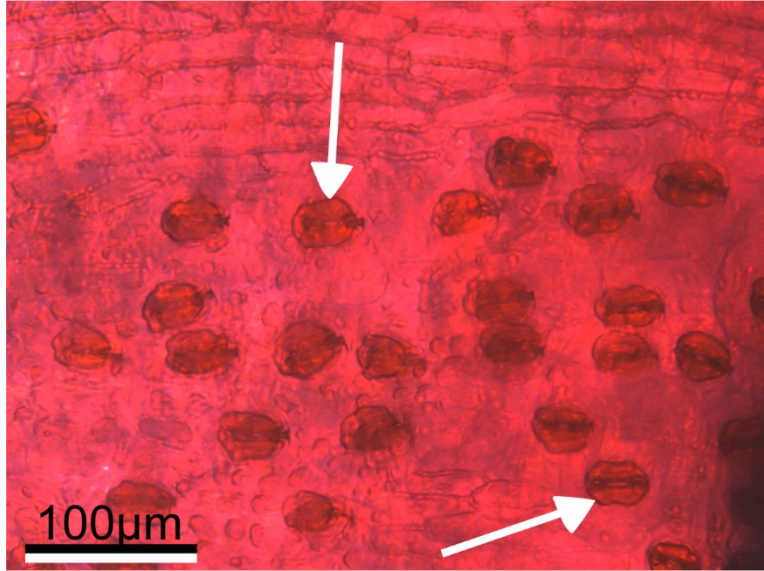


Figure 1.2 Cleared and stained stomata on a *Thuja occidentalis* leaf surface, with arrows pointing to individual stomata.

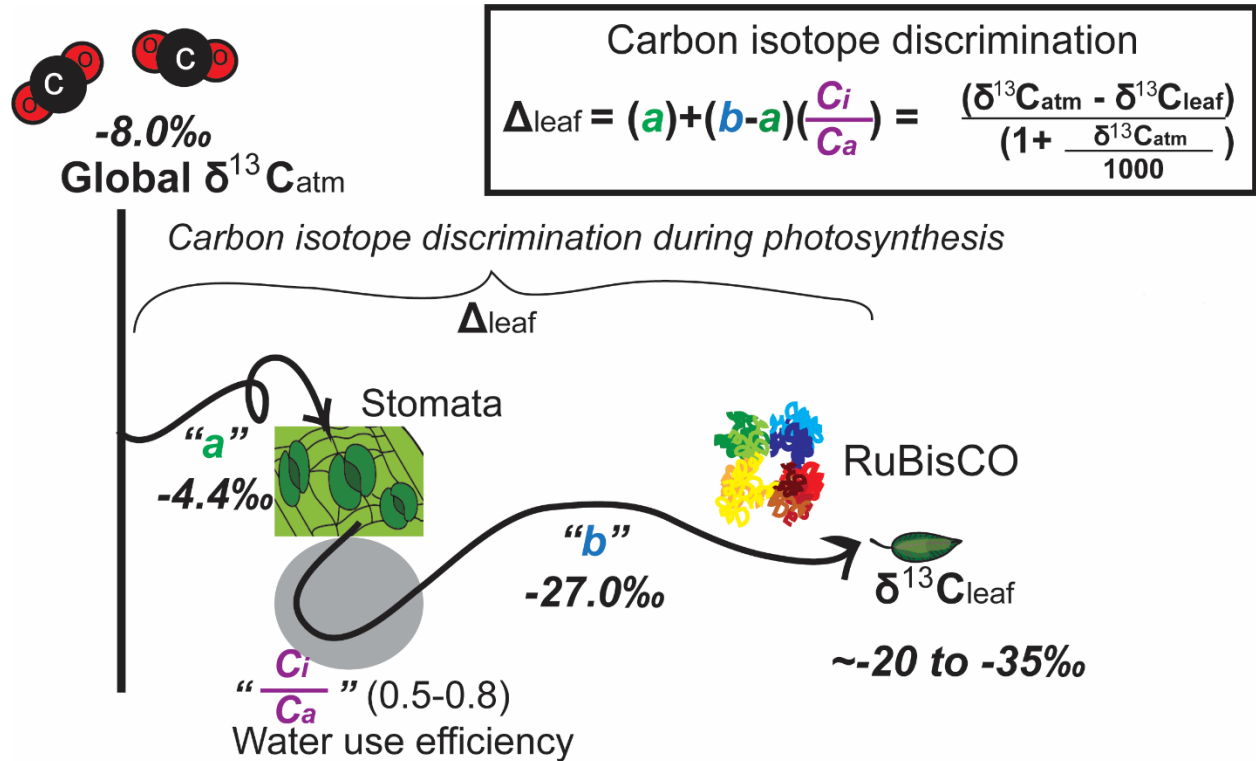


Figure 1.3 Diagram of carbon isotope discrimination during C_3 photosynthesis. The grey “ C_i/C_a ” region demonstrates the complexity of the isotopic fractionation by RuBisCO, which is controlled partially by internal and atmospheric CO_2 concentration.

1.2 The effects of climate on carbon isotope discrimination

1.2.1 CO₂

The concentration of CO₂ in the atmosphere influences stomatal distribution, shape, and size (Franks et al. 2014). As atmospheric [CO₂] increases, stomata have increased access to CO₂. [CO₂] has not been seen to have any impacts on the rate of RuBisCO activity (Campbell et al. 1988). Previous studies have examined the relationship between [CO₂] and quantity of stomata, and have determined there is an inverse relationship between [CO₂] and number of stomata (Woodward 1987; Körner 1988; Woodward & Bazzaz 1988; Apel 1989; Vatén & Bergmann 2012). While this relationship is generally seen in most plants, it does not hold up for every single species. For example, in a study plants growing next to a naturally occurring CO₂ vent in Pisa, Italy of Mediterranean shrub species (*Juniperus communis*, common juniper; Cupressaceae; *Myrtus communis*, common myrtle; Myrtaceae, *Erica arborea*, tree heather; Ericaceae), *Juniperus communis* had no change in the number of stomata, while the other two did (Tognetti et al. 2000).

Given the established connections between carbon isotope fractionation (via diffusion) and stomata, workers have looked to examine the relationship between elevated CO₂ and carbon isotope values of plant tissues. Previous workers have tested this relationship in plants grown in growth chambers (Schubert & Jahren 2012; Lomax et al. 2019), in free air concentration enrichment experiments (FACE) in modern ecosystems (Norby & Zak 2011); and in plants preserved in the fossil record (Cui & Schubert 2017; Schlanser et al. 2020). Scientists conducting growth chamber experiments with elevated CO₂ on *Arabidopsis thaliana* and *Raphanus sativus* found a strong logarithmic relationship between CO₂ and Δ_{leaf} , and have extrapolated this to use Δ_{leaf} values as a paleobarometer. These findings suggest that plants adapt to enhanced CO₂ rapidly (within a single generation), and Δ_{leaf} values increase; authors proposed that Δ_{leaf} values therefore can be used to reflect CO₂ in the fossil record (Schubert & Jahren 2012).

Complementary responses of rapid responses including increased photosynthesis and productivity with enhanced CO₂ in FACE experiments demonstrated a theoretical increase in carbon sequestration in plant products that corresponds with increased carbon isotope discrimination (Long et al. 2004; Ainsworth & Long 2004; Leakey et al. 2009). However, responses are nuanced: alternate studies also using growth chambers found increase in Δ_{leaf} was

viable when water was plentiful but was ultimately limited by when plants were experiencing water stress (Lomax et al. 2019). Longer term, effects of elevated CO₂ on plant productivity diminished over time (Nowak et al. 2004; Norby & Zak 2011). Furthermore, microfossil record compound-specific findings indicate that in fact, over a range of 200–900 ppm CO₂, after controlling for precipitation (see section 1.2.3), Δ_{leaf} response to CO₂ is small and *negative* (Schlanser et al. 2020). The relationship between plant productivity (as represented in carbon isotope space by increased discrimination — Δ_{leaf} — and/or depleted $\delta^{13}\text{C}_{\text{leaf}}$ values) and enhanced CO₂, while controversial, has predictive value for expectations and mitigation strategies as we face imminent anthropogenic climate change, and this relationship is examined in depth in **Chapters II** and **III**.

1.2.2 $\delta^{13}\text{C}_{\text{atm}}$

The isotopic value of the atmosphere ($\delta^{13}\text{C}_{\text{atm}}$) plays a direct role in controlling the isotopic values of plants ($\delta^{13}\text{C}_{\text{leaf}}$). As the carbon source for photosynthesis, changes in the atmosphere should cause a shift in carbon isotope values in plants (Fig. 1.3). In a meta-analysis by Arens et al. (2000), $\delta^{13}\text{C}_{\text{leaf}}$ values of a series of 519 land plants were compared to $\delta^{13}\text{C}_{\text{atm}}$ values. From those results, it was clear that there was a relationship between $\delta^{13}\text{C}_{\text{leaf}}$ and $\delta^{13}\text{C}_{\text{atm}}$ values (Equation 1.4; $R^2 = 0.34$, $p < 0.001$), albeit one with somewhat modest predictive value.

$$\delta^{13}\text{C}_{\text{leaf}} = (1.10 * \delta^{13}\text{C}_{\text{atm}}) - 18.67 \quad (\text{Equation 1.4})$$

If changes in $\delta^{13}\text{C}_{\text{leaf}}$ reflect changes in $\delta^{13}\text{C}_{\text{atm}}$ values exactly, this implies that $\delta^{13}\text{C}_{\text{leaf}}$ cannot be used to reconstruct other climate variables and that Δ_{leaf} remains relatively constant regardless of interfering climate variables. This also implies that $\delta^{13}\text{C}_{\text{leaf}}$ can be used as a proxy to understand changes in sources of CO₂ to the atmosphere (e.g. methane-derived or fossil-fuel combusted CO₂ is isotopically depleted at ~ -60 and $\sim -25\%$ respectively, while mantle derived CO₂ has an average $\delta^{13}\text{C}$ composition of -5.5% ; Figure 1.4). This potential proxy is tested in historical analyses in **Chapter II** of this dissertation.

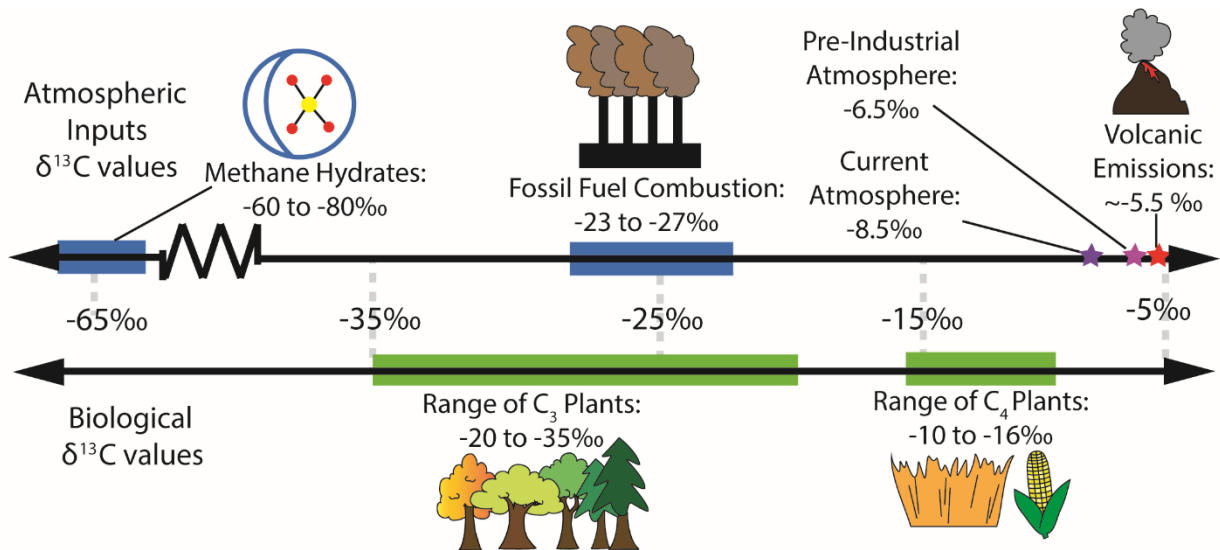


Figure 1.4 Isotopic compositions ($\delta^{13}\text{C}$) of natural sources and sinks of atmospheric CO_2 .

1.2.3 Mean annual precipitation and water availability

Carbon isotope values in plants have been linked to precipitation. Like CO_2 , this relationship is related to stomata's role in regulating transpiration. Increased water availability means that stomata can stay open without risk of desiccation, which should result in maximized carbon isotope discrimination (favoring ^{12}C ; Ehleringer 1993). Thus, increased water availability (e.g. higher mean annual precipitation rates, and/or higher growing season precipitation) for plants should result in increased carbon isotope discrimination (depleted $\delta^{13}\text{C}$ values, increased Δ_{leaf} values).

This hypothesized relationship has been empirically tested in several studies (Stewart et al. 1995; Schulze et al. 1996), including a meta-analysis that compared Δ_{leaf} values of a wide spread of C_3 plants and precipitation (Diefendorf et al. 2010). In this empirical study, there was a significant ($p < 0.001$) logarithmic relationship between carbon isotope discrimination (Δ_{leaf}) and mean annual precipitation (MAP) across a wide range of precipitation regimes (Figure 1.5; Equation 1.5; Diefendorf et al. 2010; Kohn 2010). These results affirm the hypothesis that water stress results in less carbon isotope discrimination, related to minimizing transpiration through the stomata.

$$\Delta_{leaf}(\text{‰}) = 5.54(\pm 0.22) * \log(MAP) + 4.07(\pm 0.70) \quad (\text{Equation 1.5})$$

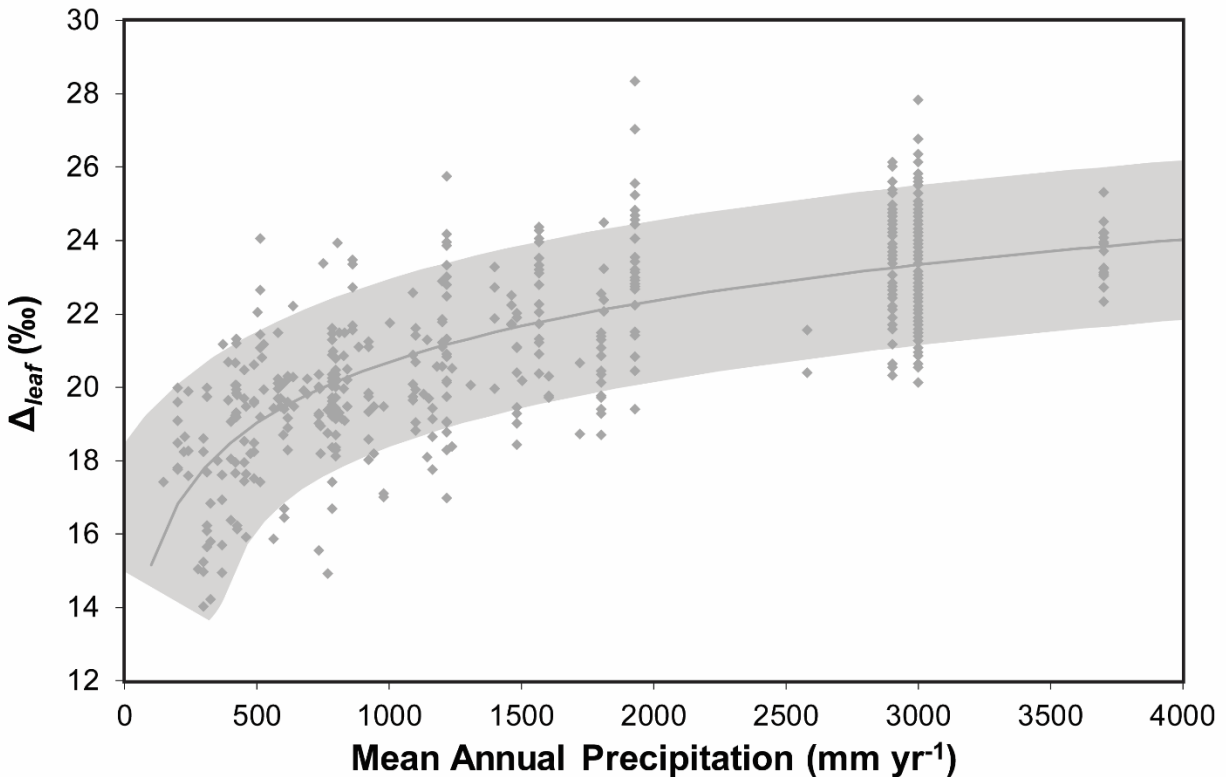


Figure 1.5 Relationship between Δ_{leaf} values (‰) and mean annual precipitation (mm yr^{-1}). Adapted after Diefendorf et al.'s (2010) meta-analysis findings. Everything within the grey box is within the standard deviation around the equation.

Relative humidity (RH) and vapor pressure deficit (VPD), both measurements representing moisture in ecosystems, have also been tested as drivers of stomatal response and subsequent fluctuations in carbon isotope discrimination (Schulze & Kupperts 1979; Hall et al. 1994). However, results have been mixed: *Lycopersicon esculentum* (tomato), *Glycine max* (soybeans), *Tagetes erecta* (marigold), and *Triticum aestivum* (wheat) were grown at controlled RH; higher humidity scenarios (RH of 75%) resulted in depletion of $\delta^{13}\text{C}_{leaf}$ values by up to -3‰ compared to low humidity counterparts (RH of 30%; Madhavan et al. 1991). Likewise, when VPD was controlled in a series of *Triticum aestivum* (winter wheat) growth experiments, VPD played a significant role, attributed to stomatal closure in high VPD conditions (Condon et al. 1992). However, when VPD was compared to carbon isotope values of *Larrea tridentate*

(creosote bush) in growth chamber experiments, VPD was not shown to affect Δ_{leaf} values (Sharifi & Rundel 1993).

1.2.4 Temperature

Activity of the RuBisCO enzyme is temperature-dependent, so natural changes in temperature are thought to affect photosynthesis, and as a proxy, $\delta^{13}\text{C}_{\text{leaf}}$ values (Arens et al. 2000). To one extreme, high air temperatures result in higher evapotranspiration rates and a decrease in RuBisCO activation (Gates 1968; Crafts-Brandner & Salvucci 2000); which have similar effects on isotope discrimination as low water availability (O’Leary 1981). On the other end, low temperatures result in depleted $\delta^{13}\text{C}_{\text{leaf}}$ values by up to -3‰ in some plants (Tieszen 1991; Körner et al. 1991) and no change in others (Gebrekirstos et al. 2009). It is worth noting that for studies that found increased discrimination with temperature, temperature was not deconvolved from latitude and altitude, so these factors should be considered as related to this climate driver (Körner et al. 1991). Furthermore, Helliker and Richter (2008) found that during the growing season, leaves maintained internal temperatures ideal for photosynthesis 21.4 ± 2.2 °C independent of external temperatures (Helliker & Richter 2008). In other words, although temperature could drive the efficiency of the enzyme RuBisCO as well as transpiration rates, in practice plants have adapted to self-regulate leaf temperatures.

1.2.5 Light and height

Light level and plant height, two local factors that are linked by growth form, are both considered potential drivers of $\delta^{13}\text{C}_{\text{leaf}}$ variability (Arens et al. 2000). These are linked because leaves higher in the canopy typically receive more ambient sunlight, while lower canopy leaves are shaded, with only intermittent irradiance (Xiao et al. 2013). Increased sunlight, an important catalyst for photosynthesis, increases opportunity for leaves to conduct photosynthesis (Knapp & Smith 1990), thus sun versus shade conditions (including as related to height) link to plants’ rates of photosynthesis. Like temperature, increased sunlight results in higher rates of evapotranspiration (as well as higher temperatures), so sun leaves typically are drier and more water stressed (Uhl & Walther 2000). Due to this water stress, sun leaves are expected to be enriched in ^{13}C compared to shade leaves (Tu et al. 2004). Heterogeneity in light availability and

associated microenvironments dependent on leaf placement on the tree is a small-scale demonstration of the importance of environmental drivers on photosynthesis and carbon isotope discrimination. Furthermore, leaves growing very close to the forest floor can have isotopic values shifted by the addition of isotopically depleted soil-respired CO₂ (Brooks et al. 1997), emphasizing the importance of carbon availability in plant carbon isotope discrimination; this issue is addressed in **Chapter III**. However, when this expectation is tested rigorously by comparing sun and shade leaves of a single species, the differences are not statistically difference (0.33‰; $p > 0.200$; Xiao et al. 2013). Therefore, though sun vs shade is an important microcosm of the importance of the water and carbon cycle in carbon isotope records and controlling plant productivity, the bias this plays when looking at environmental factors on carbon isotope ecology of leaves in modern, historical and fossil records is negligible.

1.2.6 Evolutionary lineage and history

Other potential drivers of carbon isotope discrimination differences among plants includes evolution (Rundel et al. 1999). In particular, different plant functional types and crown versus stem group lineages may have developed different carbon isotope discrimination strategies; on a broad scale, this can be seen when comparing plants using C₃, C₄ and CAM photosynthetic pathways (Tippie & Pagani 2007; Sage 2008). All of the work contained in this thesis considers the importance of evolution and of making general versus species-specific assumptions.

Textbox 1.2: Three photosynthetic pathways

C₃ plants (e.g. trees, soybeans, wheat, rice, 85% plant species) use primarily the RuBisCO enzyme to assimilate CO₂, first to 3-phosphoglycerate, a 3-carbon atom product. The majority of plant species on Earth use C₃ photosynthesis. *This dissertation focuses solely on C₃ plants, but will refer to other photosynthetic mechanisms at times.*

C₄ plants (e.g. corn, maize, sugarcane) use first an additional enzyme to assimilate CO₂, first to a 4 carbon organic acid (oxaloacetate). This step exists so that plants minimize **photorespiration** (when RuBisCO acts on oxygen, rather than CO₂), by separating initial CO₂ fixation and RuBisCO's fixation to 3-carbon products during the Calvin Cycle.

CAM plants (e.g. cacti) minimize photorespiration and save water by separating nighttime fixation with daytime Calvin Cycle.

1.3 Carbon isotope records in sediments

The translation of carbon and organic matter from plants to sediments occurs during senescence and deposition of plant matter. In modern studies and the fossil record, organic carbon in sediments has been derived from plant fossils (to reconstruct $\delta^{13}\text{C}_{\text{atm}}$ and CO_2 ; Arens et al. 2000; Cui & Schubert 2016) and leaf waxes (to reconstruct paleoecology; Tierney et al. 2011, Wu et al. 2017; Bhattacharya et al. 2018), while carbonates in sediments have been used from pedogenic carbonates and plant and animal fossils (to reconstruct CO_2 ; Cerling et al. 1991; Cerling 1992; and to reconstruct paleodiets; Koch 1998). In addition to the factors controlling carbon isotope discrimination in plants, the use of organic matter in sediments introduces additional factors, such as microbial metabolism and diagenetic alteration (^{13}C ; Wynn 2007; Fig. 1.6a). Heterotrophically respired CO_2 , which can ultimately degas from the soil, tends to be depleted in ^{13}C by about 2‰, leaving behind microbial biomass and microbial decomposition solid byproducts that are enriched by about 2‰ (Wynn et al. 2005; Wynn 2007). As you continue deeper below the surface, authigenic carbonate formed from soils-respired CO_2 can be overprinted by recrystallization, diagenetic precipitation, and inherited carbonate from soil parent materials (Wynn 2007). Pedogenic carbonates are only found in arid land soils (Cerling & Quade 1993), and thus are not useful for paleoecological interpretations from mesic environments. Because the reaction is kinetically driven, the enrichment of $\delta^{13}\text{C}$ of soil organic carbon with depth through a soil column can be summarized by Rayleigh distillation (Fig. 1.6b). The fractionation of carbon isotope values within the soil column is not comparable across all soils, and is impacted by how water-logged a soil is, which once again relates to precipitation and regional water cycles as well as soil texture, soil temperature, and microbes present (Wynn 2007). Nonetheless, the carbon isotope composition of soil carbon ($\delta^{13}\text{C}_{\text{SOM}}$) in the uppermost horizons of a soil closely matches the integrated composition of the plants growing on that soil. This suggests that quantitative relationships between $\delta^{13}\text{C}_{\text{leaf}}$ and MAP could potentially be reflected between $\delta^{13}\text{C}_{\text{leaf}}$ and MAP could potentially be reflected by $\delta^{13}\text{C}_{\text{SOM}}$ as well. This potential relationship is explored in **Chapter IV**.

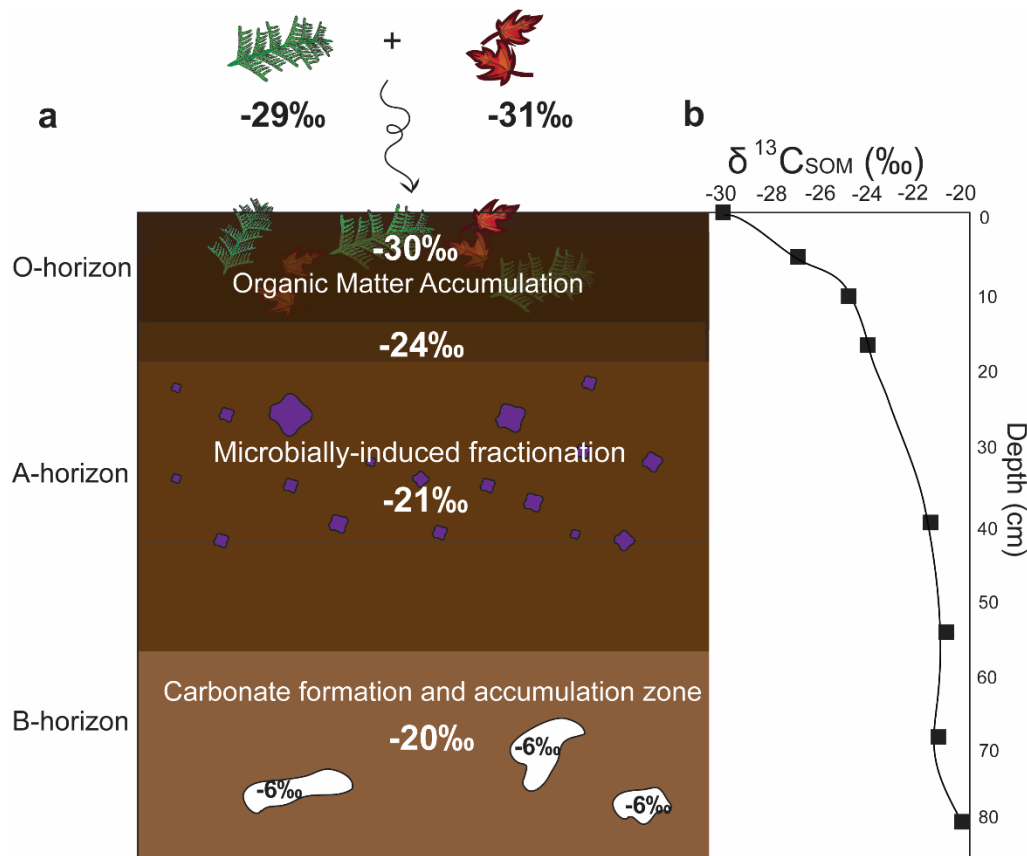


Figure 1.6 Diagram of soil carbon isotopes in a soil profile including O- through B- horizons and major driving processes. (a) An example soil profile including common horizons O- through B- and major fractionation processes, in addition to common $\delta^{13}C$ values found at each level (b) an example soil profile demonstrating Rayleigh fractionation with depth, created based on combined data from Wynn's (2007, Fig. 1) measured profiles from Kakamega Forest Reserve (Kenya), Goodwin Creek (Mississippi USA), Zengoaga (Cameroon) and Queensland (Australia).

1.4 Dissertation structure

This dissertation aims to examine the relationship between carbon isotope discrimination recorded in plants and organic matter and the carbon and water cycle in a new context. I approach the carbon isotope ecology of terrestrial ecosystems as they relate to the carbon cycle from several perspectives. This includes a study focused on the relationship between a number of potential climate factors and the carbon isotope ecology of one Great Lakes region gymnosperm (*Thuja occidentalis*, northern white cedar, **Chapter II**), and a complementary study that assesses the particular relationship between CO_2 and carbon isotope ecology of a number of woody C_3 plants (**Chapter III**). **Chapter IV** addresses the integrative properties of soil, and applications

in the fossil record in the context of the findings from previous chapters. This work takes advantage of the natural experiment of Industrialization from several angles, and incorporates the use of museum and herbarium collections to gather highly resolved temporal data. In **Chapter V**, I use findings from the previous three chapters to reconstruct many aspects of a forest ecosystem as recorded in early Eocene (hothouse) sediments. In each of the studies, the results indicate the importance of taxonomic identification and of not over-generalizing across C₃ plants.

Specifically, **Chapter II** explores the relationship between carbon isotope discrimination and fractionation (Δ_{leaf} , $\delta^{13}\text{C}_{\text{leaf}}$ respectively) and environmental and edaphic factors in a highly resolved single species study throughout Industrialization. This chapter focuses on the relationship between climate variables and the organic chemistry of *Thuja occidentalis* (northern white cedar) collected across the Great Lakes Region from the 1800s to the 2010s (and stored in herbaria). The use of the natural experiment of anthropogenic CO₂ enhancement provides a unique opportunity to look at changes in %C, %N, and carbon isotope biogeochemistry in light of rising CO₂ levels related to fossil fuels. What makes this experiment especially unique is that in addition to CO₂ rising, the isotopic value of atmospheric CO₂ becomes more depleted over this time period.

While **Chapter II** centers around one focal species, with a number of climate variables under scrutiny, **Chapter III** focuses instead around the relationship between one specific climate variable: [CO₂], and carbon isotope biogeochemistry in eight different focal species, including seven gymnosperms: *Thuja koraiensis* (Korean arborvitae), *Thuja occidentalis* (northern white cedar), *Thuja plicata* (Pacific red cedar), *Thuja standishii* (Japanese arborvitae), *Thuja sutchuenensis* (Sichuan arborvitae), *Pinus strobus* (Eastern white pine), *Platycladus orientalis* (Oriental arborvitae) and one woody angiosperm, *Populus tremuloides* (quaking aspen). This study uses collections to examine a number of species response to anthropogenic carbon enhancement over Industrialization. In addition to using historical specimens to look in depth at the response of certain species to CO₂, this study incorporates many carbon isotope values from literature and meta-analyses to examine the role that taxonomy plays in controlling plant response to CO₂.

Applications from findings in Chapters II and III are applied to **Chapter IV**, which examines previous findings relating precipitation and $\delta^{13}\text{C}_{\text{leaf}}$ through a different lens: soil. This

chapter tests $\delta^{13}\text{C}$ in soil organic matter ($\delta^{13}\text{C}_{\text{SOM}}$) as a potential complementary proxy, under the premise that soil organic matter acts as an aggregator of aboveground biomass within an ecosystem, and thus is not sensitive to changing taxonomy. This chapter includes modern organic-rich soils from C_3 -only ecosystems collected for this study and modern organic rich soils from C_3 -only ecosystems aggregated from literature. Findings based on modern studies are applied to fossilized soils (paleosols) with comparable soil and ecosystem development to modern times. Each of these paleosols had independent non- $\delta^{13}\text{C}_{\text{SOM}}$ based paleoprecipitation estimates for comparison.

Finally, findings from Chapters II, III and IV were applied in ancient early Eocene forested ecosystems (**Chapter V**). Specimens spanning a 70m stratigraphic section of alluvial, fluvial, and pedogenic sediments in the greater Green River basin were collected and analyzed for bulk geochemistry, organic geochemistry, and carbon isotope ecology. Findings from prior chapters related to organic isotope geochemistry in plants and soils are contextualized with pre-established inorganic proxies in soils and sedimentary facies, all together giving a comprehensive, robust ecosystem reconstruction. In this study, I use multiple proxies to constrain aspects of the environment, which, in conjunction with the well-documented floral assemblage of the Blue Rim escarpment, provide an excellent snapshot of the well-rounded depositional environment. Using bulk geochemical tools to constrain provenance, parent material, leaching and weathering, combined with paleosol based tools to reconstruct temperature and precipitation, I parse out climate signals and constrain hydrological inputs into the region. In addition to applying $\delta^{13}\text{C}_{\text{SOM}}$ to provide precipitation reconstructions to complement previous physiognomy-based ones, $\delta^{13}\text{C}_{\text{atm}}$ values of *Lygodium kaulfussii* were applied to constrain $\delta^{13}\text{C}_{\text{atm}}$ during the Early Eocene. In full, **Chapter V** represents the importance of using these tools, researched in Chapters II through IV, in the presence of multiple proxies when possible, to best represent the intricacies of regional ecosystems during a hothouse period often invoked as an analog for future climate change.

1.5 References

- Ainsworth, E. A., & Long, S. P. (2005). What have we learned from 15 years of free-air CO₂ enrichment (FACE)? A meta-analytic review of the responses of photosynthesis, canopy properties and plant production to rising CO₂. *New Phytologist*, *165*(2), 351-372.
- Andersson, I., & Backlund, A. (2008). Structure and function of Rubisco. *Plant Physiology and Biochemistry*, *46*(3), 275-291.
- Apel, P. (1989). Influence of CO₂ on stomatal numbers. *Biologia Plantarum*, *31*(1), 72-74.
- Arens, N. C., Jahren, A. H., & Amundson, R. (2000). Can C₃ plants faithfully record the carbon isotopic composition of atmospheric carbon dioxide? *Paleobiology*, 137-164.
- Bar-On, Y. M., & Milo, R. (2019). The global mass and average rate of rubisco. *Proceedings of the National Academy of Sciences*, *116*(10), 4738-4743.
- Berner, R. A. (1992). Weathering, plants, and the long-term carbon cycle. *Geochimica et Cosmochimica Acta*, *56*(8), 3225-3231.
- Bhattacharya, T., Tierney, J. E., Addison, J. A., & Murray, J. W. (2018). Ice-sheet modulation of deglacial North American monsoon intensification. *Nature Geoscience*, *11*(11), 848-852.
- Bolin, B. (1970). The carbon cycle. *Scientific American*, *223*(3), 124-135.
- Bowes, G. (1991). Growth at elevated CO₂: photosynthetic responses mediated through Rubisco. *Plant, Cell & Environment*, *14*(8), 795-806.
- Brooks, J. R., Flanagan, L. B., Buchmann, N., & Ehleringer, J. R. (1997). Carbon isotope composition of boreal plants: functional grouping of life forms. *Oecologia*, *110*(3), 301-311.
- Campbell, W. J., Allen, L. H., & Bowes, G. (1988). Effects of CO₂ concentration on rubisco activity, amount, and photosynthesis in soybean leaves. *Plant physiology*, *88*(4), 1310-1316.
- Cao, M., & Woodward, F. I. (1998). Dynamic responses of terrestrial ecosystem carbon cycling to global climate change. *Nature*, *393*(6682), 249-252.
- Cerling, T. E., Solomon, D. K., Quade, J. A. Y., & Bowman, J. R. (1991). On the isotopic composition of carbon in soil carbon dioxide. *Geochimica et Cosmochimica Acta*, *55*(11), 3403-3405.
- Cerling, T. E. (1992). Use of carbon isotopes in paleosols as an indicator of the p(CO₂) of the paleoatmosphere. *Global Biogeochemical Cycles*, *6*(3), 307-314.

- Cerling, T. E., Quade, J. (1993). Stable carbon and oxygen isotopes in soil carbonates. P. K Swart K. C Lohmann, J McKenzie, and S Savin eds. *Climate change in continental isotopic records. Geophysical Monograph*, 78, 217-231.
- Condon, A. G., Richards, R. A., & Farquhar, G. D. (1992). The effect of variation in soil water availability, vapour pressure deficit and nitrogen nutrition on carbon isotope discrimination in wheat. *Australian Journal of Agricultural Research*, 43(5), 935-947.
- Conroy, J. L., Overpeck, J. T., Cole, J. E., Shanahan, T. M., & Steinitz-Kannan, M. (2008). Holocene changes in eastern tropical Pacific climate inferred from a Galápagos lake sediment record. *Quaternary Science Reviews*, 27(11-12), 1166-1180.
- Crafts-Brandner, S. J., & Salvucci, M. E. (2000). RuBisCO activase constrains the photosynthetic potential of leaves at high temperature and CO₂. *Proceedings of the National Academy of Sciences*, 97(24), 13430-13435.
- Cruz-Martínez, K., Rosling, A., Zhang, Y., Song, M., Andersen, G. L., & Banfield, J. F. (2012). Effect of rainfall-induced soil geochemistry dynamics on grassland soil microbial communities. *Applied and environmental microbiology*, 78(21), 7587-7595.
- Ehleringer, J. R. (1993). Carbon and water relations in desert plants: an isotopic perspective. In *Stable isotopes and plant carbon-water relations* (pp. 155-172). Academic Press.
- Farquhar, G. D., Ehleringer, J. R., & Hubick, K. T. (1989). Carbon isotope discrimination and photosynthesis. *Annual review of plant biology*, 40(1), 503-537.
- Franks, P. J., Royer, D. L., Beerling, D. J., Van de Water, P. K., Cantrill, D. J., Barbour, M. M., & Berry, J. A. (2014). New constraints on atmospheric CO₂ concentration for the Phanerozoic. *Geophysical Research Letters*, 41(13), 4685-4694.
- Gallagher, T. M., & Sheldon, N. D. (2013). A new paleothermometer for forest paleosols and its implications for Cenozoic climate. *Geology*, 41(6), 647-650.
- Gates, D. M. (1968). Transpiration and leaf temperature. *Annual Review of Plant Physiology*, 19(1), 211-238.
- Gebrekirstos, A., Worbes, M., Teketay, D., Fetene, M., & Mitlöhner, R. (2009). Stable carbon isotope ratios in tree rings of co-occurring species from semi-arid tropics in Africa: patterns and climatic signals. *Global and Planetary Change*, 66(3-4), 253-260.
- Hall, A. E., Thiaw, S., & Krieg, D. R. (1994). Consistency of genotypic ranking for carbon isotope discrimination by cowpea grown in tropical and subtropical zones. *Field Crops Research*, 36(2), 125-132.
- Haworth, M., Elliott-Kingston, C., & McElwain, J. C. (2011). Stomatal control as a driver of plant evolution. *Journal of Experimental Botany*, 62(8), 2419-2423.

- Hendy, I. L., & Kennett, J. P. (2000). Dansgaard-Oeschger cycles and the California Current System: Planktonic foraminiferal response to rapid climate change in Santa Barbara Basin, Ocean Drilling Program hole 893A. *Paleoceanography*, *15*(1), 30-42.
- Helliker B. H., & Richter S. L. (2008). Subtropical to boreal convergence of tree-leaf temperatures. *Nature* *454*(7203), 511-514.
- Hessen, D. O., Ågren, G. I., Anderson, T. R., Elser, J. J., & De Ruiter, P. C. (2004). Carbon sequestration in ecosystems: the role of stoichiometry. *Ecology*, *85*(5), 1179-1192.
- Hopley, P. J., Weedon, G. P., Marshall, J. D., Herries, A. I., Latham, A. G., & Kuykendall, K. L. (2007). High-and low-latitude orbital forcing of early hominin habitats in South Africa. *Earth and Planetary Science Letters*, *256*(3-4), 419-432.
- Jobbágy, E. G., & Jackson, R. B. (2000). The vertical distribution of soil organic carbon and its relation to climate and vegetation. *Ecological applications*, *10*(2), 423-436.
- Knapp, A. K., & Smith, W. K. (1990). Stomatal and photosynthetic responses to variable sunlight. *Physiologia Plantarum*, *78*(1), 160-165.
- Körner, C. (1988). Does global increase of CO₂ alter stomatal density? *Flora*, *181*(3-4), 253-257.
- Körner, C., Farquhar, G. D., & Wong, S. C. (1991). Carbon isotope discrimination by plants follows latitudinal and altitudinal trends. *Oecologia*, *88*(1), 30-40.
- Leakey, A. D., Ainsworth, E. A., Bernacchi, C. J., Rogers, A., Long, S. P., & Ort, D. R. (2009). Elevated CO₂ effects on plant carbon, nitrogen, and water relations: six important lessons from FACE. *Journal of experimental botany*, *60*(10), 2859-2876.
- Long, S. P., Ainsworth, E. A., Rogers, A., & Ort, D. R. (2004). Rising atmospheric carbon dioxide: plants FACE the future. *Annual Reviews in Plant Biology*, *55*, 591-628.
- Madhavan, S., Treichel, I., & O'Leary, M. H. (1991). Effects of relative humidity on carbon isotope fractionation in plants. *Botanica Acta*, *104*(4), 292-294.
- McElwain, J. C. (1998). Do fossil plants signal palaeoatmospheric carbon dioxide concentration in the geological past? *Philosophical Transactions of the Royal Society of London. Series B: Biological Sciences*, *353*(1365), 83-96.
- McElwain, J. C., & Steinthorsdottir, M. (2017). Paleoecology, ploidy, paleoatmospheric composition, and developmental biology: a review of the multiple uses of fossil stomata. *Plant Physiology*, *174*(2), 650-664.
- Norby, R. J., & Zak, D. R. (2011). Ecological lessons from free-air CO₂ enrichment (FACE) experiments. *Annual review of ecology, evolution, and systematics*, *42*.

- Nowak, R. S., Ellsworth, D. S., & Smith, S. D. (2004). Functional responses of plants to elevated atmospheric CO₂—do photosynthetic and productivity data from FACE experiments support early predictions? *New Phytologist*, *162*(2), 253-280.
- O'Leary, M. H. (1981). Carbon isotope fractionation in plants. *Phytochemistry*, *20*(4), 553-567.
- Ojima, D. S., Dirks, B. O., Glenn, E. P., Owensby, C. E., & Scurlock, J. O. (1993). Assessment of C budget for grasslands and drylands of the world. *Water, Air, and Soil Pollution*, *70*(1-4), 95-109.
- Pennisi, E. (2008). Getting to the root of drought responses. *Science*, *320*(5873), 173-173.
- Peppe, D. J., Royer, D. L., Cariglino, B., Oliver, S. Y., Newman, S., Leight, E., Enikolopov, G., Fernandez-Burgos, M., Herrera, F., Adams, M. J. & Correa, E. (2011). Sensitivity of leaf size and shape to climate: global patterns and paleoclimatic applications. *New Phytologist*, *190*(3), 724-739.
- Peppe, D. J., Baumgartner, A., Flynn, A., & Blonder, B. (2018). Reconstructing paleoclimate and paleoecology using fossil leaves. In *Methods in Paleoecology* (pp. 289-317). Springer, Cham.
- Ponton, S., Flanagan, L. B., Alstad, K. P., Johnson, B. G., Morgenstern, K. A. I., Kljun, N., Black, T. A., & Barr, A. G. (2006). Comparison of ecosystem water-use efficiency among Douglas-fir forest, aspen forest and grassland using eddy covariance and carbon isotope techniques. *Global Change Biology*, *12*(2), 294-310.
- Royer, D. L. (2001). Stomatal density and stomatal index as indicators of paleoatmospheric CO₂ concentration. *Review of Palaeobotany and Palynology*, *114*(1-2), 1-28.
- Sage, R. F. (2008). Environmental and evolutionary preconditions for the origin and diversification of the C₄ photosynthetic syndrome. *Plant Biology*, *3*(3), 202-213.
- Schlanser, K., Diefendorf, A. F., Greenwood, D. R., Mueller, K. E., West, C. K., Lowe, A. J., Basinger, J. F., Currano, E. D., Flynn, A. G., Fricke, H. C. & Geng, J. (2020). On geologic timescales, plant carbon isotope fractionation responds to precipitation similarly to modern plants and has a small negative correlation with pCO₂. *Geochimica et Cosmochimica Acta*, *270*, 264-281.
- Schlesinger, W. H., & Jasechko, S. (2014). Transpiration in the global water cycle. *Agricultural and Forest Meteorology*, *189*, 115-117.
- Scholz, C. A., Johnson, T. C., Cohen, A. S., King, J. W., Peck, J. A., Overpeck, J. T., Talbot, M. R., Brown, E. T., Kalindekaffe, L., Amoako, P. Y. & Lyons, R. P. (2007). East African megadroughts between 135 and 75 thousand years ago and bearing on early-modern human origins. *Proceedings of the National Academy of Sciences*, *104*(42), 16416-16421.
- Schubert, B. A., & Jahren, A. H. (2018). Incorporating the effects of photorespiration into terrestrial paleoclimate reconstruction. *Earth-Science Reviews*, *177*, 637-642.

- Schulze, E. D., & Küppers, M. (1979). Short-term and long-term effects of plant water deficits on stomatal response to humidity in *Corylus avellana* L. *Planta*, 146(3), 319-326.
- Sharifi, M. R., & Rundel, P. W. (1993). The effect of vapour pressure deficit on carbon isotope discrimination in the desert shrub *Larrea tridentata* (creosote bush). *Journal of Experimental Botany*, 44(2), 481-487.
- Sheldon, N. D., Retallack, G. J., & Tanaka, S. (2002). Geochemical climofunctions from North American soils and application to paleosols across the Eocene-Oligocene boundary in Oregon. *The Journal of geology*, 110(6), 687-696.
- Sheldon, N. D., Smith, S. Y., Stein, R., & Ng, M. (2020). Carbon isotope ecology of gymnosperms and implications for paleoclimatic and paleoecological studies. *Global and Planetary Change*, 184, 103060.
- Stein, R. A., Sheldon, N. D., & Smith, S. (2019). Rapid response to anthropogenic climate change by *Thuja occidentalis*: implications for past climate reconstructions and future climate predictions. *PeerJ*, 7, e7378.
- Sterling, T. M. (2005). Transpiration: water movement through plants. *Journal of Natural Resources and Life Sciences Education*, 34(1), 123-123.
- Stewart, G. R., Turnbull, M. H., Schmidt, S., & Erskine, P. D. (1995). ¹³C natural abundance in plant communities along a rainfall gradient: a biological integrator of water availability. *Functional Plant Biology*, 22(1), 51-55.
- Teodoridis, V., Mazouch, P., Spicer, R. A., & Uhl, D. (2011). Refining CLAMP—investigations towards improving the Climate Leaf Analysis Multivariate Program. *Palaeogeography, Palaeoclimatology, Palaeoecology*, 299(1-2), 39-48.
- Tierney, J. E., Lewis, S. C., Cook, B. I., LeGrande, A. N., & Schmidt, G. A. (2011). Model, proxy and isotopic perspectives on the East African Humid Period. *Earth and Planetary Science Letters*, 307(1-2), 103-112.
- Tierney, J. E., Pausata, F. S., & deMenocal, P. B. (2017). Rainfall regimes of the Green Sahara. *Science advances*, 3(1), e1601503.
- Tipple, B. J., & Pagani, M. (2007). The early origins of terrestrial C₄ photosynthesis. *Annual Reviews of Earth and Planetary Science*, 35, 435-461.
- Tognetti, R., Minnocci, A., Peñuelas, J., Raschi, A., & Jones, M. B. (2000). Comparative field water relations of three Mediterranean shrub species co-occurring at a natural CO₂ vent. *Journal of Experimental Botany*, 51(347), 1135-1146.
- Tu, T. T. N., Kürschner, W. M., Schouten, S., & Van Bergen, P. F. (2004). Leaf carbon isotope composition of fossil and extant oaks grown under differing atmospheric CO₂ levels. *Palaeogeography, Palaeoclimatology, Palaeoecology*, 212(3-4), 199-213.

- Uhl, D., & Walther, H. (2000). Sun leaf or shade leaf?—Known facts in the light of new data with implications for palaeobotany. *Feddes Repertorium*, 111(3-4), 165-174.
- Warren, C. R., & Adams, M. A. (2001). Distribution of N, Rubisco and photosynthesis in *Pinus pinaster* and acclimation to light. *Plant, Cell & Environment*, 24(6), 597-609.
- Woodward, F. I. (1987). Stomatal numbers are sensitive to increases in CO₂ from pre-industrial levels. *Nature*, 327(6123), 617-618.
- Woodward FI, Bazzazz FA (1988). The responses of stomatal density to CO₂ partial pressure. *Journal of Experimental Botany*, 39(12), 1771-1781.
- Tipple, B. J., Meyers, S. R., & Pagani, M. (2010). Carbon isotope ratio of Cenozoic CO₂: A comparative evaluation of available geochemical proxies. *Paleoceanography*, 25(3), PA3202.
- Vatén A., Bergmann, D. C. (2012). Mechanisms of stomatal development: an evolutionary view. *EvoDevo*, 3(11).
- Wu, M. S., Feakins, S. J., Martin, R. E., Shenkin, A., Bentley, L. P., Blonder, B., /Salinas, N., Asner, G. P., & Malhi, Y. (2017). Altitude effect on leaf wax carbon isotopic composition in humid tropical forests. *Geochimica et Cosmochimica Acta*, 206, 1-17.
- Wynn, J. G., Bird, M. I., & Wong, V. N. (2005). Rayleigh distillation and the depth profile of ¹³C/¹²C ratios of soil organic carbon from soils of disparate texture in Iron Range National Park, Far North Queensland, Australia. *Geochimica et cosmochimica acta*, 69(8), 1961-1973.
- Wynn, J. G. (2007). Carbon isotope fractionation during decomposition of organic matter in soils and paleosols: implications for paleoecological interpretations of paleosols. *Palaeogeography, Palaeoclimatology, Palaeoecology*, 251(3-4), 437-448.
- Xiao, L., Yang, H., Sun, B., Li, X., & Guo, J. (2013). Stable isotope compositions of recent and fossil sun/shade leaves and implications for paleoenvironmental reconstruction. *Review of Palaeobotany and Palynology*, 190, 75-84.
- Zhu, J., Poulsen, C. J., & Tierney, J. E. (2019). Simulation of Eocene extreme warmth and high climate sensitivity through cloud feedbacks. *Science advances*, 5(9), eaax1874.

CHAPTER II

Rapid Response to Anthropogenic Climate Change by *Thuja occidentalis*: Implications for Past Reconstructions and Future Climate Predictions¹

2.1 Abstract

Carbon isotope values of leaves ($\delta^{13}\text{C}_{\text{leaf}}$) from meta-analyses and growth chamber studies of C_3 plants have been used to propose generalized relationships between $\delta^{13}\text{C}_{\text{leaf}}$ and climate variables such as mean annual precipitation (MAP), atmospheric concentration of carbon dioxide ($[\text{CO}_2]$), and other climate variables. These generalized relationships are frequently applied to the fossil record to create paleoclimate reconstructions. Although plant evolution influences biochemistry and response to environmental stress, few studies have assessed species-specific carbon assimilation as it relates to climate outside of a laboratory. We measured $\delta^{13}\text{C}_{\text{leaf}}$ values and C:N ratios of a wide-ranging evergreen conifer with a long fossil record, *Thuja occidentalis* (Cupressaceae) collected 1804–2017, in order to maximize potential paleo-applications of our focal species. This high-resolution record represents a natural experiment from pre-Industrial to Industrial times, which spans a range of geologically meaningful $[\text{CO}_2]$ and $\delta^{13}\text{C}_{\text{atm}}$ values. Δ_{leaf} values (carbon isotope discrimination between $\delta^{13}\text{C}_{\text{atm}}$ and $\delta^{13}\text{C}_{\text{leaf}}$) remain constant across climate conditions, indicating limited response to environmental stress. Only $\delta^{13}\text{C}_{\text{leaf}}$ and $\delta^{13}\text{C}_{\text{atm}}$ values showed a strong relationship (linear), thus, $\delta^{13}\text{C}_{\text{leaf}}$ is an excellent record of carbon isotopic changes in the atmosphere during Industrialization. In contrast with previous free-air concentration enrichment experiments, no relationship was found between C:N ratios and increasing $[\text{CO}_2]$. Simultaneously static C:N ratios and Δ_{leaf} in light of increasing CO_2 highlights plants' inability to match rapid climate change with increased carbon assimilation as previously expected; Δ_{leaf} values are not reliable tools to reconstruct MAP and $[\text{CO}_2]$, and $\delta^{13}\text{C}_{\text{leaf}}$ values only decrease with $[\text{CO}_2]$ in line with atmospheric carbon isotope changes.

¹Published under the citation:

Stein, R. A., Sheldon, N. D., & Smith, S. (2019). Rapid response to anthropogenic climate change by *Thuja occidentalis*: implications for past climate reconstructions and future climate predictions. *PeerJ*, 7, e7378.

2.2. Introduction

The concentration ($[\text{CO}_2]$) and isotopic value ($\delta^{13}\text{C}_{\text{atm}}$) of atmospheric CO_2 are changing at a pace unprecedented in geologic time (Keeling et al., 2005; Zhang et al., 2013). These changes have been accompanied by regional changes in mean annual temperature (MAT), mean annual precipitation (MAP), maximum summer temperature, and other climate variables (Yonetani & Gordon, 2001). The rapid decline in the carbon isotopic composition of CO_2 ($\delta^{13}\text{C}_{\text{atm}}$) due to fossil fuel combustion, deforestation, and other human inputs, is known as the Suess Effect, and is a chemical representation of anthropogenic changes to the atmosphere—and more broadly, the environment. $\delta^{13}\text{C}_{\text{atm}}$ values provide a useful way to see changes in CO_2 sources, sinks, and fluxes in the modern environment (Keeling, 1979; Boutton, 1991; Deines, 1992). It can also be applied to geologic problems (Schmitt et al., 2012) due to the naturally differing isotopic compositions of different CO_2 sources (e.g., methane, volcanism). $\delta^{13}\text{C}_{\text{atm}}$ values are particularly useful because they are parameters in models that reconstruct past changes to atmospheric $[\text{CO}_2]$ using paleosol carbonates (Cerling et al., 1991, 1992) or atmospheric $[\text{CO}_2]$ using plant stomatal parameters (Franks et al., 2014). Direct measurements of $\delta^{13}\text{C}_{\text{atm}}$ values only go back 50 years due to technological limitations, and longer-reaching ice core CO_2 bubbles ($\sim 800,000$ years) are poorly resolved for recent times and limited by the presence of glacial ice (Keeling & Whorf, 2004; Augustin et al., 2004; Barnola et al., 1987; Trudinger et al., 1999; Petit et al., 1999). The biosphere provides an excellent system that directly interacts with the atmosphere and fills the gap to provide high-resolution recent and long-term records, potentially extending into geologic time (Arens, Jahren & Amundson, 2000).

This direct interaction means that plants potentially provide a robust record of $\delta^{13}\text{C}_{\text{atm}}$ values in their own leaf carbon isotope values ($\delta^{13}\text{C}_{\text{leaf}}$) and fractionation values (Δ_{leaf} , Equation 2.1; Farquhar, Ehleringer & Hubick, 1989; Feng, 1999; Farquhar & Sharkey, 1982), which gives insight into changes in carbon assimilation over time. In Equation 2.1, a represents the fractionation of $\delta^{13}\text{C}$ due to diffusion in air (4.4‰) and b represents the fractionation due to the carboxylation (instigated by the Rubisco enzyme, 27‰; Farquhar, Ehleringer & Hubick, 1989). These fractionation factors are compiled and multiplied by the ratio of C_i (intercellular $[\text{CO}_2]$) to C_a (atmospheric $[\text{CO}_2]$), a ratio that is often used to represent water use efficiency.

$$\Delta_{\text{leaf}} = \frac{\delta^{13}\text{C}_{\text{atm}} - \delta^{13}\text{C}_{\text{leaf}}}{(1 + \delta^{13}\text{C}_{\text{leaf}}/1000)} = a + (b - a)\left(\frac{C_i}{C_a}\right) \quad (\text{Equation 2.1})$$

While a and b are thought to be constant, we know that $\delta^{13}\text{C}_{\text{atm}}$ and C_a are changing rapidly. This could result in a corresponding change in Δ_{leaf} values as plants adapt to increased $[\text{CO}_2]$ or subsequent regional climate changes, for example, systematic changes in local precipitation). Alternatively, Δ_{leaf} values of leaves may stay constant but show marked changes in $\delta^{13}\text{C}_{\text{leaf}}$ values corresponding to changes in $\delta^{13}\text{C}_{\text{atm}}$ values if leaves are incorporating $\delta^{13}\text{C}_{\text{atm}}$ into leaf tissues at a rate unaffected by other climate conditions.

2.2.1 Carbon isotopes related to climate variables

Previous studies have related Δ_{leaf} values to climate variables such as MAP, water availability and soil moisture (Diefendorf et al., 2010; Kohn, 2010; Wernerehl & Givnish, 2015; Mårtensson et al., 2017), MAT (Troughton & Card, 1975; O’Leary, 1993); latitude (Diefendorf et al., 2010; Kohn, 2010), $[\text{CO}_2]$ (Schubert & Jahren, 2012, 2018), altitude (Korner, Farquhar & Wong, 1991; O’Leary, 1993), seasonality (Ehleringer, Phillips & Comstock, 1992), and $\delta^{13}\text{C}_{\text{atm}}$ values during growth seasons (Peñuelas & Azcón-Bieto, 1992; Arens, Jahren & Amundson, 2000; Pedicino et al., 2002). The studies that incorporate potential influence from a wide range of climate variables have been conducted via meta-analysis with no normalized collection procedure or investigated species, or via growth chamber experiment conducted under idealized conditions. The few studies that have used naturally-obtained specimens (i.e., natural history collections such as herbaria) to look at isotope change over time and changing atmospheric conditions ($[\text{CO}_2]$ and $\delta^{13}\text{C}_{\text{atm}}$ values) have focused on localized regions with little range in climate (i.e., all dry, mid- to high- altitude, hot regions of eastern Arizona/western New Mexico, or the Mediterranean climate of Catalonia; Peñuelas & Azcón-Bieto, 1992; Pedicino et al., 2002). These collections-based experiments are limited in scope and while they provide information on specific ecosystems, do not address these biosphere-atmosphere interactions across climate regimes or on a regional and global scale. Very little is known about whether individual species respond to any, some, or all of these potential forcings across a range of climatic conditions.

2.2.2 Potential Climate Drivers

2.2.2.1 CO₂ and elevation

We would expect higher [CO₂] to affect biochemical discrimination because of the known effects elevated [CO₂] has on stomata (size, density, and conductance; Woodward, 1987; Woodward & Bazzaz, 1988; Tognetti et al., 2000; Ainsworth & Rogers, 2007). In a meta-analysis of trees in European temperate and boreal forests, leaves responded to an increase in [CO₂] with a significant (21%) decrease in stomatal conductance (the rate of passage of atmospheric CO₂ into plant tissue; Medlyn et al., 2001). Increased [CO₂] also causes a decrease in stomatal density (the number of pores on a leaf surface) and stomatal index (the number of pores compared to the number of total epidermal cells); these indices have been liberally applied to the geologic record to reconstruct [CO₂] (Retallack, 2001; Beerling & Royer, 2002; Roth-Nebelsick et al., 2014). Because stomata directly control the flow of carbon dioxide into leaves and control carbon isotope fractionation by diffusion (Farquhar, Ehleringer & Hubick, 1989), changes in stomatal parameters could affect fractionation as well. Additional factors must be considered; the dependence of Δ_{leaf} on [CO₂] may in part be due to isotopic discrimination associated with photorespiration (Schubert & Jahren, 2018). Indeed, previous growth chamber studies in prescribed CO₂ environments showed increased carbon isotope fractionation with increased [CO₂]; Schubert & Jahren (2012) found a strong hyperbolic correlation ($r > 0.94$) between [CO₂] and Δ_{leaf} values in two species of herbaceous angiosperms. Based upon these growth chamber experiments (Schubert & Jahren, 2012, 2018), the relationship between [CO₂] and Δ_{leaf} is expected to be most sensitive at geologically low [CO₂] (including pre-Industrial to present values) as it was in the levels present during plant growth in this study.

Elevation has been shown to factor into carbon isotope discrimination but is frequently not evaluated independently, due to its covariant relationship with climate variables such as temperature, vapor pressure, partial pressure of CO₂ ($p\text{CO}_2$), soil [CO₂], and soil texture (Diefendorf et al., 2010). A study looking at *Salix herbacea* leaves along an altitudinal gradient (2,000–2,800 m) in Austria showed a decrease in carbon isotope value with increased altitude, did not account for corresponding changes in other climate variables (Beerling, Matthey & Chaloner, 1993). Another study done in Utah and New Mexico using a number of desert and woodland species, including angiosperms and gymnosperms, found similar negative trends in $\delta^{13}\text{C}_{\text{leaf}}$ with increased altitude without controlling for other climate variables (Van de Water, Leavitt & Betancourt, 2002). In 2010, a meta-analysis assessing carbon isotope fractionation and discrimination values across a wide range of C₃ plants (Diefendorf et al., 2010) found that when

combined with MAP, elevation explained 61% of variability in Δ_{leaf} values. Based upon these studies, we included elevation as a potential variable in our study, however, we chose sample locations to minimize changes in elevation because it is difficult to completely separate this variable from regional variation in $[\text{CO}_2]$ and $\delta^{13}\text{C}_{\text{atm}}$.

2.2.2.2 $\delta^{13}\text{C}_{\text{atm}}$

With the current increase in $[\text{CO}_2]$, we have observed the aforementioned Suess Effect, wherein $\delta^{13}\text{C}_{\text{atm}}$ has changed in response to increased inputs of more isotopically negative CO_2 into the atmosphere (Keeling, 1979). The composition of CO_2 involved in the making of organic tissue is likely to affect the composition of that organic tissue (Arens, Jahren & Amundson, 2000); our study will test if this effect is compounded or mitigated by changes in other climate variables over this chronologically robust natural experiment.

2.2.2.3 Latitude

Latitude is expected to affect stomatal traits and therefore be related to carbon isotope fractionation due to its inverse relationship with light (specifically length of growing season and length of day) and temperature, and consequent effects on the maximum operating times for photosynthesis. A meta-analysis across 760 species in nine Chinese forest ecosystems showed a latitudinal variation in stomatal density and stomatal length at the community level (Wang et al., 2015). Given these morphological changes due to latitude, and the relationship between latitude and temperature, we might expect that Δ_{leaf} values would be inversely related to latitude as well (Farquhar, Ehleringer & Hubick, 1989; Equation 2.1). The relationship between Δ_{leaf} and latitude (15.9°S through 69.5°N) was observed in results of a meta-analysis of plants that used C_3 photosynthetic pathways ($n = 506$) (Diefendorf et al., 2010), but any changes in Δ_{leaf} as a function of latitude disappeared when latitude was decoupled from temperature and precipitation.

2.2.2.4 Precipitation

The stomata act as an inlet for CO_2 uptake as well as an outlet for leaf water loss via transpiration, which is why one might expect a relationship between carbon isotope fractionation and available water (represented in the paleo-record as reconstructed MAP). With decreased available water (i.e., decreased MAP) comes increased need for plant “water use efficiency” (as

measured by the ratio of water used in photosynthesis to water lost through transpiration); plants therefore minimize water loss through the same stomata by fully closing, resulting in decreased carbon isotope fractionation (Farquhar, Ehleringer & Hubick, 1989). Previous meta-analyses, such as those by Diefendorf et al. (2010) and Kohn (2010), compared Δ_{leaf} values of a wide variety of modern C_3 plants from many regions with MAP and found that Δ_{leaf} varied significantly with MAP (p-value = 0.0001 and $R^2 = 0.57$; Diefendorf et al., 2010).

2.2.2.5 Temperature and seasonality

In addition to the climate variables with pre-established and applied relationships with Δ_{leaf} values ($[\text{CO}_2]$, MAP), various hypotheses have been proposed about the relationships between carbon isotope discrimination and other climate variables. For example, MAT could also constrain photosynthetic processes and associated carbon isotope fractionation because it gives a rough representation of extreme conditions and growing season length during which carbon assimilation occurs. For this reason, MAT is a well-addressed climate variable in previous isotope fractionation studies, but none have identified a relationship between fractionation and MAT (Arens, Jahren & Amundson, 2000; Diefendorf et al., 2010; Kohn, 2010; Schubert & Jahren, 2012). Furthermore, Helliker & Richter (2008) found that leaves maintained a constant internal temperature ideal for photosynthesis of 21.4 ± 2.2 °C (total range of measurements), independent of external temperatures. In addition to MAT, maximum summer temperatures (particularly, the extreme highs associated with a warming climate) are expected to increase (Mirza, 2003). Increased maximum summer temperatures lead to increased evapotranspiration and more plant stress, which might affect carbon assimilation rates and stomatal conductivity (Farquhar, Ehleringer & Hubick, 1989; Diefendorf et al., 2010).

Seasonal variation is also thought to affect isotopic discrimination, resulting in a change in $\delta^{13}\text{C}_{\text{leaf}}$ of up to 1–2‰ (Ehleringer, Phillips & Comstock, 1992; Arens, Jahren & Amundson, 2000), or in some deciduous trees such as maples, up to 6‰ between early spring and late fall (Lowdon & Dyck, 1974). Typically, more positive values are found in the winter (indicative of less isotopic discrimination) and more negative values occur in the summer (indicative of more discrimination). This effect strongest in arid and semiarid environments because they experience amplified seasonal temperature, precipitation, and evaporation effects (up to 4‰; Ehleringer,

Phillips & Comstock, 1992). Our choice of sample locations should minimize this effect, as our specimens come from humid regions.

Though we do not expect a correlation between temperature and seasonality with Δ_{leaf} values, nor are there good proxies for these variables in the fossil record, we include them here for completeness. This ensures that any observed noise is random or unaccountable for in the fossil record, rather than related to variables that are commonly measured and potentially relevant in plant isotope discrimination (Farquhar, Ehleringer & Hubick, 1989; Arens, Jahren & Amundson, 2000).

2.2.2.6 Finding a focal species

In addition to potentially confounding climate variables, variation in $\delta^{13}\text{C}_{\text{leaf}}$ and Δ_{leaf} values can be related to species-inherent carbon isotope fractionation. In a recent meta-analysis of C_3 plants conducted by Diefendorf et al. (2010), Δ_{leaf} values ranged from 13.4‰ for *Pinus edulis* in Utah, USA (Van de Water, Leavitt & Betancourt, 2002) to 28.4‰ for *Cryptocarya concinna* in Guangdong Province, China (Ehleringer, Phillips & Comstock, 1992). However, the focus on geographic and climatic variability within that dataset resulted in a small number of analyses of any individual species. Thus, while some previous studies have proposed a universal Δ_{leaf} value that represents C_3 plants on average (Arens, Jahren & Amundson, 2000; Gröcke, 2002), we focus here instead on an individual species (*Thuja occidentalis*; Cupressaceae) in order to avoid interspecific variation and phylogenetic/evolutionary effects in plant biochemistry.

Thuja occidentalis is a widespread evergreen gymnosperm with a distribution today extending throughout temperate deciduous and boreal forests in North America, and an extensive fossil record in localities across North America dating back to the Late Cretaceous (~71 million years ago; LePage, 2003; Eckenwalder, 2009). *T. occidentalis* leaves have longer life spans (>1 year) than deciduous trees (Givnish, 2002; Pease, 1917), which makes them less vulnerable to seasonal variability and harder in sedimentary archives (Diefendorf, Leslie & Wing, 2015). While some studies of other individual species have demonstrated unexplained internal isotopic variation of up to 3‰ (Tieszen, 1991), Mervenne (2015) found that Δ_{leaf} values of *T. occidentalis* showed the least amount of internal isotopic variation within a single species grown in a common garden site (e.g., $18.91 \pm 0.46\text{‰}$ vs. *Taxus*: $20.05 \pm 1.93\text{‰}$) when compared to 56

species native to temperate forests. This makes *T. occidentalis* an excellent focal taxon for a single-species study.

This study incorporates the natural shifts in [CO₂] concentrations as driven by fossil fuel combustion and other anthropogenic inputs since the Industrial Revolution (280 ppm: Pre-Industrial, to ~410 ppm in 2014; IPCC, 2014) and $\delta^{13}\text{C}_{\text{atm}}$ values (from -6.5‰: Pre-Industrial to -8.5‰: present; Araus & Buxó, 1993; Elsig et al., 2009; White, Vaughn & Michel, 2015) to examine the relationship between *T. occidentalis*' carbon isotope fractionation and leaf chemistry (C:N ratios) within a range of climate variables. The patterns of Δ_{leaf} values over a range of $\delta^{13}\text{C}_{\text{atm}}$ values highlight the limitations of $\delta^{13}\text{C}_{\text{leaf}}$ change as a tool for better understanding the biosphere and atmosphere. If $\delta^{13}\text{C}_{\text{leaf}}$ values change in sync with $\delta^{13}\text{C}_{\text{atm}}$ values, this could mean that carbon assimilation is continuing in this species as it was prior to Industrialization, perhaps indicating *T. occidentalis*' lack of adaptation to increased [CO₂]. Additionally, it may indicate that $\delta^{13}\text{C}_{\text{leaf}}$ provides another way to track anthropogenic changes to the environment in the recent past and the future.

2.3 Materials and Methods

We measured $\delta^{13}\text{C}_{\text{leaf}}$ values of *T. occidentalis* extending from present-day to Pre-Industrial historical records using both newly collected and herbarium material. This included collecting leaf material of *T. occidentalis* specimens (n = 142 collected between 1804 and 2017 with four unknown dates of collection) from across the Great Lakes region from herbaria (Figs. 2.1A and 2.1B; Table A1) and in natural present-day occurrences across a range of climate conditions (see Table A2). *Thuja* has small, 1–10 mm long scale-leaves addressed along a small branch. Three cm portions of branches representing a single growth year with multiple scale-leaves were cleaned in an ultrasonic bath of deionized water to remove surface debris, oven dried at 50 °C for 48 h and homogenized; this removes any within-leaf isotopic variation. Aliquots of each *T. occidentalis* specimen (0.6–0.8 mg) were placed into tin capsules and placed in a Costech elemental analyzer to measure %C and %N (as well as C:N ratio). Second aliquots of each *T. occidentalis* specimen (0.6–0.8 mg) were placed into tin capsules and placed in a combustion module inlet coupled to a Picarro G2201-i cavity ring-down spectrometer (CRDS) to measure $\delta^{13}\text{C}$ values of each specimen. Duplicates were run on both machines to insure homogeneity. Results of each CRDS run were internally calibrated using nine acetanilide standards ($\delta^{13}\text{C} =$

$-28.17 \pm 0.16\text{‰}$), two IAEA-600 caffeine standards ($\delta^{13}\text{C} = -27.77 \pm 0.04\text{‰}$) and two IAEA-CH-6 sucrose standards ($\delta^{13}\text{C} = -10.45 \pm 0.03\text{‰}$) in each run, as seen in Cotton, Sheldon & Strömberg (2012) study. Reproducibility of replicate analyses was better than 0.3‰.

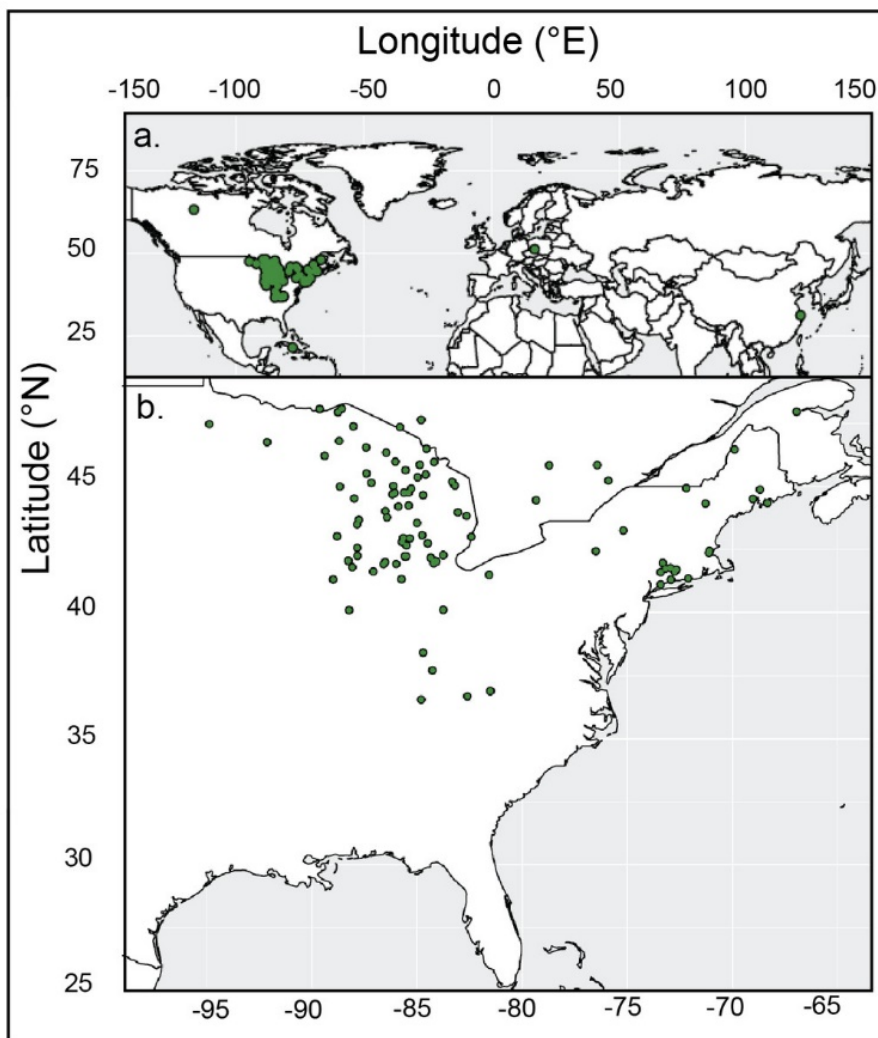


Figure 2.1 Map of locations of *Thuja occidentalis* specimens. Locations of (A) collections of *Thuja occidentalis* from across the world. (B) Specimens collected in Eastern North America (in the typical habitat of *Thuja occidentalis*).

To test whether other climate variables confounded the relationship between $\delta^{13}\text{C}_{\text{atm}}$ and $\delta^{13}\text{C}_{\text{leaf}}$, we calculated carbon isotope fractionation values (Δ_{leaf}) for each specimen using known yearly $\delta^{13}\text{C}_{\text{atm}}$ values (Equation 2.1). We derived global $\delta^{13}\text{C}_{\text{atm}}$ values from direct (Rubino et al., 2013) and interpolated ice and firn core measurements according to the year of sampling (White, Vaughn & Michel, 2015). This does not account for ecosystem or microbiome-level deviations in $\delta^{13}\text{C}_{\text{atm}}$, but does account for the greater source isotopic value. Δ_{leaf} values made it possible to

de-couple the human-driven relationship between increased $[\text{CO}_2]$ and decreased $\delta^{13}\text{C}_{\text{leaf}}$ values (the Suess Effect; Keeling, 1979) because they were calculated by isolating leaf isotope ratios from the atmospheric isotopic signal.

For each specimen locality, environmental data expected to affect $\delta^{13}\text{C}_{\text{leaf}}$ values (MAP, MAT, and maximum summer temperature; Farquhar, Ehleringer & Hubick, 1989) were derived from global databases using exact latitude and longitude coordinates of specimen origin (PRISM Climate Group, 2004; Fick & Hijmans, 2017; Government of Canada, 2018). All contiguous United States data was compiled from Oregon State University's PRISM database, which interpolates data from local weather stations at a resolution of four km (PRISM Climate Group, 2004). $\delta^{13}\text{C}_{\text{leaf}}$ values were also compared with $\delta^{13}\text{C}_{\text{atm}}$ and $[\text{CO}_2]$ values at collection times, as retrieved from NOAA databases documenting values found at Mauna Loa Observatory in Hawaii (White, Vaughn & Michel, 2015) and measured on an isotope-ratio mass spectrometer at the institute of arctic and alpine research (INSTAAR) in the University of Colorado, Boulder. $\delta^{13}\text{C}_{\text{leaf}}$ values for which $\delta^{13}\text{C}_{\text{atm}}$ values were unavailable were not included in Δ_{leaf} calculations or comparisons to climate variables (Table A3). While Δ_{leaf} values combine $\delta^{13}\text{C}$ values measured in this experiment on the CRDS with $\delta^{13}\text{C}_{\text{atm}}$ values measured on the IRMS at INSTAAR, we did not have access to individual errors for $\delta^{13}\text{C}_{\text{atm}}$ and could not propagate the error. Therefore, we used our reproducibility error of 0.3‰, which is larger than the expected error for the IRMS (0.1‰), to be conservative.

Five-point moving averages of $\delta^{13}\text{C}_{\text{leaf}}$ values were calculated to eliminate random noise caused by estimating older specimens' exact collection dates (a result of long collecting expeditions and limited recording resources). We regressed isotope values against climate variables (MAT, MAP, $\delta^{13}\text{C}_{\text{atm}}$ and annual $[\text{CO}_2]$) to examine potential drivers of the $\delta^{13}\text{C}_{\text{leaf}}$ values. We calculated the best-fit line using linear least squares regression to minimize the average distance between modeled y-values and actual y-values ($\delta^{13}\text{C}_{\text{leaf}}$ and Δ_{leaf}) and calculated coefficients of determination. We used R^2 to determine predictive relationship between the given x-variable and y-variable. Additionally, we calculated p-values using the F-test to determine the chance of null hypothesis (p-value > 0.05).

The map of sampling location was created using R version 3.5.0 (R Core Team, 2014), and the ggplot2 (Wickham, 2016) and maps (v3.3.0, Becker & Wilks, 2018) packages. The full code is available in the Supplemental Files.

2.4 Results

Values of $\delta^{13}\text{C}_{\text{leaf}}$ ranged from -21.92‰ (collected in 1899) to -28.51‰ (collected in 2017), with a mean of $-25.05 \pm 1.32\text{‰}$ (standard deviation; Table A2). Δ_{leaf} values ranged from 15.11‰ to 20.97‰ (mean: $17.93 \pm 1.11\text{‰}$ standard deviation). Minimum, maximum, and mean values for climate variables are shown in Table A2. All data can be found in Table A3.

2.4.1 Δ_{leaf} vs MAT, maximum summer temperature, latitude, seasonality and MAP

There was no relationship between Δ_{leaf} values of *T. occidentalis* and MAT (Fig. A1A; $R^2 = 0.0152$, p-value = 0.19), nor between Δ_{leaf} of *T. occidentalis* and maximum summer temperature (Fig. A1B; $R^2 = 0.0051$, p-value = 0.51) in the temperature range listed in Table A2. No relationship was found between Δ_{leaf} and latitude (Fig. A1C; $R^2 = 0.0057$, p-value = 0.42). Additionally, no relationship was found using a multivariate linear regression approach to combine codependent variables: MAT and latitude ($R^2 = 0.002$, p-values = 0.92, 0.79 respectively). There was no relationship between Δ_{leaf} of *T. occidentalis* and MAP (Fig. 2.2; Fig. AD; $R^2 = 0.0138$, p-value = 0.21), nor was there a relationship between Δ_{leaf} of *T. occidentalis* and elevation (Fig. A4A; $R^2 = 0.0138$, p-value = 0.55).

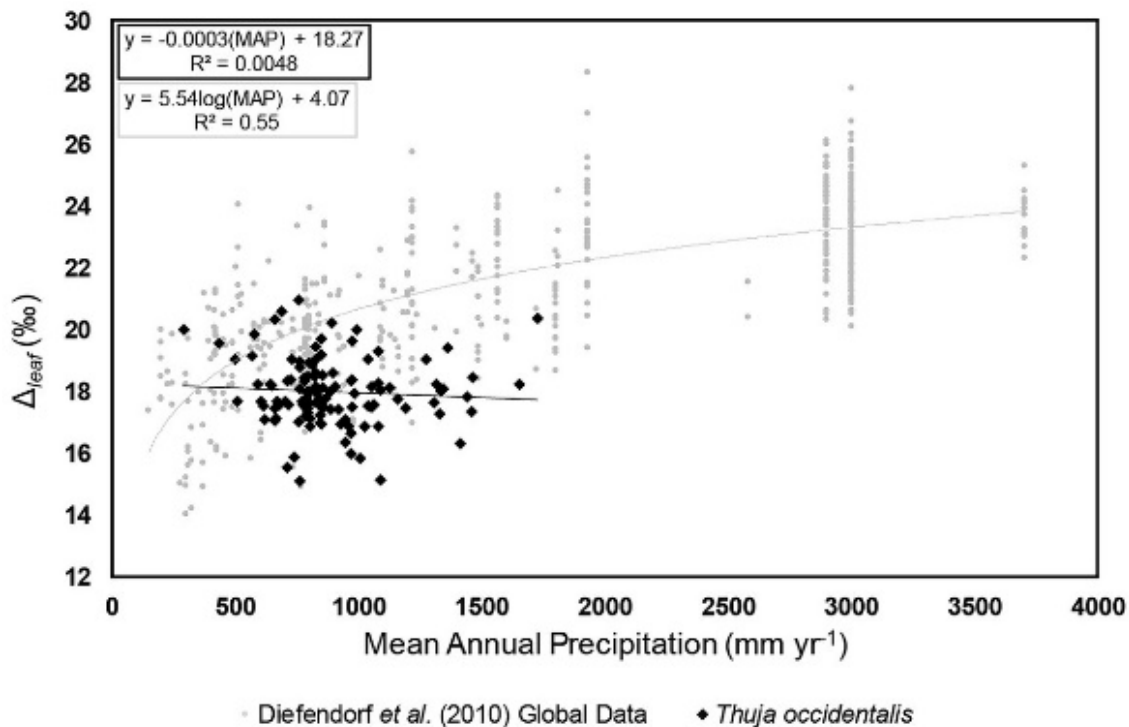


Figure 2.2 Δ_{leaf} vs. mean annual precipitation for *Thuja occidentalis* (black filled diamonds; $\Delta_{\text{leaf}} = -0.0003(\text{MAP}) + 18.75$, $R^2 < 0.01$). Data are compared with Diefendorf et al.'s (2010) global study (gray circles; $\Delta_{\text{leaf}} = 5.54(\log\text{MAP}) + 4.07$, $R^2 = 0.55$), showing C_3 specimens growing from 147 to 3,700 mm yr^{-1} . Error bars along the y-axis represent the $\pm 0.3\%$ replicate reproducibility of standards.

There was no relationship between Δ_{leaf} of *T. occidentalis* and month of collection. T-test results showed that the mean residual Δ_{leaf} values for each season were not significantly different (Spring: 0.19, Summer: -0.13 , Fall: -0.01 , Winter: -0.20 ; Fig. A5A; Month-by-month $R^2 = 0.0057$; Fig. A5B).

2.4.2 %C, %N and C:N ratios

Values of %C ranged from 30.56 weight % to 61.44 weight % ($\pm 7.90\%$), with a dataset average of 48.86 %C. %N values ranged from 0.55 weight % to 2.28 weight %, with a dataset average of 1.31% ($\pm 0.21\%$). C:N ratios ranged from 20.1:1 (due to high %N) to 86.2:1 with an average C:N value of 40.7:1 (± 7.9 C:N). There was no relationship between C:N ratios and time, $\delta^{13}\text{C}_{\text{leaf}}$, Δ_{leaf} , or $[\text{CO}_2]$ ($R^2 = 0.0227$, p-value = 0.25; $R^2 = 0.0297$, p-value = 0.68; $R^2 = 0.0157$, p-value = 0.94; and $R^2 = 0.0029$, p-value = 0.18, respectively; Fig. 2.3; Figs. A2A–A2C).

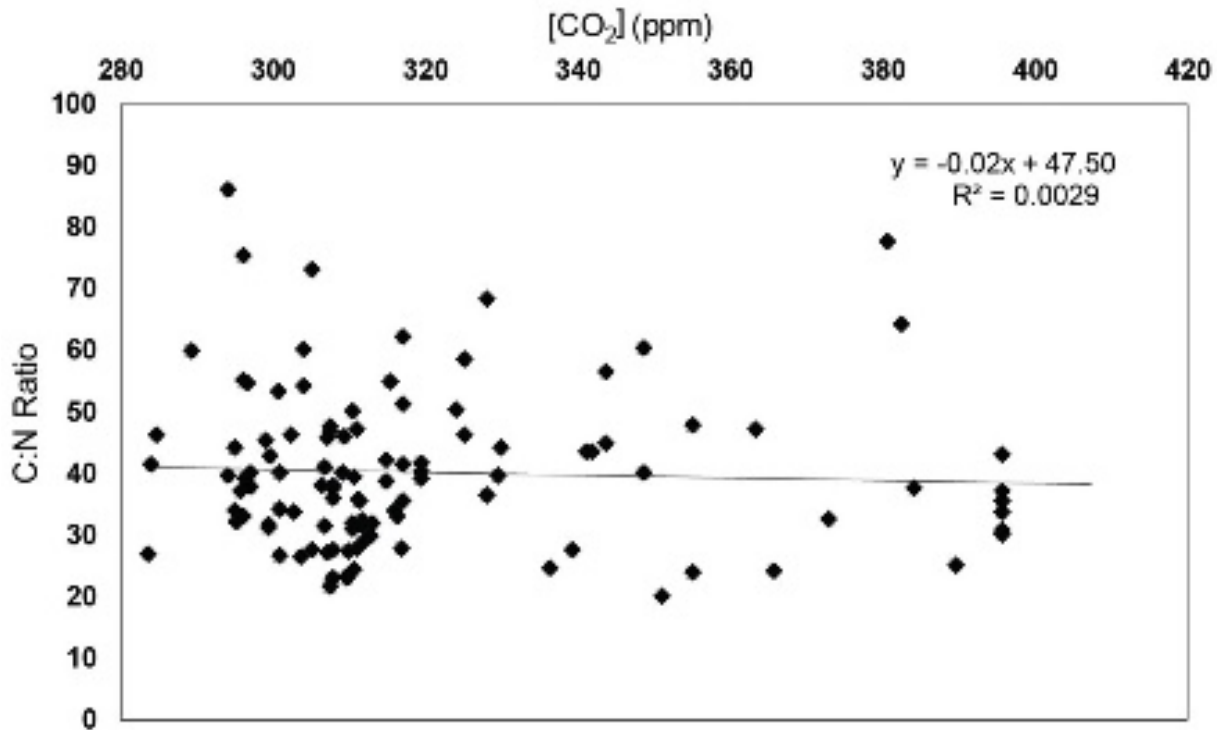


Figure 2.3 C:N ratios of specimens vs. $[\text{CO}_2]$ (ppm) from 280–410 ppm. Error bars are associated with the 0.9% replicate reproducibility of standards.

2.4.3 The atmosphere: $\delta^{13}\text{C}_{\text{leaf}}$ and Δ_{leaf} vs $[\text{CO}_2]$

There was a linear relationship between $\delta^{13}\text{C}_{\text{leaf}}$ and $[\text{CO}_2]$ (Fig. A3; $R^2 = 0.61$, p -value < 0.001), but there was no relationship between Δ_{leaf} and $[\text{CO}_2]$ (Fig. 2.4; Fig. A4; $R^2 = 0.0059$, p -value = 0.38). Because Δ_{leaf} stayed constant, with simultaneous changes in $\delta^{13}\text{C}_{\text{leaf}}$ and $\delta^{13}\text{C}_{\text{atm}}$, we can determine that changing $\delta^{13}\text{C}_{\text{leaf}}$ with increased CO_2 was an effect of the changing isotopic composition of atmospheric CO_2 ($\delta^{13}\text{C}_{\text{atm}}$) and was not related to $[\text{CO}_2]$.

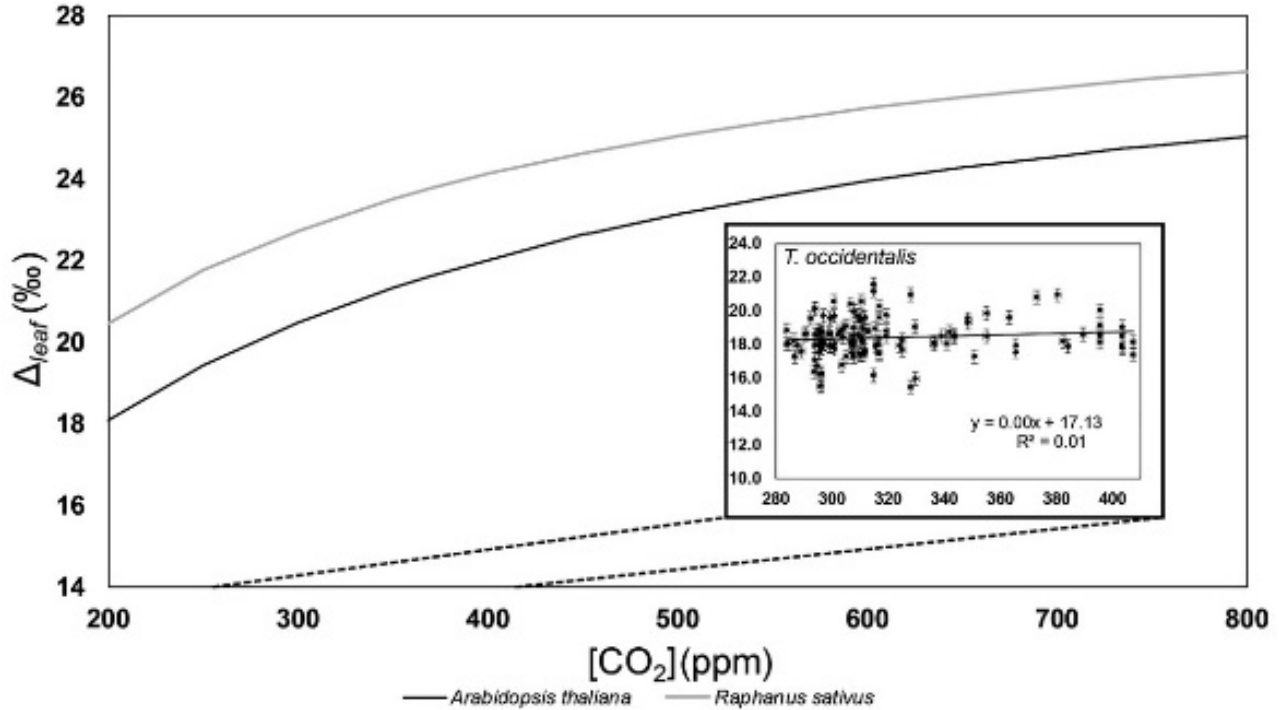


Figure 2.4. Δ_{leaf} vs. $[\text{CO}_2]$ for *Thuja* and dicots. Shown are *Thuja occidentalis* (black empty triangles; $\Delta_{\text{leaf}} = 0.0029([\text{CO}_2]) + 17.04$, $R^2 = 0.0085$) and Schubert & Jahren's (2012) growth chamber studies with replicates of *Raphanus sativus* and *Arabidopsis thaliana* (black and grey smooth lines). Schubert & Jahren's data shows C_3 specimens growing at 15 levels of $[\text{CO}_2]$ from 370 to 4,200 ppm.

2.4.4 $\delta^{13}\text{C}_{\text{atm}}$ and $\delta^{13}\text{C}_{\text{leaf}}$

There was a relationship between $\delta^{13}\text{C}_{\text{leaf}}$ and $\delta^{13}\text{C}_{\text{atm}}$ (Fig. 2.5; $R^2 = 0.74$, p -value < 0.001) as represented by Equation 2.2. The y-intercept (-16.52) represents the average offset between $\delta^{13}\text{C}_{\text{atm}}$ and $\delta^{13}\text{C}_{\text{leaf}}$, otherwise expressed as the fractionation value, Δ_{leaf} . The slope of 1.20 (with 95% confidence intervals between 1.07 and 1.32) further indicates relatively little impact of other environmental variables on leaf fractionation from atmospheric CO_2 . This relationship was compared to that as extrapolated from the regression found in Jahren, Arens & Harbenson (2008; Equation 2.3; Fig. 2.5) study using *Raphanus sativus* in growth chamber experiments.

$$\delta^{13}C_{leaf} = 1.20 (\pm 0.06) \times \delta^{13}C_{atm} - 16.52 (\pm 0.44) \quad (\text{Equation 2.2})$$

$$\delta^{13}C_{leaf} = 0.95 \times \delta^{13}C_{atm} - 25.4 \quad (\text{Equation 2.3})$$

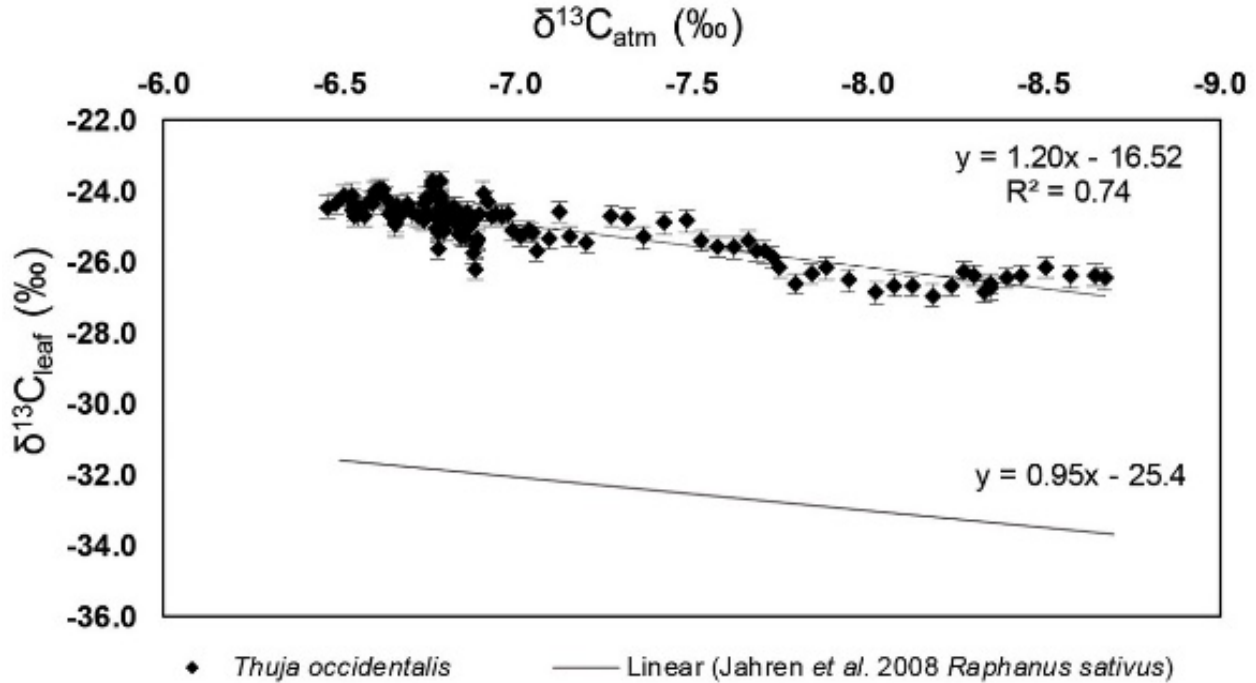


Figure 2.5 $\delta^{13}C_{atm}$ versus $\delta^{13}C_{leaf}$ values (‰) of *T. occidentalis*. This linear relationship is defined by $\delta^{13}C_{leaf} = 1.20 (\pm 0.06 \text{ standard error}) * (\delta^{13}C_{atm}) - 16.52 (\pm 0.44 \text{ standard error})$ with an R^2 value of 0.74 and a p-value < 0.001 . Error bars along the y-axis represent the $\pm 0.3\text{‰}$ replicate reproducibility of standards, error bars along the x-axis represent the $\pm 0.1\text{‰}$ replicate reproducibility associated with the isotope-ratio mass spectrometer at the Institute of Arctic and Alpine Research (INSTAAR) in Boulder, Colorado. Data points represent specimens collected for this study. The regression line below is derived from Jahren, Arens & Harbenson (2008), which used *Raphanus sativus* grown under elevated $[CO_2]$ within growth chambers to look at the relationship between $\delta^{13}C_{leaf}$ and $\delta^{13}C_{atm}$ values.

2.5 Discussion

2.5.1 Potentially complicating factors

Herbarium specimens are a useful way to look in high-resolution on this time scale, but were not necessarily consistently sampled between expeditions and years. Thus some factors such as maturity and height of tree, which have been shown to relate to carbon isotope discrimination (Brienen et al., 2017), are not specifically accounted for here. However, Brienen et al. (2017) found that height was not a significant factor in $\delta^{13}C_{leaf}$ values of the gymnosperm used (*P. sylvestris*), in contrast to broadleaf species (*Quercus robur*, *Fagus sylvatica*, *Cedrela odorata*) where there was an influence. Additionally, regional variations in $\delta^{13}C_{atm}$ resulting from proximity to respiring soil could provide a different baseline $\delta^{13}C_{atm}$ value than the global one

used based upon Mauna Loa Observatory's gas samples (Wehr & Saleska, 2015). While we were unable to control exactly where on the tree each sample was taken from nor the ecosystem-specific parameters that might influence $\delta^{13}\text{C}_{\text{atm}}$, each herbarium record includes notes on the sampling location, often including approximate maturity of the tree and height sampled from. Additionally, as expeditions are done without heavy machinery, it is likely that our specimens were sampled from approximately the height of a human, which is well out of the range of isotopic influence from soil respired CO_2 (Bazzaz & Williams, 1991). Finally, differences in $\delta^{13}\text{C}_{\text{leaf}}$ values differ depending on where on the leaf isotopes are sampled from (Gao et al., 2015). We controlled for this effect by homogenizing several entire leaves per sample and running duplicate isotope analyses, which all came within machine error (0.3‰) of one another.

Complex nitrogen dynamics, as well as those of other macro- and micro-nutrients, may play a role in vital effects that relate ultimately to carbon assimilation and/or carbon isotope fractionation, but these changes are very difficult and complicated to reconstruct in the geologic record and thus were not investigated in this study (Godfrey & Glass, 2011). It is not possible to understand shifts in regional nitrogen availability fully even within the historical record: without soil cores collected and preserved from the same sites and times of leaf collection, it is not straightforward to consider anything other than nitrogen content. Given that no one collected soils at each historical site, we cannot address changes in nitrogen dynamics quantitatively. Furthermore, for geologic applications fossil leaves and corresponding paleosols (fossil soils) are not typically preserved together. In order to account for the potential range in nitrogen dynamics, we focus here on using many specimens from across a wide landscape of different land-uses and thus a wide range of potential nitrogen dynamics, but under known $[\text{CO}_2]$ conditions. To account for historical and geological limitations of reconstructing the nitrogen cycle, this study focuses instead on the relationship between systemic changes in C:N ratios in relation to $\delta^{13}\text{C}_{\text{leaf}}$, $\delta^{13}\text{C}_{\text{atm}}$, or as indication of changes in carbon dynamics.

2.5.2 Δ_{leaf} , temperature, latitude and seasonality

There were a number of climate variables that we did not expect to have a correlative relationship with Δ_{leaf} , but we addressed to ensure that they were not confounding variables (MAT, maximum summer temperature, latitude, seasonality). Due to the consistent internal temperature and lack of relationship between Δ_{leaf} to MAT in previous studies, we expected no

relationship between Δ_{leaf} and MAT nor maximum summer temperature. As we expected, MAT showed no significant relationship with Δ_{leaf} values neither in meta-analyses, growth chamber experiments (Diefendorf et al., 2010; Schubert & Jahren, 2012) nor this study (Fig. A1A).

Because MAT and latitude are inherently related, we expected Δ_{leaf} values to relate to latitude in the same way as when compared to MAT. As predicted, there was no relationship between Δ_{leaf} of *T. occidentalis* and latitude. In order to ensure that these two codependent variables were treated as such, we ran a multiple linear regression, which gave a similarly low coefficient of determination ($R^2 = 0.002$) comparing actual Δ_{leaf} values with Δ_{leaf} values predicted using this regression. Thus, we are confident that both treated as independent and co-dependent variables, MAT and latitude do not play a role in variance of Δ_{leaf} values.

Additionally, we took into account variation in time of year specimen was collected and found no significant relationship between season and Δ_{leaf} (Figs. A5A and A5B). This is likely because *T. occidentalis* is not deciduous and does not shed its leaves annually, thus, once homogenized, the isotopic composition of the leaf is representative of average discrimination during the leaf's exposure.

2.5.3 Δ_{leaf} and CO₂

In this study we found no relationship between Δ_{leaf} and [CO₂] from 280 to 410 ppm (Fig. 2.4; Fig. A4). It is possible that the relationship observed by Schubert & Jahren (2012) exists only for idealized controlled growth chamber conditions and not in natural environments (Lomax et al., 2019). Alternatively, gymnosperms may respond more slowly than angiosperms to increases in [CO₂] due to their longer average lifespans and lack of senescence (Brodribb, Pittermann & Coomes, 2012). The changes in carbon assimilation as represented by increased carbon fractionation under short-term, ideal growth chamber conditions cannot be used to predict biological response to rapid changes in [CO₂]. In other words, plants, especially slow-growing woody plants, may not successfully adapt to anthropogenic changes of the present and future (Jump & Peñuelas, 2005).

2.5.4 Δ_{leaf} and mean annual precipitation

When Δ_{leaf} values of *T. occidentalis* were compared with MAP, Diefendorf et al.'s (2010) previously established relationship did not hold (Fig. 2.2), especially in low precipitation regimes

(<1,000 mm yr⁻¹) where the change in Diefendorf et al.'s Δ_{leaf} values was most sensitive to changes in MAP. One explanation for the lack of relationship between Δ_{leaf} of *T. occidentalis* and MAP is that this relationship breaks down on the single-species, or even plant functional type, level. In the aforementioned meta-analyses, plant functional type, species, and region were not controlled. Δ_{leaf} values may be inherent to specific biomes but may not be representative of a general trend of any given plant or plant type to MAP. It is possible that the relationships seen in the meta-analyses by Diefendorf et al. (2010) and Kohn (2010) instead represent an array of taxon-specific constant isotopic values that collectively show a meta-relationship. This experiment could be further explored by performing the same experiment in natural settings across different biomes and different plant functional types. Assuming that Δ_{leaf} values are indicative of water use (Givnish, 1979; Farquhar, Ehleringer & Hubick, 1989), this lack of relationship may also mean that plants with specific water use efficiencies and representative Δ_{leaf} values are generally located in areas where they are not living in conditions that are stressed for water given their evolutionary adaptations. Geologically, this could mean that the presence of a particular taxon in fossil localities could provide a quantitative estimate for range of MAP, which could allow more specificity of paleoclimate regimes based on macrofossils (Nearest Living Relative and/Coexistence Approach; Mosbrugger & Utescher, 1997; Mosbrugger, 2009). In terms of future climate, this is indication that the chemistry of C₃ plants may not respond to regional changes as previously thought. This is of particular concern because the velocity of climate change, especially for continued high emission rate scenarios, is substantially faster than trees will be able to adapt to (Loarie et al., 2009; Diffenbaugh & Field, 2013).

It is also possible that the predicted relationship between Δ_{leaf} and MAP is present for plants that are more responsive to their environment and/or have less extensive roots (to access deeper water sources), and thus the signal seen by Diefendorf et al. (2010) is a result of incorporating sensitive plants. Indeed, other studies using rapidly growing, highly sensitive herbaceous angiosperms have found a relationship between water treatment and carbon isotope discrimination (Lomax et al., 2019). However, the fossil record is biased toward preserving less sensitive, often woody plants due to preservation potential as well as presence within the fossil record (Looy et al., 2014); therefore, the utility of relationships based on highly sensitive plants may be muted in the fossil record.

Another explanation is that MAP is not an appropriate metric for measuring plant-available water, and while Δ_{leaf} is still a measure of water use efficiency and this value is dynamic over conditions, snowmelt volumes and/or soil water—as driven by soil porosity and other factors—are better indicators of plant-available water. Further investigations using these variables will better constrain which water-related variables affect Δ_{leaf} values of leaf tissues. The weak R^2 value between Δ_{leaf} of *T. occidentalis* and MAP (0.0138) means that Δ_{leaf} of *T. occidentalis* cannot be used to reconstruct paleo-MAP using the relationship determined by Diefendorf et al. (2010). Additional single-species experiments, particularly within angiosperms, should be conducted to look for correlations between Δ_{leaf} and MAP to test whether the lack of relationship is due to a difference inherent to gymnosperms.

2.5.5 Carbon biomass (%C) and elemental leaf chemistry (%N, C:N ratios) as related to climate variables

In addition to the response of $\delta^{13}\text{C}_{\text{leaf}}$ values to climate variables, %C alone has been shown to respond directly to elevated $[\text{CO}_2]$. Ci/Ca ratios (the ratio of internal $[\text{CO}_2]$ to atmospheric $[\text{CO}_2]$) of old growth *T. occidentalis* trees along Lac Duparquet, Quebec, increased under anthropogenic CO_2 fertilization, indicating tree response to enhanced CO_2 (Giguère-Croteau et al., 2019). This increase in tree productivity was demonstrated in the results of free-air concentration enrichment (FACE) experiments as well; in northern USA mid-latitude forests with loblolly pines (*P. taeda*), FACE experiment results indicated that elevated CO_2 induced increased carbon assimilation, resulting in increased carbon biomass, in woody tissues and increased %C of foliar storage as compared to trees grown under ambient CO_2 (Oren et al., 2001; Ainsworth & Long, 2005; Talhelm et al., 2013). Preliminary work in herbarium leaves found that increased $[\text{CO}_2]$ related to Industrialization resulted in an increase in foliar %C with no change in %N (as source of N remains constant), and thus increased C:N ratios in some species (Merveille, 2015). In order to contextualize changes in $\delta^{13}\text{C}_{\text{leaf}}$, this study examined coeval trends in leaf chemistry through elemental analysis of C and N (using N as a comparison point to see whether %C changes significantly with time).

These FACE experiments also showed that when run over longer time scales, trees reached a point of CO_2 acclimation and stopped increased carbon assimilation under enhanced CO_2 ; thus, predicted shifts in tree C-uptake may be short-lived, a pattern that will be inevitably

discernable in a long-term study incorporating pre-Industrial leaf tissues through the present (Nowak, Ellsworth & Smith, 2004). Based on FACE experiments, we expected %C to have increased in leaves sampled from the early 1800s to the present, though we might see the rate of increase slow with time. However, we saw no relationship between %C, nor C:N ratios and time nor increase in [CO₂].

In fact, *T. occidentalis* specimens collected between 1804 and 2017 did not show changes in assimilation rates due to elevated CO₂. C:N values of *T. occidentalis* showed no response to changes over time (with increased [CO₂]) or with atmospheric isotopic value (Figs. A2A and A2B). Though other organs in previous experiments responded to [CO₂], leaves, which are instrumental in the photosynthetic process as they are the organs directly in-taking atmospheric CO₂, do not. A better understanding of all plant organ behavior is imperative to defining and quantifying potential carbon sinks or plant chemistry responses to global change (Goodale et al., 2002).

2.5.6 $\delta^{13}\text{C}_{\text{leaf}}$ and $\delta^{13}\text{C}_{\text{atm}}$

Strong relationships have been found between above ground tissue and $\delta^{13}\text{C}_{\text{atm}}$ values ($p < 0.001$; Jahren, Arens & Harbenson, 2008; Fig. 2.5), and this study provides a higher resolution look at the relationship between $\delta^{13}\text{C}_{\text{leaf}}$ and $\delta^{13}\text{C}_{\text{atm}}$ in a long-lived species within a natural system. In this initial natural experiment, the $\delta^{13}\text{C}_{\text{leaf}}$ of *T. occidentalis* tracked changes in $\delta^{13}\text{C}_{\text{atm}}$ ($R^2 = 0.74$, $p\text{-value} < 0.0001$), mostly unencumbered by other climate factors. The slope for the linear relationship between $\delta^{13}\text{C}_{\text{leaf}}$ and $\delta^{13}\text{C}_{\text{atm}}$ is close to, but not exactly, 1, likely because the rate of change for $\delta^{13}\text{C}_{\text{atm}}$ has not been linear, and acceleration in the change of $\delta^{13}\text{C}_{\text{atm}}$ may not have been recorded immediately. Additionally, while there is no statistically significant relationship between any of the climate variables we tested and Δ_{leaf} , it is unlikely that climate variables, especially in aggregate, play no role in carbon isotope discrimination within this species. Because $\delta^{13}\text{C}_{\text{leaf}}$ showed a strong coefficient of determination with $\delta^{13}\text{C}_{\text{atm}}$, and no climate variables showed significant relationships with Δ_{leaf} values, we can assume that $\delta^{13}\text{C}_{\text{leaf}}$ values of modern *T. occidentalis* are strongly affected by $\delta^{13}\text{C}_{\text{atm}}$ values. Additional work must be done to evaluate error in paleo uses of $\delta^{13}\text{C}_{\text{leaf}}$ values of *T. occidentalis*, and future experiments should recreate more geologically reasonable conditions and climate changes (independent of anthropogenic factors). The relationship between $\delta^{13}\text{C}_{\text{leaf}}$ and $\delta^{13}\text{C}_{\text{atm}}$ values has

implications for paleoclimate reconstructions of $\delta^{13}\text{C}_{\text{atm}}$ as well as reconstructions of $[\text{CO}_2]$ (Cerling et al., 1991; Franks et al., 2014). We emphasize how important it is to identify the value of $\delta^{13}\text{C}_{\text{atm}}$, such as in Tipple, Meyers & Pagani (2010) study, rather than just using the Pre-Industrial value of -6.5‰ (Cerling et al., 1991) because the $\delta^{13}\text{C}_{\text{atm}}$ value has such a dramatic effect on the terrestrial part of the carbon cycle.

2.6 Conclusions

Though $\delta^{13}\text{C}_{\text{leaf}}$ and Δ_{leaf} values have been proposed as a proxy for $[\text{CO}_2]$ and MAP based on previous research, this natural-world, species-controlled study shows no indication of such relationships. Thus, the use of Δ_{leaf} values to reconstruct MAP and $[\text{CO}_2]$ in the fossil record without taxonomic identification should be reconsidered. The relationship between $\delta^{13}\text{C}_{\text{leaf}}$ and $\delta^{13}\text{C}_{\text{atm}}$ values is more informative, and may provide a new proxy ($\delta^{13}\text{C}_{\text{leaf}}$ values of *Thuja*) for reconstructing paleo- $\delta^{13}\text{C}_{\text{atm}}$ or may indicate a lag in plant adaptation to unprecedentedly rapid climate change. *Thuja* extends up to 100 million years back to the Late Cretaceous, which makes this relationship potentially useful throughout the Cenozoic and into the Mesozoic era (Berry, 1915).

While this study focuses on one single species, further work is needed to assess other taxa at the species, genus, and family levels to examine whether the relationship between $\delta^{13}\text{C}_{\text{atm}}$ and $\delta^{13}\text{C}_{\text{leaf}}$ is consistent, and furthermore, generalizable. $\delta^{13}\text{C}_{\text{leaf}}$ values of individual fossil leaves (in particular of *Thuja* leaves) cannot be used to reconstruct paleo-MAP as proposed by Kohn (2010), but average $\delta^{13}\text{C}_{\text{leaf}}$ values of sites, as recorded in bulk soil organic matter, may allow us to predict precipitation ranges. Aboveground $\delta^{13}\text{C}_{\text{leaf}}$ is thought to translate directly into the isotopic value of soil carbon ($\delta^{13}\text{C}_{\text{org}}$; Arens, Jahren & Amundson, 2000). Bulk soil organic matter ($\delta^{13}\text{C}_{\text{org}}$) is the combination of $\delta^{13}\text{C}$ of all decaying material from the ecosystem, with leaves especially abundant due to sheer volume. The average $\delta^{13}\text{C}_{\text{leaf}}$ value of all trees found in a certain region will be found in the soil; therefore, soil $\delta^{13}\text{C}_{\text{org}}$ values could be more reflective of particular precipitation at time of deposition than $\delta^{13}\text{C}_{\text{leaf}}$ values. Further studies could evaluate the reliability of $\delta^{13}\text{C}_{\text{org}}$ as a tool for MAP prediction and reconstruction.

This study implies constant carbon and nitrogen use and isotope fractionation relative to $\delta^{13}\text{C}_{\text{atm}}$ by *T. occidentalis*. Due to the unprecedentedly rapid changes $\delta^{13}\text{C}_{\text{atm}}$ and $[\text{CO}_2]$ throughout Industrialization, this lack of change in carbon assimilation patterns, despite previous

studies using modern $\delta^{13}\text{C}_{\text{leaf}}$ values to reconstruct $[\text{CO}_2]$, may indicate that modern systems are not appropriate analogues for many periods of the geologic record during which climate evolved more slowly. Modern climate change may be too rapid for plants to adapt, though more research should be done to evaluate whether this response is replicable in other species, genera, and plant functional types. It is possible that the pace of anthropogenic climate change makes modern relationships inappropriate analogues for paleoclimate.

2.7 Acknowledgments

We thank Drs. A. Reznicek and R. Rabeler and the University of Michigan Herbarium (MICH), Drs. M. Donoghue and P. Sweeney and the Yale Peabody Museum (Y), Dr. T. Lumbsch and C. Niezgodka and the Chicago Field Museum (F), M. J. Bian and the Shanghai Botanical Garden (SG), and Dr. A. Fryday and the Michigan State Herbarium (MSC). We would additionally like to thank S. Fernandes at the University of Michigan's School for Environment and Sustainability (UM-SEAS), and R. Dzombak, A. Hamersma and M. Ng in the Department of Earth and Environmental Sciences at the University of Michigan (UM EES) for the assistance obtaining historical and present-day collections.

2.8 References

- Ainsworth E. A. & Long S. P. (2005). What we have learned from 15 years of free-air CO_2 enrichment (FACE)? A meta-analytic review of the responses of photosynthesis, canopy properties, and plant production to rising CO_2 . *New Phytologist* 165(2):351-371
- Ainsworth E. A., & Rogers A. (2007). The response of photosynthesis and stomatal conductance to rising $[\text{CO}_2]$: mechanisms and environmental interactions, *Plant, Cell & Environment* 30(3), 258-270
- Araus J. L., & Buxó R. (1993). Changes in carbon isotope discrimination in grain cereals from the north-western Mediterranean Basin during the past seven millennia. *Functional Plant Biology* 20(1), 117-128
- Arens N. C., Jahren A. H., & Amundson R. (2000). Can C_3 plants faithfully record the carbon isotopic composition of atmospheric carbon dioxide? *Paleobiology* 26(1), 137-164
- Augustin L., Barbante C., Barnes P. R., Barnola J. M., Castellano E., & Dreyfus G. (2004). Eight glacial cycles from an Antarctic ice core. *Nature* 429(6992), 623-628

- Barnola J. M., Raynaud D., Korotkevich Y. S., & Lorius C. (1987). Vostok ice core provides 160,000-year record of atmospheric CO₂. *Nature* 329(6138), 408-414
- Bazzaz F. A., & Williams W. E. (1991). Atmospheric CO₂ concentrations within a mixed forest: implications for seedling growth. *Ecology* 72(1):12-16
- Beerling D. J., Matthey D. P., & Chaloner W. G. (1993). Shifts in the $\delta^{13}\text{C}$ composition of *Salix herbacea* L. leaves in response to spatial and temporal gradients of atmospheric CO₂ concentration. *Proceedings of the Royal Society of London. Series B: Biological Sciences* 253(1336), 53-60
- Beerling D. J., & Royer D. L. (2002). Fossil plants as indicators of the Phanerozoic global carbon cycle. *Annual Review of Earth and Planetary Sciences* 30(1), 527-556
- Berry E. W. (1915). The age of the Cretaceous flora of southern New York and New England. *Journal of Geology* 23(7), 608-618
- Boutton T. W. (1991). Stable carbon isotope ratios of natural materials: II. Atmospheric, terrestrial, marine, and freshwater environments. *Carbon Isotope Techniques 1*, 173-185
- Brienen R. J. W., Gloor E., Clerici S., Newton R., Arppe L., Boom A., Bottrell S., Callaghan M., Heaton T., Helama S., Helle, G., Leng, M. J., Mielikainen, K., Oinonen, M., Timonen, M. (2017). Tree height strongly affects estimates of water-use efficiency responses to climate and CO₂ using isotopes. *Nature Communications* 8(299), 1-10
- Brodribb T. J., Pittermann J., Coomes D. A. (2012). Elegance versus speed: examining the competition between conifer and angiosperm trees. *International Journal of Plant Sciences* 173(6), 673-694
- Cerling T. E. (1992). Use of carbon isotopes in paleosols as an indicator of the p(CO₂) of the paleo atmosphere. *Global Biogeochemical Cycles*, 6(3), 307-314
- Cerling T. E., Solomen D. K., Quade J., Bowman J. R. (1991). On the isotopic composition of carbon in soil carbon dioxide. *Geochimica et Cosmochimica Acta* 55(11), 3403-3405
- Cotton J. M., Sheldon N. D., Strömberg C. A. E. (2012). High-resolution isotopic record of C₄ photosynthesis in a Miocene grassland. *Palaeogeography, Palaeoclimatology, Palaeoecology* 337–338, 88-98
- Deines P. (1992). Mantle carbon: concentration, mode of occurrence, and isotopic composition. In: Schidlowski M., Golubic S., Kimberley M. M., McKirdy D. M., Trudinger P. A., eds. *Early Organic Evolution: Implications for Mineral and Energy Resources*. Berlin, Heidelberg: Springer.
- Diefendorf A. F., Leslie A. B., Wing S. L. (2015). Leaf wax composition and carbon isotopes vary among major conifer groups. *Geochimica et Cosmochimica Acta* 170, 145-156

- Diefendorf A. F., Mueller K. E., Wing S. L., Koch P. L., Freeman K. H. (2010). Global patterns in leaf ^{13}C discrimination and implications for studies of past and future climate. *Proceedings of the National Academy of Sciences* 107(13), 5738-5743
- Diffenbaugh N. S., & Field C. B. (2013). Changes in ecologically critical terrestrial climate conditions. *Science*, 341(6145), 486-492
- Eckenwalder J. E. (2009). Conifers of the world: the complete reference. China: Timber Press.
- Ehleringer J. R., Phillips S. L., Comstock J. P. (1992). Seasonal variation in the carbon isotopic composition of desert plants. *Functional Ecology* 6(4), 396-404
- Elsig J., Schmitt J., Leuenberger D., Schneider R., Eyer M., Leuenberger M., Stocker T. F. (2009). Stable isotope constraints on Holocene carbon cycle changes from an Antarctic ice core. *Nature* 461(7263), 507-510
- Farquhar G. D., Ehleringer J. R., Hubick K. T. (1989). Carbon isotope discrimination and photosynthesis. *Annual Review of Plant Biology and Plant Molecular Biology* 40(1), 503-537.
- Farquhar G. D., Sharkey T. D. (1982). Stomatal conductance and photosynthesis. *Annual Review of Plant Physiology* 33(1), 317-345
- Feng X. (1999). Trends in intrinsic water-use efficiency of natural trees for the past 100–200 years: a response to atmospheric CO_2 concentration. *Geochimica et Cosmochimica Acta* 63(13–14), 1891-1903
- Fick S. E., Hijmans R. J. (2017). WorldClim 2: new 1-km spatial resolution climate surfaces for global land areas. *International Journal of Climatology* 37(12), 4302-4315
- Franks P. J., Royer D. L., Beerling D. J., Van de Water P. K., Cantrill D. J., Barbour M. M., Berry J. A. (2014). New constraints on atmospheric CO_2 concentration for the Phanerozoic. *Geophysical Research Letters* 41(13), 4685-4694
- Gao L., Guimond J., Thomas E., Huang Y. (2015). Major trends in leaf wax abundance, $\delta^2\text{H}$ and $\delta^{13}\text{C}$ values along leaf venation in five species of C_3 plants: physiological and geochemical implications. *Organic Geochemistry* 78,144-152
- Giguère-Croteau C., Boucher E., Bergeron Y., Girardin M. P., Drobyshch I., Silva L. C. R., Helie J. F., Garneau M. (2019). North America's oldest boreal trees are more efficient water users due to increased $[\text{CO}_2]$, but do not grow faster. *Proceedings of the National Academy of Sciences* 116(7), 2749-2754
- Givnish T. (1979). On the adaptive significance of leaf form. In: Solbrig OT, Jain S, Johnson GB, Raven PH, eds. Topics in Plant Population Biology. London: Palgrave. 375-407
- Givnish T. (2002). Adaptive significance of evergreen vs. deciduous leaves: solving the triple paradox. *Silva Fennica* 36(3):703-743

- Godfrey L. V., Glass J. B. (2011). The geochemical record of the ancient nitrogen cycle, nitrogen isotopes, and metal cofactors. *Methods in Enzymology* 486, 483-506
- Goodale C. L., Apps M. J., Birsey R. A., Field C. B., Heath L. S., Houghton R. A., Jenkins J. C., Kohlmaier G. H., Kurz W., Liu S., Nabuurs, G.-J., Nilsson, S., Shvidenko, A. Z. (2002). Forest carbon sinks in the northern hemisphere. *Ecological Applications* 12(3), 891-899
2018. 1981–2010 Climate Normals & Averages. Retrieved from Canadian Climate Normals website (accessed 15 February 2018)
- Gröcke D. R. (2002). The carbon isotope composition of ancient CO₂ based on higher-plant organic matter. *Philosophical Transactions of the Royal Society of London. Series A: Mathematical, Physical and Engineering Sciences* 360(1793), 633-658
- Helliker B. H., & Richter S. L. (2008). Subtropical to boreal convergence of tree-leaf temperatures. *Nature* 454(7203), 511-514.
- IPCC. 2014. Intergovernmental panel on climate change guidelines. IPCC Fifth Assessment Report
- Jahren A. H., Arens N. C., Harbenson S. A. (2008). Prediction of atmospheric $\delta^{13}\text{C}\text{O}_2$ using fossil plant tissues. *Reviews of Geophysics* 46(1),1-12
- Jump A. S., Peñuelas J. (2005). Running to stand still: adaptation and the response of plants to rapid climate change. *Ecology Letters* 8(9), 1010-1020.
- Keeling C. D. (1979). The Suess effect: ¹³Carbon-¹⁴Carbon interrelations. *Environment International* 2(4–6), 229-300
- Keeling C. D., Piper S. C., Bascatow R. B., Wahlen M., Whorf T. P., Heimann M., Meijer H. A. (2005). Exchanges of atmospheric CO₂ and ¹³CO₂ with the terrestrial biosphere and oceans from 1978-2000: observations and carbon cycle implications. In: Ehleringer J. R., Cerling T., Dearing M. D., eds. *A History of Atmospheric CO₂ and its Effects on Plants, Animals, and Ecosystems*. New York: Springer. 177:83-113
- Keeling C. D., & Whorf T. P. (2004). Atmospheric CO₂ from continuous air samples at Mauna Loa observatory. Hawaii: Carbon Dioxide Information Analysis Center, Oak Ridge National Laboratory.
- Kohn M. J. (2010). Carbon isotope compositions of terrestrial C₃ plants as indicators of (paleo) ecology and (paleo) climate. *Proceedings of the National Academy of Sciences* 107(46), 19691-19695
- Korner C., Farquhar G. D., Wong S.C. (1991). Carbon isotope discrimination by plants follows latitudinal and altitudinal trends. *Oecologia* 88(1), 30-40

- LePage B. A. (2003). A new species of *Thuja* (Cupressaceae) from the Late Cretaceous of Alaska: implications of being evergreen in a polar environment. *American Journal of Botany* 90(2), 167-174
- Loarie S. R., Duffy P. B., Hamilton H., Asner G. P., Field C. B., Ackerly D. D. (2009). The velocity of climate change. *Nature* 462, 1052-1055
- Lomax B. H., Lake J. A., Leng M. J., Jardine P. E. (2019). An experimental evaluation of the use of $\Delta^{13}\text{C}$ as a proxy for palaeoatmospheric CO_2 . *Geochimica et Cosmochimica Acta* 247, 162-174
- Looy C., Kerp H., Duijnste I., DiMichele B. (2014). The late Paleozoic ecological-evolutionary laboratory, a land-plant fossil record perspective. *Sedimentary Record* 12(4), 4-18
- Lowdon J., & Dyck W. (1974). Seasonal variations in the isotope ratios of carbon in maple leaves and other plants. *Canadian Journal of Earth Sciences* 11(1), 79-88
- Mårtensson L. M., Carlsson G., Prade T., Kørup K., Lærke P. E., Jensen E. S. (2017). Water use efficiency and shoot biomass production under water limitation is negatively correlated to the discrimination against ^{13}C in the C_3 grasses *Dactylis glomerata*, *Festuca arundinacea* and *Phalaris arundinacea*. *Plant Physiology and Biochemistry* 113, 1-5
- Medlyn B. E., Barton C. V. M., Broadmeadow M. S. J., Ceulemans, R., De Angelis, P., Forstreuter, M., Freeman, M., Jackson, S. B., Kellomaki, S., Laitat, E., Rey A., Roberntz P., Sigurdsson B. D., Strassemeier J., Wang K., Curtis P. S., Jarvis P. G. (2001). Stomatal conductance of European forest species after long-term exposure to elevated $[\text{CO}_2]$: a synthesis of experimental data. *New Phytologist* 149, 247-264
- Merven C. (2015). *Isotope ecology of temperate conifers*. (Master's Thesis University of Michigan, Ann Arbor, MI, United States of America).
- Mirza M. M. Q. (2003). Climate change and extreme weather events: can developing countries adapt? *Climate Policy* 3(3), 233-248
- Mosbrugger V. (2009). Nearest-living-relative method. In: Gornitz V., ed. *Encyclopedia of Paleoclimatology and Ancient Environments*. Dordrecht: Springer. 607-609
- Mosbrugger V., Utescher T. (1997). The coexistence approach—a method for quantitative reconstructions of Tertiary terrestrial palaeoclimate data using plant fossils. *Palaeogeography, Palaeoclimatology, Palaeoecology* 134(1-4), 61-86.
- Nowak R. S., Ellsworth D. S., Smith S. D. (2004). Functional responses of plants to elevated atmospheric CO_2 - do photosynthetic and productivity data from FACE experiments support early predictions? *New Phytologist* 162(2), 253-280.
- O'Leary M. H. (1993). Biochemical basis of carbon isotope fractionation. *Stable Isotopes and Plant Carbon-Water Relations* 1993, 19-28.

- Oren R., Ellsworth D. S., Johnsen K. H., Phillips N., Ewers B. E., Maier C., Schafer K. R., McCarthy H., Hendrey G., McNulty S. G., Katul, G. G. (2001). Soil fertility limits carbon sequestration by forest ecosystems in a CO₂-enriched atmosphere. *Nature* 411(6836), 469-472.
- Original S code by Richard A. Becker, Allan R. Wilks. R version by Ray Brownrigg.
Enhancements by Thomas P Minka and Alex Deckmyn. 2018. Maps: draw geographical maps. R package Version 3.3.0 software
- Pease V. A. (1917). Duration of leaves in evergreens. *American Journal of Botany* 4(3), 145-160
- Pedicino L. C., Leavitt S. W., Betancourt J. L., Van de Water P. K. (2002). Historical variations in $\delta^{13}\text{C}_{\text{leaf}}$ of herbarium specimens in the southwestern U. S. *Western North American Naturalist* 62(3), 348-359
- Peñuelas J., & Azcón-Bieto J. (1992). Changes in leaf $\Delta^{13}\text{C}$ of herbarium plant species during the last 3 centuries of CO₂ increase. *Plant, Cell & Environment* 15(4), 485-489
- Petit J. R., Jouzel J., Raynaud D., Barkov N. I., Barnola J. M., Basile I., Bender M., Chappellaz J, Davis M., Delaygue G., Delmotte, M., Kotlyakov, V. M., Legrand, M., Lipenkov, V. Y., Lorius, C., Pepin, L., Ritz, C., Saltzman, E., Stievenard, M. (1999). Climate and Atmospheric History of the Past 420,000 years from the Vostok Ice Core, Antarctica. *Nature* 399, 429-436
- PRISM Climate Group. 2004. Oregon State University. created 4 February 2004
- R Core Team. 2014. R: a language and environment for statistical computing. Vienna: R Foundation for Statistical Computing.
- Retallack G. J. (2001). A 300-million-year record of atmospheric carbon dioxide from fossil plant cuticles. *Nature* 411(6835), 287-290
- Roth-Nebelsick A., Oehm C., Grein M., Utescher T., Kunzmann L., Friedrich J. P., Konrad W. (2014). Stomatal density and index data of *Platanus neptuni* leaf fossils and their evaluation as a CO₂ proxy for the Oligocene. *Review of Palaeobotany and Palynology* 206, 1-9
- Rubino M., Etheridge D. M., Trudinger C. M., Allison C. E., Battle M. O., Langenfelds R. L., Jenk T. M. (2013). A revised 1000 year atmospheric $\delta^{13}\text{C}$ -CO₂ record from Law Dome and South Pole, Antarctica. *Journal of Geophysical Research: Atmospheres* 118(15), 8482-8499
- Schmitt J., Schneider R., Elsig J., Leuenberger D., Laurantou A., Chappellaz J., Köhler P., Joos F., Stocker T. F., Leuenberger M., Fischer H. (2012). Carbon isotope constraints on the deglacial CO₂ rise from ice cores. *Science* 336(711), 711-713
- Schubert B. A., & Jahren A. H. (2012). The effects of atmospheric CO₂ concentration on carbon isotope fractionation in C₃ land plants. *Geochimica et Cosmochimica Acta* 96, 29-43

- Schubert B. A., & Jahren A. H. (2018). Incorporating the effects of photorespiration into terrestrial paleoclimate reconstruction. *Earth-Science Reviews* 177,637-642
- Talhelm A. F., Pregitzer K., Kubiske M., Zak D., Company C., Burton A. (2013). Elevated CO₂ and O₃ alter productivity and carbon storage in Northern Temperate Forests: results from Aspen FACE. *AGUFM, 2013*, B21A-0461.
- Tieszen L. L. (1991). Natural variations in the carbon isotope values of plants: implications for archaeology, ecology, and paleoecology. *Journal of Archaeological Science* 18(3), 227-248
- Tipple B. J., Meyers S. R., Pagani M. (2010). Carbon isotope ratio of Cenozoic CO₂: a comparative evaluation of available geochemical proxies. *Paleoceanography* 25(3).
- Tognetti R., Minnocci A., Penuelas J., Rachi A., Jones M. B. (2000). Comparative field water relations of three Mediterranean shrub species co-occurring at a natural CO₂ vent. *Journal of Experimental Botany* 51(347), 1135-1146.
- Troughton J. H., & Card K. A. 1975. Temperature effects on the carbon-isotope ratio of C₃, C₄ and Crassulacean-acid-metabolism (CAM) plants. *Planta* 123(2), 185-190
- Trudinger C. M., Enting I. G., Francey R. J., Etheridge D. M., Rayner P. J. (1999). Long-term variability in the global carbon cycle inferred from a high-precision CO₂ and δ¹³C ice-core record. *Tellus B: Chemical and Physical Meteorology* 51(2), 233-248
- Van de Water P. K., Leavitt S. W., Betancourt J. L. (2002). Leaf δ¹³C variability with elevation, slope aspect, and precipitation in the southwest United States. *Oecologia* 132(3), 332-343
- Wang R., Yu G., He N., Wang Q., Zhao N., Xu Z., Ge J. (2015). Latitudinal variation of leaf stomatal traits from species to community level in forests: linkage with ecosystem productivity. *Scientific Reports* 5, 14454
- Wehr R., & Saleska S. R. (2015). An improved isotopic method for partitioning net ecosystem-atmosphere CO₂ exchange. *Agricultural and Forest Meteorology* 214–215, 515-531
- Wernerehl R. W., & Givnish T. J. (2015). Relative roles of soil moisture, nutrient supply, depth, and mechanical impedance in determining composition and structure of Wisconsin prairies. *PLOS ONE* 10(9), e0137963
- White J. W. C., Vaughn B. H., Michel S. E. (2015). University of Colorado, Institute of Arctic and Alpine Research (INSTAAR), stable isotopic composition of atmospheric carbon dioxide (¹³C and ¹⁸O) from the NOAA ESRL carbon cycle cooperative global air sampling network, 1990–2014. Version 2015-10-26 software.
- Wickham H. (2016). *ggplot2: elegant graphics for data analysis*. New York: Springer-Verlag.
- Woodward F. I. (1987). Stomatal numbers are sensitive to increases in CO₂ from pre-industrial levels. *Nature* 327(6123):617-618

- Woodward F. I., & Bazzaz F. A. (1988). The responses of stomatal density to CO₂ partial pressure. *Journal of Experimental Botany* 39(12), 1771-1781
- Yonetani T., & Gordon H. B. (2001). Simulated changes in the frequency of extremes and regional features of seasonal/annual temperature and precipitation when atmospheric CO₂ is doubled. *Journal of Climate* 14(8), 1765-1779
- Zhang Y. G., Pagani M., Liu Z., Bohaty S. M., DeConto R. (2013). A 40-million-year history of atmospheric CO₂. *Philosophical Transactions of the Royal Society: Mathematical, Physical and Engineering Sciences* 371(2001), 20130096

CHAPTER III

C₃ Plant Carbon Isotope Discrimination Does Not Respond to CO₂ Concentration on Decadal to Centennial Timescales²

3.1 Abstract

(1) Plant carbon isotope discrimination is complex, and could be driven by climate, evolution, and/or edaphic factors. We tested the climate drivers of carbon isotope discrimination in modern and historical plant chemistry, and focus in particular on the relationship between rising [CO₂] over Industrialization and carbon isotope discrimination.

(2) We generated temporal records of plant carbon isotopes from museum specimens collected over a climo-sequence to test plant response to climate and atmospheric change over the past 200 years (including *Pinus strobus*, *Platycladus orientalis*, *Populus tremuloides*, *Thuja koraiensis*, *Thuja occidentalis*, *Thuja plicata*, *Thuja standishii*, *Thuja sutchuenensis*). We aggregated our results with a meta-analysis of a wide range of C₃ plants to do a comprehensive study of the distribution of carbon isotope discrimination and values among different plant types.

(3) We show that climate variables (e.g. mean annual precipitation, temperature, and *key to this study*, CO₂ in the atmosphere) do not drive carbon isotope discrimination.

(4) Plant isotope discrimination is intrinsic to each taxon, and could link phylogenetic relationships and adaptation to climate quantitatively over ecological to geological time scales.

²Accepted to *New Phytologist* on the 13th of October 2020 under the citation: Stein, R. A., Sheldon, N. D., & Smith, S. (in press). C₃ plant carbon isotope discrimination does not respond to CO₂ concentration on decadal to centennial timescales. *New Phytologist*. doi: 10.1111/nph.17030

3.2 Introduction

Plants grow in direct contact with the changing atmosphere and surrounding environment, so they have the potential to record changes in environmental conditions and related stress (Farquhar et al. 1989; Arens et al. 2000). The carbon isotope chemistry of plants has been used by both the geological and ecological scientific communities to monitor climate change, plant biochemistry, and plant productivity (e.g. Feng et al. 1999; Diefendorf et al. 2010; Kohn 2010). Carbon isotope discrimination in plants (represented by $\Delta^{13}\text{C}_{\text{plant}}$ values) is the combined effects of fractionation selecting for light carbon due to diffusion through the leaf surface (^{12}C ; 4.4‰; noted as “a” in Equation 3.1), fractionation due to Rubisco’s selective preference for light carbon (27–30‰; noted as “b” in Equation 3.1), and an array of biochemical and environmental factors that are sometimes collectively termed “water use efficiency” (c_i/c_a is the ratio of internal to atmospheric CO_2 concentration; Equation 3.1; e.g. Farquhar et al. 1989).

$$\Delta^{13}\text{C}_{\text{plant}} = a + (b - a) \frac{c_i}{c_a} \text{ (Equation 3.1)}$$

Plant carbon isotope discrimination ($\Delta^{13}\text{C}_{\text{plant}}$) represents the difference between the isotopic composition of the atmosphere ($\delta^{13}\text{C}_{\text{CO}_2}$) and plants ($\delta^{13}\text{C}_{\text{plant}}$; Farquhar et al. 1989; Feng et al. 1999; Equation 3.2).

$$\Delta^{13}\text{C}_{\text{plant}} = \frac{\delta^{13}\text{C}_{\text{CO}_2} - \delta^{13}\text{C}_{\text{plant}}}{1 + \frac{\delta^{13}\text{C}_{\text{plant}}}{1000}} \text{ (Equation 3.2)}$$

Scientists typically interpret carbon isotope values ($\delta^{13}\text{C}_{\text{plant}}$) and $\Delta^{13}\text{C}_{\text{plant}}$ values as related to and affected by environmental drivers like mean annual precipitation (Diefendorf et al. 2010; Kohn 2010; Kohn 2016) or the amount of carbon dioxide in the atmosphere ($[\text{CO}_2]$; Schubert and Jahren, 2012; Cui and Schubert, 2016; Cui & Schubert 2020), or to reflect a fundamental plant trait with variability due to local effects like edaphic factors (Araus et al. 2002; Bonal et al. 2007). Our ability to use carbon isotope discrimination as recorded in plants to think about either past or future problems is dependent on understanding which combination of those factors drive discrimination.

3.2.1 Background

The direct interaction that plants have with the environment around them makes it such that leaf (and other plant part) tissues record environmental conditions (Schlanser et al. 2020). Global change biologists and geologists aim to leverage this fact in order to look at past ecosystems and to understand biotic responses to elevated carbon dioxide concentration of the atmosphere ($[\text{CO}_2]$) as well as related changes in seasonal and annual temperature, evapotranspiration, and precipitation (Jones et al. 1998). Previous studies have suggested that $\Delta^{13}\text{C}_{\text{plant}}$ values are sensitive to changes in $[\text{CO}_2]$ (Ehleringer & Cerling 1995; Schubert & Jahren 2012) and workers have proposed a $\Delta^{13}\text{C}_{\text{plant}}$ -paleobarometer to reconstruct $[\text{CO}_2]$ in the fossil record based upon those empirical relationships (Schubert & Jahren 2012; Cui & Schubert 2017). In this scenario, $\Delta^{13}\text{C}_{\text{plant}}$ values increase as the pool of available CO_2 increases, indicating that the mechanism of $[\text{CO}_2]$ uptake is altered in response to elevated $[\text{CO}_2]$ (Cornwell et al. 2018). Other studies have argued that water use efficiency, c_i/c_a (Equation 3.1), is not constant and that plants modify their leaf gas exchange properties in response to CO_2 , meaning that discrimination and CO_2 cannot be directly linked (Ehleringer & Cerling 1995; Beerling & Royer 2002).

$\Delta^{13}\text{C}_{\text{plant}}$ values also are cited as representative of intrinsic water use efficiency (iWUE; Farquhar & Richards 1984; Farquhar et al. 1989; Araus et al. 2002; Bonal et al. 2007); this is likely related to evolutionary components. If $\Delta^{13}\text{C}_{\text{plant}}$ values are genetically influenced, members of the same species should have constant $\Delta^{13}\text{C}_{\text{plant}}$ values (with minor variability within a species related to genotypic diversity and local environmental factors regardless of global drivers). Because genetic and edaphic drivers are measurable in the present, relationships between $\Delta^{13}\text{C}_{\text{plant}}$ and those drivers can be used directly to predict future ecosystem response to local and regional environmental change (Ainsworth & Long 2005; Nowak et al. 2004; Mueller et al. 2016; Yan et al. 2017). An additional implication of using $\Delta^{13}\text{C}_{\text{plant}}$ values as intrinsic traits is that other variables used to link physiologically-driven fractionation to isotopic values (Equation 3.1) become solvable. These assumptions still have geological implications: if climate variables are not driving $\Delta^{13}\text{C}_{\text{plant}}$ values, variability in $\Delta^{13}\text{C}_{\text{plant}}$ values is still representative of water use efficiency (Equation 3.1), which can be reconstructed in deep time to reconstruct water stress of a plant. However, due to the difficulty of measuring genetic diversity in the fossil record and the infrequency of coeval fossil soil and plant preservation due to different taphonomic filters (Looy

2014), the scope of $\Delta^{13}\text{C}_{\text{plant}}$ applications would be more limited for geologic problems or attempts to use the geologic record to project future change. Furthermore, most ecological validation studies of this concept have been based on single site or single taxon data collection or on short-term free-air concentration experiments (FACE) where environmental variability has either not been considered or has only been examined over short (< 10 years) time periods. As a result, questions remain about whether relationships observed in short-term records (e.g. on annual scale) would persist over the longer time periods necessary to project the impacts of future climate change.

If the previously proposed relationship between $\Delta^{13}\text{C}_{\text{plant}}$ and $[\text{CO}_2]$ is consistent across plants, it indicates that overall, plants are responsive and adaptive to $[\text{CO}_2]$ in real time. This paleobarometer potentially circumvents common problems of other deep-time paleo-barometric tools, like high error at high CO_2 concentrations or issues with statistical robustness, taphonomic bias, effects specific to certain taxonomy, and convolved environmental effects (e.g., oceanographic; Royer et al. 2004). The relationship between $\Delta^{13}\text{C}_{\text{plant}}$ and $[\text{CO}_2]$ has been tested previously in growth chamber experiments (Cui & Schubert 2017; Lomax et al. 2019) and fossil plants directly with an independent proxy constraint on CO_2 (Schlanser et al. 2020). Growth chamber experiments showed increased $\Delta^{13}\text{C}_{\text{plant}}$ values with increasing $[\text{CO}_2]$ in *Arabidopsis thaliana* (thale cress) and *Raphanus sativus* (wild radish), two weedy herbaceous angiosperms. This relationship was substantiated with selectively sampled literature values to demonstrate that sensitivity (S) of plant isotopic response to $[\text{CO}_2]$ peaked ~ 200 ppm with $S = 0.03\text{‰ ppm}^{-1}$ increase in discrimination and began to flatten around 1000 ppm with values closer to $S = 0.0025\text{‰ ppm}^{-1}$ (Schubert & Jahren 2012). The highest sensitivity values were collected from literature, but Schubert and Jahren's (2012) meta-analysis specifically only sampled studies that saw increases in discrimination with $[\text{CO}_2]$, excluding all studies that did not. Each of the species used to create this model have completely sequenced genomes and have been widely studied as model organisms; in addition to well-constrained biochemistry, these species are both easy to grow quickly for real-time experiments. Results from experiments using *A. thaliana* and *R. sativus* have been extrapolated to other groups of plants (Schubert & Jahren 2012; Shen et al. 2013; Cui et al. 2020). This empirically-derived relationship has been used with carbon isotope measurements in fossils ($\delta^{13}\text{C}_{\text{fossil}}$) to reconstruct $[\text{CO}_2]$ during geologic warm periods (Cui & Schubert, 2017; Cui et al. 2020), and has been used as evidence to support a future plant

response to anthropogenically-driven rise in [CO₂]. When Lomax et al. (2019) attempted to use $\Delta^{13}\text{C}_{\text{plant}}$ as a paleobarometer in growth chamber experiments with varied water regimes, they found that low water availability led to under-predicting [CO₂] values for high [CO₂] treatments designed to simulate most of the geologic past. This suggests that [CO₂] cannot be implicated as the main driver for carbon isotope discrimination without considering water availability, but even this may be further complicated by evolution. The studies used to formulate a $\Delta^{13}\text{C}_{\text{plant}}$ - paleobarometer model have not distinguished plant growth rate nor plant growth habit, and have assumed that there is no difference between angiosperms and any other type of plant. *Raphanus* and *Arabidopsis* have limited fossil records (Miocene–present; e.g., Beilstein et al., 2010) and first evolved during periods of low [CO₂]; therefore, there are questions about the reliability of a *Raphanus sativus*-*Arabidopsis thaliana*-focused model as a paleobarometer for a high CO₂ world or for non-angiosperm plants. This approach to study the relationship between [CO₂] and $\Delta^{13}\text{C}_{\text{plant}}$ is high resolution and well-controlled, and assumes that [CO₂] is the main driving factor and does not address other climate and edaphic factors (e.g. soil moisture, nitrogen and nutrient availability, salinity; Bowman et al. 1989; Condon et al. 1992; Högberg et al. 1993; Guehl et al. 1995; Dawson et al. 2002).

Additional geological studies to examine the relationship between [CO₂] and $\Delta^{13}\text{C}_{\text{plant}}$ values in deep time have mixed results. Paleogene plants collected from the Paleocene Fort Union Formation and the Eocene Willwood Formation demonstrate no observable response to large changes in [CO₂] (Diefendorf et al. 2015). Kohn (2016), however, found a small gradual increase in $\Delta^{13}\text{C}_{\text{plant}}$ values in Pleistocene-Holocene sediments, that, when corrected for mean annual precipitation, could be linked to increased [CO₂]. However, this same study found a slight decrease in $\Delta^{13}\text{C}_{\text{plant}}$ values in Pleistocene and Tertiary herbivore data (Kohn 2016). Recent work using leaf waxes collected from sediments of both the Cretaceous and Oligocene shows that $\Delta^{13}\text{C}_{\text{plant}}$ values in these sediments had no clear positive [CO₂]-dependence and in fact, responded negatively, perhaps related to adaptation to minimize water loss (Schlanser et al. 2020). Testing in geological sediments is important and relevant to the utility of this paleobarometer, but would be strengthened by adding an additional timescale between prior geologic studies and growth chamber experiments.

To test to what extent $\Delta^{13}\text{C}_{\text{plant}}$ values of plants are responsive to changes in $[\text{CO}_2]$ and how taxon-specific is this response, we turned to Industrialization as a natural experiment. This historical approach has the benefits of high-resolution, semi-annual data while also accounting for natural influence from environmental, edaphic, and other variables that would be seen in the fossil record and can offset changes in water use efficiency and $\Delta^{13}\text{C}_{\text{plant}}$ (Giguère-Croteau, et al. 2019). In this study, we measured $\Delta^{13}\text{C}_{\text{plant}}$ response to the Industrialization-driven rise in $[\text{CO}_2]$ in several plant species; non-barometric climate variables are not controlled but are constrained and considered. Industrialization (1850–present) provides a unique, natural $[\text{CO}_2]$ enrichment “experiment” wherein $[\text{CO}_2]$ values range from 280 ppm to nearly 420 ppm (i.e., an increase of ~50%), allowing us to track actual plant $\Delta^{13}\text{C}_{\text{plant}}$ responses to rising $[\text{CO}_2]$. Previous works have tested the relationship of $\Delta^{13}\text{C}_{\text{plant}}$ values to environmental, edaphic, and genetic factors among modern plants (e.g. Cornwell et al. 2018). However, most of those studies reflect only present-day or near present-day CO_2 levels and only rarely have tracked the long-term (> 100 years) response of individual species (e.g. Stein et al. 2019). Based upon growth chamber experiments, Industrialization provides a range of $[\text{CO}_2]$ wherein plant $\Delta^{13}\text{C}_{\text{plant}}$ responses are thought to be extremely sensitive (Schubert & Jahren 2012). In tandem with changes in $[\text{CO}_2]$, the isotopic composition of atmospheric CO_2 has changed significantly over this time due to the burning of fossil fuels (from a value of -6.7 to -8.5‰; Keeling et al. 2001), allowing us to examine changes in $\Delta^{13}\text{C}_{\text{plant}}$ versus changes in $\delta^{13}\text{C}_{\text{plant}}$ values (Fig. 3.1a-c) during this interval.

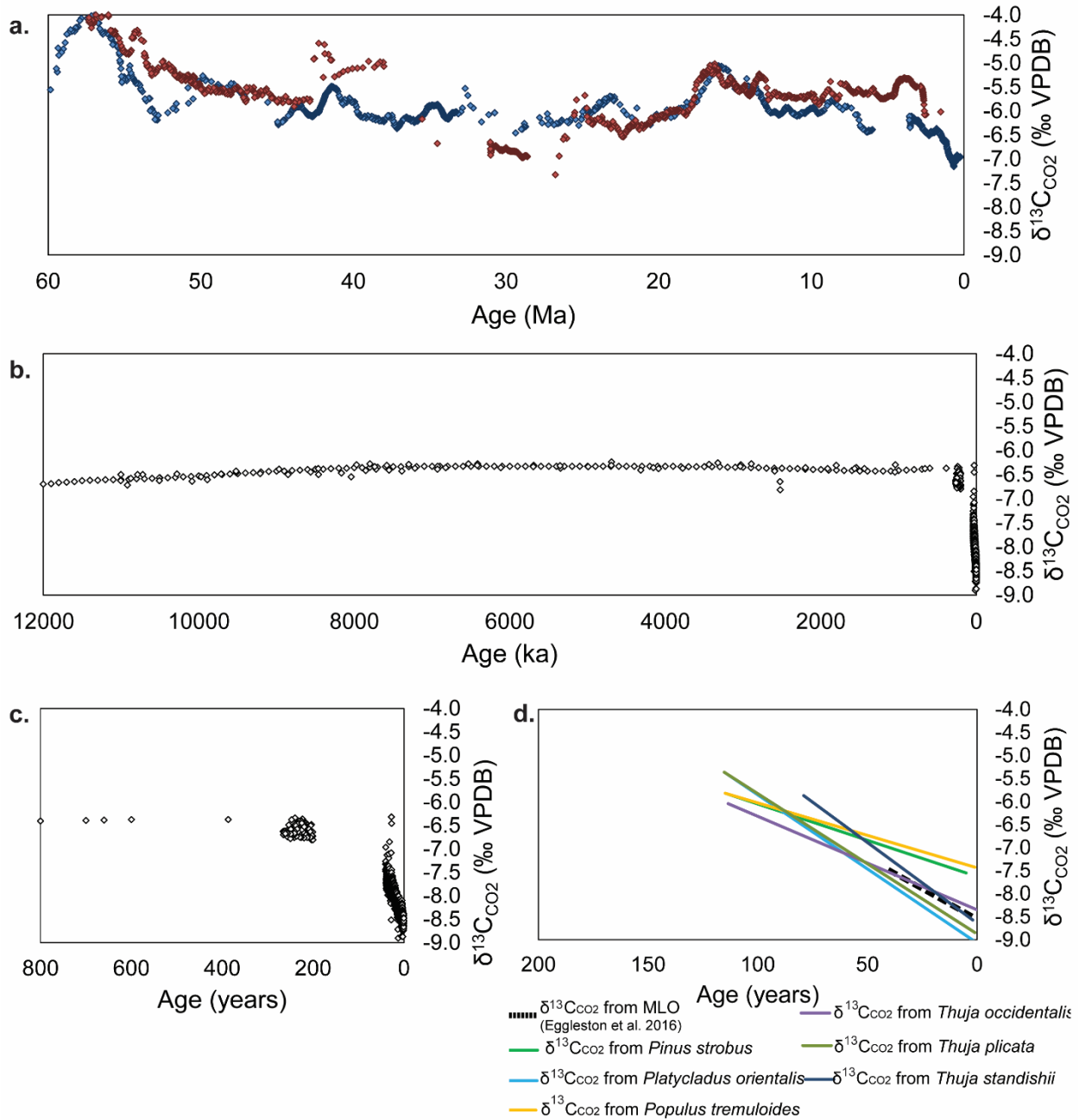


Figure 3.1 Evolution of $\delta^{13}\text{C}_{\text{CO}_2}$ (‰) over time, including the Cenozoic, 12,000 years ago, the past 800 years, and the past 200 years including values reconstructed from $\delta^{13}\text{C}_{\text{leaf}}$ values. (a) 60 million years ago to present, with red diamonds representing values reconstructed using planktonic foraminifera and blue diamonds representing values reconstructed using benthic foraminifera (Tippie et al. 2010), (b) over the last 12,000 years with white diamonds representing $\delta^{13}\text{C}_{\text{CO}_2}$ from ice cores (Elsig et al. 2009, Bauska et al. 2018), (c) over the past 800 years with white diamonds representing $\delta^{13}\text{C}_{\text{CO}_2}$ from ice cores (Elsig et al. 2009, Bauska et al. 2018), (d) over Industrialization, 200 years ago to present, including $\delta^{13}\text{C}_{\text{CO}_2}$ values as measured from Mauna Loa Observatory (MLO; Keeling et al. 2001, Keeling et al. 2005, Eggleston *et al.*

2016) and $\delta^{13}\text{C}_{\text{CO}_2}$ values reconstructed using $\Delta^{13}\text{C}_{\text{plant}}$ values from six species we collected ($n \geq 10$ specimens).

The high-resolution temporal datasets tracking several species are supplemented by modern samples of the same species, to examine whether there are relationships between other climate variables and $\Delta^{13}\text{C}_{\text{plant}}$ values (Sheldon et al. 2020). In addition, we have compiled $\delta^{13}\text{C}_{\text{plant}}$ values and calculated $\Delta^{13}\text{C}_{\text{plant}}$ values for a wide range of herbaceous and woody C_3 plants to compare between plant groups and growth strategies. Compiled literature data include herbaceous and woody angiosperms, and bryophytes (Fig. 3.3, Supp. Figs. B2; B3–Supp. Table B1). The total dataset includes 2585 isotope analyses, with data collected for this study accompanied with measured climate variables.

3.3 Materials and Methods

We used records from 11 herbaria and museum collections facilities (COLO, CS, F, HMAS, KHD, KUN, MICH, MSC, SG, WTU, YU) to evaluate the relationship between carbon isotope chemistry ($\Delta^{13}\text{C}_{\text{plant}}$ and $\delta^{13}\text{C}_{\text{plant}}$) and changing environmental drivers of a number of woody gymnosperms species and one woody angiosperm over the period of Industrialization. We collected modern gymnosperm (2015-2019) leaf material from across the Northern Hemisphere ($n = 469$) of *Pinus strobus*, *Platycladus orientalis*, *Thuja koraiensis*, *Thuja occidentalis*, *Thuja plicata*, *Thuja standishii*, and *Thuja sutchuenensis* as well as additional modern species from another angiosperm, *Populus tremuloides* species ($n = 1264$ total specimens for modern and historical specimens, combined) from between 1806 and 2019, spanning a wide range of climate conditions (Table B2). Specimens were washed in deionized (DI) water within an ultrasonic bath for thirty minutes to remove herbarium glue and other sediments, then dried in a 50°C oven for 48 hours, and finally ground to homogeneity with an agate mortar and pestle. Ground specimens were stored in air-tight glass vials within sealed chambers with desiccant to absorb water vapor. Specimen aliquots were weighed into tin capsules from 0.600 mg to 0.800 mg and run on a Picarro Cavity Ring Down Spectroscopy (CRDS) for $\delta^{13}\text{C}$ values, with official IAEA standards (IAEA-CH6: sucrose, $\delta^{13}\text{C} = -10.45\text{‰}$; IAEA-600: caffeine, $\delta^{13}\text{C} = -27.77\text{‰}$) and laboratory internal standards (C_3 sugar: $\delta^{13}\text{C} = -26.14\text{‰}$, C_4 sugar: $\delta^{13}\text{C} = -12.71\text{‰}$, acetanilide: $\delta^{13}\text{C} = -28.17\text{‰}$). CRDS machine specifications

indicate reproducibility of $\pm 0.3\%$, but our standard reproducibility was $\pm 0.12\%$. These same specimens were also run on a Costech Elemental Analyzer for %C and %N and C:N ratio using laboratory standards (acetanilide: 71.09%C, 10.34%N, and atropine: 70.56%C, 4.84%N) in University of Michigan's Earth System Science Laboratory.

Climate variables (MAP, MAT, Maximum Summer Temperature) associated with each specimen were obtained from PRISM Climate Group (Prism Climate Group 2004) for samples obtained in the contiguous United States and WorldClim (version 2 at 2.5km resolution; Fick & Hijmans 2017) and Vostok Ice Core ($[\text{CO}_2]$, $\delta^{13}\text{C}_{\text{CO}_2}$; White et al. 2015). Altitude and latitude were also gathered for samples and compared to isotope analysis results. $\Delta^{13}\text{C}_{\text{plant}}$ values were calculated using $\delta^{13}\text{C}_{\text{CO}_2}$ as collected from the Vostok Ice Core and Mauna Loa Observatory (White et al. 2015) using Equation 3.2 (e.g. Feng et al. 1999; Diefendorf et al. 2010).

We compared our historical findings regarding the relationship between $\delta^{13}\text{C}_{\text{plant}}$ values and $\delta^{13}\text{C}_{\text{CO}_2}$ with Arens et al.'s (2000) generalized empirical relationship between $\delta^{13}\text{C}_{\text{plant}}$ values and $\delta^{13}\text{C}_{\text{CO}_2}$ values in C_3 plants (Equation 3.3).

$$\delta^{13}\text{C}_{\text{plant}} = 1.05(\delta^{13}\text{C}_{\text{CO}_2}) - 18.72 \text{ (Arens et al. 2000) (Equation 3.3)}$$

Additional carbon isotopic values were obtained from previously published studies with coincident $[\text{CO}_2]$ and $\delta^{13}\text{C}_{\text{CO}_2}$ values to compare this study's focal plant results with a wider range of plant functional types ($n = 2585$; Dataset B1). We excluded all genera and families with fewer than 20 and 25 isotopic measurements (respectively) when comparing taxa and isotope discrimination values, but included these in plant habit or plant reproductive group comparisons. To test whether these genera, families, and/or plant habits/reproductive strategies $\Delta^{13}\text{C}_{\text{plant}}$ values had the same mean and variances as the $\Delta^{13}\text{C}_{\text{plant}}$ values from the Schubert & Jahren (2012) study, we conducted F-tests where the null hypothesis was equal variance, then conducted two sample t-tests assuming unequal variances wherein the null hypothesis was equal mean values (Table B3). We included analysis of plant specimens grown under $[\text{CO}_2]$ values from 280–1000 ppm, because although atmospheric $[\text{CO}_2]$ is ~ 410 ppm at present, concentrations of CO_2 as high as 1800 ppm have been observed at ground level within very dense canopy on a very nutrient-rich Mollisol (Bazzaz & Williams 1991) – to account for this potential fluctuation, of our sites,

we included values for plants grown at [CO₂] levels up to 1000 ppm. We excluded values from the literature from plants that were grown at >1000 ppm.

Equation 3.4 (Cui & Schubert 2016) was used to reconstruct values of [CO₂] for each isotope value we collected, then compared reconstructed values with our known values collected from Mauna Loa Observatory and ice cores (Prism Climate Group 2004; White et al. 2015).

$$\Delta^{13}\text{C} = [(28.26)(0.21)(p\text{CO}_2 + 25)]/[28.26 + (0.21)(p\text{CO}_2 + 25)] \text{ (Schubert \& Jahren 2012; Cui \& Schubert 2016; Equation 3.4)}$$

where 28.26 represents A, the maximum fractionation value, while 0.21 and 25 represent B and C, constants derived iteratively to find the best fit curve, and $p\text{CO}_2 = [\text{CO}_2]$ (Cui & Schubert 2016).

3.4 Results

Six of the eight focal species showed significant shifts in $\delta^{13}\text{C}_{\text{plant}}$ in tandem with $\delta^{13}\text{C}_{\text{CO}_2}$ values. These plants (*Pinus strobus*, *Platycladus orientalis*, *Populus tremuloides*, *Thuja occidentalis*, *Thuja plicata*, *Thuja standishii*), when corrected for each species' average $\Delta^{13}\text{C}_{\text{plant}}$ values, demonstrated changes in $\delta^{13}\text{C}_{\text{CO}_2}$ over Industrialization comparable to those recorded in ice and at Mauna Loa Observatory (Fig. 3.1c-d). *Populus tremuloides* displayed a slope and intercept similar to the generalized relationship found in the Arens et al. (2000) study (1.08 and -18.77, respectively), though the gymnosperms tested had different responses in $\delta^{13}\text{C}_{\text{plant}}$ values to changing $\delta^{13}\text{C}_{\text{CO}_2}$ (Table B4). The other focal species (*Thuja koraiensis*, *Thuja sutchuenensis*) did not span a sufficient period of time to examine the direction; *Thuja sutchuenensis* was only rediscovered recently (Qiaoping et al. 2002) after over a century of being listed as extinct in the wild (EW) by IUCN standards.

Over the span of Industrialization, none of the eight species studied showed any significant changes in $\Delta^{13}\text{C}_{\text{plant}}$ nor significant relationship with [CO₂] (Fig. 3.2 shows the four largest datasets; others are plotted in Supp. Fig. B3). We examined changes in sensitivities for all data, and for pre-1960 values (280–320 ppm) and post-1960 values (320–410 ppm), with 1960 representing where slope changes in [CO₂] increase due to more rapid industrialization of developing nations (Keeling et al. 2001; MacFarling et al. 2006) (Table B5). Of the seven

species with pre-1960 data points (<320 ppm [CO₂]) and post-1960 values (>320 ppm [CO₂]), only two (*Thuja standishii* and *Thuja occidentalis*; Cupressaceae) showed a change in sensitivity to [CO₂], and both declined rather than increasing as would have been predicted by growth chamber experiments. The sensitivity to [CO₂] (*S*; change in ‰ of $\Delta^{13}\text{C}_{\text{plant}}$ per ppm of [CO₂]) exhibited by *Arabidopsis thaliana* and *Raphanus sativus* in growth chamber experiments was not observed in any of the Industrialization-spanning historical records (Table B5). In fact, we found negative shifts in *S* for *Populus tremuloides* (Salicaceae) and *Thuja koraiensis*; none of the modern/historical species exhibited sensitivity to [CO₂] similar to the growth chamber experiments of Schubert & Jähren (2012).

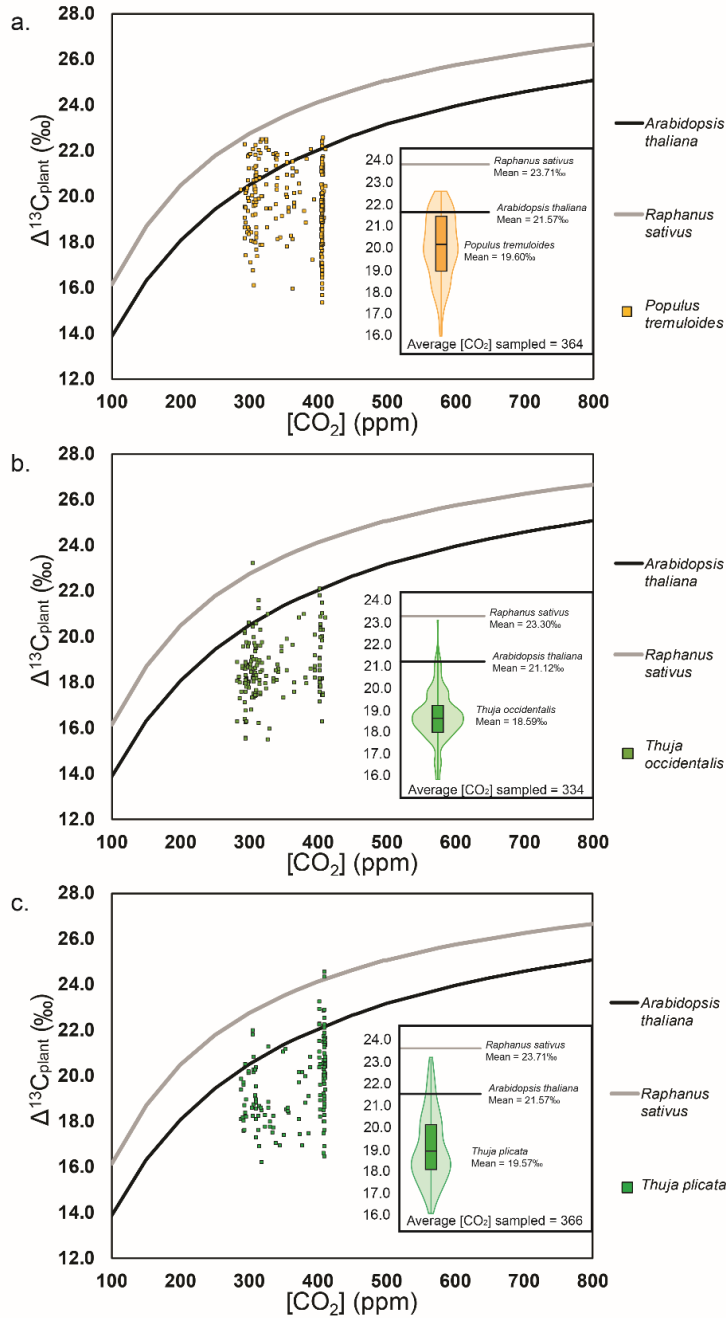


Figure 3.2 $[\text{CO}_2]$ values plotted against $\Delta^{13}\text{C}_{\text{plant}}$ for species with high-resolution records of the period of Industrialization. Data are for: (a) *Populus tremuloides* (quaking aspen), (b) *Thuja occidentalis* (northern white cedar), and (c) *Thuja plicata* (western red cedar). The outer panel shows change in $\Delta^{13}\text{C}_{\text{plant}}$ vs. $[\text{CO}_2]$ over Industrialization, while the inner panel shows the range and distribution of $\Delta^{13}\text{C}_{\text{plant}}$ values for this species. Each of the species occupies different geographic ranges and different ranges of climatic variability, but none shows a significant $\Delta^{13}\text{C}_{\text{plant}}$ response to rising $[\text{CO}_2]$ over the period of Industrialization.

This study compares $\Delta^{13}\text{C}_{\text{plant}}$ values of *Arabidopsis* and *Raphanus* with a breadth of C_3 plant functional types, representing taxa with different reproduction styles (angiosperms, gymnosperms, and bryophytes), growth habits (woody and herbaceous), and vascular systems (vascular and non-vascular). When comparing the long historical records of $\Delta^{13}\text{C}_{\text{plant}}$ with modern data from a variety of plant types from the literature, we found a distinct difference between gymnosperms, woody angiosperms, herbaceous angiosperms, and bryophytes, and *A. thaliana* and *R. sativus* for any CO_2 level <1000 ppm (Fig. 3.3). This was true even for other herbaceous, fast-growing members of the same family as the $\Delta^{13}\text{C}_{\text{plant}}$ -paleobarometer model organisms (Brassicaceae; *A. thaliana*, *R. sativus*). Values above 1000 ppm are unlikely to be found at woody tree sampling height ($\sim 1\text{--}2\text{m}$), despite the source of soil-respired CO_2 rising from the ground (Bazzaz & Williams 1991). When performing a t-test for the mean values of each of these plant functional types as compared to the two tested weeds, we found that all of the tested differences were statistically significant (Fig. 3.3; Fig. B1; Table B3), indicating that none of the wild-grown species were behaving like the growth chamber experiments. When further analyzed at higher taxonomic levels, all genera and families showed statistically different $\Delta^{13}\text{C}_{\text{plant}}$ values than *A. thaliana* and *R. sativus*.

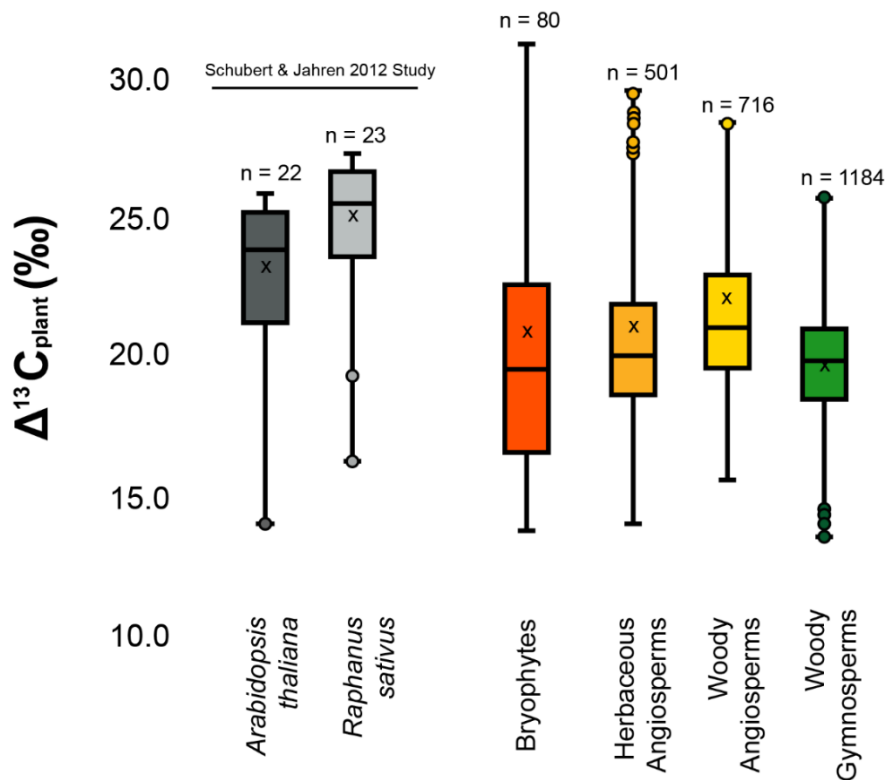


Figure 3.3 $\Delta^{13}\text{C}_{\text{plant}}$ values of plants divided by growth form, as collected from literature and this study. Meta-analysis plants are shown in color, compared to *Arabidopsis* and *Raphanus* values in grey. Xs denote mean values and circles denote outlier $\Delta^{13}\text{C}_{\text{plant}}$ values. Boxes show 75th percentile of data, while whiskers show remaining 25th percentile of data.

To test the idea that $\Delta^{13}\text{C}_{\text{plant}}$ should be related to $[\text{CO}_2]$, we compared the measured $[\text{CO}_2]$ with $[\text{CO}_2]$ reconstructed using an empirical relationship derived from growth chamber experiments (see *Methods*, Equation 3.4). The actual $[\text{CO}_2]$ values showed no significant relationship with reconstructed $[\text{CO}_2]$ values (Fig. 3.4; p-value = 0.63); often the model-reconstructed $[\text{CO}_2]$ values underestimated measured $[\text{CO}_2]$ (Fig. 3.4), which is consistent with other recent growth chamber experiments that included water stress as a variable (Lomax et al. 2019). Thus, we find no evidence that $\Delta^{13}\text{C}_{\text{plant}}$ is related to $[\text{CO}_2]$. Instead, the historical data showed consistent linear relationships between $\delta^{13}\text{C}_{\text{plant}}$ and $\delta^{13}\text{C}_{\text{CO}_2}$ for all tested species, with each having a slope close to 1:1 (Stein et al. 2019; Sheldon et al. 2020), and where the observed $\delta^{13}\text{C}_{\text{atm}}$ values correspond closely to $\delta^{13}\text{C}_{\text{atm}}$ values reconstructed using $\delta^{13}\text{C}_{\text{plant}}$ measurements (Fig. 3.1d). In addition, most individual measurements of a given species' $\Delta^{13}\text{C}_{\text{plant}}$ value are within ± 1.5 ‰ of the mean $\Delta^{13}\text{C}_{\text{plant}}$ value found for that species, independent of other climate variables (Fig. 3.3; Fig. B2; Fig. B3; Sheldon et al. 2020).

3.5 Discussion

3.5.1 Carbon isotope discrimination and $[\text{CO}_2]$

Our results indicate that $\Delta^{13}\text{C}_{\text{plant}}$ values are not driven by $[\text{CO}_2]$ for any of the studied plants. $\Delta^{13}\text{C}_{\text{plant}}$ values remained flat for a given genus, plant functional type, and species as $[\text{CO}_2]$ increased over Industrialization (Fig. 3.2; Fig. B1). $\delta^{13}\text{C}_{\text{plant}}$ values, in contrast, closely tracked observed changes in $\delta^{13}\text{C}_{\text{CO}_2}$ driven by human-combusted fossil fuels, which are isotopically more negative than natural CO_2 sources (i.e. volcanic emissions; Keeling et al. 2001). $\delta^{13}\text{C}_{\text{plant}}$ values tracked $\delta^{13}\text{C}_{\text{CO}_2}$ in multiple species, though individual species exhibited stronger or weaker carbon isotope discrimination. Our study confirms the previously evaluated connection between $\delta^{13}\text{C}_{\text{plant}}$ values and atmospheric CO_2 sources in the geologic record (Arens et al. 2000).

Regardless of growth habit or reproductive mode (i.e., angiosperm versus gymnosperm; seed vs. spore), the newly collected data and collated literature values for our aggregate meta-analysis exhibited $\Delta^{13}\text{C}_{\text{plant}}$ values significantly lower than expected under current and historic $[\text{CO}_2]$ ranges based upon growth-chamber derived values. These results indicate $\Delta^{13}\text{C}_{\text{plant}}$ values of all of our tested plants, including herbaceous, fast-growing plants and bryophytes, which are known for their high discrimination against ^{13}C due to their primitive vascular system (Rundel et al. 1979; Proctor et al. 1992; Royles et al. 2016), are driven by something other than the atmospheric $[\text{CO}_2]$. Thus, previously observed $\Delta^{13}\text{C}_{\text{plant}}-[\text{CO}_2]$ dependence may instead represent an intrinsic trait of a limited range of highly water-use efficient, weedy plants, may reflect plant response under unnaturally consistent conditions in growth chambers, or may be related to the range of $[\text{CO}_2]$ studied or length of study. This affirms previous findings that though short-term $[\text{CO}_2]$ enhancement experiments can result in increased $\Delta^{13}\text{C}_{\text{plant}}$ values, decadal-scale plant responses, like adjustment of stomatal size and density, counteract this effect (Peñuelas & Azcón-Bieto 1992; Saurer et al. 2004; Diefendorf & Freimuth 2017). This is important for modern ecological studies that look to extrapolate broad implications from smaller, shorter, and/or local experiments. We add a note of caution not to over-generalize results.

While our historical records confirm that the $\Delta^{13}\text{C}_{\text{plant}}\text{-paleobarometer}$ typically under-predicted $[\text{CO}_2]$ in the natural world (Fig. 3.4), in the context of previous findings (Stein et al. 2019; Sheldon et al. 2020), we interpret this as due to $\Delta^{13}\text{C}_{\text{plant}}$ values being an intrinsic plant trait, and not driven by individual climate parameters. Previous workers (e.g. Kohn 2016, Lomax et al. 2019) have suggested that while there is potential for this $\Delta^{13}\text{C}_{\text{plant}}\text{-paleobarometer}$, climate factors related to water availability (e.g. mean annual precipitation, humidity) and/or nutrient availability (Giguère-Croteau et al. 2019) could confound the relationship between $[\text{CO}_2]$ and $\Delta^{13}\text{C}_{\text{plant}}$ values because of water's fundamental role in controlling photosynthesis and carbon uptake (Diefendorf et al. 2010; Franks et al. 2013). We found that none of those other climate variables significantly impacted the $\Delta^{13}\text{C}_{\text{plant}}$ at the species to family level, nor did a combination of $[\text{CO}_2]$ and precipitation (Stein et al. 2019; Sheldon et al. 2020; Supp. Table B6). The most parsimonious explanation is that the previous $\Delta^{13}\text{C}_{\text{plant}}\text{-paleobarometer}$ predicts a much greater sensitivity (S ; expressed in $\% \Delta^{13}\text{C}_{\text{plant}}/\text{ppm } [\text{CO}_2]$; Table B5) than is observable in nature; this demonstrates that $[\text{CO}_2]$ is not the main driver of $\Delta^{13}\text{C}_{\text{plant}}$ values based on highly-selected, single or few-species experiments over limited ranges in $[\text{CO}_2]$ (e.g. Van de Water et al. 1994; Peñuelas

& Estiarte 1997; Saurer et al. 2004). By sampling a wide range of taxa, we show that the discrepancy between our $\Delta^{13}\text{C}_{\text{plant}}$ values and those expected based on a $\Delta^{13}\text{C}_{\text{plant}}$ -paleobarometer are not due to the taxa used and that $\Delta^{13}\text{C}_{\text{plant}}$ values vary between taxa. In other words, $\Delta^{13}\text{C}_{\text{plant}}$ values are intrinsic to a given taxon; the evolutionary implications of intrinsic discrimination could quantitatively link phylogenetic relationships and adaptation to climate. Variability within species' $\Delta^{13}\text{C}_{\text{plant}}$ values is related to genotypic diversity and/or unmeasured but relevant-to-growth edaphic effects, but not related to the measured climate drivers and not sensitive to $[\text{CO}_2]$.

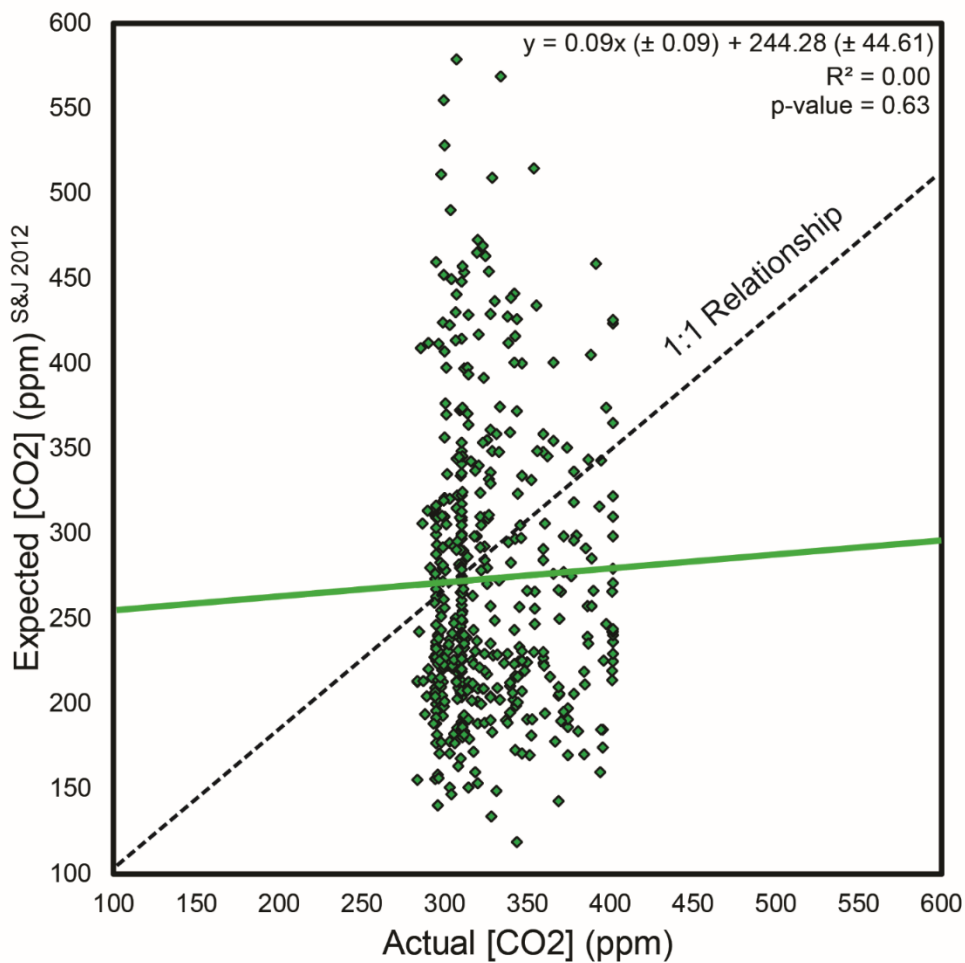


Figure 3.4 $[\text{CO}_2]$ (ppm) values as measured at MLO ($[\text{CO}_2]_a$), compared to reconstructed $[\text{CO}_2]$ values ($[\text{CO}_2]_r$) based on the proposed $\Delta^{13}\text{C}_{\text{plant}}$ -paleobarometer (Equation 3.4; Schubert & Jahren 2012; Cui & Schubert 2016). Solid line shows trendline for our data ($[\text{CO}_2]_r = 0.09 (\pm 0.09) * [\text{CO}_2]_a + 244.28 (\pm 44.61)$; $R^2 = 0.00$, $p\text{-value} = 0.63$), while dashed line shows expected relationship if reconstructed $[\text{CO}_2]$ values were equal to measured $[\text{CO}_2]$ values ($[\text{CO}_2]_r = [\text{CO}_2]_a$).

3.5.2 Ancient bio-atmosphere implications

Our results indicate we may be able to use $\delta^{13}\text{C}_{\text{plant}}$ values to reconstruct paleo- $\delta^{13}\text{C}_{\text{CO}_2}$ values as experimented with in previous studies (i.e. Arens et al. 2000; Fig. 3.1d) given that the other tested environmental factors were not significant drivers of $\delta^{13}\text{C}_{\text{plant}}$ (Supp. Table B6). We suggest that using species-specific plant-atmosphere isotope relationships to track $\delta^{13}\text{C}_{\text{CO}_2}$, rather than a generalized relationship, will add certainty, and takes a step to address the critiques raised by Beerling & Royer (2002) that the generalized empirical relation by Arens et al. (2000; Equation 3.3) does not account for variability in c_i/c_a within or between plant lineages. While this “universal” relationship based on a range of species works, we found that the responses of each species in our historical dataset to changing $\delta^{13}\text{C}_{\text{CO}_2}$ were different (as represented by equations relating the $\delta^{13}\text{C}_{\text{plant}}$ values of each species to $\delta^{13}\text{C}_{\text{CO}_2}$ values; Table B4). The woody angiosperm, *Populus tremuloides*, behaved similarly to the generalized relationship found in the Arens et al. (2000) study, but the other species tested, all gymnosperms, had vastly different responses in $\delta^{13}\text{C}_{\text{plant}}$ values to changing $\delta^{13}\text{C}_{\text{CO}_2}$. This highlights the importance of evolution in response to changing climate and atmospheric variables.

For plants with pre-instrument or fossil records, modern $\Delta^{13}\text{C}_{\text{plant}}$ values are a key input parameter in many other tools (including paleo-barometric techniques) previously applied in the fossil record, and are a key tracer of $[\text{CO}_2]$ sources and fluxes in deep time (Franks et al. 2014). With the depth and breadth of our study, we provide robustly constrained $\Delta^{13}\text{C}_{\text{plant}}$ values of several species (*Thuja occidentalis*, *Thuja plicata*, *Pinus strobus*, *Populus tremuloides*), and validate that $\Delta^{13}\text{C}_{\text{plant}}$ values are approximately constant. Although carbon isotope discrimination is complex and influenced by many factors (Diefendorf & Freimuth 2017), in tandem with previous works (Merveille 2015; Stein et al. 2019; Sheldon et al. 2020), we support that many measures of temperature (e.g., MAT, growing season temperature) and moisture (e.g. MAP, wettest three months) do not have predictive relationships with $\Delta^{13}\text{C}_{\text{plant}}$ values (Supp. Table B6). This means that while there are diagenetic and preservation-related factors to take into account before using $\delta^{13}\text{C}_{\text{plant}}$ to reconstruct paleo- $\delta^{13}\text{C}_{\text{CO}_2}$, it is plausible to look at relative perturbations in $\delta^{13}\text{C}_{\text{CO}_2}$ in time using plants over time scales from hundreds to millions of years to track

changes in the carbon cycle. This would be an excellent terrestrial complement to Tipple et al.’s (2010) foraminifera-derived $\delta^{13}\text{C}_{\text{CO}_2}$ record and would provide a way to compare marine-terrestrial reconstructions and to time-calibrate major paleoclimatic transitions.

Our results affirm previous experiments that calculated paleo-water use efficiency in *Metasequoia* and *Thuja* fossils based on $\delta^{13}\text{C}$ values, which assumed no confounding climate factors (e.g. Sheldon et al. 2020; Supp. Table B6). While $\Delta^{13}\text{C}_{\text{plant}}$ values should not be used to reconstruct environmental drivers like $[\text{CO}_2]$, they can be used to identify water use efficiency in ancient plants. Ancient plants’ water use efficiency provides insight into general adaptation to climate events and evolutionary history—a critical aspect of how the past can inform the future (McElwain 2018).

3.5.3 Modern and future climate change

This study’s markedly longer duration of the “natural experiments” considered provides context and validation for important shorter experiments, like growth chamber (Lomax et al. 2019) and FACE experiments (Ainsworth & Long 2005; Norby & Zak 2011). These experiments have been used to show short-term plant adaptation to enhanced CO_2 in certain plants, but muted response with longer time and a wider breadth of plant types (Long et al. 2006; Hickler et al. 2011; Norby & Zak 2011). We have demonstrated responses over the entirety of Industrialization, validating the value of those shorter-term experiments for predicting future response. Our results suggest that extending these experiments and incorporating a number of comparative species of different plant functional types grown in the same environment would be useful to determine longer-term and broader plant reactions to elevated CO_2 .

If $\Delta^{13}\text{C}_{\text{plant}}$ values are inherent to species, soil chemistry, a catchment of aboveground ecosystem inputs, may demonstrate relationships with environmental drivers related to the biogeography of plant adaptation and distribution (Cornwell et al. 2018). Previous works have demonstrated that $\Delta^{13}\text{C}_{\text{plant}}$ values provide insight into plant health associated with measurable genotypic and edaphic effects (Reich et al. 2006); to isolate the effects of these variables, additional future studies could examine foliar to critical zone carbon isotope variability over natural experiment of Industrialization with measured soil parameters (e.g. soil moisture, texture, pH, nutrient availability, microbiota; Kaplan et al. 2002; McKee et al. 2002; Cornwell et al.

2018). With deeper understanding of what edaphic, morphological, and genetic factors drive variability, we can use $\Delta^{13}\text{C}_{\text{plant}}$ values to understand plant biochemistry in response to things like water stress, yield, and growth success and strategically manage landscapes to maximize plants as a biological carbon sink.

3.6 Acknowledgments

For assistance with herbarium collections, we thank Ryan Allen (COLO), Tim Hogan (COLO), Erin Tripp (COLO), Jennifer Ackerfield (CS), Christine Niezgoda (F), Thorsten Lumbsch (F), Xiao-Guo Xiang (HMAS), Melissa Islam (KHD), Liu Ende (KUN), Richard Rabeler (MICH), Anton Reznicek (MICH), Alan Fryday (MSC), Mo Jian Bin (SG), Caroline Strömberg (WTU), Michael Donoghue (YU), Shusheng Hu (YU) and Patrick Sweeney (YU). We thank Mike Blakeman (United States Forest Service: Rio Grande National Forest), Steve Baumann (National Park Service: El Malpais National Monument), Matthew Dubeau (NPS: Olympic National Park), Scott Esser (NPS: Rocky Mountain National Park), Susana Fernandes (University of Michigan School for Environment and Sustainability), Matthew Klein (USFS: White River National Forest), Jayne Lebeda (USFS: Fishlake National Forest), Su Tao (Xishuangbanna Tropical Botanical Garden) and Jason Zayatz (USFS: Coconino National Forest) for assistance with sampling permissions. Additional thanks to Steve Baumann, Susana Fernandes, Molly Ng, Rebecca Dzombak and Ashley Hamersma for assistance in the field. Finally, we thank Dr. Aaron Diefendorf and an anonymous reviewer for the helpful feedback that improved this manuscript, as well as Dr. Peter Franks, the handling editor, for overseeing the editorial process at *New Phytologist*. This work was partially funded by NSF Award #1812949 to NDS. Fieldwork by RAS was supported by the Geological Society of America's Graduate Research grants.

3.7 References

- Ainsworth, E. A., & Long, S. P. (2005). What have we learned from 15 years of free-air CO₂ enrichment (FACE)? A meta-analytic review of the responses of photosynthesis, canopy properties and plant production to rising CO₂. *New Phytologist*, 165(2), 351-372.
- Araus, J. L., Slafer, G. A., Reynolds, M. P., & Royo, C. (2002). Plant breeding and drought in C₃ cereals: what should we breed for? *Annals of botany*, 89(7), 925-940.

- Arens, N. C., Jahren, A. H., & Amundson, R. (2000). Can C₃ plants faithfully record the carbon isotopic composition of atmospheric carbon dioxide? *Paleobiology*, 26(1), 137-164.
- Bauska, T. K., Brook, E. J., Marcott, S. A., Baggenstos, D., Shackleton, S., Severinghaus, J. P., & Petrenko, V. V. (2018). Controls on millennial-scale atmospheric CO₂ variability during the last glacial period. *Geophysical Research Letters*, 45(15), 7731-7740.
- Bazzaz, F. A., & Williams, W. E. (1991). Atmospheric CO₂ concentrations Within a Mixed Forest: Implications for Seedling Growth. *Ecology*, 72(1), 12-16.
- Beerling, D. J., & Royer, D. L. 2002. Fossil plants as indicators of the Phanerozoic global carbon cycle. *Annual Review of Earth and Planetary Sciences*, 30(1), 527-556.
- Beilstein, M. A., Nagalingum, N. S., Clements, M. D., Manchester, S. R., & Mathews, S. (2010). Dated molecular phylogenies indicate a Miocene origin for *Arabidopsis thaliana*. *Proceedings of the National Academy of Sciences*, 107(43), 18724-18728.
- Bowman, W. D., Hubick, K. T., von Caemmerer, S., & Farquhar, G. D. (1989). Short-term changes in leaf carbon isotope discrimination in salt-and water-stressed C₄ grasses. *Plant physiology*, 90(1), 162-166.
- Bonal, D., Born, C., Brechet, C., Coste, S., Marcon, E., Roggy, J. C., & Guehl, J. M. (2007). The successional status of tropical rainforest tree species is associated with differences in leaf carbon isotope discrimination and functional traits. *Annals of Forest Science*, 64(2), 169-176.
- Condon, A. G., Richards, R. A., & Farquhar, G. D. (1992). The effect of variation in soil water availability, vapour pressure deficit and nitrogen nutrition on carbon isotope discrimination in wheat. *Australian Journal of Agricultural Research*, 43(5), 935-947.
- Cornwell, W. K., Wright, I. J., Turner, J., Maire, V., Barbour, M. M., Cernusak, L. A., Dawson, T., Ellsworth, D., Farquhar, G.D., Griffiths, H., Keitel, C., Knohl, A., Reich, P.B., Williams, D.G., Bhaskar, R., Cornelissen, J.H.C., Richards, A., Schmidt, S., Valladares, F., Korner, C., Schulze, E-D., Buchmann, N., & Santiago, L.S. (2018). Climate and soils together regulate photosynthetic carbon isotope discrimination within C₃ plants worldwide. *Global Ecology and Biogeography*, 27(9), 1056-1067.
- Cui, Y., & Schubert, B. A. (2016). Quantifying uncertainty of past pCO₂ determined from changes in C₃ plant carbon isotope fractionation. *Geochimica et Cosmochimica Acta*, 172, 127-138.
- Cui, Y., & Schubert, B. A. (2017). Atmospheric pCO₂ reconstructed across five early Eocene global warming events. *Earth and Planetary Science Letters*, 478, 225-233.
- Cui, Y., Schubert, B. A., & Jahren, A. H. (2020). A 23-my record of low atmospheric CO₂. *Geology*, 48, (9), 888-892.

- Dawson, T. E., Mambelli, S., Plamboeck, A. H., Templer, P. H., & Tu, K. P. (2002). Stable isotopes in plant ecology. *Annual review of ecology and systematics*, 33(1), 507-559.
- Diefendorf, A. F., Mueller, K. E., Wing, S. L., Koch, P. L., & Freeman, K. H. (2010). Global patterns in leaf ^{13}C discrimination and implications for studies of past and future climate. *Proceedings of the National Academy of Sciences*, 107(13), 5738-5743.
- Diefendorf, A. F., Freeman, K. H., Wing, S. L., Currano, E. D., & Mueller, K. E. (2015). Paleogene plants fractionated carbon isotopes similar to modern plants. *Earth and Planetary Science Letters*, 429, 33-44.
- Diefendorf, A. F., & Freimuth, E. J. (2017). Extracting the most from terrestrial plant-derived n-alkyl lipids and their carbon isotopes from the sedimentary record: A review. *Organic Geochemistry*, 103, 1-21.
- Eggleston, S., Schmitt, J., Bereiter, B., Schneider, R., & Fischer, H. (2016). Evolution of the stable carbon isotope composition of atmospheric CO_2 over the last glacial cycle. *Paleoceanography*, 31(3), 434-452.
- Ehleringer, J. R., & Cerling, T. E. (1995). Atmospheric CO_2 and the ratio of intercellular to ambient CO_2 concentrations in plants. *Tree physiology*, 15(2), 105-111.
- Elsig, J., Schmitt, J., Leuenberger, D., Schneider, R., Eyer, M., Leuenberger, M., ... & Stocker, T. F. (2009). Stable isotope constraints on Holocene carbon cycle changes from an Antarctic ice core. *Nature*, 461(7263), 507-510.
- Farquhar, G. D., & Richards, R. A. (1984). Isotopic composition of plant carbon correlates with water-use efficiency of wheat genotypes. *Functional Plant Biology*, 11(6), 539-552.
- Farquhar, G. D., Ehleringer, J. R., & Hubick, K. T. (1989). Carbon isotope discrimination and photosynthesis. *Annual review of plant biology*, 40(1), 503-537.
- Feng, X. (1999). Trends in intrinsic water-use efficiency of natural trees for the past 100–200 years: a response to atmospheric CO_2 concentration. *Geochimica et Cosmochimica Acta*, 63(13-14), 1891-1903.
- Fick, S. E., & Hijmans, R. J. (2017). WorldClim 2: new 1-km spatial resolution climate surfaces for global land areas. *International journal of climatology*, 37(12), 4302-4315.
- Franks, P., Adams, M., Amthor, J. S., Barbour, M., Berry, J., Ellsworth, D. S, Ghannoum, O., Lloyd, J., Lloyd, J., McDowell, N.G., Norby, R.J., Tissue, D., von Caemmerer, S., & Farquhar, G.D. (2013). Sensitivity of plants to changing atmospheric CO_2 concentration: from the geological past to the next century. *New Phytologist*, 197(4), 1077-1094.
- Franks, P. J., Royer, D. L., Beerling, D. J., Van de Water, P. K., Cantrill, D. J., Barbour, M. M., & Berry, J. A. (2014). New constraints on atmospheric CO_2 concentration for the Phanerozoic. *Geophysical Research Letters*, 41(13), 4685-4694.

- Giguère-Croteau, C., Boucher, É., Bergeron, Y., Girardin, M. P., Drobyshev, I., Silva, L. C., Hélie, J-F. & Garneau, M. (2019). North America's oldest boreal trees are more efficient water users due to increased [CO₂], but do not grow faster. *Proceedings of the National Academy of Sciences*, 116(7), 2749-2754.
- Guehl, J. M., Fort, C., & Ferhi, A. (1995). Differential response of leaf conductance, carbon isotope discrimination and water-use efficiency to nitrogen deficiency in maritime pine and pedunculate oak plants. *New Phytologist*, 131(2), 149-157.
- Hickler, T., Smith, B., Prentice, I. C., Mjöfors, K., Miller, P., Arneth, A., & Sykes, M. T. (2008). CO₂ fertilization in temperate FACE experiments not representative of boreal and tropical forests. *Global Change Biology*, 14(7), 1531-1542.
- Högberg, P., Johannisson, C., & Hällgren, J. E. 1993. Studies of ¹³C in the foliage reveal interactions between nutrients and water in forest fertilization experiments. *Plant and Soil*, 152(2), 207-214.
- Jones, T. H., Thompson, L. J., Lawton, J. H., Bezemer, T. M., Bardgett, R. D., Blackburn, T. M., ... & Howson, G. 1998. Impacts of rising atmospheric carbon dioxide on model terrestrial ecosystems. *Science*, 280(5362), 441-443.
- Kaplan, J. O., Prentice, I. C., & Buchmann, N. (2002). The stable carbon isotope composition of the terrestrial biosphere: Modeling at scales from the leaf to the globe. *Global Biogeochemical Cycles*, 16(4), 8-1.
- Keeling, C.D., Piper, S.C., Bacastow, R.B., Wahlen, M., Whorf, T.P., Heimann, M., & Meijer, H.A. 2005. Atmospheric CO₂ and ¹³CO₂ exchange with the terrestrial biosphere and oceans from 1978 to 2000: Observations and carbon cycle implications. In *A history of atmospheric CO₂ and its effects on plants, animals, and ecosystems* (pp. 83-113). Springer, New York, NY.
- Kohn, M. J. (2010). Carbon isotope compositions of terrestrial C₃ plants as indicators of (paleo) ecology and (paleo) climate. *Proceedings of the National Academy of Sciences*, 107(46), 19691-19695.
- Kohn, M. J. (2016). Carbon isotope discrimination in C₃ land plants is independent of natural variations in pCO₂. *Geochemical Perspectives Letters*, 2(1), 35-43.
- Lomax, B. H., Lake, J. A., Leng, M. J., & Jardine, P. E. (2019). An experimental evaluation of the use of Δ¹³C as a proxy for palaeoatmospheric CO₂. *Geochimica et Cosmochimica Acta*, 247, 162-174.
- Long, S. P., Ainsworth, E. A., Leakey, A. D., Nösberger, J., & Ort, D. R. (2006). Food for thought: lower-than-expected crop yield stimulation with rising CO₂ concentrations. *Science*, 312(5782), 1918-1921.

- Looy, C., Kerp, H., Duijnste, I., & DiMichele, B. (2014). The late Paleozoic ecological-evolutionary laboratory, a land-plant fossil record perspective. *The Sedimentary Record*, 12(4), 4-18.
- Macfarling Meure, C., Etheridge, D., Trudinger, C., Steele, P., Langenfelds, R., Van Ommen, T., Smith, A. & Elkins, J. (2006). Law Dome CO₂, CH₄ and N₂O ice core records extended to 2000 years BP. *Geophysical Research Letters*, 33(14).
- McElwain, J. C. (2018). Paleobotany and global change: Important lessons for species to biomes from vegetation responses to past global change. *Annual review of plant biology*, 69, 761-787.
- Merven, C. (2015). *Isotope ecology of temperate conifers* (Masters' Thesis, University of Michigan, Ann Arbor, MI, United States of America).
- McKee, K. L., Feller, I. C., Popp, M., & Wanek, W. (2002). Mangrove isotopic ($\delta^{15}\text{N}$ and $\delta^{13}\text{C}$) fractionation across a nitrogen vs. phosphorus limitation gradient. *Ecology*, 83(4), 1065-1075.
- Mueller, K. E., Blumenthal, D. M., Pendall, E., Carrillo, Y., Dijkstra, F. A., Williams, D. G., Follett R. F., & Morgan, J. A. (2016). Impacts of warming and elevated CO₂ on a semi-arid grassland are non-additive, shift with precipitation, and reverse over time. *Ecology Letters*, 19(8), 956-966.
- Norby, R. J., & Zak, D. R. (2011). Ecological lessons from free-air CO₂ enrichment (FACE) experiments. *Annual Review of Ecology, Evolution, and Systematics*, 42, 181-203.
- Nowak, R. S., Ellsworth, D. S., & Smith, S. D. (2004). Functional responses of plants to elevated atmospheric CO₂—do photosynthetic and productivity data from FACE experiments support early predictions? *New Phytologist*, 162(2), 253-280.
- Peñuelas, J., & Azcón-Bieto, J. (1992). Changes in leaf $\Delta^{13}\text{C}$ of herbarium plant species during the last 3 centuries of CO₂ increase. *Plant, Cell & Environment*, 15(4), 485-489.
- PRISM Climate Group, Oregon State University, <http://prism.oregonstate.edu>, created 4 Feb 2004.
- Proctor, M. C. F., Raven, J. A., & Rice, S. K. (1992). Stable carbon isotope discrimination measurements in *Sphagnum* and other bryophytes: physiological and ecological implications. *Journal of Bryology*, 17(2), 193-202.
- Qiaoping, X., Fajon, A., Zhenyu, L., Likuo, F., & Zhengyu, L. (2002). *Thuja sutchuenensis*: a rediscovered species of the Cupressaceae. *Botanical Journal of the Linnean Society*, 139(3), 305-310.
- Reich, P. B., Hungate, B. A., & Luo, Y. (2006). Carbon-nitrogen interactions in terrestrial ecosystems in response to rising atmospheric carbon dioxide. *Annual Review of Ecology, Evolution, and Systematics*, 37, 611-636.

- Royer, D. L., Berner, R. A., Montañez, I. P., Tabor, N. J., & Beerling, D. J. (2004). CO₂ as a primary driver of Phanerozoic climate. *GSA today*, 14(3), 4-10.
- Royles, J., Amesbury, M. J., Roland, T. P., Jones, G. D., Convey, P., Griffiths, H., Hodgson, D.A., & Charman, D. J. (2016). Moss stable isotopes (carbon-13, oxygen-18) and testate amoebae reflect environmental inputs and microclimate along a latitudinal gradient on the Antarctic Peninsula. *Oecologia*, 181(3), 931-945.
- Rundel, P. W., Stichler, W., Zander, R. H., & Ziegler, H. (1979). Carbon and hydrogen isotope ratios of bryophytes from arid and humid regions. *Oecologia*, 44(1), 91-94.
- Saurer, M., Siegwolf, R. T., & Schweingruber, F. H. (2004). Carbon isotope discrimination indicates improving water-use efficiency of trees in northern Eurasia over the last 100 years. *Global Change Biology*, 10(12), 2109-2120.
- Schlanser, K., Diefendorf, A. F., Greenwood, D. R., Mueller, K. E., West, C. K., Lowe, A. J., Basinger, J. F., Currano, E. D., Flynn, A. G., Fricke, H. C., Geng, J., Meyer, H. W., Peppe, D. J. (2020). On geologic timescales, plant carbon isotope fractionation responds to precipitation similarly to modern plants and has a small negative correlation with pCO₂. *Geochimica et Cosmochimica Acta*, 270, 264-281.
- Schubert, B. A., & Jahren, A. H. (2012). The effect of atmospheric CO₂ concentration on carbon isotope fractionation in C₃ land plants. *Geochimica et Cosmochimica Acta*, 96, 29-43.
- Shen, D., Sun, H., Huang, M., Zheng, Y., Qiu, Y., Li, X., & Fei, Z. (2013). Comprehensive analysis of expressed sequence tags from cultivated and wild radish (*Raphanus* spp.). *BMC genomics*, 14(1), 721.
- Sheldon, N. D., Smith, S. Y., Stein, R., & Ng, M. (2020). Carbon isotope ecology of gymnosperms and implications for paleoclimatic and paleoecological studies. *Global and Planetary Change*, 184, 103060.
- Stein, R. A., Sheldon, N. D., & Smith, S. (2019). Rapid response to anthropogenic climate change by *Thuja occidentalis*: implications for past climate reconstructions and future climate predictions. *PeerJ*, 7, e7378.
- Tipple, B. J., Meyers, S. R., & Pagani, M. (2010). Carbon isotope ratio of Cenozoic CO₂: A comparative evaluation of available geochemical proxies. *Paleoceanography*, 25(3), PA3202.
- White, J.W.C., Vaughn, B.H., Michel, S.E. (2015). University of Colorado, Institute of Arctic and 720 Alpine Research (INSTAAR), Stable Isotopic Composition of Atmospheric Carbon Dioxide (¹³C and ¹⁸O) from the NOAA ESRL Carbon Cycle Cooperative Global Air Sampling Network, 722 1990-2014, Version: 2015-10-26.
- Yan, W., Zhong, Y., & Shangguan, Z. (2017). Contrasting responses of leaf stomatal characteristics to climate change: a considerable challenge to predict carbon and water cycles. *Global Change Biology*, 23(9), 3781-3793.

CHAPTER IV

Soil Carbon Isotope Values and Paleo-Precipitation Reconstruction³

4.1 Abstract

Anthropogenic climate change has significant impacts at the ecosystem scale including widespread drought, flooding, and other natural disasters related to precipitation extremes. To contextualize modern climate change, scientists often look to ancient environmental changes, such as shifts to ancient precipitation ranges. Previous studies have used fossil leaf organic chemistry and paleosol inorganic chemistry as paleo-precipitation proxies, but have largely ignored the organic soil layer, which acts as a bridge between aboveground biomass and belowground inorganic accumulation, as a potential recorder of precipitation. We investigate the relationship between carbon isotope values in soil organic matter ($\delta^{13}\text{C}_{\text{SOM}}$) and a variety of seasonal and annual climate parameters in modern ecosystems and find a significant relationship between $\delta^{13}\text{C}_{\text{SOM}}$ values and mean annual precipitation (MAP). After testing the relationship between actual and reconstructed precipitation values in modern systems, we test this potential paleo-precipitation proxy in the geologic record by comparing precipitation values reconstructed using $\delta^{13}\text{C}_{\text{SOM}}$ to other reconstructed paleoprecipitation values based on the same paleosols. This study provides a promising new proxy that can be applied to ecosystems post-Devonian to the Miocene, and in mixed C_3/C_4 ecosystems in the geologic record with additional paleobotanical and palynological information. It also extends paleo-precipitation reconstruction to more weakly developed paleosol types, such as those lacking B- horizons, than previous inorganic proxies and is calibrated for wetter environments.

4.2 Introduction

Anthropogenic climate change has caused major shifts in global and regional precipitation regimes (IPCC 2007), and it is imperative that we understand the impacts these

³Submitted to *Paleoceanography & Paleoclimatology* under the citation:
Stein, R. A., Sheldon, N. D., & Smith, S. Soil carbon isotope values can be used to reconstruct paleo-precipitation.

shifts have on ecosystems to drive effective conservation. In addition to being a fundamental necessity to life, precipitation and subsequent plant water availability controls ecosystems' distribution and health and the magnitude of soil carbon sinks (Cotton et al. 2013). Major changes in precipitation could cause complete turnover of ecosystems; our understanding of the impacts of global climate change on future precipitation distributions is often influenced by ancient precipitation changes, especially as they relate to recorded ecosystem turnover.

In order to reconstruct ancient precipitation, we use clues from the geologic record, often in the form of chemical records in sediments or preserved micro- and macro geology (Thompson et al. 1999; Shucheng & Evershed 2001; Stinchcomb et al. 2016). Ancient precipitation patterns clarify changes in precipitation as a function of modern climate change, and can affect climate model outputs (Dai 2006). They also inform interpretations of other parameters, including paleo-topography and soil CO₂ concentration (Cerling et al. 1991; Cerling et al. 1992; Ekart et al. 1999; Breecker et al. 2009). Furthermore, paleo-precipitation plays an important role in our understanding of paleo-temperature reconstructions (Gallagher et al. 2019), as the magnitude and timing of precipitation constrains the effects of ground heating in soils and the offset between water temperature and air temperate in lakes (Hren and Sheldon, 2012).

Previous workers have used $\delta^{13}\text{C}$ values of aboveground plant mass ($\delta^{13}\text{C}_{\text{leaf}}$) to reconstruct precipitation (Weiguo et al. 2005; Youfeng et al. 2008; Wang et al. 2013). This approach relies on the premise that $\delta^{13}\text{C}_{\text{leaf}}$ values are linked to water availability because stomata (leaf pores) are the centralized location where plant-atmosphere gas exchange occurs, including associated processes such as carbon isotope fractionation and transpiration (Livingston & Spittlehouse 1996; Farquhar 1989; Arens et al. 2000). This relationship has been substantiated by empirical studies, which have demonstrated a reasonably strong logarithmic relationship between carbon isotope discrimination in C₃ plants (Δ_{leaf} , Equation 4.1) and mean annual precipitation ($\Delta_{\text{leaf}} = 5.54(\log\text{MAP}) + 4.07$; $R^2 = 0.55$, p-value < 0.001; Diefendorf et al. 2010; Kohn et al. 2010).

$$\text{Equation (4.1)} \quad \Delta_{\text{leaf}} = \frac{\delta^{13}\text{C}_{\text{atm}} - \delta^{13}\text{C}_{\text{leaf}}}{\left(1 + \frac{\delta^{13}\text{C}_{\text{leaf}}}{1000}\right)}$$

These meta-analyses indicate a systemic relationship between water availability and plant isotope discrimination, but this relationship does not carry over on a species-specific scale (Stein et al. 2019; Sheldon et al. 2020; Stein et al. in press). Within any given precipitation regime, there is significant variation in $\delta^{13}\text{C}_{\text{leaf}}$ values among plants, and for any given taxon, the $\delta^{13}\text{C}_{\text{leaf}}$ values are essentially invariant regardless of whether the plant is growing in wetter or dryer conditions. Instead, $\delta^{13}\text{C}_{\text{leaf}}$ values reflect species-specific C isotope discrimination behavior and the atmospheric input isotopic composition (Stein et al., 2019; Sheldon et al. 2020; Stein et al. in press). Thus, the meta-relationship observed reflects the integration of the whole ecosystem, rather than any individual taxon's behavior (Sheldon et al. 2020). This makes it difficult to apply the directly measured $\delta^{13}\text{C}_{\text{leaf}}$ values of geologic plants (Kohn 2010) or reconstructed $\delta^{13}\text{C}_{\text{leaf}}$ values based on fossil teeth (Quade et al. 1995; Wang et al. 2008; Passey 2017) as paleo-precipitation proxies without taxonomic identification. However, an aggregated record of an ecosystem (i.e. carbon isotope values of soil, $\delta^{13}\text{C}_{\text{SOM}}$, or the difference between the carbon isotope value of the atmosphere and of soil; Δ_{SOM} ; Equation 4.2) should demonstrate a similar but taxonomically independent relationship as the meta-analyses demonstrated. We propose that soils act as the “great integrator,” and that organic matter can be used as an average of the aboveground ecosystem (Powell et al. 2012; Sheldon et al. 2020). This has been previously demonstrated by water isotopes (Deuterium, $\delta^2\text{H}$ or δD , and oxygen, $\delta^{18}\text{O}$) recorded in topsoil along a precipitation transect, where topsoil water isotope values reflected the isotopic value of incoming precipitation (Struck et al. 2020). We expect that the relationship between carbon isotope values in leaves ($\delta^{13}\text{C}_{\text{leaf}}$) and precipitation will also be recorded as carbon isotopic values in surface-most soil organic matter ($\delta^{13}\text{C}_{\text{SOM}}$ values).

$$\Delta_{\text{SOM}} = \frac{\delta^{13}\text{C}_{\text{atm}} - \delta^{13}\text{C}_{\text{SOM}}}{\left(1 + \frac{\delta^{13}\text{C}_{\text{SOM}}}{1000}\right)} \text{ (Equation 4.2)}$$

Previous studies have evaluated the relationship between weathering and precipitation in soils, based on the principle that increased precipitation drives increased chemical weathering and leaching of nutrients (Stewart et al. 2001), which consequently affects soil geochemistry and soil horizonization. The link between weathering and precipitation is an additional reason to expect a demonstrable relationship between mean annual precipitation and soil chemistry. This idea has been evaluated in distribution of mobile versus immobile inorganic compounds,

although it has largely been untested using organic compounds. Past work has used quantifiable weathering (via chemistry) to reconstruct precipitation (CIA, CIA-K, CALMAG, PPM_{1.0}; Jenny & Leonard 1934; Retallack 1994; Royer 2001; Sheldon et al. 2002; Nordt & Driese 2010; Stinchcomb et al. 2016; Beverly et al. 2018). Each of these methods for precipitation reconstruction has been applied as a paleoprecipitation proxy, but as tested in modern conditions, each are confined to certain precipitation regimes or soil types (Jenny & Leonard 1934; Retallack 1994; Royer 2001; Sheldon et al. 2002; Nordt & Driese 2010), except for PPM_{1.0} (paleosol-paleoclimate model), a nonlinear spline and partial least squares regression model. Although PPM_{1.0} is generalizable for many soil types, this tool trades versatility for high error and uncertainty (Stinchcomb et al. 2016). The error associated with each of these soil paleoprecipitation proxies increases in soils that receive > 1500 mm yr⁻¹, such as sub-tropical and tropical soils. This limits these proxies during paratropical climate regimes, which are common during geologic times, including the Eocene and many earlier, pre-Cenozoic times (Harrington et al. 2004).

We aim to provide a new tool using organic geochemistry in soils ($\delta^{13}\text{C}_{\text{SOM}}$, Δ_{SOM}) that can be used to supplement existing paleoprecipitation tools in organic-rich land ecosystems and settings with weaker soil formation. This tool, which should be less susceptible to high precipitation error due to leaching than inorganic proxies, can improve the accuracy of paleoprecipitation reconstruction in high rainfall regimes.

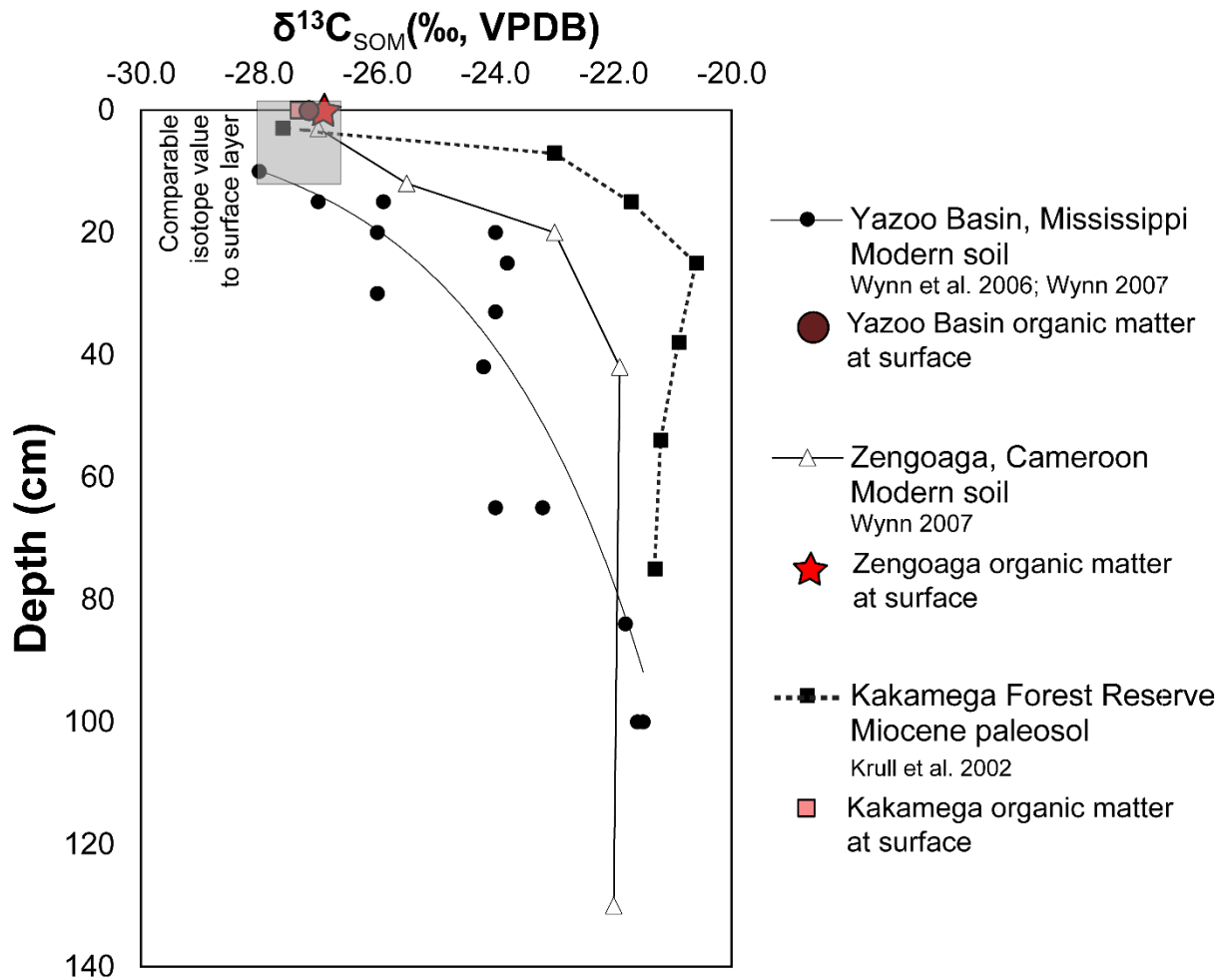


Figure 4.1: Modern soils from Wynn (2007) and a paleosol from Krull et al. (2002), displaying carbon isotope values ($\delta^{13}\text{C}_{\text{SOM}}$) with depth, demonstrating Rayleigh distillation processes. The surface values are shown in red symbols at 0m. The zone where organic carbon isotope values are comparable to the surface for these soils is shown in transparent grey box (up to ~10cm in depth).

Similar to chemical weathering and sub-surface horizon development, $\delta^{13}\text{C}_{\text{SOM}}$ is not constant with depth. While topsoil should reflect the above and belowground biomass coming into the system directly, as organic matter is buried, the carbon chemical composition of the soil changes, and processes like microbial recycling and oxidation (driving Rayleigh distillation) cause isotope enrichment through the profile, stabilizing in the B- horizon (e.g. ~70 cm depth; Wynn 2007; Fig. 4.1). This Rayleigh distillation is not constant between all soils; for example, disparate texture results in different carbon isotope changes with depth (Krull et al. 2005). However, as Figure 1 shows, the O horizon and uppermost A horizon of soils closely matches

the vegetation. To evaluate $\delta^{13}\text{C}_{\text{SOM}}$ as a precipitation proxy, we conducted $\delta^{13}\text{C}$ analyses specifically on O-horizon (topsoil) soils from three specific ecosystems (dominated by *Thuja occidentalis*, *Thuja plicata* and *Populus tremuloides*) across a climosequence and supplemented these ecosystem-specific soils with modern $\delta^{13}\text{C}$ values of organic topsoil layers from the literature. We tested the applicability of the new proxy by comparing reconstructed results from Paleozoic-Cenozoic paleosols that had independent paleo-precipitation estimates.

4.3 Methods

We collected O-horizon soils as well as living leaves from tree branches from *Thuja occidentalis* (northern white cedar, including six branchlets and 20 soils), *Thuja plicata* (Pacific red cedar, including three leaves and five soils), and *Populus tremuloides* (quaking aspen, including nine leaves and 23 soils) dominated ecosystems in 15 locations (Fig. 2) using a 2 ¼" diameter auger ($n = 67$) to compare $\delta^{13}\text{C}_{\text{SOM}}$ values in conifer and angiosperm-dominated ecosystems, respectively. We determined these locations for collection based on sampling a precipitation gradient and with the assistance of the iNaturalist citizen science observation application (iNaturalist 2018) to find exact locations of these specific tree species.

Upon collection, soils were dried in a 50°C oven to eliminate risk of continued respiration and alteration of isotopic values. Soils were brought to the Earth Systems Science (ESS) Laboratory at the University of Michigan, Ann Arbor, acidified in 5% dilute hydrochloric acid (HCl) solution on a 50°C hotplate to remove authigenic or inherited carbonate, and allowed to settle out for 30 minutes. Excess liquid was removed with transfer pipettes. This process was repeated three times and/or until soils did not exhibit further reactivity to HCl. Soils were rinsed with deionized water as many times as they were exposed to HCl (e.g., three times for three HCl baths, five times for five HCl baths) to remove all excess HCl, then placed in a 50°C oven to dry again.

Soils were loaded into tin capsules and run on low carbon setting (20–200 ppm) on a Picarro G2201-i cavity ring down spectrometer (CRDS; replicate standard deviation $\pm 0.3\text{‰}$). Results were calibrated using internal laboratory acetanilide standards (-28.17‰) ranging from 0.100 mg to 1.400 mg, and run with additional standards calibrated by the International Atomic

Energy Agency: IAEA-CH-6 (-10.45‰; sucrose) and IAEA-600 (-27.77‰; caffeine), as well as additional internal laboratory standards: homogenized sugar from C₃ sugarbeet (-26.14‰) and C₄ sugarcane (-12.71‰).

We aggregated climate data (mean annual temperature, maximum summer temperature, vapor pressure deficit, mean annual precipitation, growing season precipitation) for all soils collected for this study using data interpolated on a 10-km scale from PRISM Climate Group through Oregon State University (PRISM Climate Group 2014). We also compared isotopic values to CO₂ gas concentrations collected from ice cores (pre-1958; Etheridge et al. 1998) and Mauna Loa Observatory's *in situ* atmospheric CO₂ measurements (post-1958; Keeling & Whorf 2004; White et al. 2015) from 1900–2017. Because carbon in the O-horizon of soils is recalcitrant, most carbon in soil is hundreds to thousands of years old (Lorenz et al. 2007; Kleber 2010). Therefore, when calculating Δ_{SOM} (Equation 4.2), we used a fixed Pre-Industrial $\delta^{13}\text{C}_{\text{atm}}$ value (-6.5‰).

To supplement soils collected through the ESS Lab at the University of Michigan, we collated organic carbon isotope values from previous studies with included climate data (n = 106; Supp. Table C1; Supp. Table C3; Fig. 4.2). For any missing climate information for soils from the contiguous United States in the original publications, we supplemented using PRISM Climate Group's interpolated values and other sources (see Supp. Table C3). We collected values only for soils that had been treated to remove carbonate.

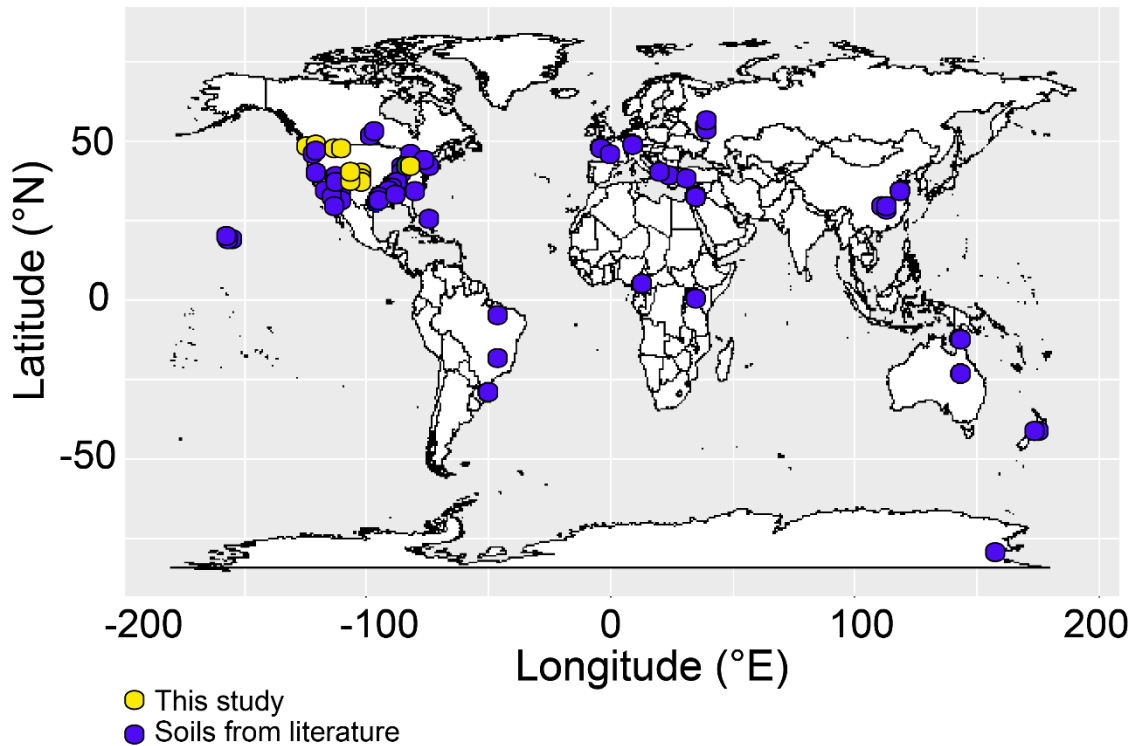


Figure 4.2 Map of modern soils. Yellow circles indicate soils collected by the Earth Systems Science Lab at the University of Michigan; dark blue circles are values collated from previous studies.

Additionally, we collected organic carbon isotope values from geological literature for paleosol analyses ($n = 62$; Cerling et al. 1992; Mora et al. 1996; Hatte et al. 2001; Nordt et al. 2002; Pustovoytov & Terhorst 2004; Sheldon 2006; Gutierrez & Sheldon 2012; Hyland & Sheldon 2013; Harris et al. 2017; Lukens et al. 2017; Tabor et al. 2017; Supp. Fig. C5; Supp. Table C3). $\delta^{13}\text{C}_{\text{SOM}}$ -reconstructed results provided without coeval precipitation estimates (sometimes from other publications) were excluded.

4.4 Results

There was a significant logarithmic relationship between $\delta^{13}\text{C}_{\text{SOM}}$ and mean annual precipitation within studied soils ($\delta^{13}\text{C}_{\text{SOM}} = -2.04 \ln(\text{MAP}) - 11.99$; $R^2 = 0.68$; $p\text{-value} < 0.001$; Fig. 4.3). There was also a strong relationship between Δ_{SOM} and mean annual precipitation

($\Delta_{\text{SOM}} = -2.14\ln(\text{MAP}) + 5.37$; $R^2 = 0.64$; $p\text{-value} = 1.29 \times 10^{-38}$; Fig. 4). There was a demonstrable relationship between growing season precipitation (mm yr^{-1}) and $\delta^{13}\text{C}_{\text{SOM}}$ ($\delta^{13}\text{C}_{\text{SOM}} = -0.90\ln(\text{GSP}) - 20.08$, $R^2 = 0.24$; $p\text{-value} = 4.44 \times 10^{-7}$; Supp. Fig. C2), but this relationship was only modestly predictive. To determine outliers, we excluded all values from the regressions that had residuals from the expected value greater than twice the standard deviation of the mean of all residuals ($n = 3$). We found that the $\delta^{13}\text{C}_{\text{SOM}}$ and Δ_{SOM} values of soils collected in Olympic National Park ($\text{MAP} = 3350 \text{ mm yr}^{-1}$) were outliers—over two standard deviations (0.95%) from the expected values based on the full dataset. Each of these soils had $\delta^{13}\text{C}_{\text{SOM}}$ and Δ_{SOM} values of $>2.00\%$ from expected. All other soils included in this study (both collected in the field for this study, and from literature) were formed at precipitation regimes $<2500 \text{ mm yr}^{-1}$, and the outlier Olympic Peninsula soils collected were sampled at sites with precipitation values of 3350 mm yr^{-1} .

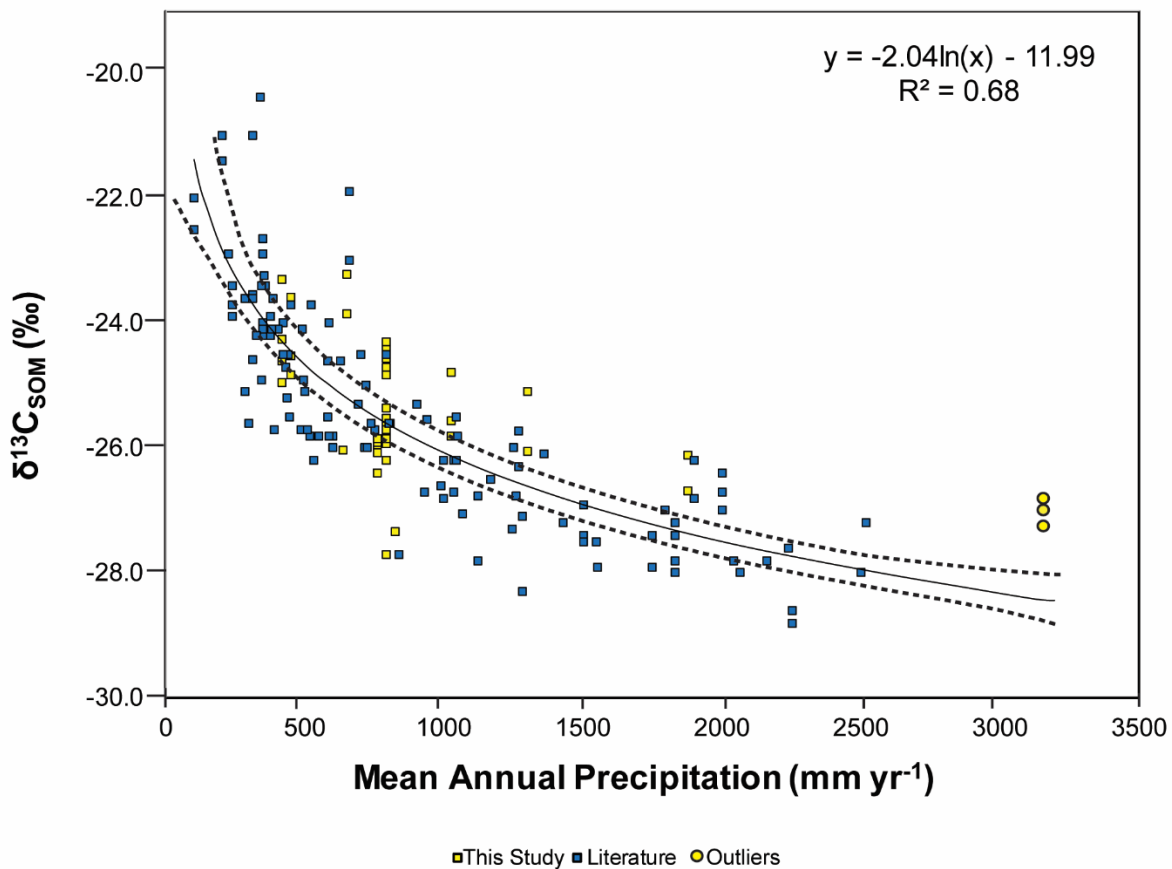


Figure 4.3 $\delta^{13}\text{C}_{\text{SOM}}$ values compared to mean annual precipitation (mm yr^{-1}) for modern soils. New data are shown in yellow squares, literature data is shown in blue squares, and outliers (from our dataset,

measured MAP = 3350 mm yr⁻¹) are shown in yellow circles. 95% confidence intervals are shown in dashed lines.

All other climate variables tested had coefficients of determination that were not strongly predictive ($R^2 \leq 0.25$). Latitude and $\delta^{13}\text{C}_{\text{SOM}}$ values did not have any predictive relationship, though there was a change in range related to region (Fig. 4.4). For elevation, longitude, mean annual temperature, maximum growing season temperature, vapor pressure deficit (annual minimum and maximum), predictive relationships were consistently low (Supplemental Fig. C1). Significance (p-values) and coefficients of determination (R^2 values) for relationships between $\delta^{13}\text{C}_{\text{SOM}}$ values and Δ_{SOM} values and other climate variables are provided in Table 4.1.

Table 4.1 Statistical results (p-value, significance test and R^2 -value, coefficient of determination) for carbon isotope values ($\delta^{13}\text{C}_{\text{SOM}}$ and Δ_{SOM} values) compared to environmental and sampling location variables. Strong predictive relationships ($R^2 > 0.50$) are shown in dark green, moderately predictive relationships (0.25-0.50) are denoted in light green, and weakly predictive relationships are shown in yellow (0.10-0.25). If there was no predictive value in the relationship, it is not highlighted. All relationships that are significant (p-value < 0.001) are shown in light green.

Variable	Unit	p-value		R^2 value	
		$\delta^{13}\text{C}_{\text{SOM}}$ (‰)	Δ_{SOM} (‰)	$\delta^{13}\text{C}_{\text{SOM}}$ (‰)	Δ_{SOM} (‰)
Latitude	°N	<0.001	<0.001	0.10	0.10
Latitude	°	0.02	0.02	0.03	0.03
Longitude	°E	<0.001	<0.001	0.11	0.11
Elevation (m)	meters	<0.001	<0.001	0.25	0.25
Mean Annual Temperature	°C	0.03	0.03	0.04	0.04
Maximum Growing Season Temperature	°C	0.10	0.10	0.03	0.03
Mean Annual Precipitation	mm yr ⁻¹	<0.001	<0.001	0.68	0.64
Growing Season Precipitation	mm / season	<0.001	<0.001	0.24	0.24
Vapor Pressure Deficit Minimum	hPa	<0.001	<0.001	0.15	0.15
Vapor Pressure Deficit Maximum	hPa	0.64	0.64	<0.01	<0.01

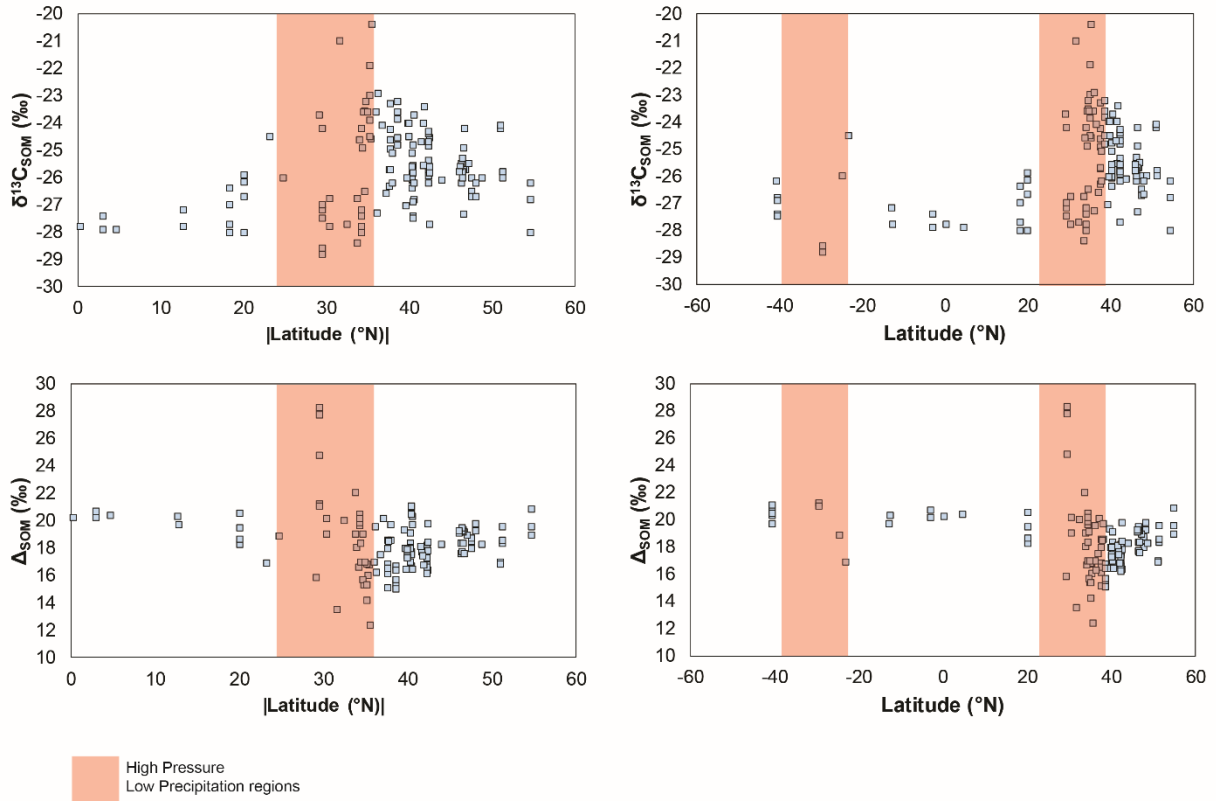


Figure 4.4 The relationship between $\delta^{13}\text{C}_{\text{SOM}}$, Δ_{SOM} and latitude (both absolute value of latitude, or degrees distance from the equator, and actual latitude). Transparent red areas show desert regions as determined by atmospheric convergent and divergent zones.

Previous workers focused on the relationship between $\delta^{13}\text{C}_{\text{leaf}}$ and climate variables found that a multivariate logarithmic regression incorporating both MAP and altitude showed the most predictive relationship with $\delta^{13}\text{C}$ values (Equation 4.3; $R^2 = 0.59$; Diefendorf et al. 2010; Kohn 2010), so we tested this in soils. Modeled after Diefendorf et al.’s multiple regression (Equation 4.3), we evaluated the relationship between Δ_{SOM} , precipitation, and the square root of elevation and found the multiple linear regression less predictive than the MAP-only regression findings (Equation 4.4; $R^2 = 0.62$, $p\text{-value} = 4.48 \times 10^{-32}$; Supp. Table C2).

$$\Delta_{\text{leaf}} = 4.20(\pm 0.26) * \log(\text{MAP}) - 0.06(\pm 0.01) * \sqrt{\text{elevation}} + 9.35(\pm 0.90) \text{ (Equation 4.3)}$$

$$\Delta_{\text{SOM}} = 5.24(\pm 0.57) * \log(\text{MAP}) - 0.01(\pm 0.01) * \sqrt{\text{elevation}} + 4.7; R^2 = 0.62, p\text{-value} = 4.48 \times 10^{-32} \text{ (Equation 4.4)}$$

We conducted multivariate analyses looking at the combined factors between MAP and any variable with a demonstrated single-variable relationship with Δ_{SOM} and $\delta^{13}\text{C}_{\text{SOM}}$ (specific

criteria: $p\text{-value} < 0.001$, $R^2 \geq 0.10$; Table 4.1). None of these relationships was more predictive than that between mean annual precipitation and Δ_{SOM} and/or $\delta^{13}\text{C}_{\text{SOM}}$ alone, but introducing additional variables increases uncertainty, especially with regard to the geologic record (Supp. Table C2).

4.5 Discussion

4.5.1 Overall relationships between climate variables and $\delta^{13}\text{C}_{\text{SOM}}$

There were neither strong nor predictive relationships between $\delta^{13}\text{C}_{\text{SOM}}$ and mean annual temperature, maximum summer temperature, vapor pressure deficit, atmospheric partial pressure of CO_2 ($p\text{CO}_2$), or latitude (R^2 value < 0.25 for all studied climate and spatial variables, p -values included in Supp. Table C2). Some of the variability in $\delta^{13}\text{C}_{\text{SOM}}$ values that is not explained by mean annual precipitation can be explained by elevation ($R^2 = 0.25$), but we cannot discount that this relationship is related to topographic controls on precipitation (Duckstein et al. 1973). It is likely that high temperatures and high vapor pressure deficit and their subsequent impacts on evapotranspiration (resulting in increased water demand from soils and soil drying) during the warm (and presumably growing) season, were counteracted by water availability from the non-growing season months. It is also likely that the highest temperatures originate in tropical regions, where precipitation is high as well, which is why we did not see a relationship between $\delta^{13}\text{C}_{\text{SOM}}$ values and temperature. Complementary multivariate regressions examining the relationship between (MAP + any variable with a statistically significant R^2 value > 0.10 ; see Table 4.1) and Δ_{SOM} did not improve the relationship between MAP alone and carbon isotope values in soil (Supp. Table C2). The inclusion of additional variables for reconstructive purposes, while adding specificity, also adds uncertainty, thus, we propose solely considering MAP for the new $\delta^{13}\text{C}_{\text{SOM}}$ -precipitation proxy. These findings indicate that it is possible to apply $\delta^{13}\text{C}_{\text{SOM}}$ values to reconstruct paleo-precipitation without worrying about interference from other tested climate variables. This is especially useful because many of the other tested variables (elevation, latitude, growing season precipitation, and vapor pressure deficit) are difficult to constrain in the geologic record, and reliance on these additional variables being defined adds more uncertainty and limitations to this proxy.

While there was no predictive relationship between latitude and $\delta^{13}\text{C}_{\text{SOM}}$ or Δ_{SOM} values (Fig. 5; $R^2 < 0.10$), the isotopic variability of soils collected at the horse latitudes ($\sim 30^\circ\text{N}$ and 30°S) was wider (-20 to -29‰) as compared to non-horse latitudes (-23 to -28‰). This variability could be linked to precipitation (discussed further below); precipitation and latitude are interdependent, and at these latitudes, converging dry air masses result in deserts and extremely low precipitation values. As a result, plants growing in the horse latitudes are more stressed and more susceptible to variability in the timing of rainfall, rather than the average annual precipitation. During extended periods of high precipitation, soils are likely to have depleted $\delta^{13}\text{C}_{\text{SOM}}$ signatures and high Δ_{SOM} values, but during long droughts, show enriched $\delta^{13}\text{C}_{\text{SOM}}$ signatures and low Δ_{SOM} values. This variability and wide range of $\delta^{13}\text{C}_{\text{SOM}}$ values between 20°N and 40°S indicate the sensitivity of these regions to drought conditions. The impacts of drought at these latitudes can collapse empires: for example, the end of the Maya Classic Period coincided with a ~ 200 -year period of intense drought as recorded in Lake Chichancanab sediments on the Yucatan Peninsula ($\sim 20^\circ\text{N}$; Hodell et al. 1995; Douglas et al. 2016), so future concentrated work on isotope biogeochemistry in these areas of possible climate stress may allow us to predict humanitarian disasters.

4.5.2 Water availability and $\delta^{13}\text{C}_{\text{SOM}}$

There is a clear and significant relationship between precipitation (both seasonal and annual) and carbon isotope values of soils (as measures of integrated plant values), comparable to the logarithmic trend between precipitation and $\delta^{13}\text{C}_{\text{leaf}}$ values in previous leaf-based meta-analyses (Diefendorf et al. 2010; Kohn 2010). The relationship between the actual measured precipitation and reconstructed precipitation using the new $\delta^{13}\text{C}_{\text{SOM}}$ model was significant (Equation 4.5; Supp. Fig. C3; $R^2 = 0.68$, $p\text{-value} < 0.001$), and most importantly, the slope of the relationship (1.02 ± 0.05) between reconstructed and actual precipitation indicates that our $\delta^{13}\text{C}_{\text{SOM}}$ model predicts reasonable precipitation values. Similarly, although the intercept indicates a modest positive offset of $44.85 (\pm 60.19) \text{ mm yr}^{-1}$ of precipitation between predicted values compared to measured values, this is an insubstantial amount of precipitation when distinguishing between different biomes (Whitaker 1975), and is within error of no offset.

Reconstructed MAP = $1.02(\pm 0.05) * (\text{Actual MAP}) + 44.85 (\pm 60.19)$ (Equation 4.5)

While there is a positive logarithmic relationship between Δ_{SOM} and mean annual precipitation (complementary with the negative logarithmic relationship between $\delta^{13}\text{C}_{\text{SOM}}$ and MAP), it shows slightly weaker predictive value than that seen between $\delta^{13}\text{C}_{\text{SOM}}$ and MAP ($R^2 = 0.64$). Assumptions about $\delta^{13}\text{C}_{\text{atm}}$ values introduce uncertainty in calculating Δ_{SOM} related to age and homogeneity of the atmosphere. First, soil organic matter is hundreds to thousands of years old (e.g., Trumbore 2000) and turns over slowly; this means that $\delta^{13}\text{C}_{\text{atm}}$ values were not constant throughout the lifetime of soil organic carbon. We used set pre-Industrial values (-6.5‰) as the most widely representative value, but the rapidly changing $\delta^{13}\text{C}_{\text{atm}}$ values introduce some noise and uncertainty into the data (Sanderman et al. 2017). However, we have no evidence that $\delta^{13}\text{C}_{\text{atm}}$ values have changed at such an unprecedented rate as today (Tippie et al. 2010), so this noise should not be problematic in the geologic record (Keeling 1979). Secondly, because of micro-environmental variability in $\delta^{13}\text{C}_{\text{atm}}$ related to differences in topography and regional, $\delta^{13}\text{C}_{\text{atm}}$ values close to the soil surface are heterogeneous (Francey et al. 1985; Broadmeadow et al. 1992) and can exceed the variability in $\delta^{13}\text{C}_{\text{atm}}$ on the timescale of soil collection. $\delta^{13}\text{C}_{\text{atm}}$ is important for reconstructions, but $\delta^{13}\text{C}_{\text{atm}}$ is not well-constrained in the geologic record at short (<10 ka) timescales, and soil carbon spans hundreds to thousands of years in age. Therefore, during times with dynamic climate atmospheric C changes (e.g. glacial-interglacial periods, Paleocene-Eocene transition, middle Miocene climatic optimum; Tippie et al. 2010), it is recommended to use the $\delta^{13}\text{C}_{\text{SOM}}$ -MAP, but not Δ_{SOM} -MAP, relationship to reconstruct mean annual precipitation (useful adjustments using the independent foraminiferal-derived $\delta^{13}\text{C}_{\text{atm}}$ proxy that spans the Cenozoic are discussed below).

There is a negative logarithmic relationship between $\delta^{13}\text{C}_{\text{SOM}}$ values and growing season precipitation (GSP) but this relationship is weaker than that observed between $\delta^{13}\text{C}_{\text{SOM}}$ and mean annual precipitation ($\delta^{13}\text{C}_{\text{SOM}} = -0.90(\text{GSP}) - 20.08$; $R^2 = 0.24$; Supp. Fig. C2a). Some of the relationship can be explained by the high correlation between growing season precipitation and mean annual precipitation (p-value < 0.001 , $R^2 = 0.57$; Supp. Fig. C2b). The muted relationship between GSP and isotopic fractionation compared to mean annual precipitation demonstrates the importance of soil water storage to growth season productivity even when this water is accrued

during plant dormancy (e.g. snowmelt, wintertime precipitation, etc.). Previous workers have demonstrated variability in moisture deficit that does not necessarily correspond to peak growing season or dormancy (Tabor et al. 2013; Gallagher et al. 2016). The new results reaffirm the importance of non-growing season precipitation (e.g. soil water, frozen soil water, snowpack) in providing water ultimately used by plants during the subsequent growing season.

4.5.3 A case study in the geologic record

In order to test the veracity of this paleoprecipitation proxy in the geologic record, we reconstructed paleo-precipitation using the modern $\delta^{13}\text{C}_{\text{SOM}}$ -model for a number of paleosols described in the literature. The applications of this proxy to the geologic record are limited by development and preservation of soil horizons, so we compared $\delta^{13}\text{C}_{\text{SOM}}$ -paleoprecipitation values based on upper (O- and A-; undistinguished) horizons with MAP reconstructed using other paleoprecipitation proxies (Fig. 4.6). The comparative proxies included CIA-K (Sheldon et al. 2002), CALMAG (Nordt & Driese 2010), depth to Bk horizons (Retallack 2005), leaf area index (LAI; Pfeifer et al. 2012) and CLAMP (Spicer et al. 2009), with physiognomic data called “flora” and semi-quantitative methods (e.g. existence of carbonate, types of vegetation) are categorized as “other” (Supp. Fig. C7). Some of the methods used for comparison, like CIA-K and LAI, are thought to under-predict precipitation related to over-representation of clay content and taphonomic bias favoring preservation of small leaves, respectively (Spicer 2000; Stinchcomb et al. 2016). CLAMP, on the other hand, has been shown to overpredict mean annual precipitation in modern forests, due to the approximation of statistical fits associated with this tool (Wilf et al. 1998). The slope of the relationship (1.01) between precipitation reconstructed using other proxies and $\delta^{13}\text{C}_{\text{SOM}}$ values is very close to 1, indicating that relative changes in precipitation reconstructed using both proxies are approximately equal. Despite these stipulations for other paleoprecipitation proxies, the quality of comparison between $\delta^{13}\text{C}_{\text{SOM}}$ -paleoprecipitation and paleoprecipitation values reconstructed using other established proxies was random, not systematically biased depending on the proxy (Supp. Fig. C7). In this study, the $\delta^{13}\text{C}_{\text{SOM}}$ -reconstructed values produce higher MAP reconstructions than other proxies by 373 mm yr^{-1} , but this over-prediction is still within the standard error (400 mm yr^{-1}) of an exact 1:1 relationship and it is unclear whether this is systemic based on individual alternate proxy errors

or $\delta^{13}\text{C}_{\text{SOM}}$ -reconstruction overprediction. When error is introduced for both $\delta^{13}\text{C}_{\text{SOM}}$ based reconstructions and other paleo-proxies, most of this study's data fall within the realm of a 1:1 relationship between other proxy reconstructions. It is possible that precipitation is conflated with time during weathering, affecting some paleoprecipitation proxies more than others, and making it difficult to compare $\delta^{13}\text{C}_{\text{SOM}}$ with chemical weathering proxies like CIA-K and CALMAG; in other words, it is not clear which (if either) proxy is necessarily accurate. Systemic over-prediction of precipitation using the $\delta^{13}\text{C}_{\text{SOM}}$ -precipitation proxy could be related to weathering biases, or could relate to selective degradation of compounds with positive isotopic signatures, leaving behind lipids, which are more depleted in ^{13}C (Canuel et al. 2003) in acidic conditions. Systemic under-prediction using the $\delta^{13}\text{C}_{\text{SOM}}$ -precipitation proxy could be related to oxidation of microbial digestion and mobilization of ^{12}C as soil-respired gas, leaving behind more enriched organic matter (e.g. Wynn 2007). The comparison between reconstructed precipitation from each established proxy and the new $\delta^{13}\text{C}_{\text{SOM}}$ -precipitation was randomly distributed, indicating that there was no systematic over- or under-prediction for any given proxy (Supp. Fig. C7). The comparable values reconstructed using the $\delta^{13}\text{C}_{\text{SOM}}$ proxy and other established proxies demonstrates that this would make an excellent complementary tool to use in paleoclimate reconstructions.

4.5.4 General paleo-limitations and implications

While the relationship between $\delta^{13}\text{C}_{\text{SOM}}$ and precipitation is geographically robust (in reference to modern calibration; Fig. 2), there are certain limitations to where this relationship can be used. This relationship was tested in C_3 -dominated ecosystems only, so this tool will work best before ~30 million years ago (Cerling et al. 1993; Edwards et al. 2010), or in more recent cases where there is an independent constraint on C_3 vs. C_4 plant abundance (e.g. paleobotanical evidence, phytoliths; Germeraad et al. 1968; Royer et al. 2001; Piperno 2006; Stromberg & McInerney 2011; Hyland et al. 2014; Smiley et al. 2018). As shown in Figure 1, this excludes major grass-dominated ecosystems from the Miocene through the modern without additional independent evidence of flora (e.g. savannas), which makes this relationship not currently applicable for large equatorial regions with widespread C_4 plants such as exist in modern and Neogene ecosystems. Pre-Neogene ecosystems can be treated as C_4 -free due to the lack of

abundance of C₄ plants in the Paleogene and earlier (Tippie & Pagani 2007). Bookending the oldest time wherein paleosols are comparable to modern day soils due to fundamental ecosystem structure is the Devonian Period; before land plants developed adaptations such as seed habits, arborescence, and deeper rooting systems in the Devonian, pedogenic development was weak and many of the most widespread modern soil orders (Histosols, Alfisols, Ultisols, Mollisols) were not yet in existence (Retallack 2008).

Additional deep-time nuances to consider regarding the oldest practical use of this proxy include the radiation of angiosperms: although paleosols developed similarly to those of today post-Devonian, they did not include angiosperms until sometime in the mid-Jurassic to early Cretaceous (Li et al. 2019; but see Coiro et al. 2019, Sokoloff et al. 2019, Bateman 2020). Angiosperms are the most widespread plant types in modern ecosystems (and ever since their radiation in the mid-Cretaceous; Li et al. 2019), so the past ~144 million years should be directly comparable, but what about for gymnosperm dominated ecosystems of the Paleozoic and earlier Mesozoic? To test the importance of the presence of angiosperms, we compared angiosperm-dominated soils (n = 55) with gymnosperm-dominated soils (n = 23) based on ecosystem-specified (*Populus* (angiosperm), *Thuja* (gymnosperm)) collections for this study and flora provided in literature (Supp. Fig. C6). T-test results determined that the difference between $\delta^{13}\text{C}_{\text{SOM}}$ for angiosperm- and gymnosperm- dominated ecosystems was not significant, and that the ranges of these two ecosystems were comparable (Supp. Fig. C6). Thus, the proposed proxy relationship can be used on paleosols prior to the origin and radiation of angiosperms.

When applying this relationship to the geologic record, we must consider that $\delta^{13}\text{C}$ values in soils can potentially be altered by chemical, biological, and biological processes (Wynn et al. 2005). Very high precipitation values can result in organic carbon, which is fairly mobile, leaching completely from local soils. Furthermore, even if organic carbon is not completely removed from an ecosystem, dissolved organic carbon (DOC) is more likely to be translated from the upper soil horizons and accumulate in lower, B-horizons, undergoing increased oxidation-related isotopic fractionation with depth in a soil profile (e.g. Rayleigh distillation; Wynn & Byrd 2007). High precipitation can also increase microbial activity and associated diagenesis (Cruz-Martínez et al. 2012). This is further shown by empirical evidence in this study; the three outliers (Fig. 4.3, 4.5, C3), which are from the temperate rainforests on the Olympic

Peninsula of Washington with rainfall $>3000 \text{ mm yr}^{-1}$, all appear significantly more isotopically positive than expected at high rainfall. Other than these outliers, the vast majority of the soils compiled for this study were from areas with annual precipitation $<2500 \text{ mm yr}^{-1}$, so this paleo-precipitation proxy is only calibrated for use in precipitation regimes $<2500 \text{ mm yr}^{-1}$ at this time. Above these precipitation levels, most ecosystems are considered “rainforests” (Whitaker 1975) and are typically characterized by Oxisols. Although the proposed proxy is limited at very high precipitation regimes (e.g. $>2500 \text{ mm yr}^{-1}$), it is more precise than other precipitation proxies between $1500\text{--}2500 \text{ mm yr}^{-1}$. Limitations of the model connecting carbon isotope values and precipitation at high precipitation values coincides with findings by Kohn (2010), who found strong canopy effects above 2500 mm yr^{-1} (Kohn 2010) in his modern plant meta-analysis. Future studies specifically focused on testing the relationship between carbon isotope values of soils and precipitation in rainforests and other high precipitation regimes will constrain the higher end of this relationship for wider applications in the geologic record.

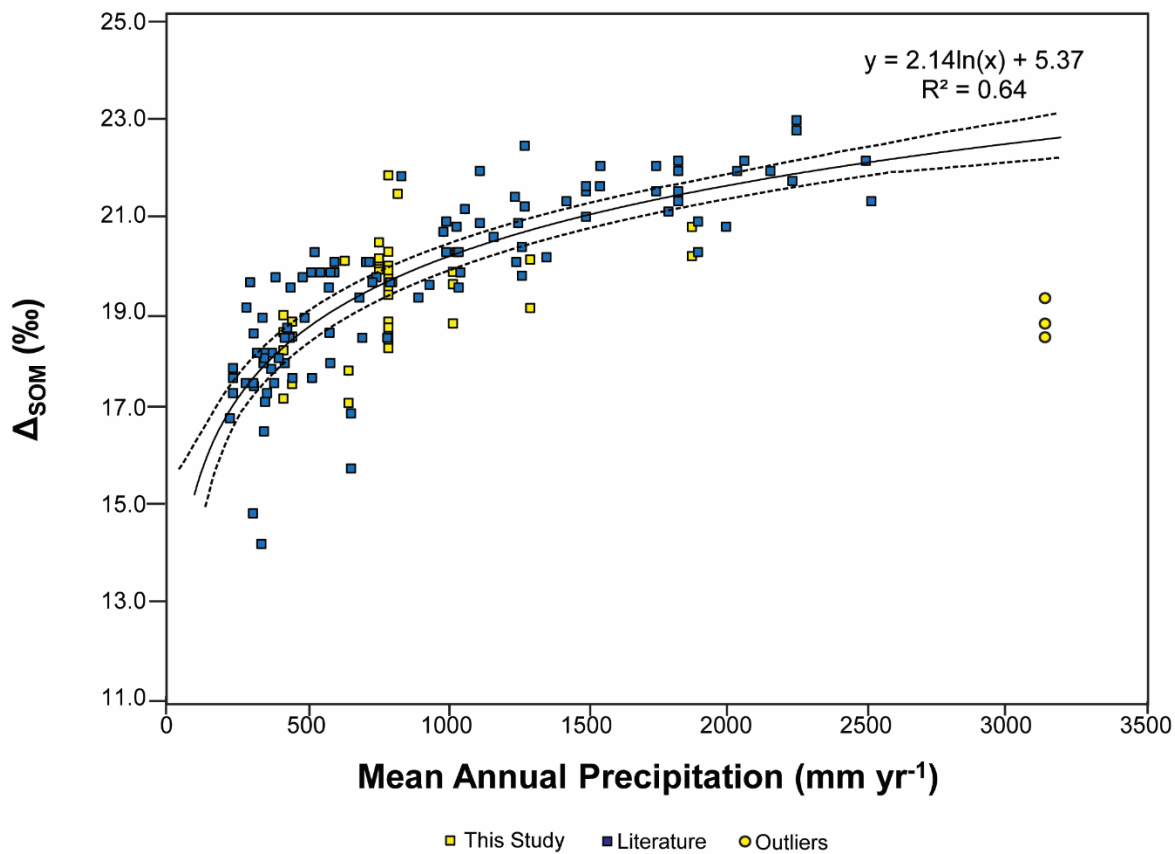


Figure 4.5: $\Delta^{13}\text{C}_{\text{SOM}}$ values compared to mean annual precipitation for modern soils. Soils from this study are shown in yellow squares, literature data is shown in blue squares, with one standard deviation shown around the best-fit logarithmic relationship model determined in this study, and outliers (from our dataset, measured MAP = 3350 mm yr⁻¹) are shown in yellow circles.

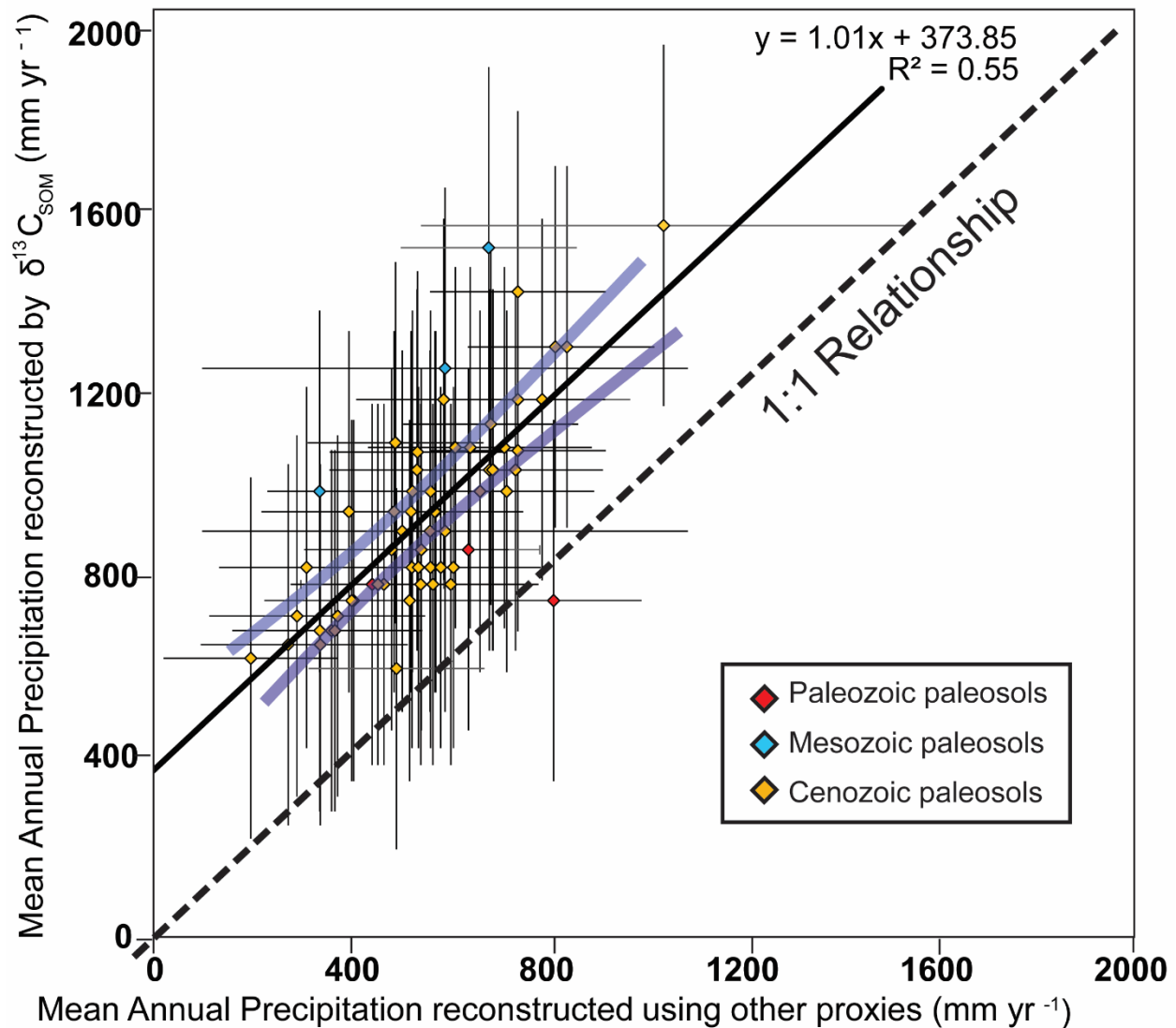


Figure 4.6: Paleosol reconstructed mean annual precipitation values over time as compared to precipitation values reconstructed with different paleoprecipitation proxies. (See Cerling et al. 1992; Mora et al. 1996; Hatté et al. 2001; Nordt et al. 2002; Pustovoytov & Terhorst 2004; Sheldon 2006; Gutierrez & Sheldon 2012; Hyland & Sheldon 2013; Harris et al. 2017; Lukens et al. 2017; Tabor et al. 2017). Shown are average mean annual precipitation values reconstructed with proxy-specific error along the x-axis and $\delta^{13}C_{SOM}$ error along the y-axis (400mm yr⁻¹). Pre-Cenozoic $\delta^{13}C_{atm}$ values (‰) are treated as -6, and Cenozoic $\delta^{13}C_{atm}$ values are calculated using Tippie et al. (2010) values. The 95% confidence intervals, indicating how the confidence in the relationship linking the new calculated values relate to the old calculated values, are shown in blue opaque lines. The 1:1 relationship, which would indicate that previous calculated values are equal to new calculated values, is shown in dashed lines. Red diamonds represent paleosols deposited in the Paleozoic, blue diamonds represent paleosols deposited in the Mesozoic, and gold diamonds represent paleosols deposited in the Cenozoic.

4.5.5 Corrections when applying to the geologic record

The isotopic value of the atmosphere ($\delta^{13}\text{C}_{\text{atm}}$) has not been constant over geological time (Tippie et al. 2010). For example, the modern atmosphere is more negative compared to most of Earth's history due to anthropogenic causes (geologic fuel combustion, deforestation; Keeling et al. 2001). Because of this, the relationship relating $\delta^{13}\text{C}_{\text{SOM}}$ and MAP needs to be corrected, using equation 4.6, for differences in $\delta^{13}\text{C}_{\text{atm}}$ when applied to the geologic record by correcting the $\delta^{13}\text{C}_{\text{SOM}}$ value of ancient soil.

$$(\delta^{13}\text{C}_{\text{atm,ancient}} - \delta^{13}\text{C}_{\text{atm,modern}}) + \delta^{13}\text{C}_{\text{SOM}} (\text{‰}) \quad (\text{Equation 4.6})$$

For example, during the early Eocene, when $\delta^{13}\text{C}_{\text{atm}}$ was approximately -5.5‰, the correction to $\delta^{13}\text{C}_{\text{SOM}}$ would be +1‰ (Tippie et al. 2010); during the Paleocene-Eocene Thermal Maximum, the correction factor would be closer to +1.5‰; and during the Mid-Miocene, the correction factor would be +0.5‰. At its most sensitive, a difference of 2.5‰ of $\delta^{13}\text{C}_{\text{atm}}$ would result in a difference between $\delta^{13}\text{C}_{\text{SOM}}$ -reconstructed precipitation values of 222 mm yr⁻¹ ($\delta^{13}\text{C}_{\text{SOM}} = -23\text{‰}$) and 739 mm yr⁻¹ ($\delta^{13}\text{C}_{\text{SOM}} = -25.5\text{‰}$). This is the difference between a desert and a grassland or savannah (Whitaker 1975).

As mentioned, the carbon isotope value of soil organic carbon is not constant through a soil profile (Krull et al. 2002; Wynn et al. 2006; Wynn 2007; Fig. 1). The organic matter at the top of the soil profile (e.g. O- horizon) is most reflective of average aboveground biomass, and should be exclusively used in applications of this model. The $\delta^{13}\text{C}_{\text{SOM}}$ down-profile becomes more enriched in ¹³C (see Fig. 1). However, this section of soil is also not always preserved (Mack et al. 1993), or is eroded and unidentifiable (Marriott et al. 2006), and the pattern of Rayleigh fractionation down-profile is contingent on factors such as soil texture and slope (Krull et al. 2002; Wynn 2007; Fig. 1). To address this constraint, when possible, carbon isotope values for the entire soil profile should be collected, such that the carbon isotope value of the topsoil can be back-calculated based on carbon isotope values and the fraction of soil organic carbon remaining for each of these samples (Wynn 2007).

4.6 Conclusions

Overall, there is a strong relationship between organic $\delta^{13}\text{C}$ values in soil and mean annual precipitation. This substantiates past work linking $\delta^{13}\text{C}$ values of aboveground plant biomass to precipitation. This $\delta^{13}\text{C}_{\text{SOM}}$ -precipitation model provides a new method for reconstructing precipitation in organic-rich sediments, particularly those without clearly preserved soil development (e.g. alluvial floodplains, wetlands), as well as more precision at precipitation levels between 1500 and 2500 mm yr^{-1} . Prior to this proxy, organic-based terrestrial precipitation proxies largely relied on taxonomy or full preservation, and paleosol-based precipitation proxies relied on full-profile development. This new tool will be especially useful in areas with poor pedogenic development, which are often found in areas near to lakes and rivers (e.g. high resolution, high preservation regions) that are vulnerable to flooding, but also especially prevalent in the fossil record. In tandem with identifiable organic material, this organic-based proxy could allow us to investigate the direct link between precipitation and organic carbon and characterize the water limitations of localized ecosystems. Future projects could use pre-determined knowledge of Rayleigh distillation isotope enrichment down-profile in soils to back-calculate topsoil $\delta^{13}\text{C}_{\text{SOM}}$ values from A- and B- horizons, which will provide a way to connect the use of B- and O- horizons of soils for paleoprecipitation reconstruction.

4.7 Acknowledgments

We thank Mike Blakeman (United States Forest Service: Rio Grande National Forest), Steve Baumann (National Park Service: El Malpais National Monument), Matthew Dubeau (NPS: Olympic National Park), Scott Esser (NPS: Rocky Mountain National Park), Susana Fernandes (University of Michigan School for Environment and Sustainability), Matthew Klein (USFS: White River National Forest), Jayne Lebeda (USFS: Fishlake National Forest), Su Tao (Xishuangbanna Tropical Botanical Garden) and Jason Zayatz (USFS: Coconino National Forest) for assistance with sampling permissions. Additional thanks to Steve Baumann and Susana Fernandes for assistance in the field. This work was partially funded by NSF Award #1812949 to NDS. Fieldwork by RAS was supported by the Geological Society of America's Graduate Research grants.

4.8 References

- Andrews, E., White, T., & del Papa, C. (2017). Paleosol-based paleoclimate reconstruction of the Paleocene-Eocene Thermal Maximum, northern Argentina. *Palaeogeography, Palaeoclimatology, Palaeoecology*, *471*, 181-195.
- Balesdent, J., Mariotti, A., & Guillet, B. (1987). Natural ¹³C abundance as a tracer for studies of soil organic matter dynamics. *Soil Biology and Biochemistry*, *19*(1), 25-30.
- Bateman, R. M. (2020). Hunting the Snark: the flawed search for mythical Jurassic angiosperms. *Journal of Experimental Botany*, *71*(1), 22-35.
- Beverly, E. J., Lukens, W. E., & Stinchcomb, G. E. (2018). Paleopedology as a tool for reconstructing paleoenvironments and paleoecology. In *Methods in paleoecology* (pp. 151-183). Springer, Cham.
- Billings, S. A., & Richter, D. D. (2006). Changes in stable isotopic signatures of soil nitrogen and carbon during 40 years of forest development. *Oecologia*, *148*(2), 325-333.
- Bol, R. A., Harkness, D. D., Huang, Y., & Howard, D. M. (1999). The influence of soil processes on carbon isotope distribution and turnover in the British uplands. *European Journal of Soil Science*, *50*(1), 41-51.
- Breecker, D. O., Sharp, Z. D., & McFadden, L. D. (2009). Seasonal bias in the formation and stable isotopic composition of pedogenic carbonate in modern soils from central New Mexico, USA. *Geological Society of America Bulletin*, *121*(3-4), 630-640.
- Broadmeadow, M. S. J., Griffiths, H., Maxwell, C., & Borland, A. M. (1992). The carbon isotope ratio of plant organic material reflects temporal and spatial variations in CO₂ within tropical forest formations in Trinidad. *Oecologia*, *89*(3), 435-441.
- Canuel, E. A., Freeman, K. H., & Wakeham, S. G. (1997). Isotopic compositions of lipid biomarker compounds in estuarine plants and surface sediments. *Limnology and Oceanography*, *42*(7), 1570-1583.
- Cerling, T. E., Solomon, D. K., Quade, J. A. Y., & Bowman, J. R. (1991). On the isotopic composition of carbon in soil carbon dioxide. *Geochimica et Cosmochimica Acta*, *55*(11), 3403-3405.
- Cerling, T. E. (1992). Use of carbon isotopes in paleosols as an indicator of the P (CO₂) of the paleoatmosphere. *Global Biogeochemical Cycles*, *6*(3), 307-314.
- Cerling, T. E., & Quade, J. (1993). Climate change in continental isotopic records. *Geophysical Monograph*, *78*, 217-231.
- Cerling, T. E., Wang, Y., & Quade, J. (1993). Expansion of C₄ ecosystems as an indicator of global ecological change in the late Miocene. *Nature*, *361*(6410), 344-345.
- Chabbi, A., Kögel-Knabner, I., & Rumpel, C. (2009). Stabilised carbon in subsoil horizons is located in spatially distinct parts of the soil profile. *Soil Biology and Biochemistry*, *41*(2), 256-261.

- Coiro, M., Doyle, J. A., & Hilton, J. (2019). How deep is the conflict between molecular and fossil evidence on the age of angiosperms? *New Phytologist*, 223(1), 83-99.
- Cotton, J. M., Jeffery, M. L., & Sheldon, N. D. (2013). Climate controls on soil respired CO₂ in the United States: implications for 21st century chemical weathering rates in temperate and arid ecosystems. *Chemical Geology*, 358, 37-45.
- Cruz-Martínez, K., Rosling, A., Zhang, Y., Song, M., Andersen, G. L., & Banfield, J. F. (2012). Effect of rainfall-induced soil geochemistry dynamics on grassland soil microbial communities. *Applied and environmental microbiology*, 78(21), 7587-7595.
- Dai, A. (2006). Precipitation characteristics in eighteen coupled climate models. *Journal of climate*, 19(18), 4605-4630.
- De Camargo, P. B., Trumbore, S. E., Martinelli, L. A., Davidson, E. A., Nepstad, D. C., & Victoria, R. L. (1999). Soil carbon dynamics in regrowing forest of eastern Amazonia. *Global Change Biology*, 5(6), 693-702.
- Diefendorf, A. F., Mueller, K. E., Wing, S. L., Koch, P. L., & Freeman, K. H. (2010). Global patterns in leaf ¹³C discrimination and implications for studies of past and future climate. *Proceedings of the National Academy of Sciences*, 107(13), 5738-5743.
- Dijkstra, P., Ishizu, A., Doucet, R., Hart, S. C., Schwartz, E., Menyailo, O. V., & Hungate, B. A. (2006). ¹³C and ¹⁵N natural abundance of the soil microbial biomass. *Soil Biology and Biochemistry*, 38(11), 3257-3266.
- Douglas, P. M., Demarest, A. A., Brenner, M., & Canuto, M. A. (2016). Impacts of climate change on the collapse of lowland Maya civilization. *Annual Review of Earth and Planetary Sciences*, 44, 613-645.
- Dümig, A., Schad, P., Rumpel, C., Dignac, M. F., & Kögel-Knabner, I. (2008). Araucaria forest expansion on grassland in the southern Brazilian highlands as revealed by ¹⁴C and δ¹³C studies. *Geoderma*, 145(1-2), 143-157.
- Du, B., Liu, C., Kang, H., Zhu, P., Yin, S., Shen, G., Hou, J. & Ilvesniemi, H. (2014). Climatic control on plant and soil δ¹³C along an altitudinal transect of Lushan Mountain in Subtropical China: Characteristics and interpretation of soil carbon dynamics. *PloS one*, 9(1).
- Duckstein, L., Fogel, M. M., & Thames, J. L. (1973). Elevation effects on rainfall: A stochastic model. *Journal of Hydrology*, 18(1), 21-35.
- Edwards, E. J., Osborne, C. P., Strömberg, C. A., Smith, S. A., & C4 Grasses Consortium. (2010). The origins of C4 grasslands: integrating evolutionary and ecosystem science. *science*, 328(5978), 587-591.
- Ekart, D. D., Cerling, T. E., Montanez, I. P., & Tabor, N. J. (1999). A 400 million year carbon isotope record of pedogenic carbonate: implications for paleoatmospheric carbon dioxide. *American Journal of Science*, 299(10), 805-827.

- Etheridge, D. M., Steele, L. P., Langenfelds, R. L., Francey, R. J., Barnola, J. M., & Morgan, V. I. (1998). Historical CO₂ records from the Law Dome DE08, DE08-2, and DSS ice cores. *Trends: a compendium of data on global change*, 351-364.
- Farquhar, G. D., Ehleringer, J. R., & Hubick, K. T. (1989). Carbon isotope discrimination and photosynthesis. *Annual review of plant biology*, 40(1), 503-537.
- Francey, R. J., Gifford, R. M., Sharkey, T. D., & Weir, B. (1985). Physiological influences on carbon isotope discrimination in huon pine (*Lagarostrobos franklinii*). *Oecologia*, 66(2), 211-218.
- Gallagher, T. M., & Sheldon, N. D. (2016). Combining soil water balance and clumped isotopes to understand the nature and timing of pedogenic carbonate formation. *Chemical Geology*, 435, 79-91.
- Gallagher, T. M., Hren, M., & Sheldon, N. D. (2019). The effect of soil temperature seasonality on climate reconstructions from paleosols. *American Journal of Science*, 319(7), 549-581.
- Germeraad, J. H., Hopping, C. A., & Muller, J. (1968). Palynology of Tertiary sediments from tropical areas. *Review of palaeobotany and palynology*, 6(3-4), 189-348.
- Givnish, T. J. (1984). Leaf and canopy adaptations in tropical forests. In *Physiological ecology of plants of the wet tropics* (pp. 51-84). Springer, Dordrecht.
- Goh, K. M., Rafter, T. A., Stout, J. D., & Walker, T. W. (1976). The accumulation of soil organic matter and its carbon isotope content in a chronosequence of soils developed on aeolian sand in New Zealand. *Journal of Soil Science*, 27(1), 89-100.
- Grant, K. E., Galy, V. V., Chadwick, O. A., & Derry, L. A. (2019). Thermal oxidation of carbon in organic matter rich volcanic soils: insights into SOC age differentiation and mineral stabilization. *Biogeochemistry*, 144(3), 291-304.
- Gutierrez, K., & Sheldon, N. D. (2012). Paleoenvironmental reconstruction of Jurassic dinosaur habitats of the Vega Formation, Asturias, Spain. *Bulletin*, 124(3-4), 596-610.
- Harrington, G., Kemp, S., & Koch, P. (2004). Palaeocene–Eocene paratropical floral change in North America: responses to climate change and plant immigration. *Journal of the Geological Society*, 161(2), 173-184.
- Harris, E. B., Strömberg, C. A., Sheldon, N. D., Smith, S. Y., & Vilhena, D. A. (2017). Vegetation response during the lead-up to the middle Miocene warming event in the Northern Rocky Mountains, USA. *Palaeogeography, Palaeoclimatology, Palaeoecology*, 485, 401-415.
- Hatté, C., Antoine, P., Fontugne, M., Lang, A., Rousseau, D. D., & Zöller, L. (2001). $\delta^{13}\text{C}$ of loess organic matter as a potential proxy for paleoprecipitation. *Quaternary Research*, 55(1), 33-38.
- Hodell, D. A., Curtis, J. H., & Brenner, M. (1995). Possible role of climate in the collapse of Classic Maya civilization. *Nature*, 375(6530), 391-394.

- Hren, M. T., Sheldon, N. D. (2012). Temporal variations in lake water temperature: Paleoenvironmental implications of lake carbonate $\delta^{18}\text{O}$ and temperature records. *Earth and Planetary Science Letters*, 337-338, 77-84.
- Hyland, E. G., & Sheldon, N. D. (2013). Coupled CO₂-climate response during the early Eocene climatic optimum. *Palaeogeography, Palaeoclimatology, Palaeoecology*, 369, 125-135.
- Hyland, E. G., Sheldon, N. D., Smith, S. Y., Cotton, J. M., & Strömberg, C. A. (2014). Dynamics of the Rise of C₄ Grasslands in Southwestern Montana. *The Paleontological Society Special Publications*, 13, 115-116.
- iNaturalist. Available from <https://www.inaturalist.org>. Accessed [May 1, 2018]
- IPCC, T. (2007). Climate change 2007: synthesis report. *Contribution of working groups I, II and III to the fourth assessment report of the intergovernmental panel on climate change*, 95-212.
- Jacobs, B. F. (1999). Estimation of rainfall variables from leaf characters in tropical Africa. *Palaeogeography, Palaeoclimatology, Palaeoecology*, 145(1-3), 231-250.
- Jenny, H., & Leonard, C. D. (1934). Functional relationships between soil properties and rainfall. *Soil Science*, 38(5), 363-382.
- Keeling, C. D., Piper, S. C., Bacastow, R. B., Wahlen, M., Whorf, T. P., Heimann, M., & Meijer, H. A. (2001). Exchanges of atmospheric CO₂ and ¹³CO₂ with the terrestrial biosphere and oceans from 1978 to 2000. I. Global aspects.
- Keeling, C. D., & Whorf, T. P. (2004). Atmospheric CO₂ concentrations derived from flask air samples at sites in the SIO network. *Trends: a compendium of data on Global Change*.
- Kleber, M. (2010). What is recalcitrant soil organic matter? *Environmental Chemistry*, 7(4), 320-332.
- Kohn, M. J. (2010). Carbon isotope compositions of terrestrial C₃ plants as indicators of (paleo) ecology and (paleo) climate. *Proceedings of the National Academy of Sciences*, 107(46), 19691-19695.
- Krull, E. S., Skjemstad, J. O., Burrows, W. H., Bray, S. G., Wynn, J. G., Bol, R., Spouncer, L. & Harms, B. (2005). Recent vegetation changes in central Queensland, Australia: Evidence from $\delta^{13}\text{C}$ and ¹⁴C analyses of soil organic matter. *Geoderma*, 126(3-4), 241-259.
- Li, H. T., Yi, T. S., Gao, L. M., Ma, P. F., Zhang, T., Yang, J. B., Gitzendanner, M. A., Fritsch, P. W., Cai, J., Luo, Y. & Wang, H. (2019). Origin of angiosperms and the puzzle of the Jurassic gap. *Nature Plants*, 5(5), 461.
- Livingston, N. J., & Spittlehouse, D. L. (1996). Carbon isotope fractionation in tree ring early and late wood in relation to intra-growing season water balance. *Plant, Cell & Environment*, 19(6), 768-774.
- Looy, C., Kerp, H., Duijnste, I., & DiMichele, B. (2014). The late Paleozoic ecological-evolutionary laboratory, a land-plant geologic record perspective. *The Sedimentary Record*, 12(4), 4-18.

- Lorenz, K., Lal, R., Preston, C. M., & Nierop, K. G. (2007). Strengthening the soil organic carbon pool by increasing contributions from recalcitrant aliphatic bio (macro) molecules. *Geoderma*, *142*(1-2), 1-10.
- Mack, G. H., James, W. C., & Monger, H. C. (1993). Classification of paleosols. *Geological Society of America Bulletin*, *105*(2), 129-136.
- Marriott, S. B., Wright, V. P., Alonso-Zarza, A. M., & Tanner, L. H. (2006). Investigating paleosol completeness and preservation in mid-Paleozoic alluvial paleosols: A case study in paleosol taphonomy from the Lower Old Red Sandstone. *SPECIAL PAPERS-GEOLOGICAL SOCIETY OF AMERICA*, *416*, 43.
- McPherson, G. R., Boutton, T. W., & Midwood, A. J. (1993). Stable carbon isotope analysis of soil organic matter illustrates vegetation change at the grassland/woodland boundary in southeastern Arizona, USA. *Oecologia*, *93*(1), 95-101.
- Mintz, J. S., Driese, S. G., Breecker, D. O., & Ludvigson, G. A. (2011). Influence of changing hydrology on pedogenic calcite precipitation in Vertisols, Dance Bayou, Brazoria County, Texas, USA: implications for estimating paleoatmospheric $p\text{CO}_2$. *Journal of Sedimentary Research*, *81*(6), 394-400.
- Mora, C. I., Sheldon, B. T., Elliott, W. C., & Driese, S. G. (1998). An oxygen isotope study of illite and calcite in three Appalachian Paleozoic vertic paleosols. *Journal of Sedimentary Research*, *68*(3), 456-464.
- Nesbitt, H., & Young, G. M. (1982). Early Proterozoic climates and plate motions inferred from major element chemistry of lutites. *Nature*, *299*(5885), 715-717.
- Nordt, L., Atchley, S., & Dworkin, S. I. (2002). Paleosol barometer indicates extreme fluctuations in atmospheric CO_2 across the Cretaceous-Tertiary boundary. *Geology*, *30*(8), 703-706.
- Nordt, L. C., & Driese, S. D. (2010). New weathering index improves paleorainfall estimates from Vertisols. *Geology*, *38*(5), 407-410.
- Olen, S. M., Ehlers, T. A., & Densmore, M. S. (2012). Limits to reconstructing paleotopography from thermochronometer data. *Journal of Geophysical Research: Earth Surface*, *117*(F1).
- Osher, L. J., Matson, P. A., & Amundson, R. (2003). Effect of land use change on soil carbon in Hawaii. *Biogeochemistry*, *65*(2), 213-232.
- Passey, B. H. (2012). Reconstructing terrestrial environments using stable isotopes in geologic teeth and paleosol carbonates. *The Paleontological Society Papers*, *18*, 167-194.
- Pfeifer, M., Gonsamo, A., Disney, M., Pellikka, P., & Marchant, R. (2012). Leaf area index for biomes of the Eastern Arc Mountains: Landsat and SPOT observations along precipitation and altitude gradients. *Remote Sensing of Environment*, *118*, 103-115.
- Piperno, D. R. (2006). *Phytoliths: a comprehensive guide for archaeologists and paleoecologists*. Rowman Altamira.

- Powell, R. L., Yoo, E. H., & Still, C. J. (2012). Vegetation and soil carbon-13 isoscapes for South America: integrating remote sensing and ecosystem isotope measurements. *Ecosphere*, 3(11), 1-25.
- Quade, J., Cerling, T. E., Andrews, P., & Alpagut, B. (1995). Paleodietary reconstruction of Miocene faunas from Paşalar, Turkey using stable carbon and oxygen isotopes of geologic tooth enamel. *Journal of Human Evolution*, 28(4), 373-384.
- Retallack, G. J. (1994). The environmental factor approach to the interpretation of paleosols. *Factors of soil formation: A fiftieth anniversary retrospective*, 33, 31-64.
- Retallack, G. J. (2008). *Soils of the past: an introduction to paleopedology*. John Wiley & Sons.
- Rothstein, D. E., Toosi, E. R., Schaetzl, R. J., & Grandy, A. S. (2018). Translocation of carbon from surface organic horizons to the subsoil in coarse-textured Spodosols: implications for deep soil C dynamics. *Soil Science Society of America Journal*, 82(4), 969-982.
- Royer, D. L., Wing, S. L., Beerling, D. J., Jolley, D. W., Koch, P. L., Hickey, L. J., & Berner, R. A. (2001). Paleobotanical evidence for near present-day levels of atmospheric CO₂ during part of the Tertiary. *Science*, 292(5525), 2310-2313.
- Sanderman, J., Creamer, C., Baisden, W. T., Farrell, M., & Fallon, S. (2017). Greater soil carbon stocks and faster turnover rates with increasing agricultural productivity, *Soil*, 1-16.
- Schermerhorn, V. P. (1967). Relations between topography and annual precipitation in western Oregon and Washington. *Water Resources Research*, 3(3), 707-711.
- Sheldon, N. D. (2006). Abrupt chemical weathering increase across the Permian–Triassic boundary. *Palaeogeography, Palaeoclimatology, Palaeoecology*, 231(3-4), 315-321.
- Sheldon, N. D., Smith, S. Y., Stein, R., & Ng, M. (2020). Carbon isotope ecology of gymnosperms and implications for paleoclimatic and paleoecological studies. *Global and Planetary Change*, 103060.
- Shucheng, X., & Evershed, R. P. (2001). Peat molecular geologies recording paleoclimatic change and organism replacement. *Chinese Science Bulletin*, 46(20), 1749.
- Smiley, T. M., Hyland, E. G., Cotton, J. M., & Reynolds, R. E. (2018). Evidence of early C₄ grasses, habitat heterogeneity, and faunal response during the Miocene Climatic Optimum in the Mojave Region. *Palaeogeography, Palaeoclimatology, Palaeoecology*, 490, 415-430.
- Sokoloff, D. D., Remizowa, M. V., El, E. S., Rudall, P. J., & Bateman, R. M. (2019). Supposed Jurassic angiosperms lack pentamery, an important angiosperm-specific feature. *New Phytologist*.
- Spicer, R. A. (2000). Leaf physiognomy and climate change. *Biotic response to global change: the last*, 145, 244-264.
- Spicer, R. A., Herman, A. B., & Wolfe, J. A. (2008). Clamp. *Encyclopedia of Paleoclimatology and Ancient Environments*, 156-158.

- Spicer, R. A., Valdes, P. J., Spicer, T. E. V., Craggs, H. J., Srivastava, G., Mehrotra, R. C., & Yang, J. (2009). New developments in CLAMP: calibration using global gridded meteorological data. *Palaeogeography, Palaeoclimatology, Palaeoecology*, 283(1-2), 91-98.
- Stein, R. A., Sheldon, N. D., & Smith, S. (2019). Rapid response to anthropogenic climate change by *Thuja occidentalis*: implications for past climate reconstructions and future climate predictions. *PeerJ*, 7, e7378.
- Stein, R. A., Sheldon, N. D., & Smith S. (in press). C₃ plant carbon isotope discrimination does not respond to CO₂ concentration on decadal to centennial timescales. *New Phytologist*. doi: 10.1111/nph.17030
- Stevenson, B. A., Kelly, E. F., McDonald, E. V., & Busacca, A. J. (2005). The stable carbon isotope composition of soil organic carbon and pedogenic carbonates along a bioclimatic gradient in the Palouse region, Washington State, USA. *Geoderma*, 124(1-2), 37-47.
- Stewart, B. W., Capo, R. C., & Chadwick, O. A. (2001). Effects of rainfall on weathering rate, base cation provenance, and Sr isotope composition of Hawaiian soils. *Geochimica et Cosmochimica Acta*, 65(7), 1087-1099.
- Stinchcomb, G. E., Nordt, L. C., Driese, S. G., Lukens, W. E., Williamson, F. C., & Tubbs, J. D. (2016). A data-driven spline model designed to predict paleoclimate using paleosol geochemistry. *American Journal of Science*, 316(8), 746-777.
- Stromberg, C. A., & McInerney, F. A. (2011). The Neogene transition from C₃ to C₄ grasslands in North America: assemblage analysis of fossil phytoliths. *Paleobiology*, 37(1), 50-71.
- Tabor, N. J., Myers, T. S., Gulbranson, E., Rasmussen, C., Sheldon, N. D., Driese, S. G., ... & McCarthy, P. J. (2013). Carbon stable isotope composition of modern calcareous soil profiles in California: implications for CO₂ reconstructions from calcareous paleosols. In *New Frontiers in Paleopedology and Terrestrial Paleoclimatology* (Vol. 104, pp. 17-34). SEPM (Society for Sedimentary Geology).
- Tabor, N. J., Sidor, C. A., Smith, R. M., Nesbitt, S. J., & Angielczyk, K. D. (2017). Paleosols of the Permian-Triassic: proxies for rainfall, climate change and major changes in terrestrial tetrapod diversity. *Journal of Vertebrate Paleontology*, 37(sup1), 240-253.
- Tipple, B. J., & Pagani, M. (2007). The early origins of terrestrial C₄ photosynthesis. *Annu. Rev. Earth Planet. Sci.*, 35, 435-461.
- Tipple, B. J., Meyers, S. R., & Pagani, M. (2010). Carbon isotope ratio of Cenozoic CO₂: A comparative evaluation of available geochemical proxies. *Paleoceanography*, 25(3).
- Thompson, R. S., Anderson, K. H., & Bartlein, P. J. (1999). *Quantitative paleoclimatic reconstructions from late Pleistocene plant macrogeologies of the Yucca Mountain region* (p. 39). US Department of the Interior, US Geological Survey.
- Torn, M. S., Lapanis, A. G., Timofeev, A., Fischer, M. L., Babikov, B. V., & Harden, J. W. (2002). Organic carbon and carbon isotopes in modern and 100-year-old-soil archives of the Russian steppe. *Global Change Biology*, 8(10), 941-953. Townsend, A. R., Vitousek,

- P. M., Desmarais, D. J., & Tharpe, A. (1997). Soil carbon pool structure and temperature sensitivity inferred using CO₂ and ¹³CO₂ incubation fluxes from five Hawaiian soils. *Biogeochemistry*, 38(1), 1-17.
- Trumbore, S. (2000). Age of soil organic matter and soil respiration: radiocarbon constraints on belowground C dynamics. *Ecological Applications*, 10(2), 399-411.
- Volkoff, B., & Cerri, C. C. (1987). Carbon isotopic fractionation in subtropical Brazilian grassland soils. Comparison with tropical forest soils. *Plant and soil*, 102(1), 27-31.
- von Fischer, J. C., & Tieszen, L. L. (1995). Carbon isotope characterization of vegetation and soil organic matter in subtropical forests in Luquillo, Puerto Rico. *Biotropica*, 138-148.
- Wang, G., Li, J., Liu, X., & Li, X. (2013). Variations in carbon isotope ratios of plants across a temperature gradient along the 400 mm isoline of mean annual precipitation in north China and their relevance to paleovegetation reconstruction. *Quaternary Science Reviews*, 63, 83-90.
- Wang, Y., Kromhout, E., Zhang, C., Xu, Y., Parker, W., Deng, T., & Qiu, Z. (2008). Stable isotopic variations in modern herbivore tooth enamel, plants and water on the Tibetan Plateau: Implications for paleoclimate and paleoelevation reconstructions. *Palaeogeography, Palaeoclimatology, Palaeoecology*, 260(3-4), 359-374.
- Ward, J. K., Tissue, D. T., Thomas, R. B., & Strain, B. R. (1999). Comparative responses of model C₃ and C₄ plants to drought in low and elevated CO₂. *Global Change Biology*, 5(8), 857-867.
- Weiguo, L., Xiahong, F., Youfeng, N., Qingle, Z., Yunning, C., & Zhisheng, A. N. (2005). δ¹³C variation of C₃ and C₄ plants across an Asian monsoon rainfall gradient in arid northwestern China. *Global Change Biology*, 11(7), 1094-1100.
- Weltzin, J. F., & McPherson, G. R. (Eds.). (2003). *Changing precipitation regimes and terrestrial ecosystems: A North American perspective*. University of Arizona Press.
- White, J. W. C., Vaughn, B. H., & Michel, S. E. (2015). University of Colorado, Institute of Arctic and Alpine Research (INSTAAR), Stable Isotopic Composition of Atmospheric Carbon Dioxide (¹³C and ¹⁸O) from the NOAA ESRL Carbon Cycle Cooperative Global Air Sampling Network, 1990–2014, Version: 2015-10-26. Path: ftp://aftp.cmdl.noaa.gov/data/trace_gases/co2c13/flask.
- Whittaker, R. (1975). Whittaker Biome Diagram.
- Wilf, P., Wing, S. L., Greenwood, D. R., & Greenwood, C. L. (1998). Using geologic leaves as paleoprecipitation indicators: an Eocene example. *Geology*, 26(3), 203-206.
- Wilf, P. (2000). Late Paleocene–early Eocene climate changes in southwestern Wyoming: Paleobotanical analysis. *Geological Society of America Bulletin*, 112(2), 292-307.
- Wynn, J. G., Bird, M. I., & Wong, V. N. (2005). Rayleigh distillation and the depth profile of ¹³C/¹²C ratios of soil organic carbon from soils of disparate texture in Iron Range

- National Park, Far North Queensland, Australia. *Geochimica et cosmochimica acta*, 69(8), 1961-1973.
- Wynn, J. G. (2007). Carbon isotope fractionation during decomposition of organic matter in soils and paleosols: implications for paleoecological interpretations of paleosols. *Palaeogeography, Palaeoclimatology, Palaeoecology*, 251(3-4), 437-448.
- Wynn, J. G., & Bird, M. I. (2007). C₄-derived soil organic carbon decomposes faster than its C₃ counterpart in mixed C₃/C₄ soils. *Global Change Biology*, 13(10), 2206-2217.
- Youfeng, N., Weiguo, L., & Zhisheng, A. (2008). A 130-ka reconstruction of precipitation on the Chinese Loess Plateau from organic carbon isotopes. *Palaeogeography, Palaeoclimatology, Palaeoecology*, 270(1-2), 59-63.

CHAPTER V

Using Multiple Proxies to Characterize a Post-Early Eocene Climatic Optimum Ecosystem in the Rocky Mountain Interior⁴

5.1 Abstract

The early Eocene climatic optimum (EECO), a warm period ~50 million years ago, is often referred to as an analog for warm-world conditions in a high-emissions anthropogenic modern climate change scenario. Thus, understanding hydroclimate at this time, particularly in areas stressed by modern climate change, is imperative to mitigating future water stress and drought. The Greater Green River Basin (GGRB), which accumulated sediment from the surrounding dynamic topography in a highly evaporative, hypersaline lake (Lake Gosiute) is known for its high resolution, well-preserved records of the EECO. In the middle of this basin, marking approximately the center of Lake Gosiute's maximum extent, the Bridger Formation and Blue Rim escarpment host pristinely preserved, well-documented floral assemblages in alluvial and fluvial sediments. Previous age constraints based on biostratigraphy estimated ages ~50–45.5 million years ago, but here absolute ages of 49.29 and 48.29 Ma are reported based on ⁴⁰Ar/³⁹Ar geochronology, placing the Blue Rim escarpment shortly after the peak warming associated with the EECO. Due to the basin's proximity to multiple potential sources of moisture and transported sediment to the west, northeast and south, there is concern that inconsistent hydrological inputs may interfere with interpretations of climate and depositional signals in the region. Using multiple geochemical proxies and fossil evidence, we demonstrate that moisture and sediment sources in the basin throughout the >1 million years of post-EECO uplift of the Rocky Mountains stayed constant, and that variability in biogeochemistry and floral preservation is related to changes in climate and biota. Our multiproxy approach using floral, organic, and inorganic proxies (CIA-K, PWI, bulk geochemical ratios to determine provenance, carbon isotope ecology, floral humidity province, Holdridge Life Zones) demonstrate that the rim of Lake Gosiute was an ephemeral wet forest ecosystem with warm temperatures (10.4–12.0 °C), medium to high precipitation (608–1167 mm yr⁻¹), moderate weathering, and sediments coming

⁴Co-authors for this manuscript upon publication include Dr. Nathan D. Sheldon & Rebecca M. Dzombak (University of Michigan), Dr. Michael E. Smith (Northern Arizona University) and Dr. Sarah E. Allen (Pennsylvania State University Altoona).

from consistent provenance. This systemic approach to a high-resolution record of late, central Lake Gosiute indicates that the region was mostly littoral and floodplain, demonstrating the overall regression of Lake Gosiute just after the EECO. The constant provenance, parent material, temperature, and precipitation imply that the development of the Laramide orogeny had largely finished in this region by the time of deposition.

5.2 Introduction

5.2.1 The Eocene Period

The anthropogenic release of fossil fuels drives a rapid and sustained increase in atmospheric carbon dioxide (CO₂) coupled with subsequent climate change (IPCC 2007). To understand the effects of elevated CO₂ on the Earth, we seek out geological periods with high temperatures and high atmospheric CO₂ for comparison (Cotton et al. 2013). Recently, the early Eocene climatic optimum (EECO) has been invoked as a climate analog for our projected future (Zhu et al. 2019). This peak warming of the EECO occurred 51.5–50.9 million years ago (Ma) and consisted of long-term global temperature maxima and high CO₂ levels but was tectonically comparable to today (Hyland & Sheldon 2013; West et al. 2020). Throughout the early Cenozoic, from the Paleocene to early Eocene, it has been inferred that much of North America was warm and wet, with extensive temperate forests (Smith et al. 2012; Breedlovestrout et al. 2014; Greenwood et al. 2016; West et al. 2020) up to high latitudes 65 °N (Dillhoff et al. 2013). As the planet warms, we are increasingly worried about water availability and dry climates getting drier (Cheeseman 2016). An example of this is the continental interior of North America: currently the North American Southwest is high-elevation desert and experiences severe droughts. It is assumed that with imminent climate change, this drought may be exacerbated (Poore et al. 2005); therefore, we are especially interested in the paleoclimate of the North American interior.

5.2.2 Continental interior and foreland basins in the Rocky Mountains

During the early Eocene, the thick-skinned Sevier orogeny transitioned into the thin-skinned Laramide orogeny mountain building events, resulting in the formation of these uplifting

mountains and basins close to sea level (Dickinson et al. 1988; Snoke et al. 1993). Subsequently, sedimentation rates increased, creating extensive sedimentary basin deposits (Dickinson et al. 1988; Snoke et al. 1993). These high sedimentation rate intracontinental lake basins are typically well-preserved in the fossil record, allowing us to study deep time in high resolution (Looy et al. 2014). One of these, Eocene Lake Gosiute, a basin east of the fold and thrust belt (Figure 5.1), is represented by lacustrine deposits of the Green River Formation (Lyman Tongue, Wilkins Peak, Laney Members; Smith et al. 2003) as well as the inter-fingering paleosols and alluvial mudstones of the Wasatch and Bridger formations (Carroll et al. 2008).

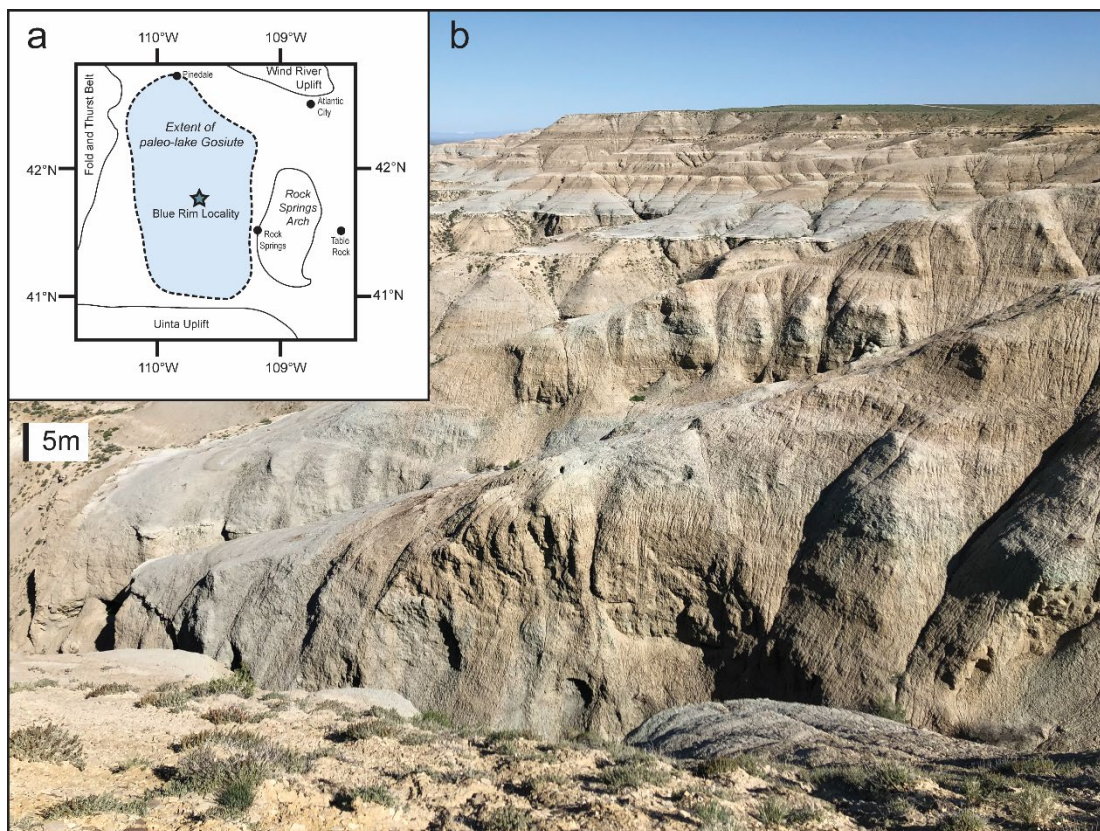


Figure 5.1: Map and profile of Blue Rim escarpment. (a) Map and location of Blue Rim escarpment (41.7985 °N, -109.5856 °E) and surrounding Eocene topography. (b) Landscape image of the escarpment from the uppermost strata.

Lake Gosiute was surrounded by the Wind River range (north), Uinta range (south), Rock Springs uplift (south, east), and Wyoming fold-and-thrust belt (west; Fig. 5.1), and as a result received water inputs from each of these sources (Murphey et al. 2011). The array of surrounding mountain ranges with high sediment input around a highly evaporative, shallow

alkaline lake has resulted in superb preservation in sediments from the EECO of paleo-lake Gosiute in the GGRB (Surdam & Stanley 1979). However, due to the multiple potential inputs, the patterns driving the local hydroclimate can interfere with climate and geochronological interpretations (Carroll et al. 2008). Previous work has speculated that our perception and interpretation of the climate and environment of the GGRB could be driven by changes in hydrological inputs related to tectonic uplift in the region. Specifically, significantly shifting geochemical data ($\delta^{18}\text{O}$ values) within calcitic mudstone spanning 100,000 years in the Green River Formation (49 Ma) was interpreted as potential changes in river and stream inputs associated with relief or lengthy distances, rather than changing temperatures or rainfall (Carroll et al. 2008). This could impact our understandings of paleoecosystems, because interpretations of environments could be influenced by allochthonous organic material, as can paleoclimate reconstructions, and even age (if geochronology is performed on grains from external sites; Smith et al. 2003; Malone et al. 2014). The origin and amplitude of hydrological inputs to Lake Gosiute is pertinent to our understanding about water availability in the region post-EECO. Better constraints on fluvial and alluvial inputs to Lake Gosiute will allow us to determine whether our interpretations of the environment are a result of inconsistent sources, or changing climate. The proximity of these lacustrine records to active tectonics in westward mountain building also results in high-frequency tephra, which allow us to constrain the age of Lake Gosiute with anomalous precision. The paleolatitude of southwestern Wyoming in the early Eocene is thought to be moderately comparable to its position today (41–41.82 °N; Wolfe et al. 1998; Hyland & Sheldon 2013), thus this region provides a tectonically constrained, biogeographically similar region to study the early Eocene continental interior.

5.2.3 Using multiple proxies to characterize an environment

There are several terrestrial proxies that can be used to reconstruct paleoclimate and paleoecology (e.g. pedogenic carbonate isotope values, floral assays, stomatal density; Cerling 1992; Royer 1999; Wilf et al. 2000; Spicer et al. 2009). This study seeks to combine these proxies to create a holistic and robust reconstruction of the Greater Green River Basin during the early Eocene. The high degree of preservation of organic and inorganic specimens, due to the tectonic assemblage of the basin currently, makes it such that the Greater Green River Basin is

an excellent location for such an approach. In light of the potential imprint of hydrological changes in climate and ecosystem interpretations, the use of multiple sources of geochemical inorganic in tandem can provide context for many aspects of depositional environment, including characterization of ecosystems, climate, hydroclimate, age and origin of sediments. Organic geochemistry can be used to demonstrate isotopic composition of the atmosphere ($\delta^{13}\text{C}_{\text{atm}}$; Arens et al. 2000; Stein et al. 2019). The $\delta^{13}\text{C}_{\text{atm}}$ value is an important environmental variable, as it reflects sources of CO_2 gas to the atmosphere, because potential C sources have different isotopic signatures (e.g. mantle $\text{CO}_2 = \sim -5.5\text{‰}$; Keeling 1979; Boutton 1991; Deines 1992). These values are also important parameters in models that reconstruct additional environmental variables, such as the concentration of atmospheric $[\text{CO}_2]$ using paleosol carbonates (Cerling et al. 1991; Cerling 1992) or using stomatal parameters (Franks et al. 2014).

The Blue Rim locality of the Bridger Formation is a well-characterized stratigraphic section (Kistner 1973) with well-studied floral assemblages (Kistner 1973; Allen 2017), and provides an opportunity to aggregate bulk and isotope geochemical proxies within sedimentary rocks, paleosols, and organic matter in a single location (Buchheim et al. 2000). The geolocation of Blue Rim escarpment was at one time the center of Lake Gosiute during its maximal extent, though the sediments deposited represent an environment littoral to the receding lake. This is a low energy environment with high accumulation rates, and thus promises high preservation and high resolution geochemical data for ecosystem and deposition analyses. In addition to new isotope and bulk geochemistry results on newly collected fossils and mudstone samples, we provide an updated age of this formation using $^{40}\text{Ar}/^{39}\text{Ar}$ geochronology.

5.3 Methods

5.3.1 Description of locality

The Bridger Formation is an 842m thick series of tuffaceous lacustrine and deltaic-alluvial sedimentary rocks (Koenig 1960). Previously, workers estimated that the Bridger Formation spanned 3.5 million years, from 49.09–45.57 Ma (Murphey & Evanoff 2001). Other estimates place the start of the Bridger Formation prior to 50 million years, spanning through to 45.6 million years, and, although there are no previous reconstructions from the oldest portion of the

Bridger Formation (Bridger A; Allen 2017), it is thought that Bridger A could be older than 48.27 Ma based on previous geochronological estimates of Bridger C and E (47.22 Ma, 46.16 Ma respectively; Murphey and Evanoff 2001; Murphey et al. 2011). The depositional context for the Bridger Formation assumes that limestones and mudstones in the Bridger formation represent wide, shallow lakes that merged with meandering streams to Lake Gosiute as it transgressed (Kistner 1973; Groll & Steidtmann 1987; Clyde et al. 2001). There are six potential sediment sources to the Bridger Formation including Absaroka Range volcanoclastics, Uinta mountain physical weathering, Wyoming Overthrust Belt physical weathering, volcanic ashfall from Challis volcanism in Idaho, and autochthonous lacustrine carbonates (Murphey & Evanoff 2001). Where the older, and in places, co-eval Green River formation (Laney Shale; Allen 2017) is composed primarily of lacustrine sediments, the Bridger formation transitions into fluvial sediments (Buchheim et al. 2000; Allen 2017). Sedimentation within the Bridger Formation is relatively continuous, with high sedimentation rates during fluvial deposition and slightly lower sedimentation rates during lacustrine sedimentation (Murphey & Evanoff 2001). Because of this, it is known for its pristine faunal and floral preservation, making it an excellent candidate for understanding ecosystem function (Stull et al. 2014; Allen 2017).

The Blue Rim escarpment of the Bridger Formation is exposed laterally over 12km, approximately 100m tall in places (Kistner 1973). The flora at this locality have been quarried and described in great depth, and are known for their preservation of multiple plant organs like leaves, flowers, fruits, seeds, wood, pollen, and spores, all from the same localities (Allen 2017). Floral assemblages at Blue Rim occupy warm, subtropical, wet biomes; examples include palms (up to 28m tall; Allen 2017). Of the two major plant quarries, the lower horizon (older) floral assemblage consists of climbing taxa such as the abundant fern *Lygodium kaulfussi* (fern, Lygodiaceae), *Asplenium* sp. (fern, Aspleniaceae), *Acrostichum* sp. (fern, Pteridaceae), *Thelypteris iddingsi* (fern, Thelypteridaceae), dicots like *Serjania rara* (soapberry, Sapindaceae), *Populus cinnamomoides* (poplar, Salicaceae) and extinct sapindalean *Landeenia arailiodes* (Sapindaceae), *Goweria bluerimensis* (Icanicaceae), and *Phoenix windmillis* (palm; Arecaceae; Wilf et al. 2000; Allen 2017). The upper horizon hosts flora like *Macginitea wyomingensis* (sycamore; Plantanaceae), *Populus cinnamomoides* (poplar, Salicaceae), *Cedrelospermum nervosum* (elm; Ulmaceae), *Serjania rara* (soapberry, Sapindaceae), and many more (Allen 2017).

5.3.2 Age constraints

Reworked volcaniclastic ashes were sampled from the charismatic blue-green marker unit approximately halfway up the section as well as two sand beds near the top of the Blue Rim escarpment (Bridger Formation) for $^{40}\text{Ar}/^{39}\text{Ar}$ geochronological dating. To prepare sanidine phenocrysts for analysis, samples were crushed, leached in dilute hydrochloric acid (HCl) and hydrofluoric acid (HF) prior to hand-picking of sanidine in refractive index oils using a petrographic microscope, and then ultrasonic cleaning in acetone and ethanol. Sanidine phenocrysts from sampled ash beds were irradiated adjacent to standard sanidine crystals from Fish Canyon tuff (FCs) in cadmium shielding within the TRIGA (Training, Research, Isotopes, General Atomics) water-cooled, low-enriched uranium/zirconium fuel reactor at Oregon State University. Single sanidine crystals were fused using a 25W CO_2 laser and then analyzed for $^{40}\text{Ar}/^{39}\text{Ar}$ composition using a MAP 215-50 mass spectrometer attached to a metal ultra-high vacuum (UHV) gas extraction and cleanup line at the University of Wisconsin Madison WiscAr laboratory. A known 28.201 Ma age for Fish Canyon sanidine standard (FCs; Kuiper et al. 2008) was used to calculate apparent ages for each laser fusion, and weighted mean ages were calculated for the youngest coherent population of sanidine grains from each sample.

5.3.3 Physical Measurements

5.3.3.1 Stratigraphy and fossils

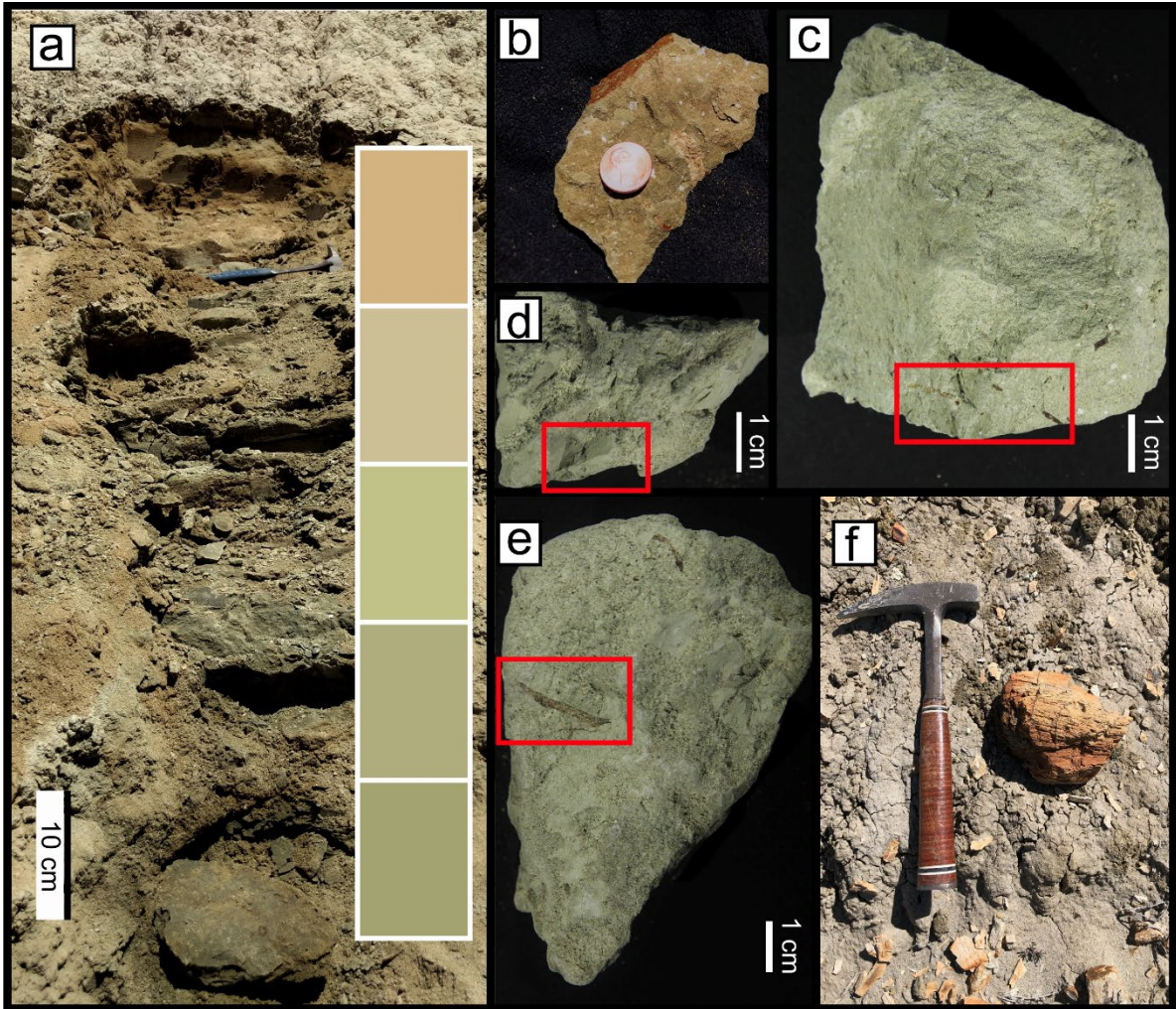


Figure 5.2 Paleosol images and features. (a) Full profile of 19BRWY3 with rock hammer for scale, (b) shows drab-haloed root trace from 19BRWY-2UB, (c) A-horizon fine organic rootlets in red box from 19BRWY2UA, (d) slickensides on 19BRWY1UA, (e) rhizoliths from 19BRWY1UA, and (f) charcoalified wood with rock hammer for scale, excavated ~3m above 19BRWY1.

Starting at the base of the Blue Rim escarpment, adjacent to the first sampled paleosol (Fig. 5.2; 5.6), an updated stratigraphic column was measured (41.7985 °N, -109.5856 °E) in September 2019 (Fig. 5.3, 5.4, 5.5). This 67m stratigraphic column traced the flanks of the escarpment to the top of the badlands. This stratigraphic column was sampled every 3m (approximately the height of one Jacob-staff) or at every interval of visual change (color, texture). In addition, plant fossils and plant hash were quarried at two locations approximately halfway (26m, 33m) and close to the top of the stratigraphic section (51.5m, 52m) for organic-rich fossil samples for isotope and bulk chemistry analysis.

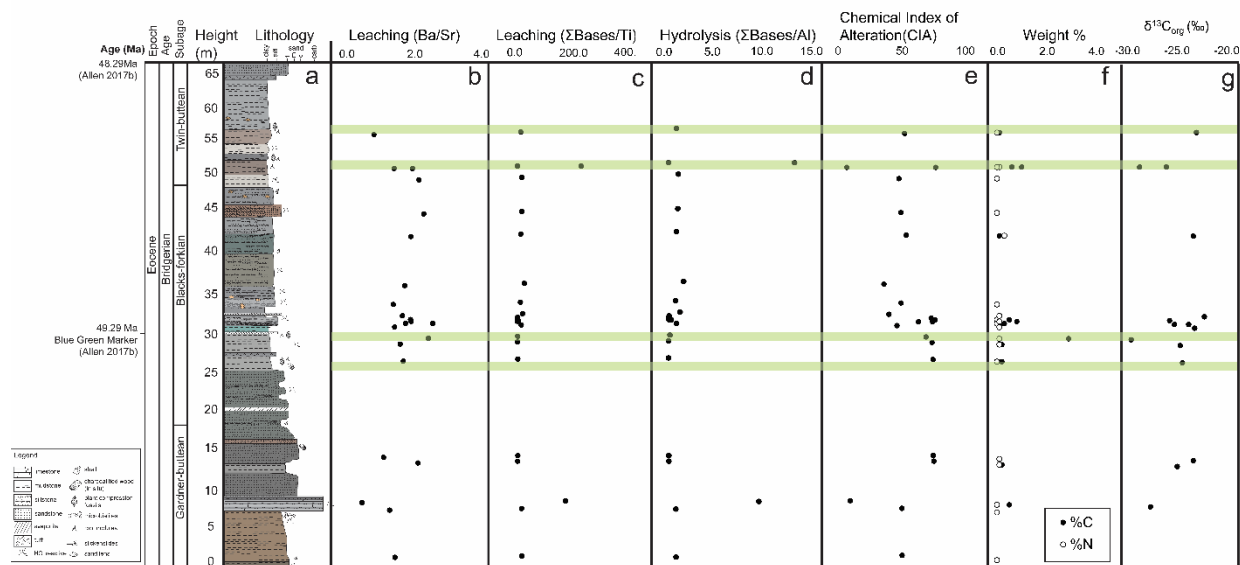


Figure 5.3 Stratigraphy with sedimentary geochemistry. (a) Stratigraphic column at the Blue Rim escarpment of the Bridger Formation. Geochemistry including (b) leaching, calculated using molar ratios of Ba:Sr, (c) leaching, calculated using the ratio of the sum of bases to Titanium, (d) hydrolysis, calculated using the ratio of the sum of bases to Aluminum, (e) chemical index of alteration to measure weathering (Equation 5.1), (f) weight % Carbon (black circles) and % Nitrogen (white circles), (g) $\delta^{13}\text{C}_{\text{org}}$ values. Light green transparent areas show stratigraphic levels containing plant fossils.

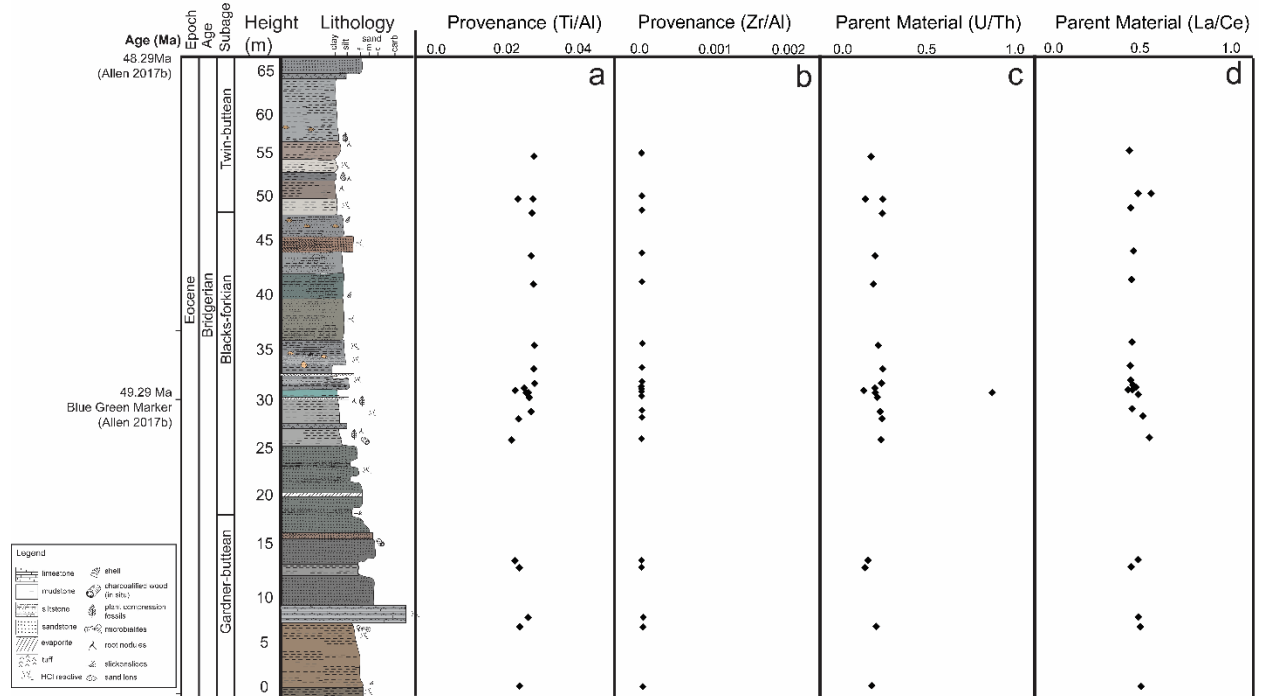


Figure 5.4 Stratigraphy with parent material and provenance proxies. (a) Provenance using molar ratios of Ti:Al, (b) provenance using molar ratios of Zr:Al, (c) parent material using molar ratios of U:Th, (d) parent material using molar ratios of La:Ce.

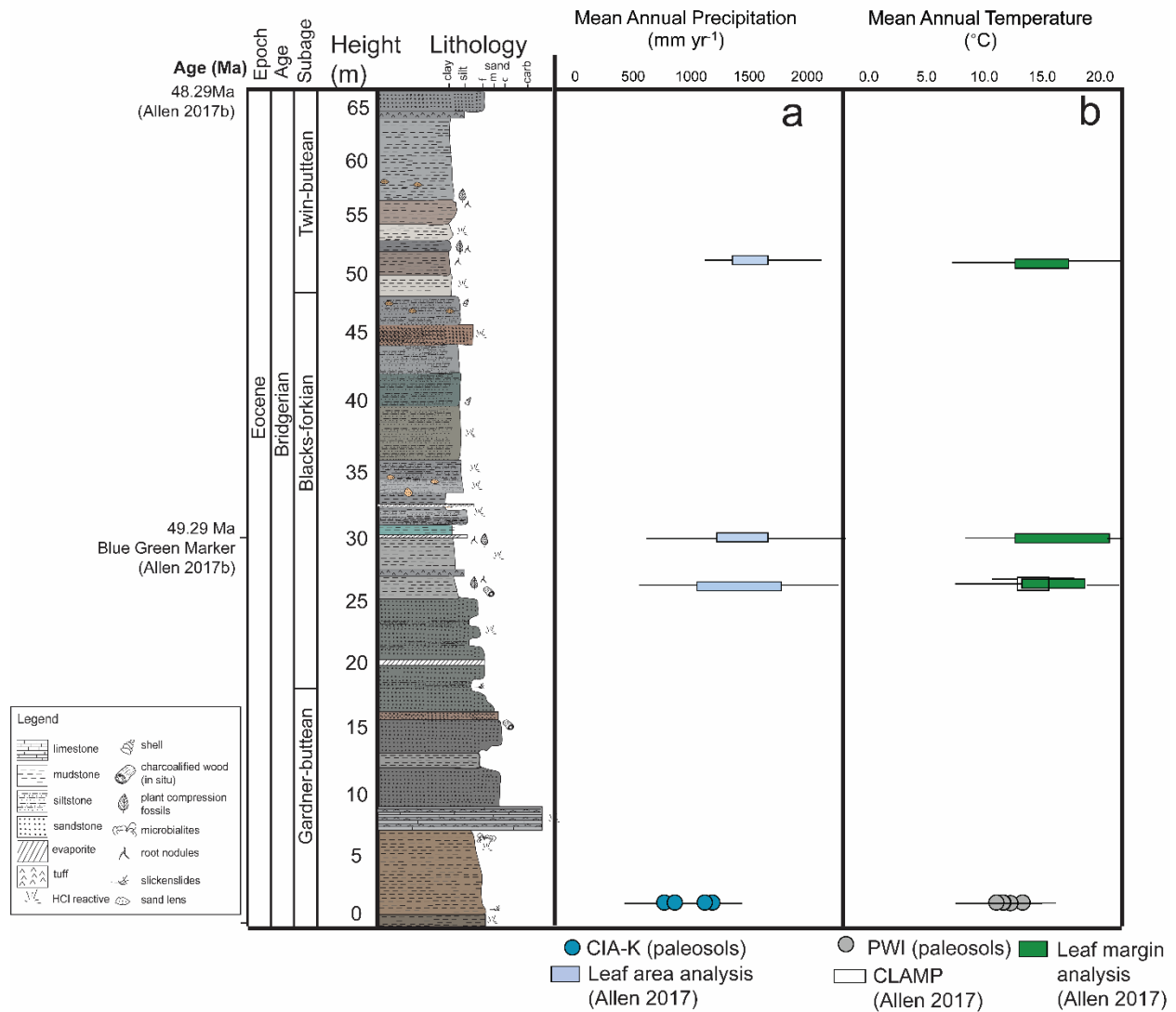


Figure 5.5 Stratigraphic column with climate proxies. (a) Reconstructed mean annual precipitation (mm yr⁻¹), and (b) mean annual temperature (°C).

5.3.3.2 Paleosol sampling

Six profiles of the same paleosol were identified and excavated along a lateral transect at the base of the Blue Rim escarpment (41.79892625, -109.58362614 (19BRWY1); Fig. 5.6). Paleosols sampled by horizon based on pedogenic features including root traces, burrows, drab-haloed and kerogenized roots, and horizonation (Fig. D1a, Table D1). Fresh rock material was excavated by digging at least 20 cm into the surface, avoiding all traces of modern pedogenesis

or surficial climate influence (i.e., modern roots or carbonate nodules). One distinctive, laterally continuous paleosol at the base of the section was sampled in five individual profiles over 440m (Fig. 5.2; Fig. 5.6; Fig. D1, D2, 19BRWY2-6). Samples were collected from each horizon present, with no fewer than three samples per paleosol profile. At each location, every present horizon (O, A, B, C) was sampled. For horizons that had color, texture, and/or other physical intra-horizonal changes, multiple samples were collected.

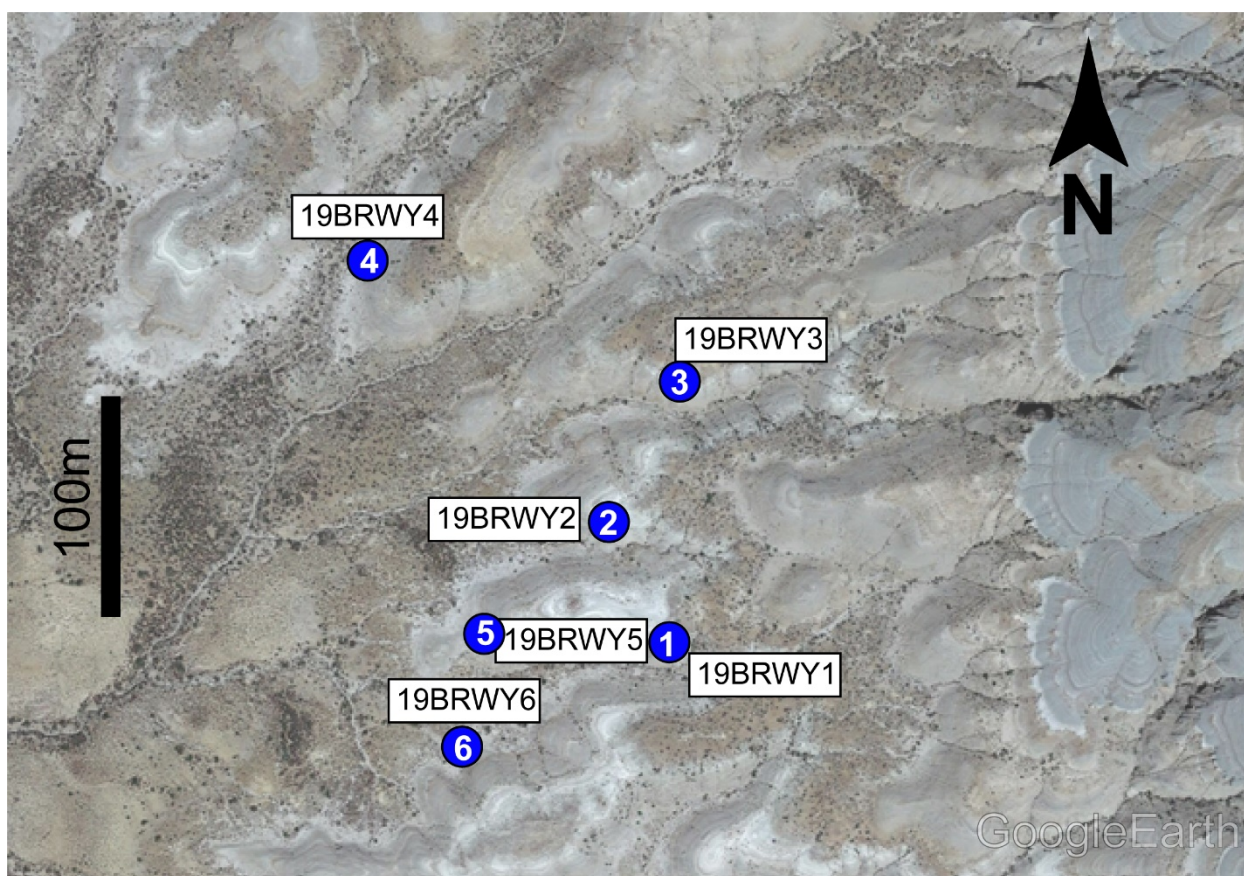


Figure 5.6 Lateral extent of paleosols. Included are paleosols 19BRWY1-6, atop image of Blue Rim escarpment topography, with a 100m scalebar. Paleosol numbers are noted in white text on blue circles. Image taken in Google earth V 9.123.0.2 (July 2019). Wyoming, USA. 41°48'02"N, 109°35'36"W, eye altitude 8611 ft.

5.3.3.3 Isotope analysis

Paleosol samples were ground to 70µm in a shatterbox. Approximately 10g aliquots of samples were measured then acidified in 5% hydrochloric acid (HCl) for 30 minutes to remove

carbonate and leave behind total organic carbon of bulk sample. After 30 minutes, these samples were decanted, then re-acidified for a total of three times (and/or until solution stopped bubbling). After these acid washes, they were rinsed with deionized water three times (or more, if given >3 acid washes). Samples were then dried in an oven at 50 °C for 72 hours.

Between 20–25mg of each sample was loaded into tin capsules and run on a Costech Elemental Analyzer to determine weight %C and %N in University of Michigan’s Earth Systems Lab with acetanilide (71.09 %C, 10.36 %N) for elemental composition calibration and acetanilide and atropine (70.56 %C, 4.18 %N) standards. The %C was used to calculate idealized loading size for isotope analysis; these samples were then run on the Picarro Cavity Ring-Down Spectroscopy (CRDS) on low carbon (Mode 9) for organic carbon isotope values ($\delta^{13}\text{C}_{\text{org}}$), with external precision better than $\pm 0.3\text{‰}$ for low-carbon samples.

5.3.3.4 Bulk Geochemistry

Approximately 10g aliquots of crushed paleosols, mudstone, and siltstone were measured and sent to ALS Laboratories in Vancouver, British Columbia, Canada for bulk elemental analysis. At ALS, samples were digested with perchloric (HClO_4), hydrofluoric (HF), nitric (HNO_3) and hydrochloric (HCl) acids, and concentrations were determined by inductively coupled plasma (ICP) optical emission spectrometry and ICP-mass spectrometry. The ICP-OES and ICP-MS were calibrated using internal standards, with major element precision better than 0.2 weight %.

5.3.3.5 Calculations

a. Weathering indices and leaching

Weathering was quantified using Chemical Index of Alteration of B horizons (CIA; Equation 5.1; Nesbitt & Young 1982), a feldspar weathering index based on the discrepancy in ion mobility during weathering.

$$CIA = \frac{Al_2O_3}{Al_2O_3 + Na_2O + CaO + K_2O} * 100 \quad (\text{Equation 5.1})$$

To test for alteration and expected pedogenic elemental trends, changes in individual element mobility and strain were explored using tau and epsilon (Equations 5.2–5.3; Chadwick et al., 1990), where epsilon represents the strain on an immobile element like Ti or Zr and tau represents the relative gain or loss of a mobile element relative to the paleosol's parent material. Average values of 2.7 g cm⁻³ and 1.5 g cm⁻³ were used for reworked ash and soil density, respectively (e.g., Sheldon & Tabor, 2009).

$$\tau_{j,w} = \frac{(\rho_w C_{j,w})}{(\rho_p C_{j,p})} * [\epsilon_{i,w} + 1] - 1 \quad (\text{Equation 5.2})$$

$$\epsilon_{i,w} = \frac{(\rho_p C_{j,p})}{(\rho_w C_{j,w})} - 1 \quad (\text{Equation 5.3})$$

The Paleosol Weathering Index (PWI; Equation 5.4; Gallagher & Sheldon 2013), which is based on differential bond strengths in cation oxides provided additional means for examining weathering. Molar concentrations are used to make calculations in Equations 5.1–5.4, rather than elemental concentrations.

$$PWI = ((4.20 * Na) + (1.66 * Mg) + (5.54 * K) + (2.05 * Ca)) * 100 \quad (\text{Equation 5.4})$$

We used several geochemical proxies to examine intensity of leaching, including the ratio of barium to strontium (Ba/Sr), which is higher with more leaching and lower with less leaching (Sheldon 2006; Retallack 2001) due to differential solubility; Sr is more soluble than Ba (Vinogradov 1959). The ratio of the sum of base cations to titanium is another metric for leaching, under the assumption that titanium is immobile, while other bases are mobile (Sheldon & Tabor 2009). The ratio of the sum of base cations to aluminum has been used as a metric for hydrolysis (Retallack 1999; Bestland 2000; Sayyed & Hundekari 2006).

b. Provenance and parent material

The molar ratios of titanium to aluminum (Ti/Al) and zirconium to aluminum (Zr/Al) was used to screen for consistency in sediment source in soils; direction of change in Ti/Al ratios is related to differences in chemical weathering, while Zr/Al ratios is related to changes in physical weathering (Sheldon & Tabor 2009). The molar ratio of uranium to thorium (U/Th), and

lanthanum to cesium (La/Ce) were used to trace potential changes in parent material composition through the stratigraphic unit, where a constant down-profile U/Th and La/Ce ratios reflect single-parent source (Sheldon 2006; Sheldon & Tabor 2009). Absolute parent material values for each of these ratios are not well calibrated, but direction of change observed at any site indicates a change in parent material, U/Th is redox-sensitive so La/Ce ratios are used as a comparative point in case of highly reduced environments.

c. Paleoclimate reconstructions

Mean annual precipitation was reconstructed using Chemical Index of Alteration minus potassium (CIA-K; Equation 5.5; 5.6; Sheldon et al. 2002; error $\pm 182 \text{ mm yr}^{-1}$), modified from CIA to control for potassium metasomatism in paleosols (Maynard 1992; Ennis et al. 2000; Sheldon et al. 2002). Mean annual temperature was calculated using PWI (Equation 5.7; error of $\pm 2.1^\circ\text{C}$; Gallagher & Sheldon 2013). We applied the empirical relationship between $\delta^{13}\text{C}_{\text{plant}}$ and $\delta^{13}\text{C}_{\text{atm}}$ values found by Arens et al. (2000; Equation 5.8; $R^2 = 0.34$) and used $\delta^{13}\text{C}_{\text{plant}}$ values of all individual fossils to reconstruct generalized, non-taxon-specific $\delta^{13}\text{C}_{\text{atm}}$ values. We compared this reconstructed value based on a generalized equation with reconstructed values based on species-specific carbon isotope discrimination values (as measured in Cornwell et al. (2018)). More specifically, we used fossils of *Lygodium* and *Acer* genera (n = 9 identified fossils used for individual measurements) to reconstruct $\delta^{13}\text{C}_{\text{atm}}$ values based on taxon-specific parameters (e.g. Stein et al. 2019).

$$CIA - K = \frac{Al_2O_3}{Al_2O_3 + Na_2O + CaO} * 100 \quad (\text{Equation 5.5})$$

$$MAP = 221e^{0.0197(CIA-K)} \quad (\text{CIA-K for paleosols; Equation 5.6})$$

$$T (^{\circ}\text{C})_{PWI} = -2.74 * \ln(PWI) + 21.39 \quad (\text{Equation 5.7})$$

$$\delta^{13}\text{C}_{\text{leaf}} = 1.1 (\delta^{13}\text{C}_{\text{atm}}) + 18.67 \quad (\text{Equation 5.8})$$

Holdridge life zones are ecoregions classified by water availability and temperature, that can be further subdivided into successional stages reflecting land use, disturbance history, latitude, altitude (Holdridge 1967; Lugo et al. 1999). The parameters for each life zone are calculated based on potential evapotranspiration and humidity provinces (Holdridge 1967; see Appendix D). Similar metrics that use evapotranspiration and precipitation to quantify ecosystems into “floral humidity provinces” based on paleosol measurements, have been established more recently by Gulbranson et al. (2011; see Appendix D). See Appendix D for methodology used to determine Holdridge life zones and Floral Humidity Provinces for paleosols (this study) and previously published floras (Leopold & MacGinitie 1972; Roehler 1993; Wing et al. 2005; Smith et al. 2008; Wing & Currano 2013; Allen 2017).

5.4 Results

5.4.1 Age

Using $^{40}\text{Ar}/^{39}\text{Ar}$ radiometric dating, weighted mean ages of two younger sanidine crystals in the base and middle of the blue-green marker bed were weighted to place the age at 49.29 ± 0.18 Ma (aligning with Bridger A/1b). These grains were found alongside pumice clasts and biotite grains along with minor detrital components following Challis volcanic field eruptions, indicating juvenile volcanic material deposition. This date was calculated using grains from BR-3, yielding an estimated age of 48.98 ± 0.38 Ma, collected at the base of the main blue layer, just above the UF 15761S plant quarry (elevation 6737 ft; Allen 2017), and grains from Sample BR-4 (collected from the lower main blue-green layer in the 2014/UF 19297 stratigraphic section at 6745 ft; Allen 2017) with a resolved estimated age of 49.43 ± 0.23 Ma. Because these two samples were collected from the same stratigraphic unit but out of stratigraphic order, they were averaged for an age of 49.29 ± 0.18 Ma.

The two sand beds sampled for $^{40}\text{Ar}/^{39}\text{Ar}$ dating at the top of the escarpment (elevation 6861 ft; Allen 2017) yielded more detrital grains, six young grains gave a weighted mean of 48.29 ± 0.45 Ma, such that the stratigraphy between the blue-green marker bed and sand beds spans Bridger B, landing the uppermost part of the Blue Rim Escarpment time equivalent to Bridger C or D/3 (Fig. 5.3, 5.4, 5.5). This constrains the lower plant horizon as slightly older

than 49.29 Ma (Allen 2017), while the upper plant horizon could be Bridger A1b or younger than 48.29 Ma.

5.4.2 Paleosol descriptions

Six profiles were sampled laterally from a single paleosol at the base of the Blue Rim escarpment (1m in the stratigraphic column; Fig. 5.3, 5.6). Paleosol profiles (Fig. 5.6; Fig. D1) typically consisted of a silty and/or sandy brown, yellow A-horizon over a parent material C-horizon of green-grey silty mudstone anywhere from ~20 to 112 cm below the surface. Paleosol #1 was missing a B-horizon due to erosion, while paleosol #4 was missing an A horizon, likely truncated during burial. Typically, each profile was lighter colored in upper horizons and darker in lower B- and C-horizons. In the paleosol profiles sampled, every A-horizon but one, and several upper B-horizons, had root traces, kerogenized roots, and/or rhizoliths. We observed drab-haloed roots in paleosols #1 and 4. Paleosol #2 had vertical burrows of up to 1cm diameter and ~3 cm length, and paleosol #1 had visible peds (Table D1; Fig. 5.2a). These soils were well-developed Inceptisols based on features, textures, and extrapolation from the local flora (Fig. 5.2a; Fig. D1; D5; Table D1).

5.4.3 Paleosol geochemistry

CIA-K (weathering profiles calculated using Equation 5.5) reference values include 100 for pure kaolinite, and values of 0 demonstrating no Al present at all. Clay-rich materials start with CIA values of 60–70 with even higher values in B-horizons and more weathered surfaces (Sheldon & Tabor 2009), while low CIA-K values occur in soils with low precipitation and high evaporite accumulation (Sheldon et al. 2002). Paleosols with sedimentary, worked parent material like those found at Blue Rim escarpment are expected to have CIA-K values of B-horizon > 60-70. On average, the lateral extent of the paleosol found at the base of the Blue Rim stratigraphic section had A-horizon values of 80 with a minimum of 40–50 in B- and C- horizons (Fig. D1b). Ti/Al values were constant throughout, ranging from 0.040 to 0.045, typical values of mudstones and sandstone parented materials (Sheldon & Tabor 2009), like those seen in sediments throughout the Blue Rim escarpment (Fig. D1c; Table D2).

Tau (used to measure mobile element transport) was calculated following Chadwick et al. (1990; Equations 5.2 and 5.3) and demonstrated in Supplemental Figure D2(a-f). Overall, tau

values for K, Mg and Na all ranged from 0 to -0.5, and tau values for Ca ranged from 0 to -1, except in paleosol #2 (which was extremely high in Ca), as is typical for Inceptisols. Tau for Rb and Fe were generally also between 0 and -0.5, though this was less consistent between profiles. To note, paleosol #1 (19BRWY1; Fig. 5.6) was excluded for paleoclimate reconstructions due to the lack of presence of the B- horizon (we identified this soil as an Entisol, which cannot be used for climate reconstructions; see Fig. 5.6 for location). Paleosol #2 (19BRWY2) was also excluded for climate reconstructions, due to the high % Ca, likely of carbonate origin as this site was reactive to HCl. Based on both field taxonomy and these geochemical results, paleosols #3-#6 are identified as Inceptisols.

5.4.4 Sedimentary geochemistry

Ba/Sr ratios, used to measure leaching intensity, were on average 1.64 (\pm 0.52 standard deviation) throughout the stratigraphic unit, with outlier values of \sim 2.54 and 2.42 at 31m and 29m, and 0.47 at 7.25m. Another proxy for leaching (sum bases/Ti) had peaks around 10m (191.19) and 52m (247.76), but otherwise consistent leaching \sim 50, with a range of 9.91 to 247.46 and average of 47.82 (Fig. 5.3b,c). Hydrolysis, as measured by sum bases/Al, peaked at 51.5m (13.69) and troughed at 26m (0.73) but otherwise demonstrated consistent leaching with an average value of 2.20 (Fig. 5.3d).

The mean chemical index of alteration (CIA), a measure of weathering, was 55.61 (\pm 20.16 standard deviation). CIA was lowest around 51.5m (CIA = 7.14) and highest around at 51.5 (CIA = 76.61) with similarly high values (73–77) at 12.5m, 26, 28.25m, 31m, 31.25m, 31.5m, and 51.5m (Fig. 5.3e). Percent carbon throughout the section was distributed similarly, with peaks at the same locations as CIA: A high of 2.9 wt. %C (29m) and a low of undetected (many places throughout the section). Percent N was highest at 42.5m (0.3%) and lowest at multiple sampling locations throughout the section (0%) (Fig. 5.3f). $\delta^{13}\text{C}_{\text{org}}$ values were lowest in these sections, with an average of -24.97‰ (\pm 2.17 standard deviation) and range of -22.13 to -29.49‰ (Fig. 5.3g).

Provenance remained nearly constant (Ti/Al ranged from 0.02 to $<$ 0.03), with a high at 32m and low at 26m (Fig. 5.4a). Parent material, likewise, remained constant for all metrics except U/Th; La/Ce ranged from 0.44 to 0.57, Zr/Al ranged from 2.37×10^{-5} to 4.83×10^{-5} (Fig.

5.4b,d). All U/Th ratios fell between 0.15 and 0.26 except for 31m at the blue-green marker, with a value of 0.87 (Fig. 5.4c).

5.4.5 Flora

At least 69 morphotypes were previously identified from Blue Rim by Allen (2017). The identifiable fossils from this specific field excursion sampled specifically for organic isotope analyses included multiple specimens of *Lygodium kaulfussi* (climbing fern, genus Lygodiaceae) compression fossils, as well as one example of *Asplenium sp.* (fern, family Aspleniaceae; as described in Allen 2017), an example of *Populus cinnamomoides* (poplar, family Salicaceae), one *Cedrela* leaf, (undefined species; mahogany, family Meliaceae; Fig. D5), several dense leaf mats, and assorted twig and branchlet fossils were recovered. These specimens were collected from the same strata as the lower horizon (e.g. UF 15761N, Allen 2017), located 26 m on the stratigraphic column included in this study (Fig. 5.3, 5.4, 5.5). There was evidence of scraps of several unidentified monocots, though no isotope analyses were run on these fossils.

5.4.6 Climate

Mean annual precipitation (MAP) values reconstructed using CIA without potash (CIA-K) on paleosol B-horizons (Equation 5.6) ranged from 608–1167 mm yr⁻¹, with an average of 845 mm yr⁻¹ (± 181 mm yr⁻¹) (Equation 5.6; Fig. 5.5; D6). The lowest estimated MAP value (288 mm yr⁻¹) was excluded due to high %Ca (10.25%) in the B horizon of paleosol 2. Mean annual temperature values (MAT) reconstructed using PWI on paleosol B-horizons (Equation 5.7) ranged from 10.4 to 12.0 °C (± 0.72 °C standard deviation), with an average of 11.0 °C.

A wide range of $\delta^{13}\text{C}_{\text{atm}}$ values were reconstructed from $\delta^{13}\text{C}_{\text{leaf}}$ from the 34 individual leaf fossils used using a generalized relationship (Arens et al. 2000). Reconstructions using the generalized Arens et al. (2000) model were done on all 34 individual leaves, even though some included unidentified fossils. Additional species-specific tests were done on all samples of *Lygodium* or *Acer* using isotope discrimination values from extant plants of these genera. 38% (n = 13) of the 34 $\delta^{13}\text{C}_{\text{atm}}$ values reconstructed using the generalized Arens et al. (2000) model suggested a $\delta^{13}\text{C}_{\text{atm}}$ value of between -5.32 and -5.82‰. 56% of all of these reconstructed values were between -5.0 and -6.0‰ (n = 19; Equation 5.8; Fig. 5.7). Limitations on this reconstruction are the species-specific nature of this proxy (Beerling & Royer 2002; Stein et al. 2019), and

values outside the range of most samples (44%) were more extreme potentially preferential diagenesis of certain compounds, driving the isotopic signature away from these values (Beerling & Royer 2002; Tu et al. 2004). Using identified *Lygodium* and *Acer* fossils ($n = 9$ total), we applied the taxon-specific isotope discrimination principle and reconstructed an average value of -4.82‰ ($\pm 0.92\text{‰}$ standard deviation). These reconstructions were based on isotope discrimination values of 20.56‰ for *Lygodium* and 20.37‰ for *Acer* (as reported in modern isotope analyses by Cornwell et al. 2018).

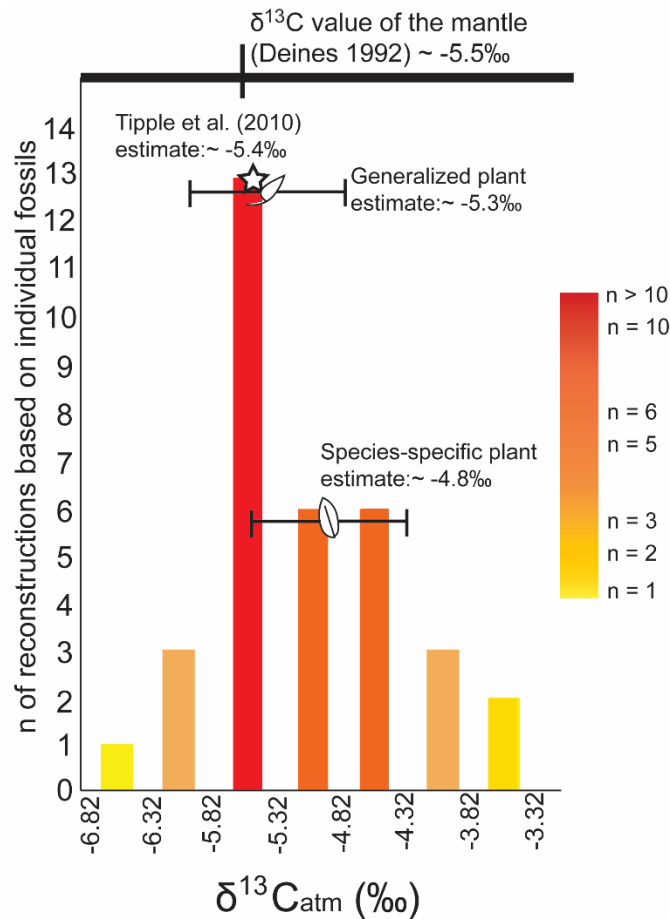


Figure 5.7 $\delta^{13}\text{C}_{\text{atm}}$ as reconstructed from $\delta^{13}\text{C}_{\text{leaf}}$ of Blue Rim fossil flora. Reconstructions utilized the generalized relationship between $\delta^{13}\text{C}_{\text{atm}}$ and $\delta^{13}\text{C}_{\text{plant}}$ (Arens et al. 2000; $n = 34$; Equation 5.8). The species-specific mean and standard deviation are shown, as are the generalized plant mean and standard deviation. The Tipple et al. (2010) foraminiferal reconstruction is denoted in a star, and the $\delta^{13}\text{C}$ value of the mantle is shown above (Deines 1992).

5.5 Discussion

5.5.1 Age

Original estimates based upon biostratigraphy placed the deposition of the Bridger Formation beginning before 50 Ma (Krishtalka et al. 1987; Alexander & Burger 2001). Early radiometric dates suggested an age between 49.09–45.57 Ma (Murphey et al. 1999). Other estimates bracketed the youngest sediments at 46.16 Ma (Sage Creek Mountain Bridger E tuff; Murphey & Evanoff 2007), or older than 48.27 Ma from a nearby, stratigraphically younger sanidine from the Church Butte tuff, also in the Bridger Basin (Murphey et al. 2011). Bookending older age estimates, the laterally correlative Big Island Tuff within the Wilkins Peak Member of the Green River Formation has been dated to 50.4 Ma \pm 1.1 Ma and 40.1 Ma \pm 1.2 Ma (Krishtalka et al. 1987; Alexander & Burger 2001; Allen 2017). The new $^{40}\text{Ar}/^{39}\text{Ar}$ dates presented here for the blue-green marker bed and sand bed above the floral quarries suggest that this section spans 49.29 Ma–48.29 Ma, making it slightly younger than the EECO, with the paleosols at the base of the section >49.29 Ma. Assuming constant sedimentation rates based on a linear interpolation between measurements, which calculates each meter of sedimentation equal to ~ 28 ka, paleosols are roughly 833,300 years older than the blue-green marker bed, or 50.1 Ma. This age lacks in precision, although it has been demonstrated that sedimentation rates in the Bridger Formation are roughly continuous (Murphey & Evanoff 2001), so the paleosols are unlikely to have been dramatically different in age. However, the shifts between different depositional environments indicate there is likely some variability in sedimentation rate. Future workers could focus on dating the sandstone features at the base of the section to constrain the oldest age of deposition in the Blue Rim escarpment better.

These new, and slightly younger dates on average, demonstrate that post-Eocene, Lake Gosiute was regressing and transgressing, though overall shrinking in size as the region dried. The Blue Rim locality is located approximately in the middle of Lake Gosiute's full extent (Fig. 5.1a), so shallowing and/or ephemeral dry land ecosystems in this region signifies that this lake's disappearance was imminent during the formation of Blue Rim. The new dates and the inferred depositional environment can be used to determine the timing and fate of the lake in conjunction with biostratigraphic evidence: fossils of *Goniobasis/Elimia* (fresh water snails, Pleuroceridae)

are prominent just above this stratigraphic section, affirming the Bridger A/B transition, as there is a biostratigraphic *Goniobasis* marker bed between Bridger A and B documented nearby (Allen 2017). *Goniobasis*' shallow lake dwelling habitats (Hanley 1976) align with the overall regression of Lake Gosiute.

5.5.2 Stratigraphy, provenance and weathering

Provenance was consistent throughout the stratigraphic section and paleosols, which can be interpreted as consistent hydrological inputs to the section. Consistent provenance does not support the idea that there might be inconsistent water sources from disparate mountain ranges causing interference in signals in the region (Doebbert et al. 2012). Parent material analyses agreed with our assumptions about parent rock and indicated that all sources were primarily sedimentary. The consistent Ti/Al, U/Th, and La/Ce ratios correspond to constant parent material throughout the one million years section covered by the Blue Rim stratigraphic column, demonstrating that basin-scale hydrology was likely not reorganized during this time. The one exception to constant parent material and provenance ratios is the anomalously high U/Th ratio in the blue-green marker bed (0.87). This proxy is redox-sensitive, so this anomalously high U/Th ratio is due to the preferential redistribution and accumulation of U in this section, as Th is insoluble and immobile (Pett-Ridge et al. 2007; Sheldon & Tabor 2009). Weathering and leaching were highest in the sections where there was high carbon content; this correlation is likely due to organic acids produced by plants in the ecosystem that contribute to chemical weathering (Fig. D4; $R^2 = 0.20$; p-value = 0.01 Ong et al. 1970; Berner 1992).

5.5.3 Paleosols

The six paleosol profiles sampled from one single paleosol, which was stratigraphically equivalent to 1m up the documented column, were all Inceptisols. This taxonomy was determined including soil features, provenance, leaching, weathering, element transport, and parent material (Fig. D1, D2). This is fitting considering the depositional history of this environment; these soils were likely formed between floods, when there was sufficient time for horizonation to occur, before being cut off by a flooding or minor lake transgression. Paleosol #1 (19BRWY1; 1m in stratigraphy; Fig. 5.3, 5.4, 5.5, 5.6) is an Entisol and was not included in paleoclimate reconstructions because it lacks a B horizon. The soil classification of these soils as

Inceptisols aligns with the interpreted depositional history of an ephemeral shallow, drying lake environment with periods of fluvial-alluvial deposition.

5.5.4 Climate

The early Eocene of North America is reconstructed as populated by generally widespread temperate to subtropical wet forests (Allen 2017). Depending on latitude, other studies indicate slightly warmer conditions than prior Blue Rim-based reconstructions (Allen 2017). Generally, mean annual temperatures reconstructed from other sites between 36 and 80 °N have ranges from 35°C (36 °N) to 8°C (80 °N; Fricke & Wing 2004). For mid-latitude floral assemblages, physiognomic reconstructions had cold month mean temperatures around 10 °C, indicating a relatively frost-free existence for plants living in the bulk of North America at the time (Wing & Greenwood 1993), which aligns very well with the paleosol-based results in this study. Specific examples include Kisinger Lakes, a floodplain deposit in the Wind River Basin (Aycross Formation; NE of the Greater Green River Basin; Berry 1930; MacGinitie 1974), which was thought to have warmer temperatures ranging 19 to 23 °C, with cold month mean temperatures calculated by Climate Leaf Analysis Multivariate Program (CLAMP) virtually frost-free. Precipitation in this region was estimated to be 890–1400 mm yr⁻¹, with most of this precipitation accumulating during the summer. Hyland et al. (2018) used PPM_{1.0}, a paleosol-based spline model, to estimate mean annual temperature, nearest living relative bioclimatic analyses to reconstruct cold month mean temperature, and clumped isotope measurements (Δ_{47}) to calculate warm month mean temperature estimates of the nearby, slightly older Wasatch Formation (~52– ~50.5 Ma). These estimates were made roughly 140 kilometers NE of the Blue Rim escarpment. The warm month mean temperatures reconstructed in these earlier nearby deposits were 18 to 34 °C +/- 3 °C (Kelson et al. 2017; Hyland et al. 2018), while cold month mean temperatures from 4.2 to 7.6 °C (Hyland et al. 2018) and mean annual temperature values ranged from 15.2 to 18.2 °C (Hyland et al. 2018). These estimates are warmer than those reconstructed at Blue Rim escarpment, though these estimates are likewise older, and span the EECO; Hyland et al. (2018) note a decreasing trend in younger temperatures reconstructed for their study. The Parachute Creek, Laney, and Fossil Butte Members of the Green River Formation, also thought to be slightly older than the Blue Rim escarpment, roughly the age of the EECO, have also been interpreted as semi-deciduous with seasonally dry subtropical taxa (Wing

1987; Allen 2015). Finally, slightly further away in the Okanagan Highlands, climate reconstructions yield temperature ranges of 10–13.5 °C (Wolfe et al. 1994; Wolfe et al. 1998; Greenwood et al. 2005).

MAP reconstructions from this study, based on inorganic proxies in paleosols ranged from 608–1167 mm yr⁻¹ (average: 845 mm yr⁻¹ ± 255 mm yr⁻¹, standard deviation). High influence of carbonate in parent material results in a lower CIA-K, and thus lower rainfall estimate (Sheldon et al. 2002). Error on CIA-K proxies is ±181 mm yr⁻¹ (Sheldon et al. 2002; Passchier et al. 2013); such that estimates from floral and inorganic geochemical proxies are within error of one another. However, overall, these inorganic-based reconstructions are slightly lower than those estimated using CLAMP and leaf area analysis (LAA). This could be due to the location in the section (lower and likely older, see Figure 5.5). The discrepancy may also be because CLAMP has been cited as often producing overestimates of precipitation (Wilf et al. 1998; Allen 2017), and leaf area analysis methodology using vein scaling also can result in overestimates of leaf size, which translate to excess precipitation values (Merkhofer et al. 2015).

Results based off inorganic geochemistry in paleosols in this study showed slightly lower temperatures than those reconstructed using physiognomy, with PWI-based temperatures from 10.4 to 12.0 °C (average 11.0 °C ± 0.7 °C standard deviation). Like precipitation, the underestimation based on PWI in paleosols could be related to location in the section, as paleosols were significantly lower than plant quarries in the section (see Figure 5.5). The discrepancy could be related to the soil taxonomy; the PWI tool used to reconstruct temperature was calibrated for Inceptisols, Alfisols and Ultisols, however none of the Inceptisols sampled were from temperatures >12 °C (Gallagher & Sheldon 2013). As such, the weathering indices these paleo-Inceptisols are based off of Inceptisols in modern ecosystems, which are typically found in cooler temperatures. Because the early Eocene was significantly warmer, it is possible that early developmental soils like Inceptisols existed at higher temperatures, especially in dynamic ecosystems with frequent flooding events like those preserved at the Blue Rim escarpment.

Despite the modest discrepancy between physiognomic and paleosol-based precipitation and temperature estimates, the life zones and floral humidity provinces calculated using Blue Rim paleosols were the same as those calculated using physiognomic techniques. When

paleosol-based climate reconstructions are plotted in floral humidity space and Holdridge life zones, our results were comparable to flora-only estimates based on Allen (2017) and Wilf et al. (2000)'s reconstructions of the early Eocene, and Wing et al.'s (2005) reconstruction of the Paleocene-Eocene thermal maximum (PETM; Fig. 5.8). This demonstrates the importance of the holistic approach: although individual proxies might not be exactly comparable, the overall ecosystem-level reconstructions, from taxonomic identity of fossils present to paleosol taxonomy to inorganic, organic, and floral climate reconstructions all align.

These fossils collected for organic analysis found at Blue Rim escarpment included charcoalfied trunks and *Lygodium kaulfussi* (Lygodiaceae), *Asplenium* (Aspleniaceae; two ferns), *Populus cinnamomoides* (Salicaceae), *Cedrela* (Meliaceae; woody angiosperms) as well as dense leaf mats. These collected fossils (sampled at 26 m on the stratigraphic section) are comparable to a smaller set of findings by Allen (2017) and MacGinitie (1969) and characteristic of mesic, forested environment. *Lygodium*, a climbing fern at present and during the Eocene, cannot grow in exceedingly wet conditions (e.g. rain forest), and *Populus* and *Cedrela* trees are found in temperate and tropical-subtropical forests and riparian areas (Hamzeh & Dayanandan 2004; Hamzeh et al. 2006). There was evidence of monocot fossils, likely a part of the herbaceous understory; this is congruent to the palynological evidence of *Phoenix windmillis*, (palm, Arecaceae) found at this site by Allen (2017), though these fossils were not sufficiently preserved to be identifiable.

This compiled, multi-proxy evidence provides confidence that this region was indeed an ephemeral wet forest along the edge of a lake and/or river, experiencing frequent and sporadic flooding from nearby freshwater sources. Floral humidity provinces and Holdridge life zones calculated from paleosol-based MAP and MAT reconstructions were compared to ones calculated from MAP and MAT as provided in published studies. Chronologically, this region went from wettest during the PETM in the proximal Bighorn Basin (rain forest; reconstructed using LMA and LAA; Wing et al. 2005) to drier and cooler (characterized as a wet forest), resulting in less evapotranspiration and less precipitation as time progressed. EECO (Bighorn Basin; Wing & Currano 2013). Blue Rim-era floral humidity provinces are all estimated to also be wet forests, which is further contextualized by fossil evidence as presented in our fossils and Allen's (2017) characterization of the escarpment. Other comparably aged Eocene climate

reconstructions based on palynological data from the Laney Member of the Green River Formation (~48.5 Ma; Smith et al. 2008), located in the same basin as the Blue Rim escarpment, appear to be closer to rainforest floral humidity provinces (Leopold & MacGinitie 1972; Roehler 1993; Smith et al. 2008; Fig. 5.8). Over the late Paleogene into Neogene and more recently, the region has continued drying and is now high desert/dry scrub, with minimal precipitation (195 mm yr⁻¹ in 2019, the year sampled; PRISM Climate Group 2004), cold winters (<0 °C from November to March; PRISM Climate Group 2004), and hot, dry summers (Fig. 5.8). The locations of each of these sites is plotted on Figure D7, to demonstrate their proximity.

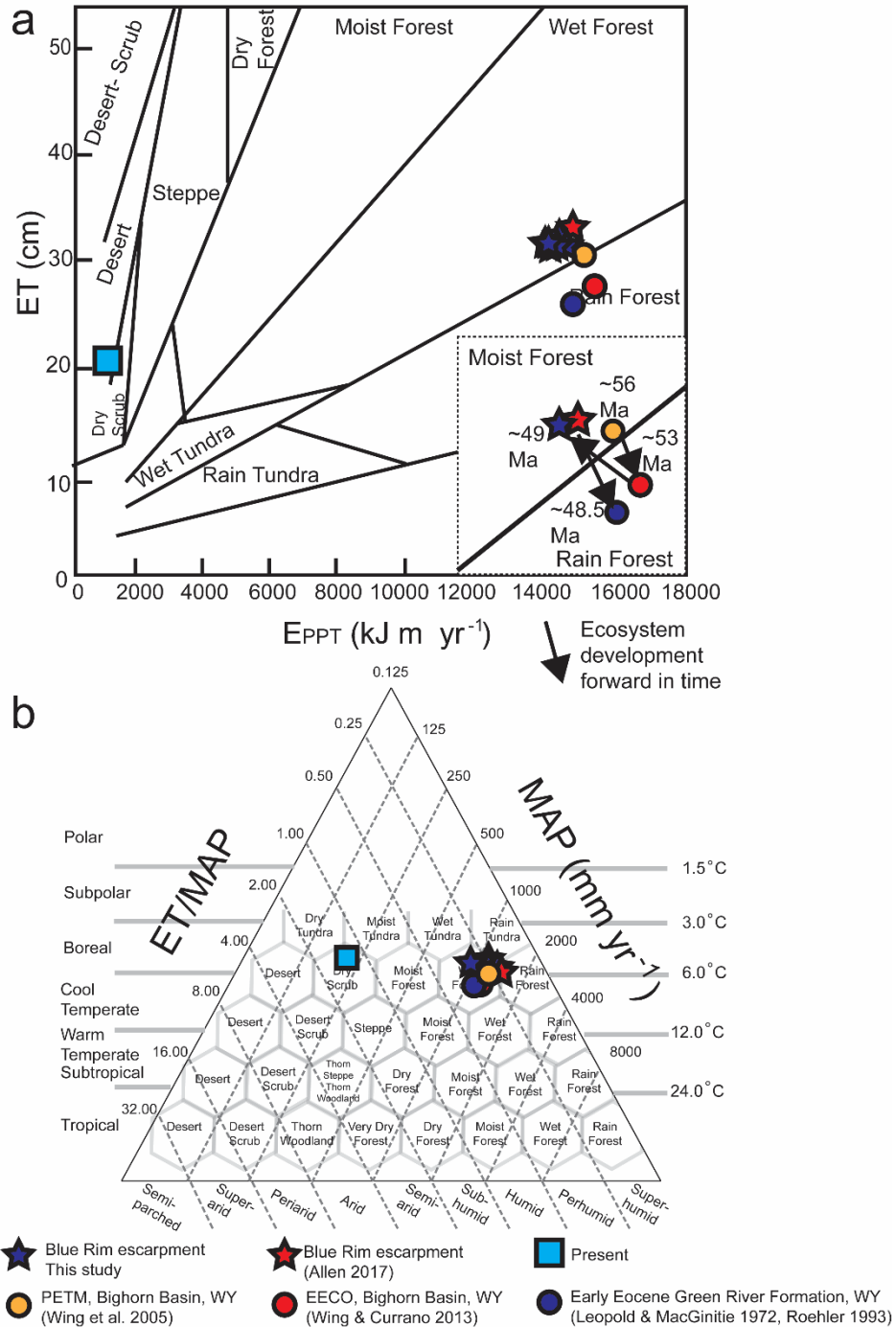


Figure 5.8 Ecosystem level characterization of Blue Rim escarpment and other Cenozoic Wyoming ecosystems. Paleosol-based (a) Floral Humidity Province and (b) Holdridge life zones (Holdridge 1967) in blue stars. (a) includes inset showing climate progression over time, with (1) showing the PETM (Bighorn Basin, ~56Ma), (2) the EECO (Bighorn Basin, ~53Ma), (3) this site (~49 Ma) and (4) the latest stage of Lake Gosiute (Green River Formation, ~48.5Ma; Smith et al. 2008). Comparative studies for this region based on nearby temperature and precipitation reconstructions are shown in yellow, red and blue circles, while the present is shown in light blue squares. Allen (2017) dissertation work using leaf margin analysis to reconstruct MAT and leaf area analysis to reconstruct MAP is shown in red stars.

As mentioned, based on the comparative Arens et al. (2000) model, $\delta^{13}\text{C}_{\text{leaf}}$ values can be used to infer $\delta^{13}\text{C}_{\text{atm}}$ values. In previous works, Stein et al. (2019) and others determined that plant carbon isotope discrimination was taxon-specific (Stein et al. 2019; Sheldon et al. 2020; Stein et al. in press). Limitations of the Arens et al. proxy include the lack of taxonomic identity and the assumption that plant water use efficiency (c_i/c_a) remains constant in long and short-term scenarios (Beerling & Royer 2002). Our large sample size of complete leaf fossils from a single horizon ($n = 34$) allows us to statistically determine the most likely $\delta^{13}\text{C}_{\text{atm}}$ value based on the assumption that Arens et al.'s (2000) model represents a general relationship between $\delta^{13}\text{C}_{\text{atm}}$ and $\delta^{13}\text{C}_{\text{leaf}}$ values. To address limitations related to taxonomic identity, we also conducted analyses with taxon-specific reconstructions using nine total *Lygodium* and *Acer* fossils, using extant members of these genera (as published in Cornwell et al. 2018) to determine isotope discrimination and reconstruct the atmosphere. Taxon-specific reconstructions had an average value of -4.82‰ ($\pm 0.92\text{‰}$ standard deviation), within error of the isotopic value of mantle CO_2 (-5.5‰ ; Deines 1992). The discrepancy between the mean and the mantle is likely because of the small sample size, and with more targeted sampling, this taxon-specific approach would yield comparable results to the generalized reconstructions and closer to the mantle. Due to our lack of sampling resolution, the higher sampling using assumptions of general C_3 photosynthesis is more appropriate in this case. We compared our reconstructed $\delta^{13}\text{C}_{\text{atm}}$ values (between -5.32 and -5.82‰) to the value reconstructed for ~ 49 Ma using benthic and planktonic foraminifera, -5.4‰ (Tippie et al. 2010), and feel confident in our use of this tool to reconstruct $\delta^{13}\text{C}_{\text{atm}}$ values. This value is aligned with the isotopic composition of the mantle, which is also identified as $\sim -5.5\text{‰}$ (Deines 1992); thus, we can assume that the majority of the source of CO_2 gas to the atmosphere at this time was volcanic in origin.

5.6 Conclusions

The age findings contained in this study constrain the time period for the Blue Rim wet forests as younger than previous estimates, with the upper half of the section clearly deposited after the EECO. Based on dating and sedimentation rates, the lower part of the section could overlap with the end of the EECO, but *the climate remains unchanged throughout the section.*

During the EECO, the Blue Rim escarpment received between 608–1167 mm yr⁻¹ of precipitation, likely related to different moisture regimes, and was a productive paratropical forest. Though reconstructed temperature and precipitation values using paleosol and sedimentological geochemistry are lower than published values reconstructed from flora, the values all fall within error of one another. Furthermore, the Holdridge life zones and floral humidity provinces calculated for both physiognomic-based and geochemistry-based reconstructions are comparable, pinpointing this region as a warm, wet forest ~49 Ma.

The presented updated age constraints, floral evidence and proxies, and inorganic and organic geochemical proxies at Blue Rim escarpment make it possible to reconstruct the depositional environment of this Lake Gosiute central region in an unprecedented way, including demonstrating the timing of the lake's demise. Geochemical tools allow us to interpret constant climate, hydrology, and provenance in the region; active tectonism was not recorded in this region. While Laramide orogenesis extended from 70 to 40 million years ago, this mountain-building was not continuous at any given location (Dickinson et al. 1988), and indeed, previous works have estimated diachronous termination of Laramide orogeny in Wyoming to be anywhere between 35 and 50 Ma (Dickinson et al. 1988). The multi-proxy results indicate that it is likely that the Blue Rim escarpment was deposited post-Laramide orogeny. The use of multiple proxies to cross-compare sites is under-utilized in paleoclimate reconstructions but affords us more confidence in our understanding of regional and more broad-scale climate regimes. Findings also contextualize the regression of Lake Gosiute, especially given the location of the Blue Rim escarpment; it is clear that at the time, Lake Gosiute was shallowing though still receiving sedimentological inputs from the same, consistent hydrological sources, with ephemeral flourishing forests on the lakeshore. Based on ample floral and geochemical data, ~49.29 to 48.29 million years ago – after the peak of the EECO – southwest Wyoming was a warm, wet forest with little to no frost and mild temperatures, in agreement with previous work.

Previous workers have worried about the interference of multiple hydrological inputs from various topographic sources due to the active tectonism in the region at the time. The consistent Ti/Al, U/Th, and La/Ce ratios to determine provenance and parent material throughout the Blue Rim stratigraphic column demonstrate that the hydrological and sedimentological inputs remained stable for this location throughout the one million years spanned by this section. This multi-proxy approach can be used in roughly contemporaneous, adjacent basins (e.g. Washakie

Basin, Uinta Basin, Sand Wash Basin, Piceance Basin); an in-depth, multi-point study of this region in the early Eocene can further elucidate the North American continental interior climate during hothouse periods, as well provide more information about hydrological inputs and tectonism in the region at this time.

5.7 Acknowledgments

We thank Nikolas C. Midttun for assistance measuring, creating, and sampling the stratigraphic column at the Blue Rim escarpment in June 2019. We thank Steven Manchester for personal communications regarding the location of floral fossil quarries at Blue Rim. We thank Selena Y. Smith for personal communications and consultation regarding fossils and for access to her camera and camera stand for fossil photographs. We would like to acknowledge Naomi E. Levin, Christopher J. Poulsen and Gretchen Keppel-Aleks for their feedback on this manuscript. This work was partially funded by NSF Award #1812949 to Nathan Sheldon and Michael Smith, and an Evolving Earth Graduate Research Grant to RAS.

5.8 References

- Allen, S. E. (2017). Reconstructing the local vegetation and seasonality of the Lower Eocene Blue Rim site of southwestern Wyoming using fossil wood. *International Journal of Plant Sciences*, 178(9), 689-714.
- Allen, S. E. (2017). The Uppermost Lower Eocene Blue Rim Flora from the Bridger Formation of Southwestern Wyoming: Floristic Composition, Paleoclimate, and Paleoecology. Doctoral Dissertation, University of Florida.
- Arens, N. C., Jahren, A. H., & Amundson, R. (2000). Can C₃ plants faithfully record the carbon isotopic composition of atmospheric carbon dioxide? *Paleobiology*, 137-164.
- Beerling, D. J., & Royer, D. L. (2002). Fossil plants as indicators of the Phanerozoic global carbon cycle. *Annual Review of Earth and Planetary Sciences*, 30(1), 527-556.
- Berner, R. A. (1992). Weathering, plants, and the long-term carbon cycle. *Geochimica et Cosmochimica Acta*, 56(8), 3225-3231.

- Berry, E. W. (1930). *Revision of the lower Eocene Wilcox flora of the southeastern states: with descriptions of new species, chiefly from Tennessee and Kentucky* (Vol. 156). US Government Printing Office.
- Bestland, E. A. (2000). Weathering flux and CO₂ consumption determined from paleosol sequences across the Eocene–Oligocene transition. *Palaeogeography, Palaeoclimatology, Palaeoecology*, 156(3-4), 301-326.
- Boutton, T. W. (1991). Stable Carbon Isotope Ratios of Natural Materials: I. Sample Preparation and Mass Spectrometric. *Carbon isotope techniques*, 1, 155.
- Brand, L. R. (2002, October). Lacustrine Deposition in the Bridger Formation: Lake Gosiute Extended. In *Geological Society of America Abstracts with Programs* (Vol. 34, No. 6, p. 557).
- Breedlovestrout, R. L., Evraets, B. J., and Parrish, J. T. (2013). New Paleogene climate analysis of western Washington using physiognomic characteristics of fossil leaves. *Palaeogeography Palaeoclimatology, Palaeoecology*, 392, 22–40.
- Buchheim, H. P., Brand, L. R., & Goodwin, H. T. (2000). Lacustrine to fluvial floodplain deposition in the Eocene Bridger Formation. *Palaeogeography, Palaeoclimatology, Palaeoecology*, 162(1-2), 191-209.
- Buck, B. J., Wolff, K., Merkle, D. J., & McMillan, N. J. (2006). Salt mineralogy of Las Vegas Wash, Nevada: morphology and subsurface evaporation. *Soil Science Society of America Journal*, 70(5), 1639-1651.
- Carroll, A. R., Doebbert, A. C., Booth, A. L., Chamberlain, C. P., Rhodes-Carson, M. K., Smith, M. E., ... & Beard, B. L. (2008). Capture of high-altitude precipitation by a low-altitude Eocene lake, western US. *Geology*, 36(10), 791-794.
- Cerling, T. E., Solomon, D. K., Quade, J. A. Y., & Bowman, J. R. (1991). On the isotopic composition of carbon in soil carbon dioxide. *Geochimica et Cosmochimica Acta*, 55(11), 3403-3405.
- Cerling, T. E. (1992). Use of carbon isotopes in paleosols as an indicator of the P(CO₂) of the paleoatmosphere. *Global Biogeochemical Cycles*, 6(3), 307-314.
- Cheeseman, J. (2016). Food security in the face of salinity, drought, climate change, and population growth. In *Halophytes for food security in dry lands* (pp. 111-123). Academic Press.
- Clyde, W. C., Sheldon, N. D., Koch, P. L., Gunnell, G. F., & Bartels, W. S. (2001). Linking the Wasatchian/Bridgerian boundary to the Cenozoic Global Climate Optimum: new magnetostratigraphic and isotopic results from South Pass, Wyoming. *Palaeogeography, Palaeoclimatology, Palaeoecology*, 167(1-2), 175-199.

- Cotton, J. M., Jeffery, M. L., & Sheldon, N. D. (2013). Climate controls on soil respired CO₂ in the United States: implications for 21st century chemical weathering rates in temperate and arid ecosystems. *Chemical Geology*, 358, 37-45.
- Cornwell, W. K., Wright, I. J., Turner, J., Maire, V., Barbour, M. M., Cernusak, L. A., Dawson, T., Ellsworth, D., Farquhar, G. D., Griffiths, H. & Keitel, C. (2018). Climate and soils together regulate photosynthetic carbon isotope discrimination within C₃ plants worldwide. *Global Ecology and Biogeography*, 27(9), 1056-1067.
- Deines, P. (1992). Mantle carbon: concentration, mode of occurrence, and isotopic composition. In *Early Organic Evolution* (pp. 133-146). Springer, Berlin, Heidelberg.
- Dickinson, K. A. (1988). Paleolimnology of Lake Tubutulik, an iron-meromictic Eocene lake, eastern Seward peninsula, Alaska. *Sedimentary Geology*, 54(4), 303-320.
- Dickinson, W. R., Klute, M. A., Hayes, M. J., Janecke, S. U., Lundin, E. R., McKittrick, M. A., & Olivares, M. D. (1988). Paleogeographic and paleotectonic setting of Laramide sedimentary basins in the central Rocky Mountain region. *Geological Society of America Bulletin*, 100(7), 1023-1039.
- Dillhoff, R. M., Dillhoff, T. A., Greenwood, D. R., DeVore, M. L., & Pigg, K. B. (2013). The Eocene Thomas Ranch flora, Allenby Formation, Princeton, British Columbia, Canada. *Botany*, 91(8), 514-529.
- Doebbert, A. C., Carroll, A. R., Mulch, A., Chetel, L. M., & Chamberlain, C. P. (2010). Geomorphic controls on lacustrine isotopic compositions: evidence from the Laney Member, Green River Formation, Wyoming. *GSA Bulletin*, 122(1-2), 236-252.
- Dzombak, R. M., Sheldon, N. D., Mohabey, D. M., & Samant, B. (2020). Stable climate in India during Deccan volcanism suggests limited influence on K–Pg extinction. *Gondwana Research*.
- Ennis, D. J., Dunbar, N. W., Campbell, A. R., & Chapin, C. E. (2000). The effects of K-metasomatism on the mineralogy and geochemistry of silicic ignimbrites near Socorro, New Mexico. *Chemical Geology*, 167(3-4), 285-312.
- Franks, P. J., Royer, D. L., Beerling, D. J., Van de Water, P. K., Cantrill, D. J., Barbour, M. M., & Berry, J. A. (2014). New constraints on atmospheric CO₂ concentration for the Phanerozoic. *Geophysical Research Letters*, 41(13), 4685-4694.
- Fricke, H. C., & Wing, S. L. (2004). Oxygen isotope and paleobotanical estimates of temperature and δ¹⁸O–latitude gradients over North America during the early Eocene. *American Journal of Science*, 304(7), 612-635.
- Gallagher, T. M., & Sheldon, N. D. (2013). A new paleothermometer for forest paleosols and its implications for Cenozoic climate. *Geology*, 41(6), 647-650.

- Greenwood, D. R., Archibald, S. B., Mathewes, R. W., & Moss, P. T. (2005). Fossil biotas from the Okanogan Highlands, southern British Columbia and northeastern Washington State: climates and ecosystems across an Eocene landscape. *Canadian Journal of Earth Sciences*, 42(2), 167-185.
- Greenwood, D. R., Pigg, K. B., Basinger, J. F., and DeVore, M. L. (2016). A review of paleobotanical studies of the Early Eocene Okanogan (Okanogan) Highlands floras of British Columbia, Canada and Washington, USA, *Canadian Journal of Earth Sciences*, 53, 548–564, <https://doi.org/10.1139/cjes-2015-0177>.
- Groll, P. E., & Steidtmann, J. R. (1987). Fluvial response to Eocene tectonism, the Bridger Formation, southern Wind River Range, Wyoming.
- Hamzeh, M., & Dayanandan, S. (2004). Phylogeny of *Populus* (Salicaceae) based on nucleotide sequences of chloroplast TRNT-TRNF region and nuclear rDNA. *American journal of botany*, 91(9), 1398-1408.
- Hamzeh, M., Périnet, P., & Dayanandan, S. (2006). Genetic Relationships among species of *Populus* (Salicaceae) based on nuclear genomic data. *The Journal of the Torrey Botanical Society*, 133(4), 519-527.
- Hanley, J. H. (1976). Paleosynecology of nonmarine Mollusca from the Green River and Wasatch formations (Eocene), southwestern Wyoming and northwestern Colorado. In *Structure and classification of paleocommunities* (pp. 235-261). Dowden, Hutchinson and Ross Stroudsburg, PA.
- Holdridge, L. R. (1967). Life zone ecology. *Life zone ecology*, (rev. ed.).
- Hyland, E. G., & Sheldon, N. D. (2013). Coupled CO₂-climate response during the early Eocene climatic optimum. *Palaeogeography, Palaeoclimatology, Palaeoecology*, 369, 125-135.
- Hyland, E. G., Huntington, K. W., Sheldon, N. D., & Reichgelt, T. (2018). Temperature seasonality in the North American continental interior during the Early Eocene Climatic Optimum. *Climates of the Past*, 14, 1391-1404.
- Keeling, C. D., MOOK, W. G., & Tans, P. P. (1979). Recent trends in the ¹³C/¹²C ratio of atmospheric carbon dioxide. *Nature*, 277(5692), 121-123.
- Kelson, J. R., Huntington, K. W., Schauer, A. J., Saenger, C., & Lechler, A. R. (2017). Toward a universal carbonate clumped isotope calibration: Diverse synthesis and preparatory methods suggest a single temperature relationship. *Geochimica et Cosmochimica Acta*, 197, 104-131.
- Kistner, F. B. (1973). Stratigraphy of the Bridger Formation in the Big Island-Blue Rim area, Sweetwater County, Wyoming. In *Masters Abstracts International*, 45(4).

- Koenig, K. J. (1960). Bridger Formation in the Bridger Basin, Wyoming. *Overthrust Belt of Southwestern Wyoming and Adjacent Areas; 15th Annual Field Conference Guidebook*, 163-168.
- Kuiper, K.F.A., Deino, F.J.K., Hilgen, W., Renne, P.R., Wijbrans, J.R. (2008). Synchronizing rock clocks of Earth history. *Science* 320: 500-504.
- Leopold, E. B., & MacGinitie, H. D. (1972). Development and affinities of Tertiary floras in the Rocky Mountains. *Floristics and Paleoflorists of Asia and Eastern North America*.
- Looy, C., Kerp, H., Duijnste, I., & DiMichele, B. (2014). The late Paleozoic ecological-evolutionary laboratory, a land-plant fossil record perspective. *The Sedimentary Record*, 12(4), 4-18.
- Love, J. D. (1961). Definition of Green River, Great Divide, and Washakie basins, Southwestern Wyoming. *AAPG Bulletin*, 45(10), 1749-1755.
- Lugo, A. E., Brown, S. L., Dodson, R., Smith, T. S., & Shugart, H. H. (1999). The Holdridge life zones of the conterminous United States in relation to ecosystem mapping. *Journal of biogeography*, 26(5), 1025-1038.
- MacGinitie, H. D. (1969). *The Eocene green River flora of northwestern Colorado and northeastern Utah*. University of California Press.
- MacGinitie, H. D. (1974). An Early Middle Eocene flora from the Yellowstone-Absaroka Volcanic Province, northwestern Wind River Basin, Wyoming, 1-103. University of California Publications in Geological Science, Berkeley, California, USA.
- Malone, D. H., Craddock, J. P., & Matheson, M. G. (2014). Origin of Allochthonous Volcanic Rocks at Squaw Peaks, Wyoming: A Distal Remnant of the Heart Mountain Slide? *The Mountain Geologist*, 4, 321-336.
- Maynard, J. B. (1992). Chemistry of modern soils as a guide to interpreting Precambrian paleosols. *The Journal of Geology*, 100(3), 279-289.
- Merkhofer, L., Wilf, P., Haas, M. T., Kooyman, R. M., Sack, L., Scoffoni, C., & Cúneo, N. R. (2015). Resolving Australian analogs for an Eocene Patagonian paleorainforest using leaf size and floristics. *American Journal of Botany*, 102(7), 1160-1173.
- Miller, I. M., Brandon, M. T., & Hickey, L. J. (2006). Using leaf margin analysis to estimate the mid-Cretaceous (Albian) paleolatitude of the Baja BC block. *Earth and Planetary Science Letters*, 245(1-2), 95-114.
- Murphey, P. C., & Evanoff, E. (2001). Stratigraphy, fossil distribution, and depositional environments of the upper Bridger Formation (Middle Eocene), Southwestern Wyoming. *Wyoming State Geological Survey*.

- Murphey, P. C., Torick, L. L., Bray, E. S., Chandler, R., & Evanoff, E. (2001). Taphonomy, fauna, and depositional environment of the Omomys Quarry, an unusual accumulation from the Bridger Formation (middle Eocene) of Southwestern Wyoming (USA). In *Eocene Biodiversity* (pp. 361-402). Springer, Boston, MA.
- Murphey, P. C., & Evanoff, E. M. M. E. T. T. (2011, April). Paleontology and stratigraphy of the middle Eocene Bridger Formation, southern Green River basin, Wyoming. In *Proceedings of the Ninth Conference on Fossil Resources: Brigham Young University Geology Studies*, 49, 83-109.
- Nesbitt, H., & Young, G. M. (1982). Early Proterozoic climates and plate motions inferred from major element chemistry of lutites. *Nature*, 299(5885), 715-717.
- Ong, H. L., Swanson, V. E., & Bisque, R. E. (1970). Natural organic acids as agents of chemical weathering. *Geological Survey Research, Paper*.
- Passchier, S., Bohaty, S. M., Jiménez-Espejo, F., Pross, J., Röhl, U., van de Flierdt, T., Escutia, C., & Brinkhuis, H. (2013). Early Eocene to middle Miocene cooling and aridification of East Antarctica. *Geochemistry, Geophysics, Geosystems*, 14(5), 1399-1410.
- Peppe, D. J., Royer, D. L., Wilf, P., & Kowalski, E. A. (2010). Quantification of large uncertainties in fossil leaf paleoaltimetry. *Tectonics*, 29(3).
- Pett-Ridge, J. C., Monastra, V. M., Derry, L. A., & Chadwick, O. A. (2007). Importance of atmospheric inputs and Fe-oxides in controlling soil uranium budgets and behavior along a Hawaiian chronosequence. *Chemical Geology*, 244(3-4), 691-707.
- Poore, R. Z., Pavich, M. J., & Grissino-Mayer, H. D. (2005). Record of the North American southwest monsoon from Gulf of Mexico sediment cores. *Geology*, 33(3), 209-212.
- Retallack, G. J. (1999). Postapocalyptic greenhouse paleoclimate revealed by earliest Triassic paleosols in the Sydney Basin, Australia. *Geological Society of America Bulletin*, 111(1), 52-70.
- Retallack, G. J. (2001). Soils of the past. An introduction to palaeopedology.
- Roehler, H. W. (1993). Eocene climates, depositional environments, and geography, greater Green River Basin, Wyoming, Utah, and Colorado. *United States Geological Survey, Professional Paper*, (1506-F).
- Royer, D. L. (1999). Depth to pedogenic carbonate horizon as a paleoprecipitation indicator?. *Geology*, 27(12), 1123-1126.
- Sayed, M. R. G., & Hundekari, S. M. (2006). Preliminary comparison of ancient bole beds and modern soils developed upon the Deccan volcanic basalts around Pune (India): Potential for palaeoenvironmental reconstruction. *Quaternary International*, 156, 189-199.

- Sheldon, N. D., Retallack, G. J., & Tanaka, S. (2002). Geochemical climofunctions from North American soils and application to paleosols across the Eocene-Oligocene boundary in Oregon. *The Journal of geology*, *110*(6), 687-696.
- Sheldon, N. D. (2006). Abrupt chemical weathering increase across the Permian–Triassic boundary. *Palaeogeography, Palaeoclimatology, Palaeoecology*, *231*(3-4), 315-321.
- Sheldon, N. D., & Tabor, N. J. (2009). Quantitative paleoenvironmental and paleoclimatic reconstruction using paleosols. *Earth-Science Reviews*, *95*(1-2), 1-52.
- Sheldon, N. D., Smith, S. Y., Stein, R., & Ng, M. (2020). Carbon isotope ecology of gymnosperms and implications for paleoclimatic and paleoecological studies. *Global and Planetary Change*, 103060.
- Smith, M. E., Singer, B., & Carroll, A. (2003). $^{40}\text{Ar}/^{39}\text{Ar}$ geochronology of the Eocene Green River Formation, Wyoming. *Geological Society of America Bulletin*, *115*(5), 549-565.
- Smith, M. E., Carroll, A. R., & Singer, B. S. (2008). Synoptic reconstruction of a major ancient lake system: Eocene Green River Formation, western United States. *GSA bulletin*, *120*(1-2), 54-84.
- Smith, R. Y., Basinger, J. F., and Greenwood, D. R. (2012). Early Eocene plant diversity and dynamics in the Falkland flora, Okanagan Highlands, British Columbia, Canada, *Palaeobiodiversity and Palaeoenvironments*, *92*(3), 309–328, <https://doi.org/10.1007/s12549-011-0061-5>.
- Snoke, A. W., Steidtmann, J. R., & Roberts, S. M. (1993). Geologic history of Wyoming within the tectonic framework of the North American Cordillera. *Geology of Wyoming: Geological Survey of Wyoming Memoir*, *5*, 2-56.
- Solomon, S. (2007). IPCC (2007): Climate change the physical science basis. *AGUFM*, 2007, U43D-01.
- Spicer, R. A., Valdes, P. J., Spicer, T. E. V., Craggs, H. J., Srivastava, G., Mehrotra, R. C., & Yang, J. (2009). New developments in CLAMP: calibration using global gridded meteorological data. *Palaeogeography, Palaeoclimatology, Palaeoecology*, *283*(1-2), 91-98.
- Stein, R. A., Sheldon, N. D., & Smith, S. (2019). Rapid response to anthropogenic climate change by *Thuja occidentalis*: implications for past climate reconstructions and future climate predictions. *PeerJ*, *7*, e7378.
- Stein, R. A., Sheldon, N. D., & Smith S. (in press). C₃ plant carbon isotope discrimination does not respond to CO₂ concentration on decadal to centennial timescales. *New Phytologist*. doi: 10.1111/nph.17030

- Stull, G. W., Allen, S. E., & Manchester, S. R. (2014). Fossils of *Iodes* (Icacinaeae) from the early Eocene Blue Rim flora (SW Wyoming) and the late Miocene Wenshan flora (SW Yunnan, China). *The Paleontological Society Special Publications*, 13, 17-18.
- Surdam, R. C., & Stanley, K. O. (1979). Lacustrine sedimentation during the culminating phase of Eocene lake Gosiute, Wyoming (Green River Formation). *Geological Society of America Bulletin*, 90(1), 93-110.
- Tipple, B. J., Meyers, S. R., & Pagani, M. (2010). Carbon isotope ratio of Cenozoic CO₂: A comparative evaluation of available geochemical proxies. *Paleoceanography*, 25(3).
- Tu, T. N., Derenne, S., Largeau, C., Bardoux, G., & Mariotti, A. (2004). Diagenesis effects on specific carbon isotope composition of plant n-alkanes. *Organic Geochemistry*, 35(3), 317-329.
- Vinogradov, A. P. (1959). Geochemistry of rare and dispersed chemical elements in soils.
- West, C. K., Greenwood, D. R., Reichgelt, T., Lowe, A. J., Vachon, J. M., Basinger, J. F. (2020). Paleobotanical proxies for early Eocene climates and ecosystems in northern North America from middle to high latitudes, *Climate of the Past*, 16, 1387-1410.
- Wilf, P., Wing, S. L., Greenwood, D. R., & Greenwood, C. L. (1998). Using fossil leaves as paleoprecipitation indicators: an Eocene example. *Geology*, 26(3), 203-206.
- Wilf, P. (2000). Late Paleocene–early Eocene climate changes in southwestern Wyoming: Paleobotanical analysis. *Geological Society of America Bulletin*, 112(2), 292-307.
- Wing, S. L. (1987). Eocene and Oligocene floras and vegetation of the Rocky Mountains. *Annals of the Missouri Botanical Garden*, 748-784.
- Wing, S. L., & Greenwood, D. R. (1993). Fossils and fossil climate: the case for equable continental interiors in the Eocene. *Philosophical Transactions of the Royal Society of London. Series B: Biological Sciences*, 341(1297), 243-252.
- Wing, S. L., Harrington, G. J., Smith, F. A., Bloch, J. I., Boyer, D. M., & Freeman, K. H. (2005). Transient floral change and rapid global warming at the Paleocene-Eocene boundary. *Science*, 310(5750), 993-996.
- Wing, S. L., & Currano, E. D. (2013). Plant response to a global greenhouse event 56 million years ago. *American Journal of Botany*, 100(7), 1234-1254.
- Wolfe, J. A. (1994). Tertiary climatic changes at middle latitudes of western North America. *Palaeogeography, Palaeoclimatology, Palaeoecology*, 108(3-4), 195-205.
- Wolfe, J. A., Forest, C. E., & Molnar, P. (1998). Paleobotanical evidence of Eocene and Oligocene paleoaltitudes in midlatitude western North America. *Geological Society of America Bulletin*, 110(5), 664-678.

Zhu, J., Poulsen, C. J., & Tierney, J. E. (2019). Simulation of Eocene extreme warmth and high climate sensitivity through cloud feedbacks. *Science advances*, 5(9), eaax1874.

CHAPTER VI

Conclusions

This dissertation is a compilation of four chapters that use carbon isotope ecology in plants and soils to examine water and carbon cycle dynamics between land and the atmosphere. Each chapter provides insights into how plants respond to changes in their water and carbon cycles, as recorded, or not, in carbon isotope records in plants and in soil organic matter. This concluding chapter emphasizes important findings and future questions based on my research. Some of these questions contain preliminary data collected over the course of my thesis, presented to emphasize hypotheses and areas for future growth.

6.1 Summary of results and key findings

In **Chapter II**, I explore the relationship between carbon isotope values ($\delta^{13}\text{C}_{\text{leaf}}$), carbon isotope discrimination ($\Delta^{13}\text{C}_{\text{leaf}}$) and a number of aspects of climate and the environment (e.g. Körner et al. 1991; Ehleringer & Dawson 1992; O’Leary 1993; Arens et al. 2000; Diefendorf et al. 2010; Schubert & Jahren 2012; Wernerehl & Givnish 2015; Mårtensson et al. 2017; Stein et al. 2019) in one species: *Thuja occidentalis* (northern white cedar, Cupressaceae). This natural experiment relies on collections of leaves from expeditions spanning the early 1800s to the present from museums and herbaria. Stable C isotopes show a relationship with carbon isotope values of the atmosphere ($\delta^{13}\text{C}_{\text{atm}}$), time, and $p\text{CO}_2$. However, when $p\text{CO}_2$ is corrected for $\delta^{13}\text{C}_{\text{atm}}$, there is no relationship with $\delta^{13}\text{C}_{\text{leaf}}$. Carbon isotope discrimination shows no relationship with any other tested climate variable, indicating that there is no clear predictive relationship between climate (tested) and carbon isotope discrimination. This effectively means that $\delta^{13}\text{C}_{\text{leaf}}$ should reflect $\delta^{13}\text{C}_{\text{atm}}$ of source gas, provided taxonomic identity is clear. The role that the heterogeneity of $\delta^{13}\text{C}_{\text{atm}}$ values at ground level plays on $\delta^{13}\text{C}_{\text{leaf}}$ variability remains unclear across ecosystems; this could be investigated with ecosystem-wide gaseous and solid

measurements (see section 6.2.1). Additional future questions raised include how this can be applied to the fossil record, and the role that taphonomy plays in preservation of leaf carbon isotope values in variable conditions (see section 6.2.2).

Chapter III approaches carbon isotope ecology from a different angle, instead focusing specifically on the Δ_{leaf} -paleobarometric model that has been applied in the fossil record previously (Schubert & Jahren 2012; Cui & Schubert 2017). Using historical specimens from herbaria and museum collections, I examine plant biogeochemical responses to enhancing carbon dioxide in the atmosphere over Industrialization in high resolution. In my findings, using this historical approach in conjunction with a literature review of stable isotope ecology for a wide range of C_3 plants, it is clear that Δ_{leaf} values are not driven by CO_2 enhancement over Industrialization. Furthermore carbon isotope values across a wide range of C_3 taxa are not comparable to those used to develop the Δ_{leaf} -paleobarometric model (*Arabidopsis thaliana*: and *Raphanus sativus*: wild radish, Brassicaceae). This suggests that this paleobarometric model, based upon growth chamber experiments, might not be representative of those plants seen in the fossil record. Previous works have found that the control of atmospheric CO_2 concentration on Δ_{leaf} values is partially mitigated by water availability (Lomax et al. 2019), so the interplay of multiple complex climate variables, as seen in natural ecosystems, leaves room for future investigation (see section 6.2.3). Likewise, the role that individual species' adaptive morphology plays in carbon isotope discrimination remains uncertain, and future work on the relationship between leaf pore and discrimination across multiple species will help to determine why we see species-specific responses to climate (see section 6.2.4).

I expand on findings from Chapter II in **Chapter IV**, with a focus on the role of organic carbon isotopes in the water cycle. Despite Diefendorf et al. (2010) and Kohn's (2010) studies that found carbon isotope discrimination changed logarithmically with increased rainfall, in the single species historical analysis from Chapter II as well as findings from multiple species' historical records presented in Sheldon et al. (2020), this relationship was not replicable. This is likely because the generalized relationship between Δ_{leaf} and precipitation described by Diefendorf et al. (2010) is actually a series of straight lines for individual species living over wide precipitation regimes, stacked to make a curve (e.g. **Figure 6.1**). However, soils aggregate carbon isotope values from aboveground biomass to act as an integrator that behaves similarly to

Diefendorf et al. (2010)'s generalized plant results, minus specific taxonomic identification. In **Chapter IV**, this was tested in both modern soil systems as well as paleosols with independent precipitation estimates from other proxies. In both scenarios, reconstructed precipitation values were predictive of actual or established reconstructions of precipitation. This work would also benefit from future work to understand how different depositional conditions affect taphonomy and whether this impacts carbon isotope values recorded in organic matter (section 6.2.2).

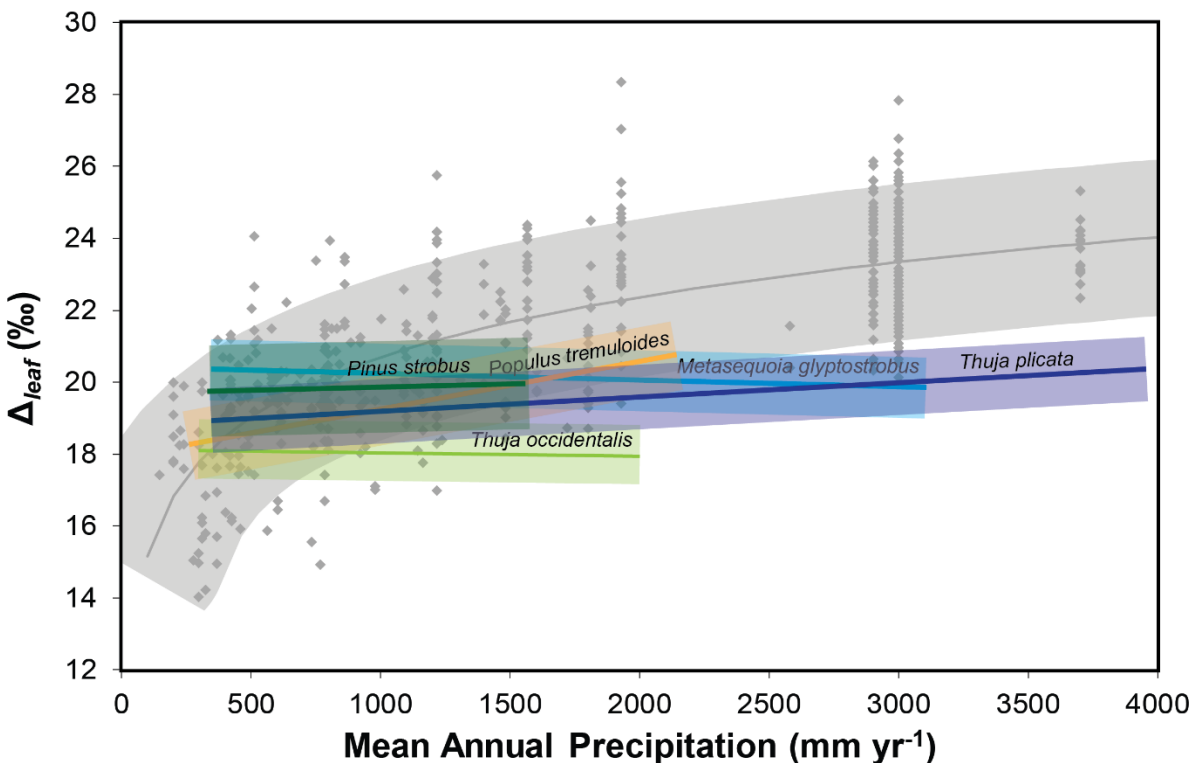


Figure 6.1 Δ_{leaf} values compared to mean annual precipitation, with individual species collected for Sheldon, Smith, Stein & Ng (*Global Planetary Change*, 2020) overlaid on Diefendorf et al.'s (2010) meta-data set.

Finally, **Chapter V** compiles the knowledge garnered from modern and ancient systems in the previous chapters and applies it to a deep time case study: the early Eocene climatic optimum (EECO). This hothouse period is now established to be a potential analog for the highest, “business as usual” scenario for future climate change created by the Intergovernmental Panel on Climate Change (Pachauri & Reisinger 2007; Zhu et al. 2019). Findings from **Chapter V** indicate that the continental interior ancient lake Gosiute, located in present day Wyoming,

Colorado and Utah, was a littoral wet forest by a regressing lake with constant hydrological inputs, medium to high rainfall, medium temperatures (10-14°C) and atmospheric carbon dioxide of mantle origin. This region is currently a high desert, with low mean annual temperature (7.4°C; 2017 value; PRISM Climate Group 2004), and precipitation (308.82 mm yr⁻¹; 2017 value; PRISM Climate Group 2004). During the early Eocene, however, the region was lush with ferns, woody angiosperms, lianas and monocots. The multiple mountain ranges surrounding the region were forming during the deposition of paleo-lake Gosiute, but changing sources did not result in climate signal interference, as provenance and parent material stayed constant throughout the section. This study provides high-resolution, valuable insight about the hydroclimate and paleoclimate of the continental interior during a modern climate analog. Findings from Chapter V, which demonstrate a more stable ecosystem than expected during a time of reconstructed dynamic global climate and dynamic regional tectonics, raise further questions about how multiple climate parameters interact, and how this affects ancient sedimentological records (section 6.2.3).

6.2 Future directions and remaining questions

In this dissertation, I have assessed the relationship between carbon isotope values in plants and soils and climate using carbon isotope values as a tool. Though not directly covered in **Chapters II-V**, this relationship is tied very closely to plant physiology and the mechanism of photosynthesis. As such, a number of outstanding questions about nuances in carbon isotope ecology relate to complexities of the carbon and water cycle. Many of these outstanding questions will address how plant morphology and physiology relate to these large biogeochemical cycles.

The carbon and water cycles are both complex, and intertwined on Earth (Wehrli 2013). As such, many of the questions raised from this work relate to how carbon and water cycle and interdependency might relate to carbon isotope records in leaves. In particular, one question raised regularly throughout this research relates to heterogeneity of the isotopic composition of the atmosphere on an ecosystem scale: the basis of carbon isotope discrimination in plants relies on a known $\delta^{13}\text{C}_{\text{atm}}$ value. However, even when the global composition is measurable (i.e. White et al. 2015) or constrainable in the fossil record (i.e. Tipple et al. 2010), variability in canopy

density and soil respiration rates cause heterogeneous $\delta^{13}\text{C}_{\text{atm}}$ values that impact interpretations of $\delta^{13}\text{C}$ values in organic matter (6.2.1). Other questions relate to the mechanism of carbon isotope discrimination in plants: the aforementioned data presented in this dissertation show empirical relationships between single climate variables and $\delta^{13}\text{C}_{\text{leaf}}$ and $\delta^{13}\text{C}_{\text{SOM}}$, but mechanistically, how is this happening? Do soil conditions (6.2.2) and/or plant morphology (6.2.4) affect the interpretations of our records? Finally, climate cannot be represented by a single parameter, and the findings demonstrated in this dissertation examine single climate variable interactions with carbon isotope discrimination. However, in the natural world, effects of the carbon and water cycle often run interference on one another (for example, increased CO_2 causes increased warming (Houghton et al. 2001), but subsequent increase in plant productivity and transpiration, leading to regional cooling; Tan et al. 2020). As such, carbon isotope discrimination in plants can and should be explored in the context of multivariable climate phenomena (6.2.3).

6.2.1 Carbon cycle: How do we account for the heterogeneity of $\delta^{13}\text{C}_{\text{atm}}$?

In **Chapter II, III, and IV** we make assumptions about $\delta^{13}\text{C}_{\text{atm}}$ assuming homogenous mixing in the atmosphere and using global values measured at Mauna Loa Observatory (MLO; White et al. 2015). However, the concentration of CO_2 can vary wildly at the soil surface and below the canopy due to soil-respired CO_2 and eddy circulation (e.g. Stoyan et al. 2000; Dore et al. 2014). This effect is strongest at night, when the forest boundary layer is thickest (e.g. Munger & Hadley 2017). Even during the day, CO_2 near the floor of wet tropical forests can be elevated by tens of ppm, and the isotopic composition of this CO_2 can be depleted by -2 to -3‰ (e.g. Broadmeadow et al. 1992; Lloyd et al. 1996; Buchmann et al. 1997; Holtum & Winter 2001). In temperate forests, these effects are muted but still present (up to 20 ppm and -1‰ depletion; Francey et al. 1985; Munger & Hadley 2017). While the location of each specimen collected in the modern portions of this study was controlled for by height, and accessibility (often related to proximity to road or trail, inherently higher air mixing regions), any shift in $\delta^{13}\text{C}_{\text{atm}}$ value from the global average measured at Mauna Loa Observatory (White et al. 2015) would result in changed carbon isotope discrimination. In these works, $\delta^{13}\text{C}_{\text{atm}}$ values used were

reasonably well constrained, though we know less about the ecosystems sampled in historical studies.

It is important for us to examine patterns in $\delta^{13}\text{C}_{\text{atm}}$ heterogeneity across ecosystems. $\delta^{13}\text{C}_{\text{atm}}$ values are not just used to calculate carbon isotope discrimination; this variable is well utilized in stomatal and pedogenic paleobarometers (Cerling et al. 1991; Cerling et al. 1992; Franks et al. 2014), as well as to provide insight into carbon sources in the atmosphere (e.g. Keeling et al. 1980). Future work could expand on the effects of heterogeneous microenvironmental air and CO_2 flow, incorporating isotopic measurements from ground to canopy. Eddy flux towers across the country at AmeriFlux, National Ecological Observation Network (NEON), Critical Zone Observatory network (CZO) and Long Term Ecological Research network (LTER) sites provide infrastructure to conduct these measurements (e.g. Thompson et al. 2011; Novick et al. 2018). The Picarro Cavity Ring-Down Spectroscopy is largely mobile and can be run on continuous flow, so this could be used to measure isotopic variation at locations along the Eddy Flux tower. The AmeriFlux, NEON, CZO and LTER networks, in total encompassing >341 flux sites, 59 of which have >10 years of data, occur across ecosystems (e.g. grasslands, shrublands, evergreen forests, mixed forests, deciduous forests, savannas, lakes, tundra, and more; Turner et al. 2003; Xiao et al. 2010; Novick et al. 2018). Flux towers have already been used to explain ecosystem productivity (e.g. Belmecheri et al. 2014); this could be expanded to examine the isotopic signature of the carbon cycle. Previous works with a Picarro CRDS have examined water isotope variability and flux in a similar way (Aron et al. 2019; Aron et al. 2020). By taking discrete and continuous measurements at different levels of ecosystems (**Figure 6.2**), it would be possible to create isotope-enabled eddy flux models and minimize uncertainty about the isotopic signature of plants' source gas. This would enhance our understanding of plants' roles in the carbon cycle.

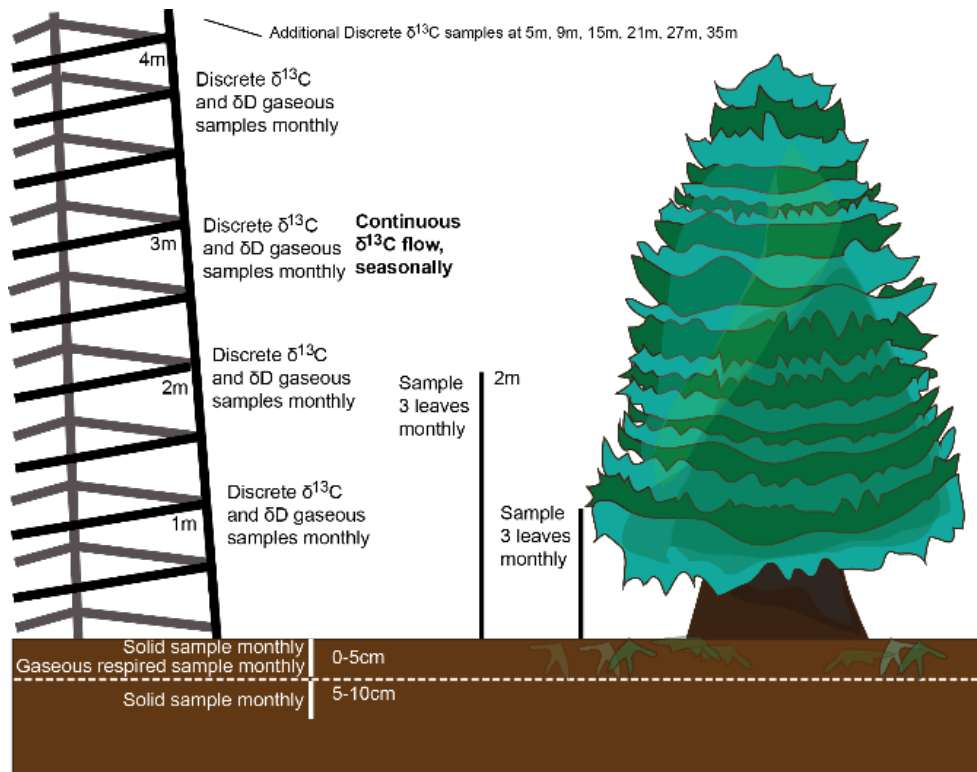


Figure 6.2 Example of potential ecosystem level ^{13}C sampling (including gaseous CO_2 from the atmosphere, leaves, soil-respired CO_2 in gaseous form, and soil organic carbon) that could constrain isotope fluxes in an ecosystem. The tower on the left represents an eddy flux tower, set up in many LTER, AmeriFlux, CZO and NEON sites across the world.

6.2.2 Water cycle: High precipitation regimes and carbon isotope values

In **Chapter IV** I explore the relationship between mean annual precipitation and $\delta^{13}\text{C}$ values of upper soil horizons. Like many proxies, $\delta^{13}\text{C}_{\text{SOM}}$ -precipitation works well at lower precipitation, and begins to behave erratically $>2500 \text{ mm yr}^{-1}$ (Stein et al. in prep., see **Chapter IV**). Of note, the range of isotope values seen in Diefendorf et al.'s (2010) dataset of $\delta^{13}\text{C}_{\text{leaf}}$ values also increased at higher precipitation values (Diefendorf et al. 2010). There is certainly a maximum carbon isotope discrimination value that can happen just based on CO_2 available and light availability, even with unlimited water availability (Farquhar 1989). Plants are not adapted to be conducting C_3 photosynthesis constantly throughout the day and night (Joo et al. 2017). Thus, we do not expect carbon isotope discrimination to increase indefinitely with increased precipitation; it is noteworthy that carbon isotope discrimination becomes unpredictable at high precipitation levels. It is possible that this is because high mean annual precipitation does not inherently mean that all of this water is available to plants; it can be run off quickly (e.g. Royer

1979), and/or moved in downward transport as colloids or in solution (Osher et al. 2003). It may be controlled by microbes present, or, other soil-specific edaphic factors such as soil texture (Dodd & Lauenroth 1997; Zhang et al. 2020). Further assessment of high precipitation ecosystems, in highly measured, resolved soils should be done to determine how and if these soil-based factors drive carbon isotope values in soils. With more effort to determine plant available water, which is more complex than just mean annual precipitation, we can better quantify plant water stress and its relationship to carbon isotope ecology in plants and soils (Zhang et al. 2020).

Furthermore, experiments looking at fractionation effects in soil acidic conditions can allow us to better understand how taphonomy affects carbon isotope values of whole and partial leaves. Carbonic acid in rain, which has a pH of 5.0, and increased weathering and leaching intensity drive soil pH to decrease with increased rainfall (USDA, unk.). The effects of this acidity on organic matter can be tested on plant material. Indeed, this has been tested in natural systems using fresh and sub-fossil leaves in mangrove ecosystems buried in peat in Belize (Wooller et al. 2003). In these experiments, sub-fossil leaf fragments and fresh leaves had comparable isotopic values (-29 to -22 ‰ and -29 to -23 ‰, respectively; Wooller et al. 2003). This can also be simulated in a lab, using set pH acid to emulate soil acidic conditions, and allowing plant fragments and full leaves to sit in acid for extended periods of time. When conducted in a closed lab experiment, using bleached and rinsed *Thuja occidentalis* leaves (to control for microbial growth), capped vials and dilute hydrochloric acid at pH = 6, (Table 6.1), results were mixed, though none were significant. Though it did appear that partial leaves became more isotopically enriched (more + isotopic values with time) and full leaves demonstrated mostly isotopic depletion with time, this experiment should be replicated in longer studies, with more data points.

Table 6.1 Taphonomic changes in $\Delta^{13}\text{C}_{\text{leaf}}$ for *Thuja occidentalis* samples over 32 weeks (sampled at 0, 2, 4, 8, 16 and 32 weeks). “P” denotes partial leaves (chopped up), “F” denotes full leaves.

Leaf	Species	Slope	Intercept	R ²	p-value
777 (P)	<i>Thuja occidentalis</i>	0.05	-29.25	0.3	0.26
778 (P)	<i>Thuja occidentalis</i>	0.1	-28.28	0.62	0.06

921 (P)	<i>Thuja occidentalis</i>	0.01	-28.92	0.58	0.16
777 (F)	<i>Thuja occidentalis</i>	0.03	-28.89	0.04	0.7
778 (F)	<i>Thuja occidentalis</i>	-0.02	-28.612	0.02	0.78
921 (F)	<i>Thuja occidentalis</i>	-0.02	-28.71	0.69	0.21

6.2.3 Water and carbon cycles: What happens to carbon isotope discrimination when you combine multiple climate variables?

This thesis has mentioned the importance of the water and carbon cycles in determining carbon isotope discrimination, fractionation and values countless times. If that is so, the two cycles can feasibly interfere with one another. As of late, most work addressing climate factors on carbon isotope discrimination focuses on one key variable; some works have tested the relationship between $\Delta^{13}\text{C}_{\text{leaf}}$ and $p\text{CO}_2$ closely in controlled environments (Schubert & Jahren 2012), and others have compared $\delta^{13}\text{C}_{\text{leaf}}$ and precipitation (Diefendorf et al. 2010) and $\delta^{13}\text{C}_{\text{atm}}$ (Arens et al. 2000). **Chapters II-IV** all use single and multivariate regressions to assess the relationship between carbon isotopes and climate variables. In **Chapter V**, these relationships are applied to the fossil record in the context of multiple variables, to assist in categorizing the landscape. However, even within controlled experiments, when additional variables are introduced (e.g. water availability, Lomax et al. 2019) idealized modeling relationships begin to fall apart. In modern ecosystems under free-air CO_2 enrichment experiments, water availability still limits stomatal conductance (Norby & Zak 2011). This introduces importance nuance to using $\delta^{13}\text{C}$ values in deep time, because never is there only one climate factor impacting a depositional environment.

There are several ways to test this; one of these is, of course, using a priori proxy data to tether climate simulations to findings, and testing what happens in dynamic earth system models (e.g. what was done with water isotopologues; Twining et al. 2006, or using ^{13}C isotope enabled CESM; Lawrence et al. 2019). Another way to do this is to compare complex climate patterns, such as the El Niño Southern Oscillation (ENSO), Pacific Decadal Oscillation (PDO), North

American Monsoon (NAM), with seasonal and annual patterns in biogeochemistry as compared to these complex teleconnections (Ito 2011; Martens et al. 2018). Previous work looked at tree growth height growth in coastal species *Picea morrisonicola* (Pinaceae; Guan et al. 2012) with measures of PDO anomalies. In preliminary data examining the relationship between $\Delta^{13}\text{C}_{\text{leaf}}$ values collected in Pacific, western montane, and Great Lakes ecosystems, $\Delta^{13}\text{C}_{\text{leaf}}$ data could be parsed to occurring on dominant ENSO/PDO timescales (Stein et al. in prep; **Figure 6.3**). The nuanced relationship between plant carbon isotope ecology and complex teleconnections could be explored throughout coastal ecosystems around the world, providing insight about the interplay of multiple climate factors in plant stress.

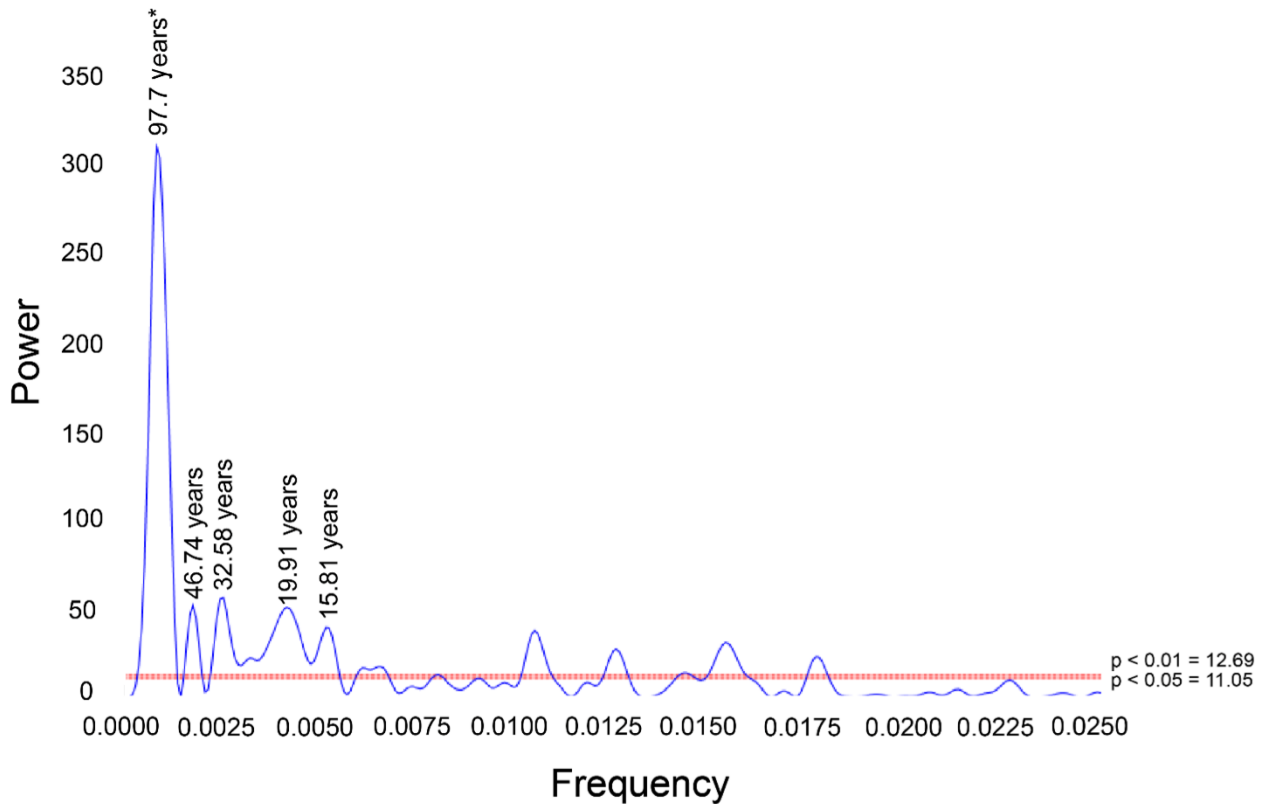


Figure 6.3 Power spectral analysis to determine strongest frequency, interpolated and regularly sampled on month (0.083 year) frequency, of *Thuja plicata* residual $\Delta^{13}\text{C}_{\text{leaf}}$ (‰) values over time.

6.2.4 Mechanisms for carbon isotope discrimination

$$\Delta_{leaf} = (a) + (b - a)\left(\frac{c_i}{c_a}\right) \quad (\text{Equation 6.1})$$

There have been established generalized equations to describe the mechanism of carbon isotope discrimination in plants (Equation 6.1), the effects that climate has on each of these sub-mechanisms is not fully understood. It has been demonstrated in many studies that stomatal density is inversely related to CO₂ (e.g. Woodward 1987; Woodward & Bazzazz 1988), but how does this factor into carbon isotope discrimination? Franks et al. (2014) designed a model that incorporated the stomatal density and isotope fractionation as a metric for the concentration of CO₂ passing into the cell to solve for *p*CO₂ of the atmosphere. This model gives us insight into the corresponding effects of stomatal shape and size on Δ¹³C_{leaf} – the stomatal density and pores can be compared to isotopic signatures as well, to connect biogeochemistry and plant morphology empirically. While currently developed based on a few case study plants, this metric can be refined with gymnosperms and other non-angiosperm biota to improve the taxon-specific accuracy of this stomatal paleobarometer.

We know that diffusion provides a mechanism for Δ¹³C_{leaf} – but to what extent? I conducted preliminary work with help from undergraduate mentees and the guidance of Dr. Dana Royer to look at the relationships between Δ¹³C_{leaf} values of *Thuja* and *Populus* specimens collected from the 1800s to present and stomatal morphology (guard cell length and width, pore length, stomatal density and stomatal volume) and found that there was no link between any stomatal parameters and isotope discrimination in these species (**Figure 6.4**). With these preliminary results, it appears that changing the aperture of stomata and density of stomata does not have effects on fractionation via diffusion. This means that changes in carbon isotope discrimination can be blamed on changes in water use efficiency (*c_i/c_a* ratios) and/or on the function of RuBisCO. Further work to constrain stomatal conductance (by using a porometer) continuously throughout the day and night before conducting these stomatal and isotopic measurements will provide even more insight about the daily patterns of carbon intake.

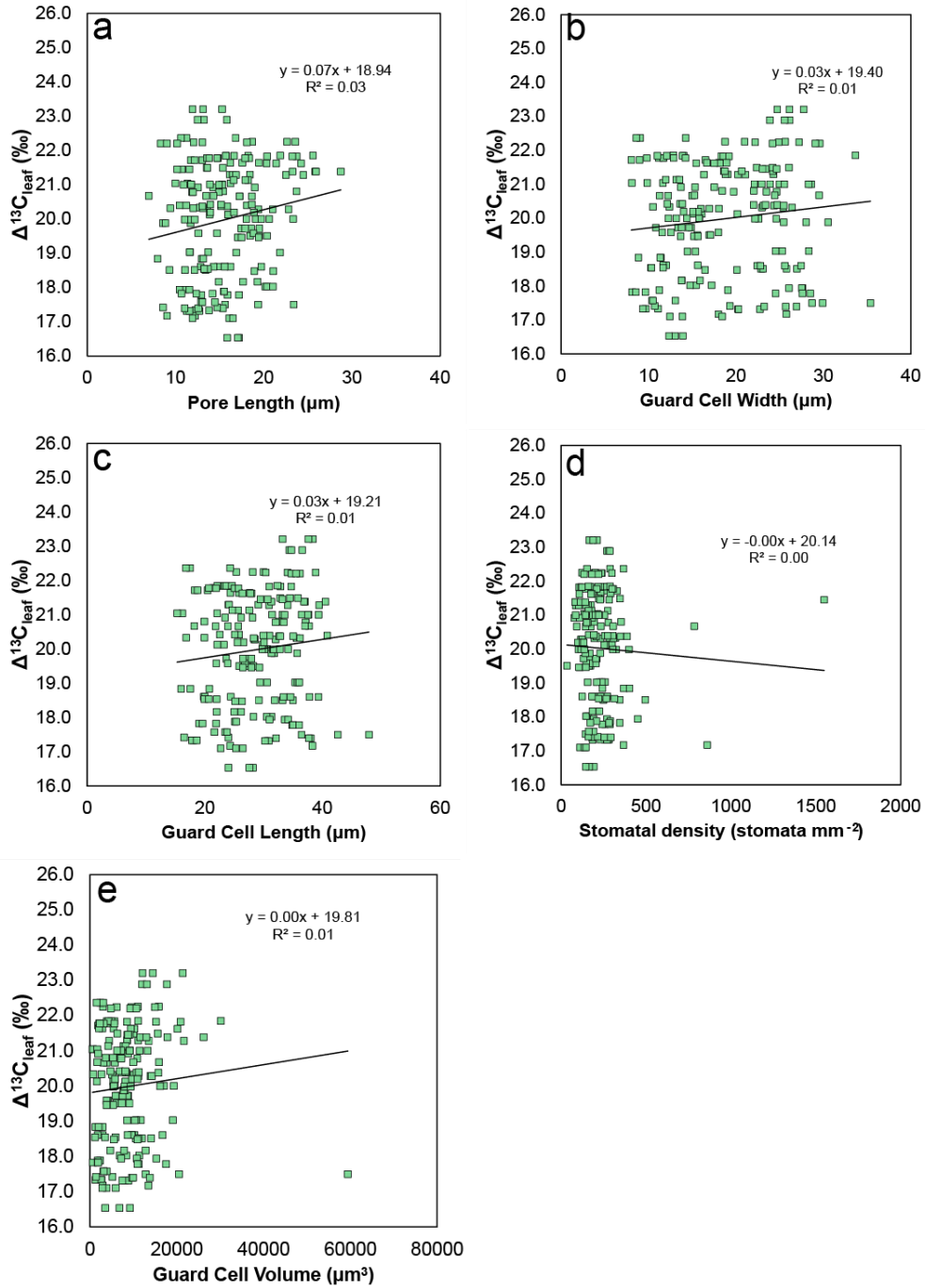


Figure 6.4 $\Delta^{13}\text{C}_{\text{leaf}}$ values (‰) vs (a) pore length (μm), (b) guard cell width (μm), (c) guard cell length (μm), (d) stomatal density (stomata mm^{-2}) and (e) guard cell volume (μm^3).

6.3 Overall areas for future exploration

Overall, the works presented in this dissertation have contributed to our understanding of carbon isotope ecology within plants and soils, especially as related to the carbon and water cycle individually. Understanding the effects of individual climate variables on plant function is useful for understanding plant carbon isotope discrimination, but leaves many outstanding questions to explore. Because we live on a dynamic planet with many interconnected environmental factors and because plants themselves are complicated, defining empirical relationships between climate and $\delta^{13}\text{C}$ values recorded in plants and soils is the tip of the iceberg. It is important that we understand the role that plants play as the carbon *and* water cycles are critically affected by anthropogenic and ancient climate change, because the biosphere plays an instrumental role as a mover of water and carbon. To do this, we must investigate the mechanism of isotope discrimination as it relates to plant adaptations, account for the nuances in each of these cycles, and determine how and when these cycles can interfere with one another in carbon isotope ecological records.

In thinking about how to approach the aforementioned problems, I would like to emphasize the tremendous room for experimental design within the herbarium and museum collections retained in facilities across the world. While there are works that have incorporated herbarium and museum collections, particularly in the biological sciences (e.g. Loiselle et al. 2008; Borchert 1996; Pedicino et al. 2002; Schmidt et al. 2005; Bieker & Martin 2018), there remain so many under-used plant specimens that were collected as early as the 1700's on expeditions by naturalists as well as samples in soil repositories (e.g. the USDA's National Soil Survey Center within the Natural Resources Conservation Service) that include O-, A-, and B-horizons across the country. As climate changes, putting stress on ecosystems and driving changes in plant community composition (Feeley et al. 2020), these facilities provide unique and important materials for us to examine the relationship between the biosphere and anthropogenic climate change (Lang et al. 2019). Though I focus on carbon isotope ecology in my work, there are many other geochemical and morphological experiments possible with these specimens, and enormous room for growth. I hope that future experimenters work to collaborate with curators, so that these resources go to good use. As science, and in particular, sustainability science becomes more interdisciplinary (Porter & Rafols 2009; Nučič 2012), the collaboration between

collections facilities, biologists, geologists, ecologists and chemists will provide new perspectives on important role that plants play in shaping our Earth's climate; I look forward to future works utilizing the natural experiment of human-driven climate change, as recorded in preserved organisms.

6.4 References

- Arens, N. C., Jahren, A. H., & Amundson, R. (2000). Can C₃ plants faithfully record the carbon isotopic composition of atmospheric carbon dioxide? *Paleobiology*, 137-164.
- Aron, P. G., Poulsen, C. J., Fiorella, R. P., & Matheny, A. M. (2019). Stable Water Isotopes Reveal Effects of Intermediate Disturbance and Canopy Structure on Forest Water Cycling. *Journal of Geophysical Research: Biogeosciences*, 124(10), 2958-2975.
- Aron, P. G., Poulsen, C. J., Fiorella, R. P., Matheny, A. M., & Veverica, T. J. (2020). An isotopic approach to partition evapotranspiration in a mixed deciduous forest. *Ecohydrology*, 13(6), e2229.
- Belmecheri, S., Maxwell, R. S., Taylor, A. H., Davis, K. J., Freeman, K. H., & Munger, W. J. (2014). Tree-ring $\delta^{13}\text{C}$ tracks flux tower ecosystem productivity estimates in a NE temperate forest. *Environmental Research Letters*, 9(7), 074011.
- Bieker, V. C., & Martin, M. D. (2018). Implications and future prospects for evolutionary analyses of DNA in historical herbarium collections. *Botany Letters*, 165(3-4), 409-418.
- Borchert, R. (1996). Phenology and flowering periodicity of Neotropical dry forest species: evidence from herbarium collections. *Journal of Tropical Ecology*, 65-80.
- Broadmeadow, M., Griffiths, H., Maxwell, C., & Borland, A. (1992). The carbon isotope ratio of plant organic material reflects temporal and spatial variations in CO₂ within tropical forest formations in Trinidad. *Oecologia*, 89, 435-441.
- Buchmann, N., Guehl, J.-M., Barigah, T., & Ehleringer, J. R. (1997). Interseasonal comparison of CO₂ concentrations, isotopic composition, and carbon dynamics in an Amazonian rainforest (French Guiana). *Oecologia*, 110, 120-131.
- Cerling, T. E., Solomon, D. K., Quade, J. A. Y., & Bowman, J. R. (1991). On the isotopic composition of carbon in soil carbon dioxide. *Geochimica et Cosmochimica Acta*, 55(11), 3403-3405.
- Cerling, T. E. (1992). Use of carbon isotopes in paleosols as an indicator of the P(CO₂) of the paleoatmosphere. *Global Biogeochemical Cycles*, 6(3), 307-314.
- Cui, Y., & Schubert, B. A. (2017). Atmospheric pCO₂ reconstructed across five early Eocene global warming events. *Earth and Planetary Science Letters*, 478, 225-233.

- Diefendorf, A. F., Mueller, K. E., Wing, S. L., Koch, P. L., & Freeman, K. H. (2010). Global patterns in leaf ^{13}C discrimination and implications for studies of past and future climate. *Proceedings of the National Academy of Sciences*, *107*(13), 5738-5743.
- Dodd, M. B., & Lauenroth, W. K. (1997). The influence of soil texture on the soil water dynamics and vegetation structure of a shortgrass steppe ecosystem. *Plant Ecology*, *133*(1), 13-28.
- Dore, S., Fry, D. L., & Stephens, S. L. (2014). Spatial heterogeneity of soil CO_2 efflux after harvest and prescribed fire in a California mixed conifer forest. *Forest Ecology and Management*, *319*, 150-160.
- Ehleringer, J. R., & Dawson, T. E. (1992). Water uptake by plants: perspectives from stable isotope composition. *Plant, cell & environment*, *15*(9), 1073-1082.
- Feeley, K. J., Bravo-Avila, C., Fadrique, B., Perez, T. M., & Zuleta, D. (2020). Climate-driven changes in the composition of New World plant communities. *Nature Climate Change*, 1-6.
- Francey, R. J., Gifford, R. M., Sharkey, T. D., & Weir, B. (1985). Physiological influences on carbon isotope discrimination in huon pine (*Lagarostrobos franklinii*). *Oecologia*, *66*(2), 211-218.
- Franks, P. J., Royer, D. L., Beerling, D. J., Van de Water, P. K., Cantrill, D. J., Barbour, M. M., & Berry, J. A. (2014). New constraints on atmospheric CO_2 concentration for the Phanerozoic. *Geophysical Research Letters*, *41*(13), 4685-4694.
- Guan, B. T., Wright, W. E., Chung, C. H., & Chang, S. T. (2012). ENSO and PDO strongly influence Taiwan spruce height growth. *Forest ecology and management*, *267*, 50-57.
- Holtum, J. & Winter, K. (2001). Are plants growing close to the floors of tropical forests exposed to markedly elevated concentrations of carbon dioxide? *Australian Journal of Botany*, *49*, 629-636.
- Houghton, J. T. (2001). *Climate Change 2001: The Scientific Basis*.
- Ito, A. (2011). Decadal variability in the terrestrial carbon budget caused by the Pacific Decadal Oscillation and Atlantic Multidecadal Oscillation. *Journal of the Meteorological Society of Japan. Ser. II*, *89*(5), 441-454.
- Joo, Y., Fragoso, V., Yon, F., Baldwin, I. T., & Kim, S. G. (2017). Circadian clock component, LHY, tells a plant when to respond photosynthetically to light in nature. *Journal of integrative plant biology*, *59*(8), 572-587.
- Keeling, C. D., Bacastow, R. B., & Tans, P. P. (1980). Predicted shift in the $^{13}\text{C}/^{12}\text{C}$ ratio of atmospheric carbon dioxide. *Geophysical Research Letters*, *7*(7), 505-508.

- Kohn, M. J. (2010). Carbon isotope compositions of terrestrial C₃ plants as indicators of (paleo) ecology and (paleo) climate. *Proceedings of the National Academy of Sciences*, 107(46), 19691-19695.
- Körner, C., Farquhar, G. D., & Wong, S. C. (1991). Carbon isotope discrimination by plants follows latitudinal and altitudinal trends. *Oecologia*, 88(1), 30-40.
- Lang, P. L., Willems, F. M., Scheepens, J. F., Burbano, H. A., & Bossdorf, O. (2019). Using herbaria to study global environmental change. *New Phytologist*, 221(1), 110-122.
- Lawrence, D. M., Fisher, R. A., Koven, C. D., Oleson, K. W., Swenson, S. C., Bonan, G., ... & Kluzek, E. (2019). The Community Land Model version 5: Description of new features, benchmarking, and impact of forcing uncertainty. *Journal of Advances in Modeling Earth Systems*, 11(12), 4245-4287.
- Lloyd, J., Kruijt, B., Hollinger, D. Y., Grace, J., Francey, R. J., Wong, S.-C., Kelliher, F. M., Miranda, A. C., Farquhar, G. D., and Gash, J.: Vegetation effects on the isotopic composition of atmospheric CO₂ at local and regional scales: theoretical aspects and a comparison between rain forest in Amazonia and a boreal forest in Siberia. *Australian Journal of Plant Physiology*, 23, 371-399, 1996.
- Loiselle, B. A., Jørgensen, P. M., Consiglio, T., Jiménez, I., Blake, J. G., Lohmann, L. G., & Montiel, O. M. (2008). Predicting species distributions from herbarium collections: does climate bias in collection sampling influence model outcomes?. *Journal of Biogeography*, 35(1), 105-116.
- Lomax, B. H., Lake, J. A., Leng, M. J., & Jardine, P. E. (2019). An experimental evaluation of the use of $\Delta^{13}\text{C}$ as a proxy for palaeoatmospheric CO₂. *Geochimica et Cosmochimica Acta*, 247, 162-174.
- Mårtensson, L. M., Carlsson, G., Prade, T., Kørup, K., Lærke, P. E., & Jensen, E. S. (2017). Water use efficiency and shoot biomass production under water limitation is negatively correlated to the discrimination against ¹³C in the C₃ grasses *Dactylis glomerata*, *Festuca arundinacea* and *Phalaris arundinacea*. *Plant Physiology and Biochemistry*, 113, 1-5.
- Martens, B., Waegeman, W., Dorigo, W. A., Verhoest, N. E., & Miralles, D. G. (2018). Terrestrial evaporation response to modes of climate variability. *NPJ Climate and Atmospheric Science*, 1(1), 1-7.
- Munger, W. & Hadley, J. (2017). CO₂ profile at Harvard Forest HEM and LPH towers since 2009, Harvard Forest Data Archive: HF197, <http://harvardforest.fas.harvard.edu:8080/exist/apps/datasets/showData.html?id=hf197>.
- Norby, R. J., & Zak, D. R. (2011). Ecological lessons from free-air CO₂ enrichment (FACE) experiments. *Annual review of ecology, evolution, and systematics*, 42.

- Novick, K. A., Biederman, J. A., Desai, A. R., Litvak, M. E., Moore, D. J., Scott, R. L., & Torn, M. S. (2018). The AmeriFlux network: A coalition of the willing. *Agricultural and Forest Meteorology*, 249, 444-456.
- Nučič, M. (2012). Is sustainability science becoming more interdisciplinary over time?. *Acta geographica Slovenica*, 52(1), 215-236.
- O'Leary, M. H. (1993). Biochemical basis of carbon isotope fractionation. In *Stable isotopes and plant carbon-water relations* (pp. 19-28). Academic Press.
- Pachauri, R. K., & Reisinger, A. (2007). IPCC fourth assessment report. *IPCC, Geneva, 2007*.
- Pedicino, L. C., Leavitt, S. W., Betancourt, J. L., & Van de Water, P. K. (2002). Historical variations in $\delta^{13}\text{C}_{\text{leaf}}$ of herbarium specimens in the southwestern US. *Western North American Naturalist*, 348-359.
- Porter, A. L., & Rafols, I. (2009). Measuring and mapping interdisciplinarity in six research fields over time (1975–2005). *Scientometrics*, 81(3), 719-745.
- PRISM Climate Group. (2004). Oregon State University. *PRISM Climate Data*.
- Royer, T. C. (1979). On the effect of precipitation and runoff on coastal circulation in the Gulf of Alaska. *Journal of Physical Oceanography*, 9(3), 555-563.
- Schubert, B. A., & Jahren, A. H. (2012). The effect of atmospheric CO₂ concentration on carbon isotope fractionation in C₃ land plants. *Geochimica et Cosmochimica Acta*, 96, 29-43.
- Schmidt, M., Kreft, H., Thiombiano, A., & Zizka, G. (2005). Herbarium collections and field data-based plant diversity maps for Burkina Faso. *Diversity and Distributions*, 11(6), 509-516.
- Sheldon, N. D., Smith, S. Y., Stein, R., & Ng, M. (2020). Carbon isotope ecology of gymnosperms and implications for paleoclimatic and paleoecological studies. *Global and Planetary Change*, 184, 103060.
- Stein, R. A., Sheldon, N. D., & Smith, S. (2019). Rapid response to anthropogenic climate change by *Thuja occidentalis*: implications for past climate reconstructions and future climate predictions. *PeerJ*, 7, e7378.
- Stoyan, H., De-Polli, H., Böhm, S., Robertson, G. P., & Paul, E. A. (2000). Spatial heterogeneity of soil respiration and related properties at the plant scale. *Plant and soil*, 222(1-2), 203-214.
- Tan, P. Y., Wong, N. H., Tan, C. L., Jusuf, S. K., Schmiele, K., & Chiam, Z. Q. (2020). Transpiration and cooling potential of tropical urban trees from different native habitats. *Science of The Total Environment*, 705, 135764.

- Thompson, S. E., Harman, C. J., Konings, A. G., Sivapalan, M., Neal, A., & Troch, P. A. (2011). Comparative hydrology across AmeriFlux sites: The variable roles of climate, vegetation, and groundwater. *Water Resources Research*, 47(10).
- Tipple, B. J., Meyers, S. R., & Pagani, M. (2010). Carbon isotope ratio of Cenozoic CO₂: A comparative evaluation of available geochemical proxies. *Paleoceanography*, 25(3), PA3202.
- Turner, M. G., Collins, S. L., Lugo, A. L., Magnuson, J. J., Rupp, T. S., & Swanson, F. J. (2003). Disturbance dynamics and ecological response: the contribution of long-term ecological research. *BioScience*, 53(1), 46-56.
- Twining, J., Stone, D., Tadros, C., Henderson-Sellers, A., & Williams, A. (2006). Moisture Isotopes in the Biosphere and Atmosphere (MIBA) in Australia: A priori estimates and preliminary observations of stable water isotopes in soil, plant and vapour for the Tumbarumba Field Campaign. *Global and Planetary Change*, 51(1-2), 59-72.
- United States Department of Agriculture (unknown). *Soil pH* [Brochure]. Retrieved from: http://www.nrcs.usda.gov/Internet/FSE_DOCUMENTS/nrcs142p2_053293.pdf.
- Wehrli, B. (2013). Biogeochemistry: Conduits of the carbon cycle. *Nature*, 503(7476), 346-347.
- Wernerehl, R. W., & Givnish, T. J. (2015). Relative roles of soil moisture, nutrient supply, depth, and mechanical impedance in determining composition and structure of Wisconsin prairies. *PloS one*, 10(9), e0137963.
- White J. W. C., Vaughn B. H., Michel S. E. (2015). University of Colorado, Institute of Arctic and Alpine Research (INSTAAR), stable isotopic composition of atmospheric carbon dioxide (13C and 18O) from the NOAA ESRL carbon cycle cooperative global air sampling network, 1990–2014. Version 2015-10-26 software.
- Woodward, F. I. (1987). Stomatal numbers are sensitive to increases in CO₂ from pre-industrial levels. *Nature*, 327(6123), 617-618.
- Woodward, F. I., & Bazzaz, F. A. (1988). The responses of stomatal density to CO₂ partial pressure. *Journal of Experimental Botany*, 39(12), 1771-1781.
- Xiao, J., Zhuang, Q., Law, B. E., Chen, J., Baldocchi, D. D., Cook, D. R., Oren, R., Richardson, A. D., Wharton, S., Ma, S. & Martin, T. A. (2010). A continuous measure of gross primary production for the conterminous United States derived from MODIS and AmeriFlux data. *Remote sensing of environment*, 114(3), 576-591.
- Zhang, C., Wang, Y., Jia, X., & An, Z. (2020). Variations in capacity and storage of plant-available water in deep profiles along a revegetation and precipitation gradient. *Journal of Hydrology*, 581, 124401.
- Zhu, J., Poulsen, C. J., & Tierney, J. E. (2019). Simulation of Eocene extreme warmth and high climate sensitivity through cloud feedbacks. *Science advances*, 5(9), eaax1874.

APPENDIX A

Supplemental Figures and Tables for Chapter II

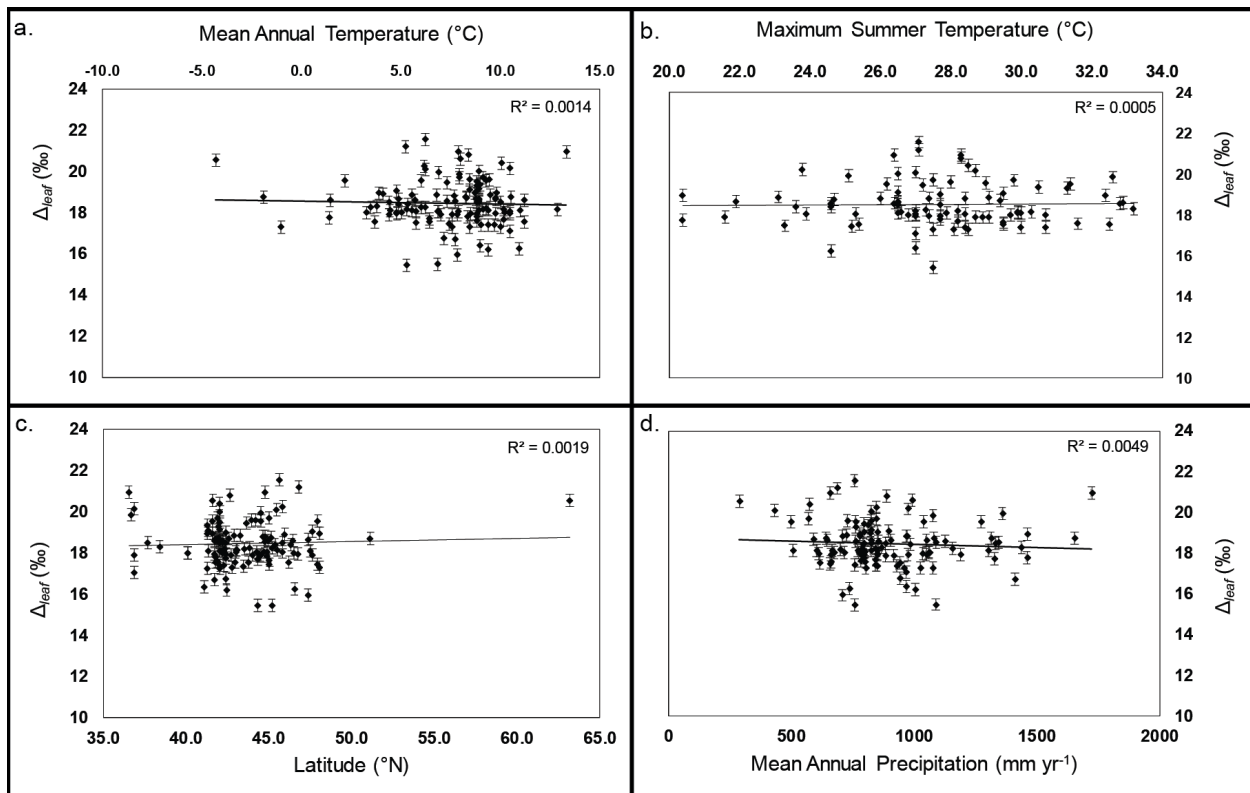


Figure A1 a) Δ_{leaf} values vs. mean annual temperature (−5 to 14°C) for collected specimens ($R^2 = 0.0001$). b) Δ_{leaf} values vs. maximum summer (growing season) temperature (20 to 33°C) for collected specimens ($R^2 = 0.0005$). c) Δ_{leaf} values vs. latitude (43 to 63°N) for collected specimens ($R^2 = 0.0002$). d) Δ_{leaf} values vs. mean annual precipitation (288 to 1724 mm yr⁻¹) for collected specimens ($R^2 = 0.0005$).

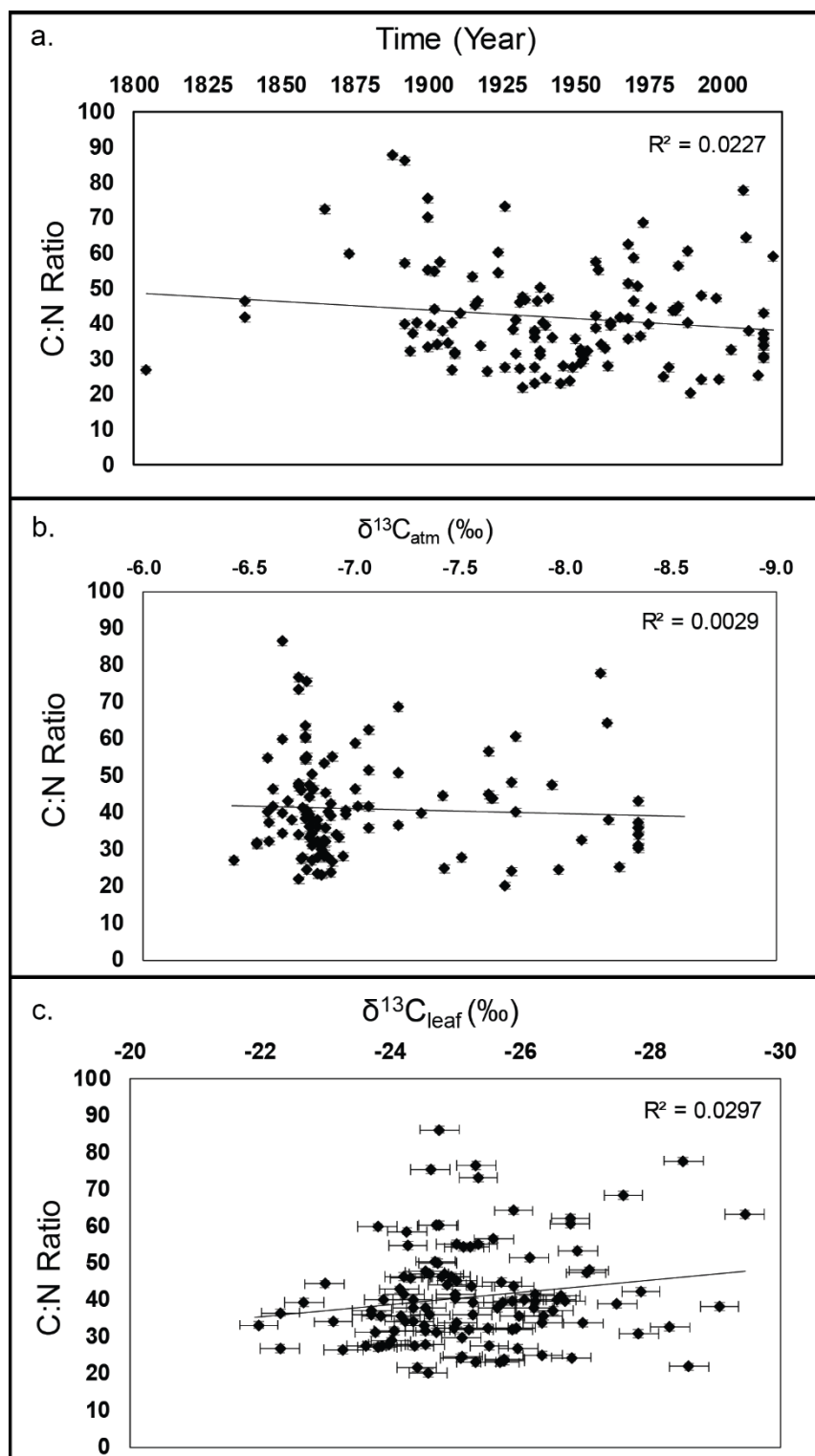


Figure A2 C:N ratios determined by wt. %C and wt. %N measured on a Costech Elemental Analyzer compared to a) time collected (year), b) $\delta^{13}\text{C}_{\text{atm}}$ values (‰), c) $\delta^{13}\text{C}_{\text{leaf}}$ values (‰). Error bars on the y-axis are associated with the 0.9% replicate reproducibility of standards. Error bars on the x-axis in c) are associated with the 0.3‰ replicate reproducibility of the Picarro CRDS standards.

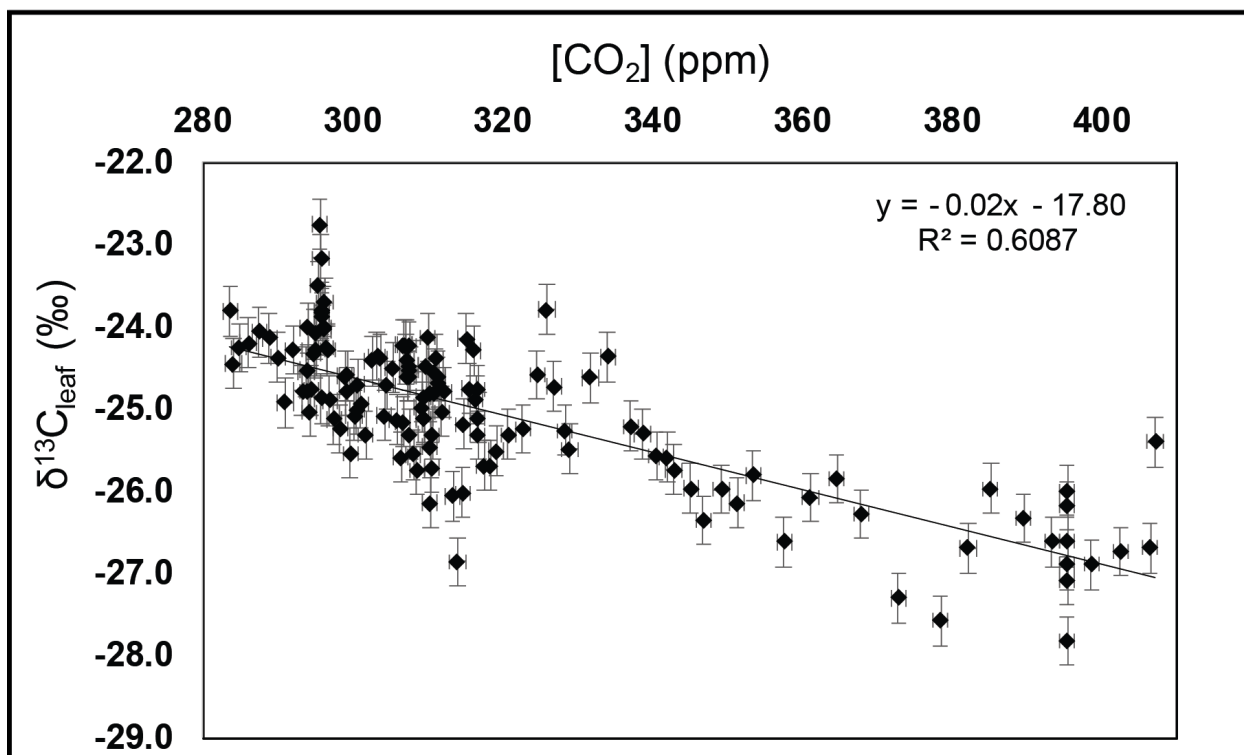


Figure A3 Linear regression between $\delta^{13}\text{C}_{\text{leaf}}$ values (‰) and $[\text{CO}_2]$ (283 to 407 ppm) for collected specimens ($R^2 = 0.61$). Error bars along the y-axis represent the $\pm 0.3\%$ replicate reproducibility of standards.

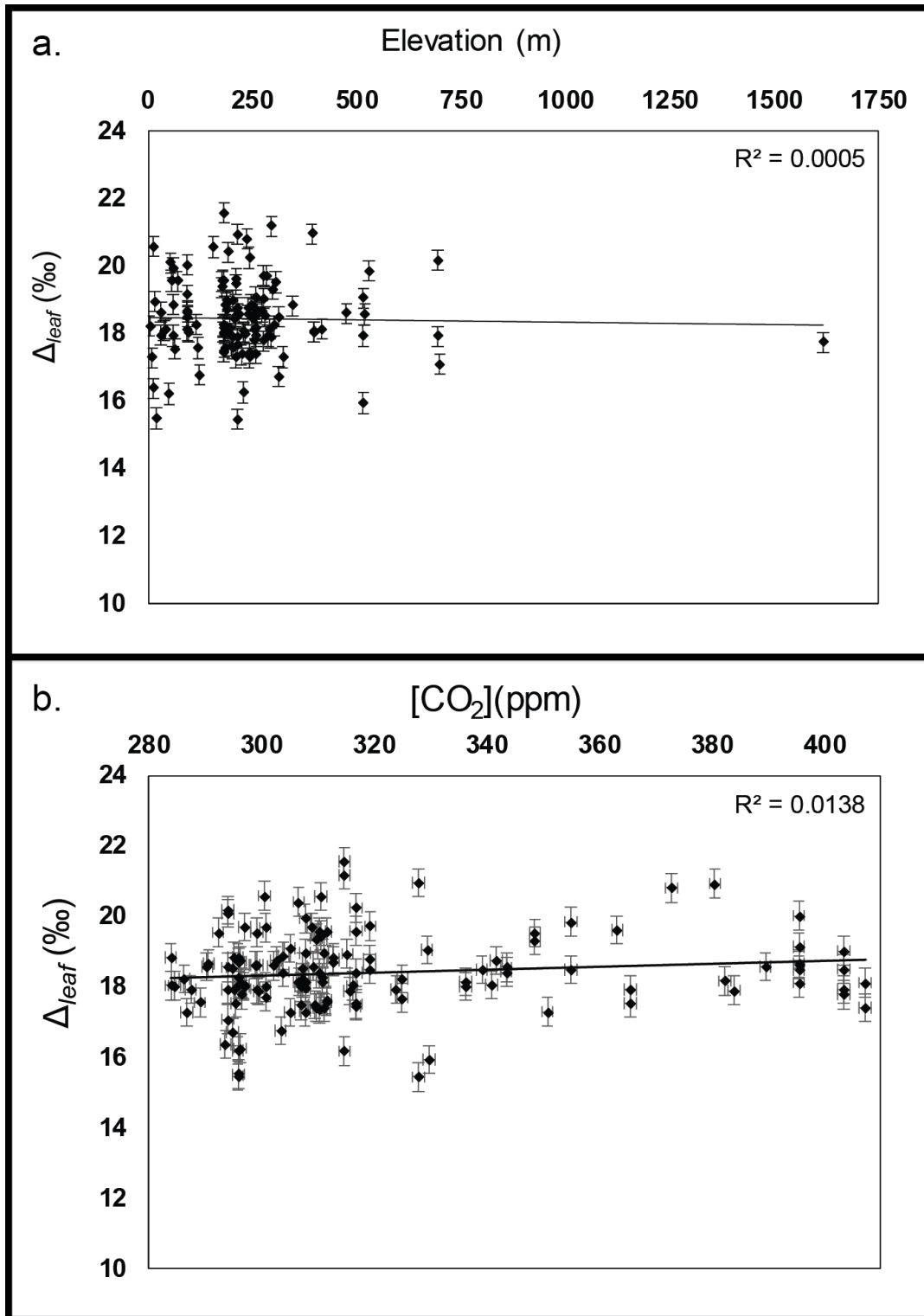


Figure A4 Linear regressions between Δ_{leaf} values and barometric measures. (a) Δ_{leaf} values versus elevation (4 to 1617 m above sea level). Error bars along the y-axis represent the $\pm 0.3\text{‰}$ replicate reproducibility of standards b) Δ_{leaf} and $p\text{CO}_2$ (283 to 407 ppm) for collected specimens ($R^2 = 0.01$). Error bars along the y-axis represent the $\pm 0.3\text{‰}$ replicate reproducibility of standards.

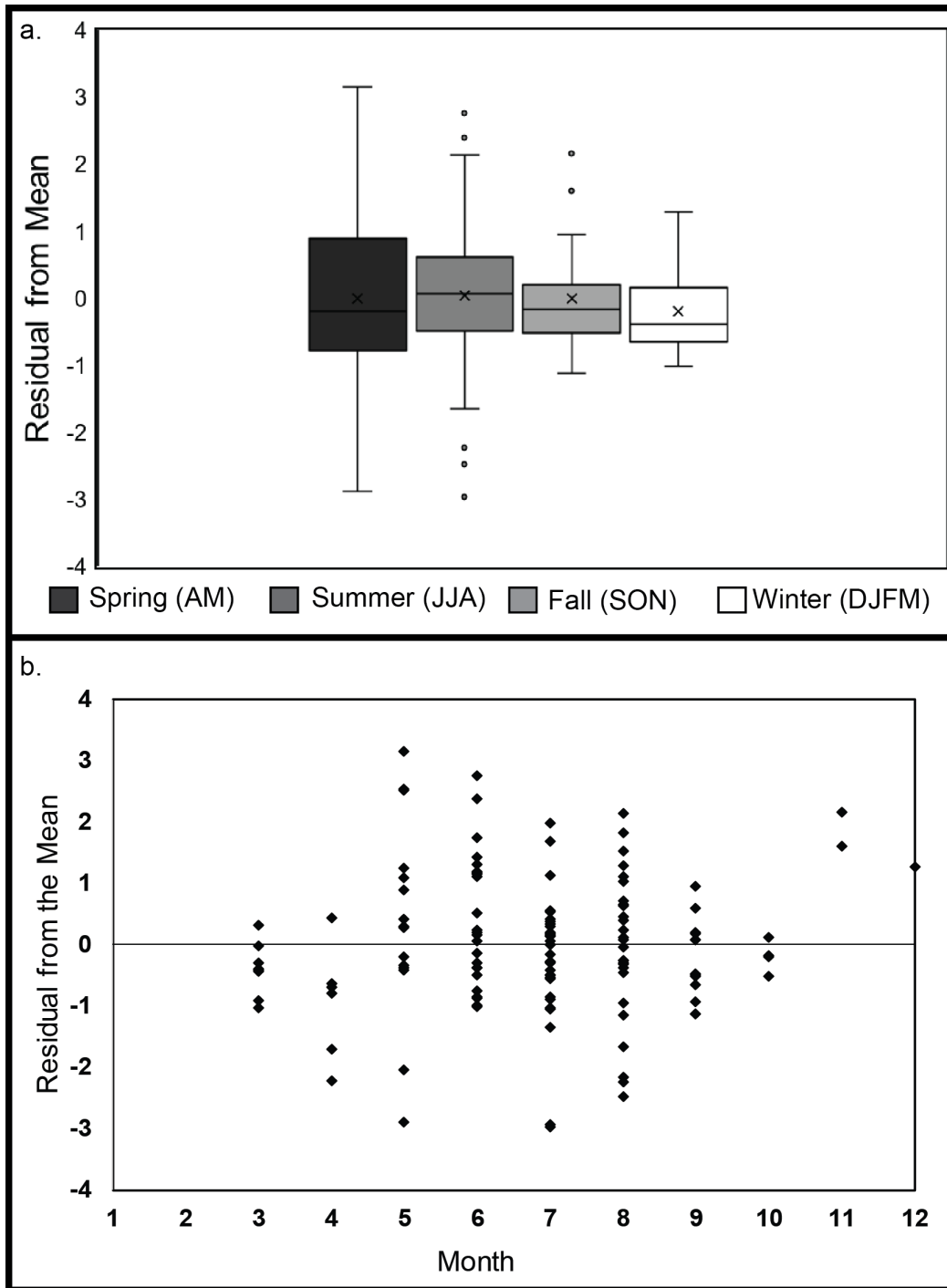


Figure A5 Box and whisker plots for Δ_{leaf} values of sampled months and seasons. a) Box and Whisker plot showing median (lines), mean and range of spring, summer, fall and winter residual values of $\delta^{13}C_{leaf}$. T-tests assuming unequal variance comparing Spring vs. Summer, Fall, Winter, Summer vs. Fall, Winter, and Fall vs. Winter could not prove a null hypothesis; that the mean for all seasonal collections was significantly different. Seasons were categorized by mean monthly temperatures $<^{\circ}C$, from 2–15 $^{\circ}C$ and rising, $>15^{\circ}C$, and between

2–15°C and falling in the Great Lakes Region (centralized lower Peninsula Michigan), b) Scatter plot including residual from mean $\delta^{13}\text{C}_{\text{leaf}}$ values as divided by month.

Table A1 Distribution of herbarium and botanical garden specimen data.

# Specimens	Collection Location	Herbarium Code	Location
70	University of Michigan Herbarium	MICH	Ann Arbor, Mich.
29	Field Museum of Natural History	F	Chicago, Ill.
22	Yale University Peabody Museum	Y	New Haven, Conn.
9	Michigan State Herbarium	MSC	East Lansing, Mich.
8	Hidden Lakes Garden	HLG	Tipton, Mich.
3	Modern Sampling	n/a	MI & OH, see supporting table S3
1	Shanghai Botanical Garden	S	Shanghai, China

Table A2 The range and mean values for measured climate variables in this study.

The minimum, maximum, and mean values for climate conditions for each specimen as obtained from NOAA ESRL Global Monitoring Division (2016), White et al. 2015, and PRISM Climate Group, as well as Government of Canada (Ed.). (2018, January 11).

	Minimum	Mean	Maximum
Latitude	36.5	43.5	63.2
[CO ₂] (ppm)	283	323	407
$\delta^{13}\text{C}_{\text{atm}}$ (‰)	-8.7	-7.1	-6.4
$\delta^{13}\text{C}_{\text{leaf}}$ (‰)	-28.5	-25.0	-21.9
MAP (mm yr ⁻¹)	288	894	1724
MAT (°C)	-4.3	7.5	13.3
Max T (°C)	20.4	27.7	33.2
Elevation (m)	4	237	1617

Table A3 All collected data.*Direct Mauna Loa measurements (NOAA ESRL Global Monitoring Division (2016) **White et al. (2015)) and Petit et al. (2001) ice core records. ***: for United States Climate Data: PRISM Climate Group Oregon State University. (2017). Data Explorer: Time Series Values for Individual Locations. Retrieved from Northwest Alliance for Computational Science & Engineering database. For Canadian Climate Data: Government of Canada (Ed.). (2018, January 11). All specimens used for isotope analysis are stored in the University of Michigan's Earth Systems Laboratory (Dr. Nathan Sheldon & Dr. Ingrid Hendy) within the University of Michigan Earth and Environmental Science Department.

Supporting Information Table S3: All collected data.*Direct Mauna Loa measurements (NOAA ESRL Global Monitoring Division (2016)

White et al. (2015)) and Petit et al. (2001) ice core records. *: for United States Climate Data: PRISM Climate Group Oregon State University. (2017).

Data Explorer: Time Series Values for Individual Locations. Retrieved from Northwest Alliance for Computational Science & Engineering database. For Canadian Climate Data: Government of Canada (Ed.). (2018, January 11). *All specimens used for isotope analysis are stored in the University of Michigan's Earth Systems Laboratory (Dr. Nathan Sheldon & Dr. Ingrid Hendy) within the University of Michigan Earth and Environmental Science Department.*

RAS ID #	Year	Collector	Original tree location	Source	Accession #	Date collected	[CO ₂ (ppm)***	δ ¹³ C _{atm} (‰)***	Latitude (°N)	Longitude (°W)	MAP (mm yr ⁻¹)***	MAT (°C)***	Mean Max T (°C)***	Elevation (m)	%N	%C	C:N (molar)	C:N (weight %)	δ ¹³ C _{leaf} (‰)	δ ¹³ C _{leaf} (‰) calculated using Feng et al. 1999)
18	2014	Mervenne	C. Lakes Garden	HLG	18	8/25/2014	395.43	-8.35	42.03	-84.11	823.7	8.9	26.5	95	1.43	48.05	39.1	33.7	-26.97	19.14
19	2014	Mervenne	C. Lakes Garden	HLG	19	8/25/2014	395.43	-8.35	42.03	-84.11	823.7	8.9	26.5	95	1.36	50.59	43.3	37.1	-26.51	18.66
20	2014	Mervenne	C. Lakes Garden	HLG	20	9/5/2014	395.43	-8.35	42.03	-84.11	823.7	8.9	26.5	95	1.42	48.10	39.5	33.9	-26.34	18.48
64	2014	Mervenne	C. Lakes Garden	HLG	64	11/1/2014	395.43	-8.35	42.03	-84.11	823.7	8.9	26.5	95	1.66	50.95	35.9	30.8	-27.82	20.03
118	2014	Mervenne	C. Lakes Garden	HLG	118	9/24/2014	395.43	-8.35	42.03	-84.11	823.7	8.9	26.5		1.65	49.93	35.2	30.2	n/a	n/a
141	2014	Mervenne	C. Lakes Garden	HLG	141	8/25/2014	395.43	-8.35	42.03	-84.11	823.7	8.9	26.5		1.16	49.87	50.1	43.0	n/a	n/a
163	2014	Mervenne	C. Lakes Garden	HLG	163	8/25/2014	395.43	-8.35	42.03	-84.11	823.7	8.9	26.5	95	1.39	49.17	41.4	35.5	-25.99	18.11
164	2014	Mervenne	C. Lakes Garden	HLG	164	8/25/2014	395.43	-8.35	42.03	-84.11	823.7	8.9	26.5	95	1.39	49.71	41.6	35.7	-26.36	18.50
171	1838	John Samples	Champaign County, Urbana, Ohio	MICH	S.N	3/24/1838	284.60	-6.62	40.11	-83.75	1059.9	10.5	30.7	98	1.05	48.61	54.0	46.3	-24.22	18.03
172	1892	S. K. and D. R. Camp	Topinabee, Michigan	MICH	#576	7/21/1892	294.00	-6.66	45.48	-84.59	432.5	6.3	27.0	55	1.27	50.54	46.4	39.8	-26.24	20.10
173	1894	Mrs. James Buchanan	Lowell, Kent County, Michigan	MICH	#51233	4/03/1894	295.10	-6.60	42.94	-85.35	972.0	9.5	29.1	60	1.59	51.13	37.5	32.2	-24.99	18.86
174	1895	Wm. Livingston Shaddick, Skeels	Grand Rapids, Michigan	MICH	#42440	7/21/1895	295.50	-6.60	42.96	-85.66	616.0	6.4	29.5	64	1.49	55.54	43.5	37.3	-23.72	17.54
175	1907	Frank C Gates	Wm. Hope Cemetery, Urbana, Illinois	MICH	#1313	3/23/1907	300.70	-6.66	40.10	-88.23	1036.0	10.2	29.7	231	1.54	52.79	40.0	34.3	-24.22	18.00
176	1908	Bartlett	Wm. Madison, New Hampshire	MICH	#1257	4/24/1908	300.70	-6.59	44.33	-71.28	1327.7	1.4	20.4	1617	1.26	50.48	46.7	40.1	-23.90	17.73
177	1916	Wm. Umbach	Portage, Michigan	MICH	#8299	7/31/1916	298.80	-6.87	42.23	-85.58	904.5	8.8	32.9	260	1.18	53.46	52.8	45.3	-25.03	18.63
178	1924	Erlanson	Peroskey, Michigan	MICH	#426	7/18/1924	303.90	-6.77	45.37	-84.97	792.0	5.3	23.6	207	0.86	51.84	70.3	60.3	-24.75	18.44
179	1924	Erlanson	Society Bay, Clark Township, Mackinac County, Michigan	MICH	#680	8/30/1924	303.90	-6.77	45.98	-84.19	723.9	4.1	23.1	187	0.96	52.06	63.2	54.2	-25.13	18.84
180	1926	Lyon Jr.	Wm. Merar Springs, Indiana	MICH	MICH# 1491323	8/18/1926	305.00	-6.74	41.33	-85.74	896.1	8.4	29.5	258	0.72	52.63	85.2	73.1	-25.36	19.10
181	1929	Unknown	Summer Lake, Doyle Township, Michigan	MICH	S.N.	8/24/1929	306.20	-6.77	45.99	-86.03	781.6	3.9	23.2		1.29	49.20	44.5	38.1	n/a	n/a
182	1930	Marcus W Lyon, Jr.	Stevensville, Michigan	MICH	MICH# 1244469	7/17/1930	306.60	-6.76	42.01	-86.52	574.3	10.1	28.5	183	1.24	50.93	47.9	41.1	-26.63	20.41
183	1931	Grassl	Chene Island, Algoma, Ontario	MICH	MICH# 1491259	7/4/1931	307.00	-6.75	46.50	-84.55	852.0	4.8		183	1.16	53.09	53.4	45.8	-24.31	18.00
184	1931	Carl O. Grassl	Siskiwit Bay Isle Royale, Michigan	MICH	#1161	8/25/1931	307.00	-6.75	47.95	-88.76	656.6	5.8	23.3	183	1.85	50.42	31.8	27.3	-23.81	17.48

185	1932	Vincent de Paul McGivney	Harbor Beach, Michigan	MICH	MICH# 1247725	10/1/1932	307.30	-6.74	43.84	-82.65	787.4	3.5	27.3	181	1.15	54.76	55.5	47.6	-24.54	18.25
186	1933	Carl O Grassl	Michigan	MICH	#3062	10/1/1932	307.30	-6.74	n/a	n/a	n/a	n/a	n/a	n/a	1.05	49.22	54.7	46.9	-24.83	18.55
187	1936	Cormack & Baldwin	Ontario	MICH	MICH# 1491290	8/4/1936	307.70	-6.83	n/a	n/a	n/a	n/a	n/a	n/a	1.22	46.35	44.3	38.0	-24.55	18.17
188	1936	Grassl	Pardee Township, Ontario	MICH	#7585	9/16/1936	307.70	-6.83	48.08	-89.63	1025.0	-1.0		323	1.39	49.97	41.9	35.9	-23.72	17.30
189	1937	Hermann	Michigan	MICH	#9256	9/13/1937	309.20	-6.81	n/a	n/a	n/a	n/a	n/a	n/a	1.11	51.24	53.8	46.2	-24.94	18.60
190	1938	Chester C Cook	Belgium, Wisconsin	MICH	MICH# 1491303	7/27/1938	310.30	-6.80	43.50	-87.85	928.1	9.1	28.4	224	1.67	51.87	36.2	31.1	-23.77	17.38
191	1938	Chester C Cook	Wisconsin	MICH	#C-142	8/16/1938	310.30	-6.80	n/a	n/a	n/a	n/a	n/a	n/a	0.98	49.07	58.4	50.1	-24.74	18.39
192	1939	Harold Neumann	Wenonah Indian Reservation, Keshena, Wisconsin	MICH	#C-1525	12/14/1939	309.00	-6.88	45.00	-88.67	568.7	9.1	29.8	284	1.28	51.38	46.8	40.1	-26.07	19.70
193	1940	Cook	Wisconsin	MICH	#K-162	8/12/1940	310.50	-6.78	43.68	-87.77	795.0	7.3	27.2	210	1.29	50.91	46.0	39.5	-25.74	19.47
194	1941	M N Zinck	Goodwin Township, Ottawa	MICH	MICH# 1491265	7/3/1941	310.80	-6.79	45.24	-75.90	868.0	6.0		115	1.07	50.47	55.0	47.2	-24.60	18.26
195	1942	Harold and Virginia Bailey	Molt Island, Isle Royale National Park	MICH	#4306	7/16/1942	311.00	-6.79	48.09	-88.58	777.2	3.9	20.4	190	1.39	49.94	41.9	35.9	-25.27	18.96
196	1946	H H Bartlett	Watson, Jackson County, Michigan	MICH	#21453	7/13/1946	310.80	-6.86	42.18	-84.35	668.0	10.2	29.9	293	1.79	49.90	32.5	27.9	-24.54	18.13
197	1948	Chase	Starved Rock State Park, Illinois	MICH	#10167	9/19/1948	309.70	-6.89	41.32	-88.99	812.3	9.0	30.5	176	2.05	48.28	27.5	23.6	-25.76	19.37
198	1950	Desmarais	Quebec	MICH	#1029	7/28/1950	311.20	-6.87							1.46	51.94	41.5	35.6	-23.86	17.41
199	1952	Virginius H Chase	Portwater, Michigan	MICH	#12669	6/28/1952	311.50	-6.86	43.78	-86.43	801.6	8.8	31.6	184	1.65	47.62	33.7	28.9	-24.02	17.58
200	1952	E G Voss	Traverse Township, Michigan	MICH	#1201	6/28/1952	311.50	-6.86	43.98	-83.06	726.9	8.4	29.0	180	1.55	50.39	37.9	32.5	-25.94	19.58
201	1954	Jennie V A Dieterle	Traverse City, Michigan	MICH	#1304	8/25/1954	312.80	-6.87	44.76	-85.62	778.0	7.7	26.0	185	1.50	48.07	37.4	32.0	-25.22	18.82
202	1957	E G Voss	Beaver Island, Michigan	MICH	#3872	5/25/1957	314.70	-6.89	45.65	-85.55	756.9	6.2	27.1	183	1.16	48.98	49.2	42.2	-27.86	21.57
203	1957	P A Hyppio	Limestone Mountain, Michigan	MICH	MICH# 1244477	6/13/1957	314.70	-6.89	46.81	-88.70	687.8	5.2	27.1	296	1.25	48.48	45.2	38.8	-27.49	21.18
204	1959	Heidenreich	Lake Simcoe, Ontario	MICH	MICH# 1491296	7/6/1959	315.70	-6.92	44.46	-79.34	885.0	4.4		295	1.40	47.58	39.6	34.0	-24.36	17.88
205	1960	Voss	Calumet, Michigan	MICH	#9456	5/15/1960	316.10	-6.93	44.25	-85.40	775.2	5.8	25.3	398	1.48	48.89	38.5	33.0	-24.53	18.04
206	1961	E. G. Voss	South Manitou Island, Leelanau County, Michigan	MICH	#9876	6/10/1961	316.70	-6.95	45.02	-86.13	757.2	7.4	25.2	182	1.74	48.65	32.6	28.0	-23.98	17.44
207	1962	Voss	Michigan	MICH	#10998	7/18/1962	319.20	-6.96	n/a	n/a	n/a	n/a	n/a	n/a	1.26	49.46	45.8	39.3	-25.28	18.80
208	1962	A Walther, A Auclair	Otter Lake, Quebec	MICH	#1491269	9/23/1962	319.20	-6.96	45.85	-76.43	885.0	4.4	n/a	210	1.22	49.21	47.0	40.3	-25.01	18.51
209	1965	Brunekt	Michigan	MICH	#578	6/19/1965	319.30	-7.02	n/a	n/a	n/a	n/a	n/a	n/a	1.14	47.48	48.6	41.6	-26.23	19.73
210	1968	Hagenah	Michigan	MICH	#6720	6/2/1968	316.80	-7.07	n/a	n/a	n/a	n/a	n/a	n/a	0.88	45.18	59.9	51.3	-26.15	19.59
211	1968	T. Reznick	Ontario	MICH	#134	3/13/1968	316.80	-7.07	n/a	n/a	n/a	n/a	n/a	n/a	1.37	48.84	41.6	35.6	-24.17	17.52
212	1968	Stuckey	Ohio	MICH	#6356	3/31/1968	316.80	-7.07	n/a	n/a	n/a	n/a	n/a	n/a	1.14	47.36	48.4	41.5	-25.01	18.40
213	1968	E. G. Voss	St. Helena Island, Moran, Michigan	MICH	#12816	8/31/1968	316.80	-7.07	45.86	-84.87	845.8	6.2	23.8	242	0.78	48.61	72.7	62.3	-26.78	20.25
214	1970	Merkle	Tom Creek, Clare County Michigan	MICH	#70-432	10/18/1970	325.00	-7.01	43.56	-85.00	843.8	6.2	28.2	302	1.06	49.00	53.9	46.2	-24.79	18.23
215	1970	Voss	Thunder Bay Island, Michigan	MICH	#13224	6/24/1970	325.00	-7.01	45.04	-83.20	843.8	6.4	28.2	215	0.82	48.08	68.4	58.6	-24.26	17.68
216	1971	C. E. Garton	Pargoma District, Ontario	MICH	#14627	7/29/1971	323.90	-7.21	47.65	-84.80	852.0	4.8	n/a	516	0.96	48.46	58.9	50.5	-24.70	17.93

217	1972	E. G. Voss	Middle Island, Alpena County, Michigan	MICH	#13980	7/14/1972	327.90	-7.21	45.19	-83.33	759.0	5.3	27.5	215	1.36	49.69	42.6	36.5	-22.32	15.45
218	1973	R. Kral	Pickett State Park, Tennessee	MICH	#49852	5/5/1973	327.90	-7.21	36.55	-84.80	1723.4	13.3	28.3	392	0.68	46.52	79.8	68.4	-27.59	20.96
219	1975	John Soper and L R Williams	Argonia District, Ontario	MICH	#149129	8/26/1975	329.39	-7.32	47.65	-84.80	852.0	4.8	n/a	516	1.24	49.18	46.3	39.7	-25.88	19.05
220	1976	J K Morton and Joan M Venn	Canoe Island, Lake Superior, Ontario	MICH	#NA 9782	8/29/1976	329.78	-7.42	47.36	-85.81	708.0	7.8	n/a	516	1.08	47.86	51.7	44.3	-23.00	15.94
221	1980	Reznicek, P M Catling	Ontario	MICH	#5486	5/25/1980	336.20	-7.43	n/a	n/a	n/a	n/a	n/a	n/a	n/a	n/a	n/a	n/a	-24.99	18.01
222	1983	W J Schepanek, A Dugal	Whitewater Lake, Ontario	MICH	#5469	8/13/1983	340.84	-7.66	45.84	-78.72	1061.5	6.8	n/a	396	1.16	50.59	50.9	43.6	-25.26	18.06
223	1985	B J Madsen	Singleton Fed, Schoolcraft County, Michigan	MICH	#MH12 44511	7/21/1985	343.50	-7.64	46.35	-86.47	983.2	4.9	24.6	252	0.86	48.58	65.9	56.5	-25.59	18.42
224	1985	Brian T Hazlett	Otter Creek, Michigan	MICH	#3504	7/22/1985	343.50	-7.64	44.75	-86.06	1090.4	7.3	24.6		1.12	50.23	52.3	44.8	-25.72	18.56
225	1988	Robert W Smith	Home Township, Michigan	MICH	#2418	5/4/1988	348.50	-7.77	41.95	-84.21	762.0	8.8	31.3	299	1.10	44.07	46.7	40.1	-26.57	19.31
226	1988	Robert W. Smith	Cambridge Township, Michigan	MICH	#2433	5/11/1988	348.50	-7.77	42.03	-84.21	760.5	8.8	31.4	305	0.89	53.84	70.6	60.5	-26.77	19.52
227	1989	W. W. Brodowicz	Byron, Kent Co., Michigan	MICH	#602	9/28/1989	350.80	-7.72	42.80	-85.71	802.6	7.6	28.1	211	1.56	31.40	23.5	20.1	-24.59	17.30
228	1993	Wacziarg, Reznicek & Wieboldt	Scott County, Virginia	MICH	#3169	6/21/1993	354.90	-7.75	36.68	-82.61	1078.0	7.9	32.6	530	1.02	48.95	56.0	48.0	-27.06	19.85
229	1993	Timothy J Higman, Thomas D Trana	Michigan	MICH	#181	6/10/1993	354.90	-7.75							1.43	34.35	28.0	24.0	-25.76	18.49
230	1998	Timothy L Walters, John Guidinger	Norman Township, Michigan	MICH	#12444 46	6/3/1998	363.11	-7.94	44.21	-85.89	825.2	9.4	28.0	212	1.00	47.28	55.1	47.3	-27.02	19.61
231	2003	Abbie Gosselink	Manitou-Lincoln Lake Barlow, Grand Rapids	MICH	#84	6/9/2003	372.79	-8.08	42.67	-85.51	888.5	8.4	28.3	238	1.20	39.04	37.9	32.5	-28.30	20.81
232	2007	Timoth L Walters, Joel Schaeffer	Whitewater Township, Grand Traverse County, Michigan	MICH	#11883	5/16/2007	380.49	-8.17	44.77	-85.40	658.9	7.9	26.4	214	0.79	61.44	90.7	77.8	-28.51	20.94
233	2008	Thomas G Lammers	Ironstone County, Escanaba River State Forest, Michigan	MICH	#12004	8/11/2008	382.31	-8.20	45.52	-87.40	700.8	5.3	26.6	182	0.90	57.79	74.9	64.2	-25.90	18.17
234	2009	David C Dister	Edgington State Park, Mason County, Michigan	MICH	#291	9/27/2009	383.84	-8.21	44.03	-86.51	917.2	7.0	21.6	204	0.81	30.56	44.0	37.7	-25.65	17.90
235	2012	Thomas G Lammers, Diane L Lammers	Kalamazoo County	MICH	#13782	6/27/2012	389.46	-8.26	42.23	-85.52	760.2	11.2	32.8	261	1.41	35.39	29.3	25.1	-26.35	18.58
296	1804		Castillo et Maldonado lectae, New Spain, Cuba	F		12/8/1804	283.40	-6.43	21.37	-77.85	1333.5	25.0		120	1.81	48.65	31.3	26.9	-22.31	16.24
297	1873	H H Babcock	Thousand Islands, Watersmeet Township, Michigan	F	FM#904 81	7/25/1873	289.10	-6.66	46.22	-89.40	662.5	3.7	25.4	520	0.85	50.87	69.8	59.8	-23.81	17.57
298	1892	Small		F	S.N.	7/23/1892	294.00	-6.66	n/a	n/a	n/a	n/a	n/a	n/a	0.55	47.40	100.5	86.2	-24.76	18.56
299	1896	M C Jenson	Lake Forest, Illinois	F	#56	3/10/1905	296.90	-6.78	42.25	-87.83	715.0	5.1	26.8	n/a	1.21	48.67	46.9	40.2	-24.35	18.01
300	1900	Lansing	Clarke, Indiana	F	#876	6/4/1900	295.90	-6.78	38.41	-84.71	1437.6	3.8	33.2	n/a	0.62	46.71	87.9	75.3	-24.62	18.29

301	1900	C Baenitz	Dreslau, Wroclaw, Poland	F	S.N.	5/9/1900	295.90	-6.78	51.14	17.06	590.0	8.3	n/a	n/a	0.87	47.97	64.3	55.1	-25.02	18.71
302	1900	C Baenitz	Germany	F	S.N.	5/16/1900	295.90	-6.79	n/a	n/a	n/a	n/a	n/a	n/a	1.45	48.08	38.7	33.2	-21.98	15.54
303	1902	Chas. J. Brand	Bemidji, Minnesota	F	#679	6/1/1902	296.40	-6.59	47.48	-94.88	603.8	4.4	27.9	417	0.88	48.18	63.8	54.8	-24.27	18.12
304	1908	Smith	Missouri	F	#623	5/25/1908	300.70	-6.80							1.87	50.15	31.3	26.8	-25.97	19.68
305	1918	C. J. Millsbaugh	Epinaim, Wisconsin	F	#4244	7/12/1918	302.60	-6.74	45.15	-87.17	1079.5	-1.9	24.7	213	1.44	48.56	39.3	33.7	-25.03	18.76
306	1926	J Francis Macbride	Trout Park, Elgin, Illinois	F	#703b	8/30/1926	305.00	-6.76	42.06	-88.27	959.9	8.4	28.5	242	1.80	49.58	32.1	27.5	-23.64	17.29
307	1930	F J Hermann	Lebanon Township, Michigan	F	#2315	7/19/1930	306.60	-6.83	43.07	-84.75	506.5	9.1	29.9	196	1.66	52.38	36.8	31.6	-24.54	18.16
308	1936	Tryon, Jr.	Immora Springs, Porter County, Indiana	F	#3088	7/2/1936	307.70	-6.83	41.63	-87.08	820.7	9.8	32.4	205	2.09	48.22	26.9	23.1	-25.32	18.97
309	1936	Olga Lakela	Duluth, Minnesota	F	#1701	8/12/1936	307.70	-6.83	46.76	-92.13	611.9	3.3	27.0	196	1.75	48.25	32.2	27.6	-24.37	17.98
310	1936	Ray C Fiesner	Waldo County, Maine	F	#10162	8/22/1936	307.70	-6.80	44.51	-69.02	1358.9	6.9	25.1	61	1.29	48.60	43.9	37.7	-26.22	19.95
311	1938	Auray Blain	Camden, canton Nemtaye, Matapedia Quebec	F	#185	7/17/1938	310.30	-6.83	47.97	-66.95	1038.0	2.2	n/a	57	1.49	47.67	37.3	32.0	-25.89	19.57
312	1940	Victorin, Boivin, Raymond, Kucyniak	Reverie, Martre, Fort Smith, Northwest Territories	F	#3825	8/18/1940	310.50	-6.78	63.17	-116.81	288.6	-4.3	n/a	157	1.93	46.99	28.4	24.3	-26.79	20.56
313	1944	Benke	Wisconsin	F	#6364	9/14/1944	309.50	-6.84	n/a	n/a	n/a	n/a	n/a	n/a	n/a	n/a	n/a	n/a	-23.92	17.49
314	1945		Par Valle Teguci, Tegucigalpa, Honduras	F		12/27/1945	309.50	-6.85	14.08	-87.20	1002.0	22.3	n/a	n/a	2.09	48.06	26.8	23.0	-25.69	19.34
315	1949	Julian A Steyermark	Trout Park, Elgin, Illinois	F	#68345	6/29/1949	309.70	-6.88	42.06	-88.27	843.5	9.7	30.7	242	1.76	48.37	32.1	27.5	-23.88	17.41
316	1952	Floyd A Swink	Walden Dunes State Park, Sawyer, Michigan	F	#838	4/26/1952	311.50	-6.86	41.92	-86.59	783.3	10.2	29.5	199	1.61	50.72	36.7	31.5	-24.06	17.63
317	1953	Swink	Kenosha County, Wisconsin	F	#2310	7/26/1953	312.70	-6.85	42.57	-87.84	640.8	9.8	29.4	190	1.61	48.00	34.8	29.8	-25.10	18.72
318	1980	M Nee	Jenerson County, Missouri	F	#19081	7/21/1980	336.20	-7.43	43.03	-88.80	768.6	12.9	30.3	257	1.98	49.03	28.9	24.8	-25.12	18.14
319	1999	Hess, Leidner, Allen, Stoyhoff, Bolger	Waldo County, Maine	F	#8818	7/15/1999	365.48	-7.97	44.51	-69.02	1189.2	8.5	27.4	61	n/a	n/a	n/a	n/a	-25.45	17.93
320	1999	Hess, Leidner, Allen, Stoyhoff, Bolger	Lisle, IL	F	unk	6/21/1999	365.48	-7.97	41.80	-88.08	943.9	11.2	32.5	204	2.02	49.05	28.3	24.3	-25.08	17.55
321	No date	Unknown	San Jose, Costa Rica	F	S.N.	No date	Unknown	Unknown	9.93	-84.12	1901.0	20.4	n/a	n/a	1.28	51.01	46.5	39.9	-26.70	n/a
322	No date	Unknown	Tres Rios, Costa Rica	F	S.N.	No date	Unknown	Unknown	9.91	-83.98	2031.0	19.2	n/a	n/a	1.50	48.41	37.6	32.3	-25.51	n/a
323	No date	Unknown	Palayias, Costa Rica	F	S.N.	No date	Unknown	Unknown	9.91	-83.81	3002.0	19.2	n/a	n/a	2.17	47.55	25.6	21.9	-28.50	n/a
324	No date	Unknown	Volcan Mirazu, Costa Rica	F	S.N.	No date	Unknown	Unknown	9.98	-83.35	3422.9	16.3	17.2	n/a	1.36	48.78	41.8	35.9	-24.61	n/a
347	1857	Unknown	New Haven, CT	Y	#6B	1857	286.70	-6.53	41.31	-72.92	1078.0	10.0	27.5	10	n/a	n/a	n/a	n/a	-23.41	n/a
348	1879	George H. Leland	Newport, VT	Y	100020477	July 1879	290.30	-6.42	44.94	-72.20	853.3	5.7	26.4	217	n/a	n/a	n/a	n/a	-24.55	18.59
349	1887	J H Schuette	Brown County, Wisconsin	Y	#282	8/2/1887	292.30	-6.42	44.53	-87.99	499.3	6.0	26.2	178	n/a	n/a	n/a	n/a	-25.47	19.54
350	1891	Anna E Carpenter	Newark, Connecticut	Y	#652	5/17/1891	293.60	-6.61	41.12	-73.42	968.9	9.0	27.0	13	n/a	n/a	n/a	n/a	-22.62	16.38
351	1892	John K Small	Mount of Hungry's Mother Creek, Smyth County, W. Virginia	Y	YU#025487	7/4/1892	294.00	-6.66	36.89	-81.52	968.0	10.5	27.0	699	n/a	n/a	n/a	n/a	-23.34	17.08

352	1899	Emile F Williams	Worcester, Massachusetts	Y	#2270	4/9/1899	295.80	-6.77	42.46	-71.09	1005.3	9.4	n/a	51	n/a	n/a	n/a	n/a	-22.61	16.21
353	1899	Emile F Williams	W. Desert, Maine	Y	#2269	7/18/1899	295.80	-6.77	44.35	-68.34	1087.6	6.8	n/a	21	n/a	n/a	n/a	n/a	-21.92	15.48
354	1901	Emile E Flynn	Burlington, Connecticut	Y	S.N.	5/17/1901	296.20	-6.79	41.77	-72.95	1652.8	8.3	n/a	254	n/a	n/a	n/a	n/a	-25.05	18.73
355	1902	Emile E Flynn	Burlington, Connecticut	Y	TO#023491	4/25/1902	296.40	-6.79	41.77	-72.95	1459.5	8.3	n/a	254	n/a	n/a	n/a	n/a	-24.15	17.79
356	1902	C K Averill	Canaan, Connecticut	Y	#417	8/31/1902	294.80	-6.79	41.97	-73.31	1343.7	7.7	n/a	239	1.10	48.56	51.5	44.1	-24.88	18.55
357	1903	E. H. Thompson	Litchfield, Connecticut	Y	TO#023457	4/25/1903	294.80	-6.80	41.74	-73.19	1410.0	7.7	n/a	313	1.36	46.33	39.7	34.1	-23.13	16.72
358	1905	O W Knight	Orono, Maine	Y	TO#023483	5/10/1905	296.90	-6.71	44.88	-68.69	798.9	5.6	n/a	38	1.20	45.48	44.2	37.9	-24.35	18.08
359	1909	H S Clark	Wethersfield, Connecticut	Y	CBS#02594	6/6/1909	299.20	-6.54	41.70	-72.67	1049.0	9.8	n/a	32	1.53	47.93	36.5	31.3	-24.71	18.63
360	1909	C H Bissell	Wethersfield, Connecticut	Y	YU#025498	9/11/1909	299.20	-6.54	41.70	-72.67	1049.0	9.8	n/a	32	1.53	48.38	36.9	31.6	-24.06	17.95
361	1909	E B Harger	New Milford, Connecticut	Y	#5565	6/17/1909	299.20	-6.54	41.60	-73.42	1272.8	9.3	n/a	70	n/a	n/a	n/a	n/a	-25.58	19.54
362	1915	H C Bigelow	Berlin, Connecticut	Y	#007	11/14/1915	300.50	-6.86	41.63	-72.75	990.9	8.0	n/a	14	0.91	48.47	62.1	53.3	-26.89	20.58
363	1917	Harold St. John and George E. Nichols	St. John Pond Township, Maine	Y	#2103	7/10/1917	302.10	-6.80	46.47	-69.90	1125.7	1.4	n/a	476	1.00	46.24	53.9	46.2	-24.94	18.60
364	1920	H Castle	Utica, New York	Y	#023409	1-Aug-20	303.40	-6.90	42.44	-76.50	944.1	7.2	n/a	124	1.77	46.68	30.8	26.4	-23.28	16.77
365	1932	K P Jansson	New London, Connecticut	Y	#13	5-Aug-32	307.30	-6.74	41.36	-72.10	1304.0	11.0	n/a	43	2.28	49.33	25.2	21.6	-24.42	18.12
366	1958	John Ebinger	New Haven, Connecticut	Y	#286	6/24/1958	315.20	-6.90	41.31	-72.93	1461.3	8.7	n/a	17	0.86	47.30	64.1	55.0	-25.36	18.94
367	1982	Doris E Taylor, Jerome Waller, Ellen Ballard, Cindy Schwind	Madison, Kentucky	Y	#1815	7/14/1982	339.15	-7.51	37.71	-84.27	1333.0	10.0	n/a	313	1.70	46.83	32.1	27.5	-25.53	18.49
368	1984	Leslie J Merhoff	Canaan, Connecticut	Y	#9536	3/16/1984	341.70	-7.65	41.97	-73.31	1313.2	10.6	n/a	239	1.07	46.65	50.8	43.6	-25.91	18.75
399	1830	Douglass Houghton	Trenon Falls, New York	MICH	MICH #1491325	July 1830	283.90	-6.53	43.26	-75.19	968.3	6.8	27.4	247	n/a	n/a	n/a	n/a	-24.90	18.84
401	1901	Bronson Barlow	Marquette County, Michigan	MICH	MICH #1491320	23-Aug-01	296.20	-6.79	46.55	-87.42	735.3	10.9	24.6	228	1.28	50.34	45.9	39.3	-22.68	16.26
402	1911	H E Sargent	Foran Lake, Antrim County Michigan	MICH	MICH #1244466	15-Jul-11	299.50	-6.69	44.92	-85.28	788.2	7.8	28.9	214	1.11	47.54	49.9	42.8	-24.14	17.88
403	1838	John Wright & George H Bull	St. Clair River, Lake Huron, Michigan	MICH	#42	June 4, 1838	283.90	-6.62	43.01	-82.42	675.7	6.9	27.0	180	1.13	46.99	48.5	41.6	-24.22	18.04
404	1957	Voss		MICH	S.N.	8/20/1957	314.70	-6.89						0.85	48.95	67.2	57.6	-22.71	16.18	
407	2017	R. Stein	Ann Arbor, MI, 4th Ave	Ann Arbor	407	3/9/2017	407.18	-8.57	42.28	-83.75	848.7	9.4	30.0	258	0.77	45.31	68.6	58.8	-25.53	17.40
408	2017	R. Stein	Ann Arbor, MI, 4th Ave	Ann Arbor	408	3/9/2017	407.18	-8.57	42.28	-83.75	848.7	9.4	30.0	256	0.66	46.26	81.7	70.1	-26.22	18.12
409	1843	Cooley	Michigan	MSC	#19-15	1843	287.40	-6.54						0.37	49.87	157.2	134.8	-24.04	17.94	
410	1865	Beal	Cambodge, Massachusetts	MSC	S.N.	5/24/1865	286.30	-6.54	42.37	-71.12	1156.9	9.3	27.0	4	0.69	49.95	84.4	72.4	-24.32	18.22
411	1888	AA Farwell	Rosebaw Co, Michigan	MSC	S.N.	June 1888	290.63	-6.55	47.39	-88.03	646.9	4.9	21.9	274	0.56	49.03	102.1	87.6	-24.75	18.66
412	1892	John K Small	Henry's Mother Creek, Four Miles North of Marion Smyth County	MSC	S.N.	6/1/1892	294.00	-6.43	36.89	-81.52	973.7	10.5	28.7	694	0.80	45.75	66.7	57.2	-23.93	17.93
413	1892	John K Small	Smyth County, Virginia	MSC	S.N.	6/8/1892	294.00	-6.66	36.89	-81.52	973.7	10.5	28.7	694	0.31	44.92	169.0	144.9	-26.31	20.18
414	1894	H. C. Skeels	Agricultural College, East Lansing, Michigan	MSC	S.N.	10/7/1894	295.10	-6.66	42.75	-84.49	660.1	7.6	29.1	260	0.51	49.86	114.0	97.8	-24.15	17.92

415	1899	Unknown	Grayling, Crawford County, Michigan	MSC	S.N.	5/27/1899	295.80	-6.60	44.66	-84.71	707.9	5.6	28.4	347	0.20	45.26	263.9	226.3	-24.96	18.83
416	1900	CFW	Crystal Lake, Montcalm County, Michigan	MSC	#141922	6/25/1900	295.90	-6.77	44.69	-86.17	796.0	7.9	28.4	229	0.67	46.87	81.6	70.0	-24.38	18.05
417	1904	Pepoon	Cass County, Michigan	MSC	#75	Aug-04	297.00	-6.78	41.93	-85.99	846.3	7.9	27.5	277	0.77	44.11	66.8	57.3	-25.98	19.71
423	2017	R. Stein	5000 Kensington Road, Cleveland Ohio	Cleveland	423	3/26/2017	407.18	-8.57	41.50	-81.57	1123.7	10.3	29.3	281	0.63	45.88	84.9	72.8	-24.44	16.27
611	2017	R. Stein	Shangri-la Botanical Garden	SG	611	7/14/2017	405.13	-8.50	31.15	121.43	1176.9	16.0	27.9	6	n/a	n/a	n/a	n/a	-28.31	20.39

APPENDIX B

Supplemental Figures, Tables and References for Chapter III

Figure B1 $[\text{CO}_2]$ values plotted against $\Delta^{13}\text{C}_{\text{plant}}$ for species with medium-resolution records of the period of Industrialization. Data are for: (a) *Pinus strobus* (Eastern white pine), (b) *Thuja sutchuenensis* (Sichuan arborvitae), (c) *Thuja koraiensis* (Korean arborvitae), (d) *Thuja standishii* (Japanese arborvitae), and (e) *Platycladus orientalis* (Chinese arborvitae). The outer panel shows change in $\Delta^{13}\text{C}_{\text{plant}}$ vs. $[\text{CO}_2]$ over Industrialization, while the inner panel shows the range and distribution of $\Delta^{13}\text{C}_{\text{plant}}$ values for this species. Each of the species occupies different geographic ranges and different ranges of climatic variability, but none shows a significant $\Delta^{13}\text{C}_{\text{plant}}$ response to rising $[\text{CO}_2]$ over the period of Industrialization.

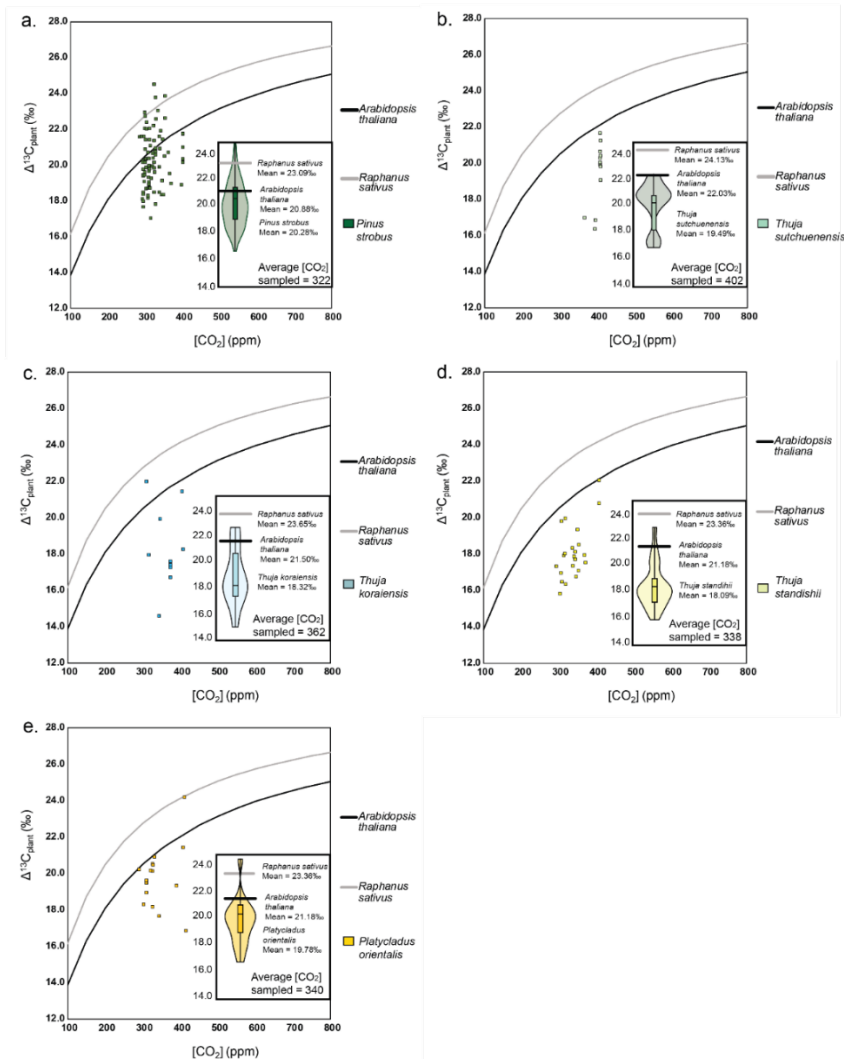


Figure B2 Comparison of $\Delta^{13}\text{C}_{\text{plant}}$ values of plants as sampled in this study, the Schubert & Jahren (2012) model, and from the literature and sorted by genera. Angiosperms are shown to the left of the diagram, while gymnosperms are shown to the right. Genera for which $n < 10$ samples within the literature, were excluded from this figure. Xs denote mean values for each genus, and lines denote median values for each genus. Each box and whisker in this figure shows a different genus with $n \geq 15$ represented isotope values from this study, Sheldon et al. (2020) and literature. Boxes show the 75th percentile of data, while whiskers show the remaining 25th percentile of data. Individual dots show outliers.

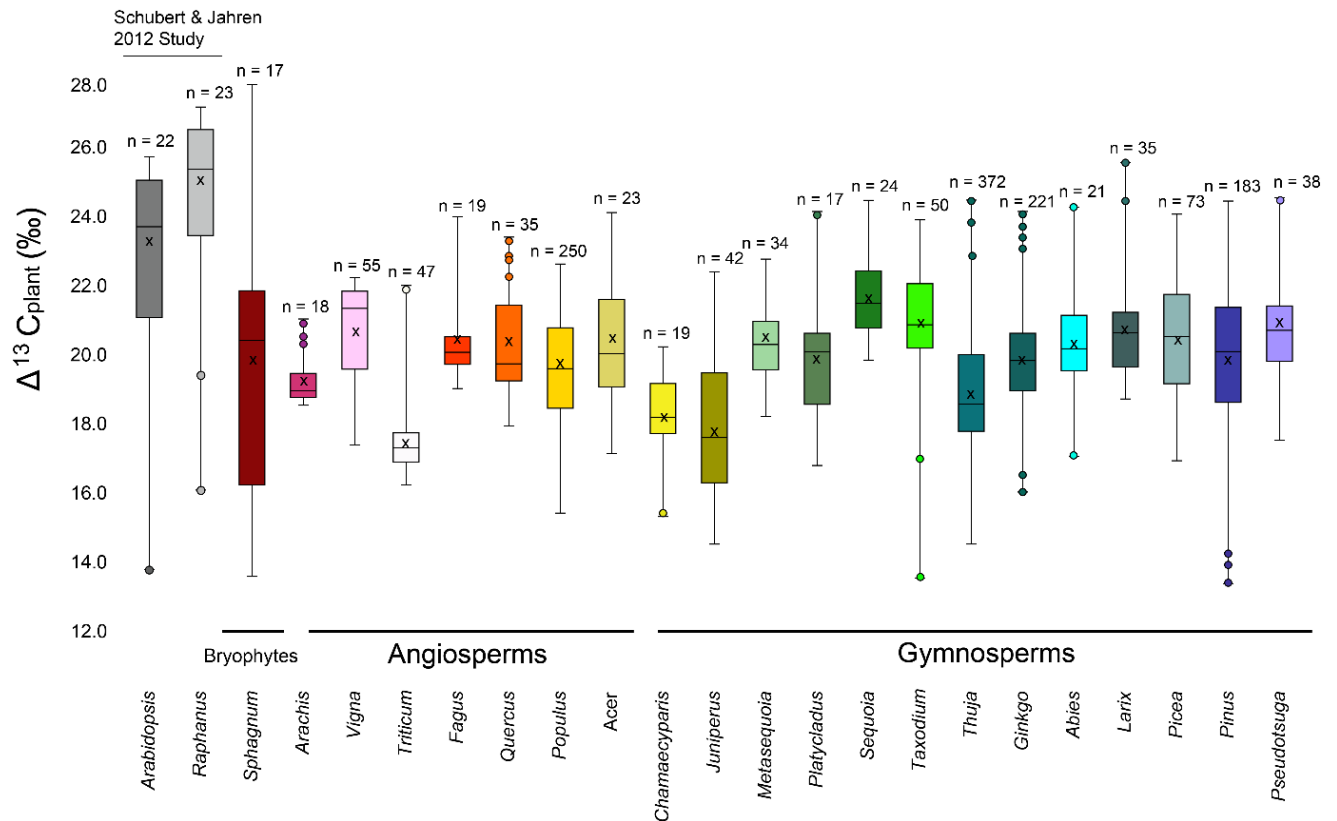


Figure B3 Comparison of $\Delta^{13}\text{C}_{\text{plant}}$ values of plants as sampled in this study, the Schubert & Jahren (2012) model, and from the literature and sorted by family. Angiosperms are shown to the left of the diagram, while gymnosperms are shown to the right. Families for which $n < 10$ samples within the literature were excluded from this figure, except for “other Brassicaceae” – members of the same family as *Arabidopsis* and *Raphanus*, for comparison. Xs denote mean values for each genus. Each box and whisker in this figure shows a different family with $n \geq 15$ represented isotope values from this study, Sheldon et al. (2020) and literature (except for Brassicaceae, which is included to show the discrepancy between model species and other Brassicaceae). Boxes show the 75th percentile of data, while whiskers show the remaining 25th percentile of data.

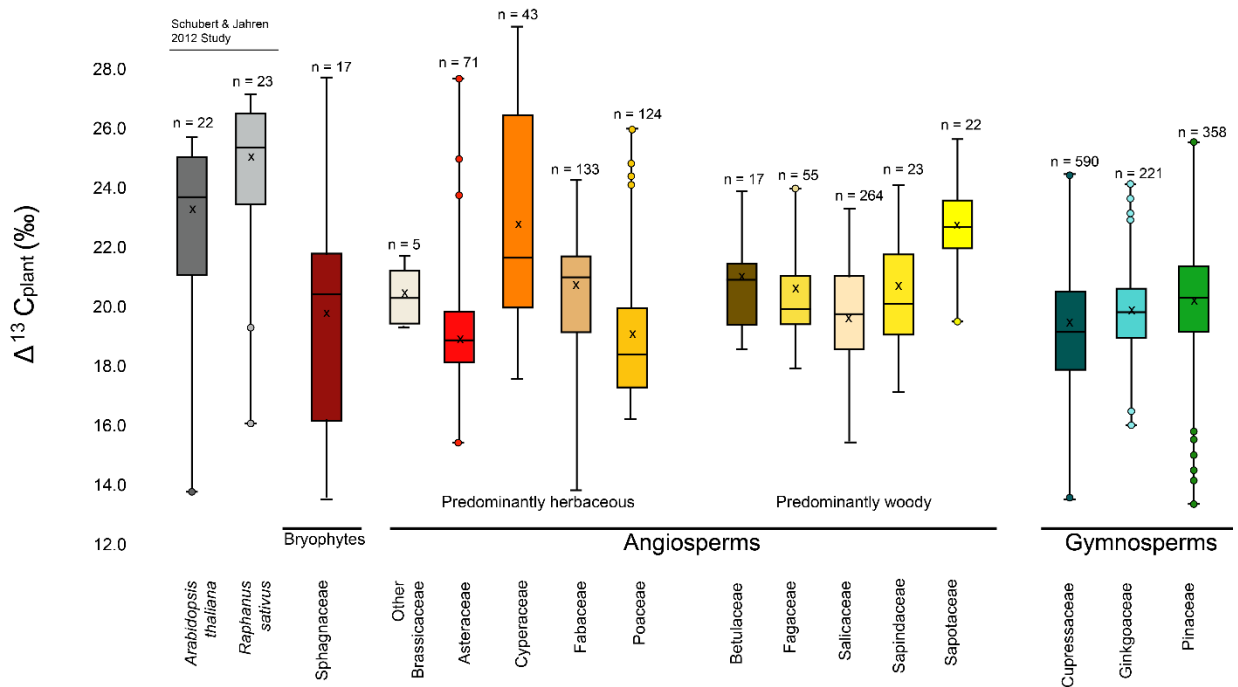


Table B1 Isotope data measurements for specimens collected in the Earth Systems Science Lab (tab labeled *ESS Lab*) and from literature (tab labeled *Literature*). References for literature and ESS data shown in tab labeled *References*. $\delta^{13}\text{C}_{\text{plant}}$ values and $\Delta^{13}\text{C}_{\text{plant}}$ values (calculated using Equation 3.2) are listed for ESS Lab and Literature values when known. Climate (PRISM Climate Group 2004) and barometric data (Etheridge et al. 1998; Keeling et al. 2001; White et al. 2015; Eggleston et al. 2016), year, collector, associated publications are listed when known and applicable. N/a denotes information not available. Equation 3.2 (see details in main text):

$$\Delta^{13}\text{C}_{\text{plant}} = \frac{\delta^{13}\text{C}_{\text{CO}_2} - \delta^{13}\text{C}_{\text{plant}}}{1 + \frac{\delta^{13}\text{C}_{\text{plant}}}{1000}}$$

(for full table, see separate file).

C₃ plant carbon isotope discrimination does not respond to CO₂ concentration on decadal to centennial timescales

Rebekah A. Stein, Nathan D. Sheldon, Selena Y. Smith

Accepted 13 October 2020

Table S1: Isotope data measurements for specimens collected in the Earth Systems Science Lab (tab labeled ESS Lab) and from literature (tab labeled Literature).

References for literature and ESS data shown in tab labeled References.

$\delta^{13}C_{plant}$ values and $\Delta^{13}C_{plant}$ values (calculated using Eq. 2) are listed for ESS Lab and Literature values when known.

Climate (PRISM Climate Group 2004) and barometric data (Etheridge et al. 1998; Keeling et al. 2001; White et al. 2015; Eggleston et al. 2016), year, collector, associated publications are listed when known and applicable.

N/a denotes information not available.

Eq. 2 (see details in main text):

$$\Delta^{13}C_{plant} = \frac{\delta^{13}C_{CO_2} - \delta^{13}C_{plant}}{1 + \frac{\delta^{13}C_{plant}}{1000}}$$

ESS Lab	et al.	2020	BHPT1498	532	#1645	William W	Gymnosperm	Woody	C3	Woody Gy	Conifer	Thuja	Thuja plicata	4/12/1998	1920	Government	US	43019194	-121.7533	306.4	-6.91	-24.85	18.40	1642	7.2	23.4	1180	0.85	47.05	64.51	65.31766
ESS Lab	et al.	2020	CO_SCP17	845	na	Rebekah S	Angiosperm	Woody	C3	Woody Ang	Salicaceae	Populus	Populus tremuloides	8/4/2018	2018	Val, Colo	US	9644414	-108.3712	407.1	-8.42	-26.11	18.16	638	4.3	23.4	2560.4	3.05	51.10	19.75	16.93443
ESS Lab	et al.	2020	CO_VRP12	849	na	Rebekah S	Angiosperm	Woody	C3	Woody Ang	Salicaceae	Populus	Populus tremuloides	8/4/2018	2018	Val, Colo	US	9644388	-108.3992	407.1	-8.42	-27.17	19.28	637	4.6	23.4	2576.3	2.78	52.78	22.29	19.11232
ESS Lab	et al.	2020	CO_VRP12	849	na	Rebekah S	Angiosperm	Woody	C3	Woody Ang	Salicaceae	Populus	Populus tremuloides	8/4/2018	2018	Val, Colo	US	9644388	-108.3992	407.1	-8.42	-27.20	19.31	637	4.6	23.4	2576.3	2.96	52.47	22.99	19.11053
ESS Lab	et al.	2020	CO_VRP12	849	na	Rebekah S	Angiosperm	Woody	C3	Woody Ang	Salicaceae	Populus	Populus tremuloides	8/4/2018	2018	Val, Colo	US	9644388	-108.3992	407.1	-8.42	-26.74	19.35	637	4.6	23.4	2576.3	2.28	51.67	23.12	22.83324
ESS Lab	et al.	2020	CSPT2000	684	9279	Holl	Angiosperm	Woody	C3	Woody Ang	Salicaceae	Populus	Populus tremuloides	6/22/2000	2000	Central CO	US	9488187	-106.3666	371.69	-8.14	-27.16	19.55	630	3.3	23.5	2743.2	4.12	48.90	13.86	11.8835
ESS Lab	et al.	2020	MHTO1294	178	8426	Eranson	Gymnosperm	Woody	C3	Woody Gy	Conifer	Thuja	Thuja occidentalis	7/18/1924	1924	Parkway	US	44537	-84.97	304.5	-6.99	-24.74	18.70	780	5.3	23.6	207.0	0.86	51.40	70.23	60.2222
ESS Lab	et al.	2020	CO_TRP17	833	na	Rebekah S	Angiosperm	Woody	C3	Woody Ang	Salicaceae	Populus	Populus tremuloides	8/3/2018	2018	Rocky Mtn	US	4033878	-105.6119	407.1	-8.42	-28.28	20.37	760	5.4	23.7	2520.3	2.56	48.47	22.46	22.668
ESS Lab	et al.	2020	CO_TRP17	833	na	Rebekah S	Angiosperm	Woody	C3	Woody Ang	Salicaceae	Populus	Populus tremuloides	8/3/2018	2018	Rocky Mtn	US	4033919	-105.6120	407.1	-8.42	-29.32	21.01	760	5.4	23.7	2521.6	2.43	49.09	23.10	20.826
ESS Lab	et al.	2020	CO_TRP17	833	na	Rebekah S	Angiosperm	Woody	C3	Woody Ang	Salicaceae	Populus	Populus tremuloides	8/3/2018	2018	Rocky Mtn	US	4033838	-105.6135	407.1	-8.42	-29.43	21.05	760	5.4	23.7	2527.7	2.38	49.15	24.08	20.5126
ESS Lab	et al.	2020	CO_FLPT12	832	na	Rebekah S	Angiosperm	Woody	C3	Woody Ang	Salicaceae	Populus	Populus tremuloides	8/3/2018	2018	Rocky Mtn	US	4032709	-105.6198	407.1	-8.42	-29.27	21.79	760	5.4	23.7	2470.3	1.97	48.20	20.59	24.11777
ESS Lab	et al.	2020	CO_FLPT12	832	na	Rebekah S	Angiosperm	Woody	C3	Woody Ang	Salicaceae	Populus	Populus tremuloides	8/3/2018	2018	Rocky Mtn	US	4032709	-105.6198	407.1	-8.42	-29.44	21.87	760	5.4	23.7	2487.4	2.08	48.63	20.68	22.26368
ESS Lab	et al.	2020	CO_FLPT12	832	na	Rebekah S	Angiosperm	Woody	C3	Woody Ang	Salicaceae	Populus	Populus tremuloides	8/3/2018	2018	Rocky Mtn	US	4033515	-105.6201	407.1	-8.42	-30.39	22.66	760	5.4	23.7	2504.2	1.73	45.31	20.54	26.19075
ESS Lab	et al.	2020	CO_FLPT12	831	na	Rebekah S	Angiosperm	Woody	C3	Woody Ang	Salicaceae	Populus	Populus tremuloides	8/3/2018	2018	Rocky Mtn	US	4033555	-105.6216	407.1	-8.42	-30.42	22.69	760	5.4	23.7	2470	3.31	49.03	17.27	14.81265
ESS Lab	et al.	2020	MHT0885	210	#1818	E. G. Voss	Gymnosperm	Woody	C3	Woody Gy	Conifer	Thuja	Thuja occidentalis	8/31/1968	1968	St Helena	US	485800	-84.8702	321.1724	-7.24	-26.78	20.07	648	6.2	23.800	242.000	0.78	48.61	72.68	62.32051
ESS Lab	et al.	2020	MHT0885	210	#1818	E. G. Voss	Gymnosperm	Woody	C3	Woody Gy	Conifer	Thuja	Thuja occidentalis	8/31/1968	1968	St Helena	US	4857956	-84.8704	325.017	-7.24	-27.53	20.87	1135	3.9	23.98	598	1.14	48.84	60.06	42.92962
ESS Lab	et al.	2020	BHPT1842	530	#1097	H. Y. Rogner	Gymnosperm	Woody	C3	Woody Gy	Conifer	Thuja	Thuja plicata	7/17/1942	1942	North Mt	US	4839142	-114.0404	310.3	-6.96	-24.42	17.90	689	4.0	23.84	844	1.05	49.30	54.75	46.95238
ESS Lab	et al.	2020	MHT1640	na	na	Molly Ng	Gymnosperm	Woody	C3	Woody Gy	Conifer	Sequoia	Sequoia sempervirens	12/20/2016	2016	Portland	US	4726625	-122.1213	404.55	-8.49	-29.30	21.43	702	13.5	23.8					
ESS Lab	et al.	2020	MHT1640	na	na	Molly Ng	Gymnosperm	Woody	C3	Woody Gy	Conifer	Sequoia	Sequoia sempervirens	12/20/2016	2016	Portland	US	4726355	-122.2118	404.55	-8.49	-29.72	21.88	702	13.5	23.8					
ESS Lab	et al.	2020	MHT1642	na	na	Molly Ng	Gymnosperm	Woody	C3	Woody Gy	Conifer	Sequoia	Sequoia sempervirens	12/20/2016	2016	Portland	US	4726352	-122.2118	404.55	-8.49	-29.96	22.11	702	13.5	23.8					
ESS Lab	et al.	2020	CSPT2000	685	#5183	Nelson	Angiosperm	Woody	C3	Woody Ang	Salicaceae	Populus	Populus tremuloides	6/29/2000	2000	North Park	US	4042414	-106.4697	371.69	-8.14	-27.55	19.95	617	3.4	23.8	2632	3.11	48.50	18.19	15.94846
ESS Lab	et al.	2020	CO_CCF17	693	na	Rebekah S	Angiosperm	Woody	C3	Woody Ang	Salicaceae	Populus	Populus tremuloides	8/18/2017	2017	Thom	US	3829082	-105.0173	405.24	-8.55	-27.79	19.79	710	6.9	23.8	2452.7	1.99	48.95	28.69	24.59799
ESS Lab	et al.	2020	CO_CCF17	693	na	Rebekah S	Angiosperm	Woody	C3	Woody Ang	Salicaceae	Populus	Populus tremuloides	8/18/2017	2017	Thom	US	3829208	-105.0171	405.24	-8.55	-29.68	21.77	710	6.9	23.8	2415.2	2.35	49.96	24.71	25.0977
ESS Lab	et al.	2020	YU101892	356	#417	C. K. Averil	Gymnosperm	Woody	C3	Woody Gy	Conifer	Thuja	Thuja occidentalis	8/31/1962	1962	Chanon	US	4196027	-73.31242	296.5	-6.82	-24.88	22.52	1344	7.7	23.29	229	1.56	48.55	54.48	44.164545
ESS Lab	et al.	2020	CLUBT186	667	#429	Green	Angiosperm	Woody	C3	Woody Ang	Salicaceae	Populus	Populus tremuloides	1992	1992	Van Laken	US	3930702	-109.3281	311.5	-7.00	-24.57	18.01	297	2.0	23.9	1999	2.54	49.45	23.54	20.18397
ESS Lab	et al.	2020	CO_FLPT12	810	na	Rebekah S	Angiosperm	Woody	C3	Woody Ang	Salicaceae	Populus	Populus tremuloides	8/3/2018	2018	Rocky Mtn	US	4033833	-105.6120	407.1	-8.42	-29.19	21.81	760	5.4	23.7	2491.1	8.42	49.20	21.81	22.82858
ESS Lab	et al.	2020	NM_TSPV1	807	na	Rebekah S	Angiosperm	Woody	C3	Woody Ang	Salicaceae	Populus	Populus tremuloides	7/31/2018	2018	Taco SM	US	3556469	-108.3928	408.9	-8.54	-25.01	16.89	768	6.3	23.9	2740.9	2.85	44.74	19.87	16.86505
ESS Lab	et al.	2020	NM_TSPV1	798	na	Rebekah S	Angiosperm	Woody	C3	Woody Ang	Salicaceae	Populus	Populus tremuloides	7/31/2018	2018	Taco SM	US	3556445	-108.4449	408.9	-8.54	-26.08	19.02	768	6.9	23.9	2651.6	2.13	48.42	28.51	22.73239
ESS Lab	et al.	2020	NM_TSPV1	806	na	Rebekah S	Angiosperm	Woody	C3	Woody Ang	Salicaceae	Populus	Populus tremuloides	7/31/2018	2018	Taco SM	US	3536842	-108.449	408.9	-8.54	-27.42	19.41	768	6.9	23.9	2740.9	1.94	48.62	28.87	24.75268
ESS Lab	et al.	2020	MHT1648	na	na	Molly Ng	Gymnosperm	Woody	C3	Woody Gy	Conifer	Sequoia	Sequoia sempervirens	12/23/2016	2016	US Santa C	US	4700082	-122.0219	404.55	-8.49	-27.84	19.91	849	13.9	24.1					
ESS Lab	et al.	2020	MHT1648	na	na	Molly Ng	Gymnosperm	Woody	C3	Woody Gy	Conifer	Sequoia	Sequoia sempervirens	12/23/2016	2016	US Santa C	US	4700222	-122.0457	404.55	-8.49	-27.31	17.76	852	4.8	24.0	1883	1.13	50.83	52.46	44.8623
ESS Lab	et al.	2020	MHT1648	na	na	Molly Ng	Gymnosperm	Woody	C3	Woody Gy	Conifer	Sequoia	Sequoia sempervirens	12/23/2016	2016	US Santa C	US	4700173	-122.0457	404.55	-8.49	-27.82	18.85	852	4.8	24.0	2116.000	1.24	49.10	46.25	39.01210
ESS Lab	et al.	2020	MHT1648	na	na	Molly Ng	Gymnosperm	Woody	C3	Woody Gy	Conifer	Sequoia	Sequoia sempervirens	12/23/2016	2016	US Santa C	US	4699792	-122.0332	404.55	-8.49	-29.69	21.85	825	14.1	24.3					
ESS Lab	et al.	2020	BHPT1857	545	S.N.	Carl A Lind	Gymnosperm	Woody	C3	Woody Gy	Conifer	Thuja	Thuja plicata	4/31/1957	1957	Aling Run	US	4829219	-122.3202	314.2	-7.07	-24.67	21.00	915	9.6	24.4	27	0.95	46.33	58.87	48.34842
ESS Lab	et al.	2020	MHT1648	na	na	Molly Ng	Gymnosperm	Woody	C3	Woody Gy	Conifer	Sequoia	Sequoia sempervirens	12/23/2016	2016	US Santa C	US	4699792	-122.0332	404.55	-8.49	-29.69	21.85	825	14.1	24.3					
ESS Lab	et al.	2020	MHT1648	na	na	Molly Ng	Gymnosperm	Woody	C3	Woody Gy	Conifer	Sequoia	Sequoia sempervirens	12/23/2016	2016	US Santa C	US	4699792	-122.0332	404.55	-8.49	-29.69	21.85	825	14.1	24.3					
ESS Lab	et al.	2020	MHT1648	na	na	Molly Ng	Gymnosperm	Woody	C3	Woody Gy	Conifer	Sequoia	Sequoia sempervirens	12/23/2016	2016	US Santa C	US	4699792	-122.0332	404.55	-8.49	-29.69	21.85	825	14.1	24.3					
ESS Lab	et al.	2020	MHT1648	na	na	Molly Ng	Gymnosperm	Woody	C3	Woody Gy	Conifer	Sequoia	Sequoia sempervirens	12/23/2016	2016	US Santa C	US	4699792	-122.0332	404.55	-8.49	-29.69	21.85	825	14.1	24.3					
ESS Lab	et al.	2020	MHT1648	na	na	Molly Ng	Gymnosperm	Woody	C3	Woody Gy	Conifer	Sequoia	Sequoia sempervirens	12/23/2016	2016	US Santa C	US														

ESS Lab	et al 2020	CO_SLPSP	871	Rebeah S	Angiosperm	Woody	C3	Woody Ang	Salicaceae	Populus	Populus tremuloides	8/20/2018	2018	Gypsum, CA	930668	-106.717	407.1	-8.42	-27.10	19.20	471	5.8	26.1	2437.8	2.36	49.39	24.41	10.327973
ESS Lab	et al 2020	CO_SLPSP	869	Rebeah S	Angiosperm	Woody	C3	Woody Ang	Salicaceae	Populus	Populus tremuloides	8/20/2018	2018	Gypsum, CA	930668	-106.717	407.1	-8.42	-27.71	19.94	471	5.8	26.1	2437.8	2.32	51.1	25.73	22.0024
ESS Lab	et al 2020	CO_SLPSP	868	Rebeah S	Angiosperm	Woody	C3	Woody Ang	Salicaceae	Populus	Populus tremuloides	8/20/2018	2018	Gypsum, CA	930668	-106.717	407.1	-8.42	-27.71	19.94	471	5.8	26.1	2437.8	2.32	51.1	25.73	22.0024
ESS Lab	et al 2020	WV_SLPSP	264	H.H. Barthe	Angiosperm	Woody	C3	Woody Ang	Prunaceae	Prunus	Prunus strobilus	9/16/1991	1991	Marathon, TX	484267	-89.7349	311.1	-6.99	-26.27	19.94	900	4.7	26.2	379.1	1.12	49.86	91.92	44.01786
ESS Lab	et al 2020	YUTO1887	343	J.H. Schuler	Gymnosperm	Woody	C3	Woody Gyr	Pinaceae	Thuja	Thuja occidentalis	8/21/1987	1987	Brown Co., NC	44.52727	-87.9933	293.6	-6.77	-25.47	19.18	499	6.0	28.2	178.8	1.24	47.27	44.46	38.120674
ESS Lab	et al 2020	WA_ML1P	n/a	Molly Ng	Gymnosperm	Woody	C3	Woody Gyr	Pinaceae	Taxodium	Taxodium distichum	9/11/2016	2016	Matthew B.	42.3004	-88.6614	401.01	-8.35	-27.07	19.24	855	8.9	26.2					
ESS Lab	et al 2020	WA_ML1P	711	Rebeah S	Angiosperm	Woody	C3	Woody Gyr	Pinaceae	Thuja	Thuja plicata	5/12/2018	2018	Ma Si Tai	47.50472	-121.7399	411.3	-8.67	-29.76	21.73	2365	10.6	26.2	1102	1.05	50.07	57.47	68.671
ESS Lab	et al 2020	FMP139	343	Chesler C	Gymnosperm	Woody	C3	Woody Gyr	Pinaceae	Pinus	Pinus strobus	8/17/1938	1938	Baldwin Har.	55.04485	-87.12423	310.2	-6.94	-26.77	20.37	874	7.1	26.3	179	1.41	47.37	39.67	34.02128
ESS Lab	et al 2020	BHP1362	288	J.V. & F. Fries	Gymnosperm	Woody	C3	Woody Gyr	Pinaceae	Pinus	Pinus strobus	7/17/1962	1962	Maadso.	44.59089	-83.02422	342.06	-7.67	-28.96	21.03	630	6.7	28.3	198	2.00	48.63	27.53	23.008
ESS Lab	et al 2020	YUTO1884	364	Leslie J. Myers	Gymnosperm	Woody	C3	Woody Gyr	Pinaceae	Thuja	Thuja occidentalis	3/16/1984	1984	Canas.	41.96627	-73.31242	345.28	-7.81	-25.91	18.98	1313	10.6	28.3	239	1.07	46.05	50.84	45.975804
ESS Lab	et al 2020	YUTO1876	369	J.F. Howell	Gymnosperm	Woody	C3	Woody Gyr	Pinaceae	Thuja	Thuja plicata	2/18/1995	1995	Savannah.	45.70244	-122.9174	297.6	-6.83	-25.38	19.01	990	10.8	28.3					
ESS Lab	et al 2020	YUTO1875	348	G.H.	Gymnosperm	Woody	C3	Woody Gyr	Pinaceae	Thuja	Thuja occidentalis	July 1875	1877	Wagon M.	44.93769	-72.20038	290.2	-6.74	-24.86	16.25	855	5.7	26.4	217	1.04	48.85	54.44	46.669201
ESS Lab	et al 2020	WA_ML1P	n/a	Molly Ng	Gymnosperm	Woody	C3	Woody Gyr	Pinaceae	Sequoia	Sequoia sempervirens	12/23/2016	2016	San Louis C.	35.27985	-120.6847	404.56	-8.49	-29.01	21.23	599	15.6	26.4					
ESS Lab	et al 2020	BHT2020	232	P.J.1883	Angiosperm	Woody	C3	Woody Ang	Salicaceae	Populus	Populus trichocarpa	5/16/2007	2007	Whitewater.	44.77000	-85.40000	386.41	-8.40	-28.81	20.70	659	7.9	26.400	214.000	0.79	41.40	90.70	77.776
ESS Lab	et al 2019	6_H2004	192	Chetema M	Angiosperm	Woody	C3	Woody Ang	Salicaceae	Acer	Acer saccharum	10/15/2014	2014	Hendon Lab	42.02897	-84.11142	395.60	-8.19	-27.88	20.26	824	8.9	26.5					
ESS Lab	et al 2019	6_00013	204	Chetema M	Angiosperm	Woody	C3	Woody Ang	Salicaceae	Acer	Acer granatum	10/15/2014	2014	Hendon Lab	42.02897	-84.11139	395.60	-8.19	-27.88	20.26	824	8.9	26.5					
ESS Lab	et al 2019	6_00013	204	Chetema M	Angiosperm	Woody	C3	Woody Ang	Salicaceae	Acer	Acer granatum	10/15/2014	2014	Hendon Lab	42.02897	-84.11139	395.60	-8.19	-27.88	20.26	824	8.9	26.5					
ESS Lab	et al 2019	6_00013	204	Chetema M	Angiosperm	Woody	C3	Woody Ang	Salicaceae	Acer	Acer granatum	10/15/2014	2014	Hendon Lab	42.02897	-84.11139	395.60	-8.19	-27.88	20.26	824	8.9	26.5					
ESS Lab	et al 2019	6_00013	204	Chetema M	Angiosperm	Woody	C3	Woody Ang	Salicaceae	Acer	Acer granatum	10/15/2014	2014	Hendon Lab	42.02897	-84.11139	395.60	-8.19	-27.88	20.26	824	8.9	26.5					
ESS Lab	et al 2019	6_00013	204	Chetema M	Angiosperm	Woody	C3	Woody Ang	Salicaceae	Acer	Acer granatum	10/15/2014	2014	Hendon Lab	42.02897	-84.11139	395.60	-8.19	-27.88	20.26	824	8.9	26.5					
ESS Lab	et al 2019	6_00013	204	Chetema M	Angiosperm	Woody	C3	Woody Ang	Salicaceae	Acer	Acer granatum	10/15/2014	2014	Hendon Lab	42.02897	-84.11139	395.60	-8.19	-27.88	20.26	824	8.9	26.5					
ESS Lab	et al 2019	6_00013	204	Chetema M	Angiosperm	Woody	C3	Woody Ang	Salicaceae	Acer	Acer granatum	10/15/2014	2014	Hendon Lab	42.02897	-84.11139	395.60	-8.19	-27.88	20.26	824	8.9	26.5					
ESS Lab	et al 2019	6_00013	204	Chetema M	Angiosperm	Woody	C3	Woody Ang	Salicaceae	Acer	Acer granatum	10/15/2014	2014	Hendon Lab	42.02897	-84.11139	395.60	-8.19	-27.88	20.26	824	8.9	26.5					
ESS Lab	et al 2019	6_00013	204	Chetema M	Angiosperm	Woody	C3	Woody Ang	Salicaceae	Acer	Acer granatum	10/15/2014	2014	Hendon Lab	42.02897	-84.11139	395.60	-8.19	-27.88	20.26	824	8.9	26.5					
ESS Lab	et al 2019	6_00013	204	Chetema M	Angiosperm	Woody	C3	Woody Ang	Salicaceae	Acer	Acer granatum	10/15/2014	2014	Hendon Lab	42.02897	-84.11139	395.60	-8.19	-27.88	20.26	824	8.9	26.5					
ESS Lab	et al 2019	6_00013	204	Chetema M	Angiosperm	Woody	C3	Woody Ang	Salicaceae	Acer	Acer granatum	10/15/2014	2014	Hendon Lab	42.02897	-84.11139	395.60	-8.19	-27.88	20.26	824	8.9	26.5					
ESS Lab	et al 2019	6_00013	204	Chetema M	Angiosperm	Woody	C3	Woody Ang	Salicaceae	Acer	Acer granatum	10/15/2014	2014	Hendon Lab	42.02897	-84.11139	395.60	-8.19	-27.88	20.26	824	8.9	26.5					
ESS Lab	et al 2019	6_00013	204	Chetema M	Angiosperm	Woody	C3	Woody Ang	Salicaceae	Acer	Acer granatum	10/15/2014	2014	Hendon Lab	42.02897	-84.11139	395.60	-8.19	-27.88	20.26	824	8.9	26.5					
ESS Lab	et al 2019	6_00013	204	Chetema M	Angiosperm	Woody	C3	Woody Ang	Salicaceae	Acer	Acer granatum	10/15/2014	2014	Hendon Lab	42.02897	-84.11139	395.60	-8.19	-27.88	20.26	824	8.9	26.5					
ESS Lab	et al 2019	6_00013	204	Chetema M	Angiosperm	Woody	C3	Woody Ang	Salicaceae	Acer	Acer granatum	10/15/2014	2014	Hendon Lab	42.02897	-84.11139	395.60	-8.19	-27.88	20.26	824	8.9	26.5					
ESS Lab	et al 2019	6_00013	204	Chetema M	Angiosperm	Woody	C3	Woody Ang	Salicaceae	Acer	Acer granatum	10/15/2014	2014	Hendon Lab	42.02897	-84.11139	395.60	-8.19	-27.88	20.26	824	8.9	26.5					
ESS Lab	et al 2019	6_00013	204	Chetema M	Angiosperm	Woody	C3	Woody Ang	Salicaceae	Acer	Acer granatum	10/15/2014	2014	Hendon Lab	42.02897	-84.11139	395.60	-8.19	-27.88	20.26	824	8.9	26.5					
ESS Lab	et al 2019	6_00013	204	Chetema M	Angiosperm	Woody	C3	Woody Ang	Salicaceae	Acer	Acer granatum	10/15/2014	2014	Hendon Lab	42.02897	-84.11139	395.60	-8.19	-27.88	20.26	824	8.9	26.5					
ESS Lab	et al 2019	6_00013	204	Chetema M	Angiosperm	Woody	C3	Woody Ang	Salicaceae	Acer	Acer granatum	10/15/2014	2014	Hendon Lab	42.02897	-84.11139	395.60	-8.19	-27.88	20.26	824	8.9	26.5					
ESS Lab	et al 2019	6_00013	204	Chetema M	Angiosperm	Woody	C3	Woody Ang	Salicaceae	Acer	Acer granatum	10/15/2014	2014	Hendon Lab	42.02897	-84.11139	395.60	-8.19	-27.88	20.26	824	8.9	26.5					
ESS Lab	et al 2019	6_00013	204	Chetema M	Angiosperm	Woody	C3	Woody Ang	Salicaceae	Acer	Acer granatum	10/15/2014	2014	Hendon Lab	42.02897	-84.11139	395.60	-8.19	-27.88	20.26	824	8.9	26.5					
ESS Lab	et al 2019	6_00013	204	Chetema M	Angiosperm	Woody	C3	Woody Ang	Salicaceae	Acer	Acer granatum	10/15/2014	2014	Hendon Lab	42.02897	-84.11139	395.60	-8.19	-27.88	20.26	824	8.9	26.5					
ESS Lab	et al 2019	6_00013	204	Chetema M	Angiosperm	Woody	C3	Woody Ang	Salicaceae	Acer	Acer granatum	10/15/2014	2014	Hendon Lab	42.02897	-84.11139	395.60	-8.19	-27.88	20.26	824	8.9	26.5					
ESS Lab	et al 2019	6_00013	204	Chetema M	Angiosperm	Woody	C3	Woody Ang	Salicaceae	Acer	Acer granatum	10/15/2014	2014	Hendon Lab	42.02897	-84.11139	395.60	-8.19	-27.88	20.26	824	8.9	26.5					
ESS Lab	et al 2019	6_00013	204	Chetema M	Angiosperm	Woody	C3	Woody Ang	Salicaceae	Acer	Acer granatum	10/15/2014	2014	Hendon Lab	42.02897	-84.11139	395.60	-8.19	-27.88	20.26	824	8.9	26.5					
ESS Lab	et al 2019	6_00013	204	Chetema M	Angiosperm	Woody	C3	Woody Ang	Salicaceae	Acer	Acer granatum	10/15/2014	2014	Hendon Lab	42.02897	-84.11139	395.60	-8.19	-27.88	20.26	824	8.9	26.5					
ESS Lab	et al 2019	6_00013	204	Chetema M	Angiosperm	Woody	C3	Woody Ang	Salicaceae	Acer	Acer granatum	10/15/2014	2014	Hendon Lab	42.02897	-84.11139	395.60	-8.19	-27.88	20.26	824	8.9	26.5					
ESS Lab	et al 2019	6_00013	204	Chetema M	Angiosperm	Woody	C3	Woody Ang	Salicaceae	Acer	Acer granatum	10/15/2014	2014	Hendon Lab	42.02897	-84.11139	395.60	-8.19	-27.88	20.26	824	8.9	26.5					
ESS Lab	et al 2019	6_00013	204	Chetema M																								

ESS Lab	et al.	2020	BHTP1982	544	5904	William H B	Gymnosperm	Woody	C3	Woody Gymnosperm	Thujaceae	Thujaceae	Thuja plicata	6/11/1992	1992	Pond Orech	43.1984	-116.3331	311.5	-7.00	-23.71	17.12	475	6.8	27.3	1960	1.07	47.41	51.67	44.30841	
ESS Lab	et al.	2020	MHT0183	399	S.N.	Douglas B	Gymnosperm	Woody	C3	Woody Gymnosperm	Thujaceae	Thujaceae	Thuja occidentalis	July 1833	1830	Trenton Fal	43.2948	-75.19287	284.4	-6.97	-24.90	18.79	958	6.8	27.4	247	1.42	48.81	39.92	34.2529437	
ESS Lab	et al.	2020	BHTP1951	543	5558	H A Stern	Gymnosperm	Woody	C3	Woody Gymnosperm	Thujaceae	Thujaceae	Thuja plicata	9/16/1951	1951	Volney L	49.9144	-116.7792	311.1	-6.99	-25.84	19.35	1662	8.5	27.4	502	0.89	41.80	54.86	47.03371	
ESS Lab	et al.	2020	BHTP1951	543	5558	Hess, Leidi	Gymnosperm	Woody	C3	Woody Gymnosperm	Thujaceae	Thujaceae	Thuja occidentalis	7/15/1959	1959	Waco Co	44.5072	-99.07194	369.7	-6.08	-25.45	17.84	1189	8.0	27.4	51	1.34	48.93	45.88	38.942023	
ESS Lab	et al.	2020	YUT01005	358	S.N.	O W Knight	Gymnosperm	Woody	C3	Woody Gymnosperm	Thujaceae	Thujaceae	Thuja occidentalis	5/10/1905	1900	Onno, Man	44.87782	-68.68756	297.6	-6.83	-24.35	17.86	799	5.6	27.4	38	1.20	45.48	44.20	37.9	
ESS Lab	et al.	2020	FMP31936	338	31444	Diga Kluge	Gymnosperm	Woody	C3	Woody Gymnosperm	Pinaceae	Pinaceae	Pinus strobus	6/23/1936	1936	DuLac, Minn	45.7797	-92.19303	308.8	-6.94	-25.4	19.46	811	2.6	27.4	409	1.49	45.31	35.46	30.494	
ESS Lab	et al.	2020	AAT02017	617	91a	Rebekah S	Gymnosperm	Woody	C3	Woody Gymnosperm	Thujaceae	Thujaceae	Thuja occidentalis	9/30/2017	2017	Ann Arbor	42.289	-83.74804	405.24	-8.55	-25.57	17.47	849	9.4	27.4	242	1.48	47.43	37.53	32.1444283	
ESS Lab	et al.	2020	AAT02017	619	91a	Rebekah S	Gymnosperm	Woody	C3	Woody Gymnosperm	Thujaceae	Thujaceae	Thuja occidentalis	9/30/2017	2017	Ann Arbor	42.288	-83.73841	405.24	-8.55	-25.67	17.57	849	9.4	27.4	288	1.41	48.07	40.17	34.4488403	
ESS Lab	et al.	2020	WA_GBP17	716	91a	Rebekah S	Gymnosperm	Woody	C3	Woody Gymnosperm	Thujaceae	Thujaceae	Thuja plicata	5/14/2018	2018	Wallace R	47.86039	-121.6721	411.3	-8.67	-27.86	19.74	2076	11.4	27.4	101.5	1.39	48.89	41.02	35.17266	
ESS Lab	et al.	2020	WA_GBP17	718	91a	Rebekah S	Gymnosperm	Woody	C3	Woody Gymnosperm	Thujaceae	Thujaceae	Thuja plicata	5/14/2018	2018	Wallace R	47.86565	-121.6719	411.3	-8.67	-28.02	19.74	2076	11.4	27.4	103.6	1.23	50.05	48.31	41.22276	
ESS Lab	et al.	2020	WA_GBP17	717	91a	Rebekah S	Gymnosperm	Woody	C3	Woody Gymnosperm	Thujaceae	Thujaceae	Thuja plicata	5/14/2018	2018	Wallace R	47.87772	-121.6704	411.3	-8.67	-30.16	22.15	2076	11.4	27.4	86.97	0.96	47.16	59.72	51.20833	
ESS Lab	et al.	2020	FMP31956	296	31759	Brian T H	Gymnosperm	Woody	C3	Woody Gymnosperm	Pinaceae	Pinaceae	Pinus strobus	5/15/1985	1985	Lelandia C	44.87088	-85.88836	344.7	-7.50	-25.40	24.36	1130	7.7	27.4	242	1.26	49.21	38.79	37.48825	
ESS Lab	et al.	2020	MHT0192	217	13880	E G Voss	Gymnosperm	Woody	C3	Woody Gymnosperm	Thujaceae	Thujaceae	Thuja occidentalis	7/14/1972	1972	Madison	45.1500	-83.3300	328.04	-7.35	-22.32	15.60	789	5.3	27.5000	215.0000	1.38	49.69	42.61	36.58767	
ESS Lab	et al.	2020	MST0104	417	4715	Pepon	Gymnosperm	Woody	C3	Woody Gymnosperm	Thujaceae	Thujaceae	Thuja occidentalis	8/11/1974	1974	Cass Conn	41.92541	-85.72841	287.2	-6.83	-25.98	17.66	846	7.5	27.4	207	0.77	44.11	66.81	47.97	36.88279
ESS Lab	et al.	2020	WA_CBPT7	714	91a	Rebekah S	Gymnosperm	Woody	C3	Woody Gymnosperm	Thujaceae	Thujaceae	Thuja plicata	5/14/2018	2018	Colton Ben	47.50373	-122.22018	411.3	-8.67	-28.13	20.02	1080	13.0	27.5	12.8	1.32	48.01	42.42	36.37121	
ESS Lab	et al.	2020	WA_CBPT7	715	91a	Rebekah S	Gymnosperm	Woody	C3	Woody Gymnosperm	Thujaceae	Thujaceae	Thuja plicata	5/14/2018	2018	Colton Ben	47.50373	-122.22017	411.3	-8.67	-28.65	20.02	1080	13.0	27.5	16.8	1.46	50.85	40.58	34.79452	
ESS Lab	et al.	2020	YUT01897	347	958	W.B.	Gymnosperm	Woody	C3	Woody Gymnosperm	Thujaceae	Thujaceae	Thuja occidentalis	1900/1905	1900	New Haven	41.31377	-72.9212	297.6	-6.83	-23.41	16.97	917	10.7	27.4	10	1.58	47.47	34.74	39.7911924	
ESS Lab	et al.	2020	YUPS1990	373	950	Anna E Cal	Gymnosperm	Woody	C3	Woody Gymnosperm	Pinaceae	Pinaceae	Pinus strobus	8/25/1990	1890	Greenfield	42.41375	-74.92297	284.2	-6.76	-26.40	17.01	867	7.4	27.6	215	1.36	46.54	39.14	34.22056	
ESS Lab	et al.	2020	M_SGT023	887	70a	Adleya Har	Gymnosperm	Woody	C3	Woody Gymnosperm	Thujaceae	Thujaceae	Thuja occidentalis	8/19/2018	2018	Seney, Mich	46.346	-85.4407	407.1	-8.42	-28.96	21.14	1223	5.6	27.6	233.5	1.41	49.81	41.21	35.32624	
ESS Lab	et al.	2020	YUT01999	352	2270	Ernie F W	Gymnosperm	Woody	C3	Woody Gymnosperm	Thujaceae	Thujaceae	Thuja occidentalis	4/9/1999	1899	Madison	42.4503	-71.19138	295.6	-6.68	-22.61	16.30	1005	9.4	27.6	51	1.34	47.73	41.54	36.6164029	
ESS Lab	et al.	2020	OR_GCTP1	754	91a	Rebekah S	Gymnosperm	Woody	C3	Woody Gymnosperm	Thujaceae	Thujaceae	Thuja plicata	5/17/2018	2018	Galles Ore	45.54023	-123.3656	411.3	-8.67	-26.18	17.98	1335	12.1	27.6	354.2	1.30	48.95	43.91	37.65885	
ESS Lab	et al.	2020	YUT01958	366	2296	John Zhang	Gymnosperm	Woody	C3	Woody Gymnosperm	Thujaceae	Thujaceae	Thuja occidentalis	6/24/1958	1958	New Haven	41.1429	-72.9383	317.24	-7.02	-25.36	18.82	1461	8.7	27.7	17	0.86	47.35	44.14	35	
ESS Lab	et al.	2020	MM16-38	n/a	n/a	Molly Ng	Gymnosperm	Woody	C3	Woody Gymnosperm	Taxodiaceae	Taxodiaceae	Taxodium distichum	8/26/2016	2016	Daves Ariz	39.97487	-82.4236	402.24	-8.42	-28.01	20.16	1037	10.4	27.7						
ESS Lab	et al.	2020	MM16-35	n/a	n/a	Molly Ng	Gymnosperm	Woody	C3	Woody Gymnosperm	Taxodiaceae	Taxodiaceae	Taxodium distichum	8/26/2016	2016	Daves Ariz	40.21983	-82.4219	402.24	-8.42	-28.31	20.16	1037	10.4	27.7						
ESS Lab	et al.	2020	MM16-37	n/a	n/a	Molly Ng	Gymnosperm	Woody	C3	Woody Gymnosperm	Taxodiaceae	Taxodiaceae	Taxodium distichum	8/26/2016	2016	Daves Ariz	39.97929	-82.42113	402.24	-8.42	-28.61	20.17	1037	10.4	27.7						
ESS Lab	et al.	2020	SWT02017	700	91a	Rebekah S	Gymnosperm	Woody	C3	Woody Gymnosperm	Thujaceae	Thujaceae	Thuja occidentalis	9/24/2017	2017	Pinecky, Mich	42.4068	-83.56431	401.01	-8.42	-26.02	18.07	794	8.8	27.7	275.8	1.89	49.46	30.52	26.1693127	
ESS Lab	et al.	2020	SWT02017	699	91a	Rebekah S	Gymnosperm	Woody	C3	Woody Gymnosperm	Thujaceae	Thujaceae	Thuja occidentalis	9/24/2017	2017	Pinecky, Mich	42.42087	-83.56568	401.01	-8.42	-26.17	18.23	794	8.8	27.7	287.4	1.87	50.21	31.18	30.620738	
ESS Lab	et al.	2020	SWT02017	698	91a	Rebekah S	Gymnosperm	Woody	C3	Woody Gymnosperm	Thujaceae	Thujaceae	Thuja occidentalis	9/24/2017	2017	Pinecky, Mich	42.28154	-83.52907	405.90	-8.39	-28.34	18.47	794	8.8	27.7	287.4	1.79	51.63	34.41	29.62968	
ESS Lab	et al.	2020	SWT02017	697	91a	Rebekah S	Gymnosperm	Woody	C3	Woody Gymnosperm	Thujaceae	Thujaceae	Thuja occidentalis	9/24/2017	2017	Pinecky, Mich	42.40638	-83.94191	401.01	-8.42	-26.71	18.20	794	8.8	27.7	281.94	1.80	50.77	32.18	31.66660	
ESS Lab	et al.	2020	SWT02017	698	91a	Rebekah S	Gymnosperm	Woody	C3	Woody Gymnosperm	Thujaceae	Thujaceae	Thuja occidentalis	9/24/2017	2017	Pinecky, Mich	42.40647	-83.94097	401.01	-8.42	-27.21	19.32	794	8.8	27.7	277.7	1.72	50.21	34.04	26.180607	
ESS Lab	et al.	2020	WA_TFTR3	704	91a	Rebekah S	Gymnosperm	Woody	C3	Woody Gymnosperm	Thujaceae	Thujaceae	Thuja plicata	10/22/2017	2017	Twin Falls	47.45183	-121.7039	401.5	-8.39	-28.44	21.63	2144	11.2	27.7	201.5	1.16	50.52	50.79	43.55172	
ESS Lab	et al.	2020	WA_TFTR3	703	91a	Rebekah S	Gymnosperm	Woody	C3	Woody Gymnosperm	Thujaceae	Thujaceae	Thuja plicata	10/22/2017	2017	Twin Falls	47.44547	-121.6991	401.5	-8.39	-29.05	21.82	2144	11.2	27.7	287	1.27	49.44	45.40	38.82913	
ESS Lab	et al.	2020	WA_TFTR3	702	91a	Rebekah S	Gymnosperm	Woody	C3	Woody Gymnosperm	Thujaceae	Thujaceae	Thuja plicata	10/22/2017	2017	Twin Falls	47.45495	-121.7039	401.5	-8.39	-29.05	21.82	2144	11.2	27.7	201.5	1.45	50.42	49.23	44.8885	
ESS Lab	et al.	2020	M_SWT01	910	n/a	Rebekah S	Gymnosperm	Woody	C3	Woody Gymnosperm	Thujaceae	Thujaceae	Thuja occidentalis	10/13/2018	2018	Stoughton	42.28154	-83.72907	405.90	-8.39	-29.84	22.14	794	8.8	27.7		0.98	50.05	60.31	31.71420	
ESS Lab	et al.	2020	M_SWT01	914	n/a	Rebekah S	Gymnosperm	Woody	C3	Woody Gymnosperm	Thujaceae	Thujaceae	Thuja occidentalis	10/13/2018	2018	Stoughton	42.28154	-83.72907	405.90	-8.39	-30.11	22.14	794	8.8	27.7		0.98	49.48	53.43	45.81481	
ESS Lab	et al.	2020	WA_TMTF3	703	91a	Rebekah S	Gymnosperm	Woody	C3	Woody Gymnosperm	Thujaceae	Thujaceae	Thuja plicata	10/22/2017	2017	Twin Falls	47.44523	-121.9794	401.5	-8.39	-30.28	22.96	2189	10.9	27.7	180.1	1.47	48.58	38.54	33.6761905	
ESS Lab	et al.	2020	YUPS1946	364	25335	Leslie J M	Gymnosperm	Woody	C3	Woody Gymnosperm	Pinaceae	Pinaceae	Pinus strobus	3/6/1946	1946	Canaan, Conn	41.9622	-73.29989	345.28	-7.81	-26.49	21.33	1239	8.3	27.7	243	1.46	51.54	40.34	34.8906	
ESS Lab	et al.	2020	CO_OTP2	843	n/a	Rebekah S	Angiosperm	Woody	C3	Woody Angiosperm	Salicaceae	Salicaceae	Populus tremuloides	8/4/2018	2018	Everson	39.95204	-105.203	407.1	-8.42	-27.25	19.36	951	8.8	27.8	228.3	2.64	49.89	22.03	18.89394	
ESS Lab	et al.																														

ESS Lab	etal.2020	MPHT194	240	31350	James F S	Gymnosper	Woody	C3	Woody Gy	Conifer	Thuja	Thuja plicata	7/9/1994	1994	Prist Lake	48.5704	-116.8227	393.50	-7.84	-25.78	18.42	696	6.9	29.4000	884.0000	0.62	51.32	96.53	82.77419
ESS Lab	etal.2020	MPHT193	171	32710	Sam	Gymnosper	Woody	C3	Woody Gy	Conifer	Thuja	Thuja occidentalis	7/20/1993	1993	Kenosis Cr	42.2577	-87.8396	311.9	-7.90	-25.10	18.35	841	9.8	28.4	190	1.61	48.00	34.77	31.93689
ESS Lab	etal.2020	MPHT192	310	32528	Ronald S	Gymnosper	Woody	C3	Woody Gy	Conifer	Thuja	Thuja occidentalis	4/21/1993	1993	Worm	41.2611	-86.9611	311.0	-7.92	-25.10	18.35	730	10.1	29.199	7.98	1.61	92.73	36.74	31.93689
ESS Lab	etal.2020	MPHT195	174	34340	Faye	Gymnosper	Woody	C3	Woody Gy	Conifer	Thuja	Thuja occidentalis	7/12/1995	1995	Green Rap	42.96	-85.66	294.4	-6.80	-23.72	17.93	616	6.4	28.5	63.7	1.42	43.90	44.42	38.08834
ESS Lab	etal.2020	CUBRT200	687	34428	Hogan & Te	Gymnosper	Woody	C3	Woody Ang	Salicaceae	Populus	Populus tremuloides	8/8/2004	2004	Black Canyon	38.57078	-107.7364	379.50	-8.29	-27.70	19.86	421	8.3	29.5	2929.8	2.16	52.10	28.45	24.38161
ESS Lab	etal.2020	YUPS1988	395	36147	K. D. Parde	Gymnosper	Woody	C3	Woody Gy	Conifer	Pinus	Pinus strobus	7/16/1988	1988	Rodding Cr	41.3138	-73.3936	352.38	-7.77	-27.72	20.26	1039	6.5	29.5	168	1.60	50.00	36.49	31.28785
ESS Lab	etal.2020	MPHT192	180	32100	N. Lyon Jr.	Gymnosper	Woody	C3	Woody Gy	Conifer	Thuja	Thuja occidentalis	8/18/1920	1920	Merrill Cr	41.3262	-85.7442	305.4	-6.91	-25.34	18.91	992	13.9	29.5	258	0.70	51.84	37.14	7.2662
ESS Lab	etal.2020	C-PHT019	607	445097	Myron Fu	Gymnosper	Woody	C3	Woody Gy	Conifer	Platycladus	Platycladus orientalis	7/25/1970	1970	M. Kuehn	45.5864	-138.3001	326.4	-7.29	-27.25	20.20	1055	8.6	29.5	73.0	1.54	46.32	80.40	30.02974
ESS Lab	etal.2020	MA AMP17	913	na	Rebekah S	Gymnosper	Woody	C3	Woody Gy	Conifer	Thuja	Thuja occidentalis	10/26/2018	2018	Burns Park	42.26516	-83.72999	405.99	-8.36	-25.79	17.89	945	10.0	29.6	1.69	51.13	35.49	30.43452	
ESS Lab	etal.2020	WA_COT1P	743	na	Rebekah S	Gymnosper	Woody	C3	Woody Gy	Conifer	Thuja	Thuja plicata	5/15/2018	2018	Cedar Cr	49.53888	-114.6758	411.3	-8.67	-27.53	19.39	826	7.2	29.6	1105.8	0.89	48.55	62.06	30.38322
ESS Lab	etal.2020	WA_COT2P	742	na	Rebekah S	Gymnosper	Woody	C3	Woody Gy	Conifer	Thuja	Thuja plicata	5/15/2018	2018	Cedar Cr	49.53888	-114.6758	411.3	-8.67	-28.18	20.07	826	7.2	29.6	1105.8	0.93	47.85	60.00	51.65161
ESS Lab	etal.2020	WA_LIT2P	741	na	Rebekah S	Gymnosper	Woody	C3	Woody Gy	Conifer	Thuja	Thuja plicata	5/15/2018	2018	Cedar Cr	49.53888	-114.6758	411.3	-8.67	-28.90	20.83	826	7.2	29.6	1119.2	0.68	48.69	83.50	71.88294
ESS Lab	etal.2020	MPHT190	173	31133	Frank C G	Gymnosper	Woody	C3	Woody Gy	Conifer	Thuja	Thuja occidentalis	3/23/1990	1990	M. Hope Cr	40.1011	-88.2286	298.5	-6.84	-24.22	17.81	1038	10.2	29.231	1.59	43.07	39.04	33.4795	
ESS Lab	etal.2020	CO_GF1P2	823	na	Rebekah S	Gymnosper	Woody	C3	Woody Ang	Salicaceae	Populus	Populus tremuloides	8/20/2018	2018	Boisler Cr	49.99488	-105.3062	407.1	-8.42	-27.17	19.27	994	11.1	29.7	2062.4	2.90	49.19	19.76	36.04828
ESS Lab	etal.2020	CO_GF1P2	827	na	Rebekah S	Gymnosper	Woody	C3	Woody Ang	Salicaceae	Populus	Populus tremuloides	8/20/2018	2018	Boisler Cr	49.99488	-105.3062	407.1	-8.42	-27.60	18.73	994	11.1	29.7	2062.4	2.30	49.22	25.31	21.70435
ESS Lab	etal.2020	MPHT193	307	32515	F. J. Hermal	Gymnosper	Woody	C3	Woody Gy	Conifer	Thuja	Thuja occidentalis	9/21/1993	1993	Madison Cr	45.9205	-88.6886	310.3	-6.99	-26.01	19.58	958	9.1	29.8	2864.0	1.31	51.25	45.77	30.24521
ESS Lab	etal.2020	BHTP1914	531	34395	W C Curtis	Gymnosper	Woody	C3	Woody Gy	Conifer	Thuja	Thuja plicata	7/20/1914	1914	Douglas Cr	54.31284	-123.2034	301.1	-8.87	-26.42	20.08	1146	11.9	29.8	216.0	0.96	47.23	97.47	49.19792
ESS Lab	etal.2020	MPHT193	307	32515	F. J. Hermal	Gymnosper	Woody	C3	Woody Gy	Conifer	Thuja	Thuja occidentalis	7/19/1993	1993	Madison Cr	45.9205	-88.7536	307.2	-6.97	-24.54	18.05	958	9.1	29.8	196	1.66	52.38	38.95	31.654180
ESS Lab	etal.2020	MPHT194	196	321483	H. H. Hart	Gymnosper	Woody	C3	Woody Gy	Conifer	Thuja	Thuja occidentalis	7/13/1948	1948	Westerlo Cr	42.1800	-84.3000	310.1	-6.98	-24.54	18.00	968	10.9	29.8	216.0	0.96	47.23	97.47	49.19792
ESS Lab	etal.2020	FMP51935	337	37180	Hermann	Gymnosper	Woody	C3	Woody Gy	Conifer	Pinus	Pinus strobus	5/9/1935	1935	Laure Lake	43.96304	-84.94716	309.4	-6.98	-25.70	19.31	1101	6.4	29.9	34.1	1.50	46.54	36.16	31.92667
ESS Lab	etal.2020	OR_MFT1P	748	na	Rebekah S	Gymnosper	Woody	C3	Woody Gy	Conifer	Thuja	Thuja plicata	5/17/2018	2018	Madison Cr	45.57719	-122.1188	411.3	-8.67	-25.13	18.69	1786	12.9	29.9	262	1.10	47.87	50.75	43.51818
ESS Lab	etal.2020	OR_TCTP1	750	na	Rebekah S	Gymnosper	Woody	C3	Woody Gy	Conifer	Thuja	Thuja plicata	5/17/2018	2018	Toke Cr	45.3982	-122.9213	411.3	-8.67	-26.47	18.29	1469	12.7	29.9	230.7	1.79	48.99	31.70	27.38872
ESS Lab	etal.2020	OR_MFT1P	747	na	Rebekah S	Gymnosper	Woody	C3	Woody Gy	Conifer	Thuja	Thuja plicata	5/17/2018	2018	Madison Cr	45.578	-122.1172	411.3	-8.67	-27.13	18.97	1786	12.9	29.9	9.1	1.82	49.41	33.50	28.72674
ESS Lab	etal.2020	OR_MFT1P	746	na	Rebekah S	Gymnosper	Woody	C3	Woody Gy	Conifer	Thuja	Thuja plicata	5/17/2018	2018	Madison Cr	45.5788	-122.1172	411.3	-8.67	-27.26	19.11	1786	12.9	29.9	9.1	1.83	49.21	61.4	39.28616
ESS Lab	etal.2020	OR_TCTP1	749	na	Rebekah S	Gymnosper	Woody	C3	Woody Gy	Conifer	Thuja	Thuja plicata	5/17/2018	2018	Toke Cr	45.3989	-122.9217	411.3	-8.67	-29.38	21.34	1469	12.7	29.9	226.6	1.41	48.63	40.22	34.48936
ESS Lab	etal.2020	MA_AAT2O	408	31100	Peiking	Gymnosper	Woody	C3	Woody Gy	Conifer	Thuja	Thuja occidentalis	3/9/2017	2017	Am Arbor	42.27545	-83.74783	407.06	-8.62	-26.22	18.07	849	9.4	30.256	0.66	46.26	81.74	70.00909	
ESS Lab	etal.2020	MA_EMP17	750	na	Rebekah S	Gymnosper	Woody	C3	Woody Ang	Salicaceae	Populus	Populus tremuloides	7/20/2018	2018	El Malpais Cr	34.98867	-108.052	408.8	-8.54	-23.08	15.48	259	10.1	30.216	1.1	50.46	27.89	31.4468	
ESS Lab	etal.2020	MA_EMP17	750	na	Rebekah S	Gymnosper	Woody	C3	Woody Ang	Salicaceae	Populus	Populus tremuloides	7/20/2018	2018	El Malpais Cr	34.98867	-108.052	408.8	-8.54	-23.08	15.48	259	10.1	30.216	1.1	50.46	27.89	31.4468	
ESS Lab	etal.2020	MA_EMP17	750	na	Rebekah S	Gymnosper	Woody	C3	Woody Ang	Salicaceae	Populus	Populus tremuloides	7/20/2018	2018	El Malpais Cr	34.98867	-108.052	408.8	-8.54	-26.33	17.27	259	10.1	30.217	1.92	49.39	30.24	25.92220	
ESS Lab	etal.2020	MA_AAT2O	407	35513	Voss	Gymnosper	Woody	C3	Woody Gy	Conifer	Thuja	Thuja occidentalis	3/9/2017	2017	Am Arbor	42.27649	-83.74772	407.06	-8.62	-25.53	17.35	849	9.4	30.258	0.77	45.31	68.82	88.841658	
ESS Lab	etal.2020	MPHT193A	250	35307	Wilfred Nat	Gymnosper	Woody	C3	Woody Gy	Conifer	Pinus	Pinus strobus	5/25/1993	1993	Grand Rap	42.92276	-85.65186	294.6	-6.79	-24.04	17.67	691	7.7	30.123	1.62	50.01	30.00	30.87037	
ESS Lab	etal.2020	MPHT193B	251	35309	Wilfred Nat	Gymnosper	Woody	C3	Woody Gy	Conifer	Pinus	Pinus strobus	6/19/1993	1993	Grand Rap	42.92276	-85.65186	294.6	-6.79	-25.70	19.40	691	7.7	30.123	1.83	49.98	25.02	21.40564	
ESS Lab	etal.2020	MPHT193C	289	35309	Chase	Gymnosper	Woody	C3	Woody Gy	Conifer	Pinus	Pinus strobus	4/13/1993	1993	Concession Cr	42.2343	-87.19176	307.2	-6.92	-27.08	20.70	538	9.4	30.2	304.0	0.96	46.02	29.25	22.105
ESS Lab	etal.2020	YUPS1989	378	31100	John K S	Gymnosper	Woody	C3	Woody Gy	Conifer	Pinus	Pinus strobus	12/28/1989	1989	Johnson Cr	39.79292	-77.01064	294.4	-6.78	-26.48	20.23	825	10.4	30.188	0.98	47.40	50.02	48.0482	
ESS Lab	etal.2020	MPHT193	310	32528	M. New	Gymnosper	Woody	C3	Woody Gy	Conifer	Thuja	Thuja occidentalis	7/21/1993	1993	Madison Cr	45.9207	-88.7805	309.6	-7.59	-25.13	17.88	769	12.9	30.257	0.88	49.03	28.88	34.92689	
ESS Lab	etal.2020	C-PHT1919	819	316369	Myron Fu	Gymnosper	Woody	C3	Woody Gy	Conifer	Thuja	Thuja standishii	8/31/1989	1989	Segetage	39.9501	-130.85949	337.6	-7.47	-24.30	17.34	1337	10.9	30.218	1.06	50.85	97.66	40.69841	
ESS Lab	etal.2020	YTO1982	367	31815	David D T	Gymnosper	Woody	C3	Woody Gy	Conifer	Thuja	Thuja plicata	7/14/1982	1982	Madison Cr	45.70854	-84.79225	342.06	-7.67	-25.50	16.32	1333	10.0	30.4	313	1.70	46.85	42.12	37.60880
ESS Lab	etal.2020	OR_TYCP1	737	na	Rebekah S	Gymnosper	Woody	C3	Woody Gy	Conifer	Thuja	Thuja plicata	5/17/2018	2018	Tyone Cr	44.54155	-122.6787	411.3	-8.67	-28.17	20.05	1188	13.7	30.4	86.6	1.28	50.90	31.70	40.36883
ESS Lab	etal.2020	WA_SVTP1	745	na	Rebekah S	Gymnosper	Woody	C3	Woody Gy	Conifer	Thuja	Thuja plicata	5/16/2018	2018	Columbia Cr	45.68444	-121.8813	411.3	-8.67	-28.76	20.08	1873	12.3	30.4	281.1	1.84	49.38	31.30	26.8396
ESS Lab	etal.2020	OR_TYCP1	734	na	Rebekah S	Gymnosper	Woody	C3	Woody Gy	Conifer	Thuja	Thuja plicata	5/17/2018	2018															

Legend

A Ehleringer DM, Steele LP, Langensfeldt RL, Franco RJ, Barnola JM, Mogan VI. Historical CO₂ records from the Law Dome DE08, DE08-2, and DSS ice cores. *Trends: a compendium of data on global change*, 351-364 (1998).

B Keeling CD, Piper SC, Bacastow RB, Wharfen M, Whorf TP, Heimann M, Meier HA, Terrestrial Biosphere and Oceans from 1978 to 2000: Observations and carbon cycle implications. In *A history of atmospheric CO₂ and its effects on plants, animals, and ecosystems* (pp. 83-113). Springer, New York, NY (2005).

C Keeling CD, Piper SC, Bacastow RB, Wharfen M, Whorf TP, Heimann M, Meier HA, Terrestrial Biosphere and Oceans from 1978 to 2000: Observations and Carbon Cycle Implications.

D Eggleston S, Schmidt J, Borer B, Schneider R, Fischer H. Evolution of the stable carbon isotope composition of atmospheric CO₂ over the last glacial cycle. *Paleoecology*, 31(3), 434-452 (2016).

E Röhrling M, Ehleringer DM, Truesdel CM, Allison CE, Battie MC, Langensfeldt RL, Jenk TM. A revised 1000 year atmospheric δ¹³C CO₂ record from Law Dome and South Pole, Antarctica. *Journal of Geophysical Research: Atmospheres*, 116(15), 8462-8469 (2011).

F Dielenford AF, Muller KE, Wang SL, Koch PL, Freeman KH. Global patterns in leaf δ¹³C discrimination and implications for studies of past and future climate. *Proceedings of the National Academy of Sciences*, 107(13), 5736-5743 (2010).

G US data from PRISM Climate Group, Oregon State University. <http://prism.oregonstate.edu>, created 4 Feb 2004.

n/a Auras JL, Reynolds MP, Acevedo E. Leaf posture, grain yield, growth, leaf structure, and carbon isotope discrimination in wheat. *Crop Science*, 33(6), 1273-1279 (1993).

n/a Arens NC, Jahren AH. Carbon isotope excursion in atmospheric CO₂ at the Cretaceous-Tertiary boundary: evidence from terrestrial sediments. *Palaios*, 15(4), 314-322 (2000).

n/a Bai E, Boutton T, Liu F, Wu X, Archer S. Variation in woody plant δ¹³C along a topographic gradient in a subtropical savanna parkland. *Oecologia*, 156:479-489 (2008).

n/a Beering DJ. Seasonal responses of resilient leaves to CO₂ enrichment. *Annals of Botany*, 75(5), 507-511 (1995).

n/a Beering DJ. δ¹³C discrimination by fossil leaves during the late-glacial climate oscillation 12-10 ka BP: measurements and physiological controls. *Oecologia*, 108(1), 29-37 (1996).

n/a Bonal D, Sabatier D, Montpied P, Treneauux D, Guehl JM. Interspecific variability of δ¹³C among trees in rainforests of French Guiana: functional groups and canopy integration. *Oecologia*, 124:454-468 (2000).

n/a Brooks JR, Flanagan LB, Buchmann N, Ehleringer JR. Carbon isotope composition of boreal plants: functional grouping of life forms. *Oecologia*, 110:301-311 (1997).

n/a Broadbent MSJ, Griffiths H, Maxwell C, Bortland AM. The carbon isotope ratio of plant organic material reflects temporal and spatial variations in CO₂ within tropical forest formations in Trinidad. *Oecologia*, 89(3), 435-441 (1992).

n/a Burt J, Wilson KL. Towards a comprehensive survey of C3 and C4 photosynthetic pathways in Cyperaceae. *Ancient Plants: A Journal of Systematic and Evolutionary Botany*, 23(1), 56-148 (2007).

n/a Buchmann N, Guehl JM, Batgah TS, Ehleringer JR. Interseasonal comparison of CO₂ concentrations, isotopic composition, and carbon dynamics in an Amazonian rainforest (French Guiana). *Oecologia*, 110:120-131 (1997).

n/a Chevillat VS, Siegwolf RTW, Pejin S, Körner C. Tissue-specific variation of δ¹³C in mature canopy trees in a temperate forest in central Europe. *Basic Appl Ecol* 6:519-534 (2005).

n/a Collater JW, Reley G, Stern B, Ehlgron G, Fry B. Compound-specific δ¹³C analyses of leaf lipids from plants with differing carbon dioxide metabolisms. *Org Geochem* 21:619-627 (1994).

n/a Condon AG, Richards RA, Farquhar GD. Relationships between carbon isotope discrimination, water use efficiency and transpiration efficiency for dryland wheat. *Australian Journal of Agricultural Research*, 44(8), 1653-1711 (1993).

n/a Dawson TE, Ehleringer JR. Isotopic enrichment of water in the "woody" tissues of plants: implications for plant water source, water uptake, and other studies which use the stable isotopic composition of cellulose. *Geochimica et Cosmochimica Acta*, 57(14), 3487-3492 (1993).

n/a De Lillis M, Matteucci G, Valentini R. Carbon assimilation, nitrogen, and photochemical efficiency of different Himalayan tree species along an altitudinal gradient. *Photosynthesis* 42:597-605 (2004).

n/a DeLucia EH, Schlesinger WH. Resource-use efficiency and drought tolerance in adjacent Great Basin and Sierran plants. *Ecology* 72:51-58 (1991).

n/a Dode MB, Luennhoff WK, Welker JM. Differential water resource use by herbaceous and woody plant life-forms in a shrubgrass steppe community. *Oecologia*, 117:504-512 (1998).

n/a Donawick JA, Ehleringer JR. Ecophysiological differences among desert plants of several woody species. *Oecologia*, 86:594-597 (1991).

n/a Durgal JAJ, Docherty G, Straker V, Ewershaw P. Interspecific variation in bulk tissue, fatty acid and monosaccharide δ¹³C values of leaves from a mesotrophic grassland plant community. *Phytochemistry* 69:2041-2051 (2008).

n/a Dupouey JL, Levail S, Chouane E, Jourdain S. Modelling carbon isotope fractionation in tree rings based on effective evapotranspiration and soil water status. *Plant, Cell & Environment*, 16(8), 939-947 (1993).

n/a Ehleringer JR, Cerling TE. Atmospheric CO₂ and the ratio of intercellular to ambient CO₂ concentrations in plants. *Tree physiology*, 15(2), 105-111 (1995).

n/a Ehleringer JR, Lin ZF, Field CB, San GO, Xiao YQ. Leaf carbon isotope ratios of plants from a subtropical monsoon forest. *Oecologia*, 72:108-114 (1987).

n/a Ehleringer JR, Phillips SL, Schuster WS, Sandquist DR. Differential utilization of summer rains by desert plants. *Oecologia*, 88(3), 430-434 (1991).

n/a Ehleringer JR, Phillips SL, Comstock JP. Seasonal variation in the carbon isotope composition of desert plants. *Funct Ecol* 6:396-404 (1992).

n/a Ehleringer JR, Hall AE, Farquhar GD (Eds.). Stable isotopes and plant carbon-water relations (Vol. 109129). San Diego: Academic Press (1993).

n/a Escudero A, Medavilla S, Hellmeier H. Leaf longevity and drought: avoidance of the costs and risks of early leaf abscission as inferred from the leaf carbon isotopic composition. *Funct Plant Biol* 35:705-713 (2008).

n/a Franco RJ, Duarte HM, Gajjar A, de Matos EA, Nairn M, Renssenberg H, Lüttge U. In situ measurements of carbon and nitrogen distribution and composition, photochemical efficiency and stable isotope ratios in *Alnus incana angustifolia*. *Trees*, 19(4), 422-430 (2005).

n/a Friend AD, Woodward FI, Switzer VR. Field measurements of photosynthesis, stomatal conductance, leaf nitrogen and δ¹³C along altitudinal gradients in Scotland. *Functional Ecology*, 11:172 (1989).

n/a Garten CT, Taylor GE, Foliar δ¹³C within a temperate deciduous forest: spatial, temporal, and species sources of variation. *Oecologia* 90:1-7 (1992).

n/a Gerd R, Bucum P, Marchesini R, Bragazza L. Water- and nutrient-use efficiency of a deciduous species, *Vaccinium myrtillus*, and an evergreen species, *V. vitis-idaea*, in a subalpine dwarf shrub heath in the southern Alps. *Italy, Oikos* 88:19-32 (2000).

n/a Gutierrez MV, Meinzer FC. Carbon isotope discrimination and photosynthetic gas exchange in coffee hedgerows during canopy development. *Functional Plant Biology*, 21(2), 207-219 (1994).

n/a Guy RD, Reid DM. Photosynthesis and the influence of CO₂ enrichment on δ¹³C values in a C3 halophyte. *Plant, Cell & Environment*, 9(11), 65-72 (1986).

n/a Hall AE, Richards RA, Condon AG, Wright GC, Farquhar GD. Carbon isotope discrimination and plant breeding. *Plant breeding reviews*, 12(81), 113 (1984).

n/a Hansen D, Siegel I. Comparison of water use efficiency and internal leaf carbon dioxide concentration in juvenile leaves and phylloides of *Acacia koa* (leguminosae) from Hawaii, estimated by two methods. *American Journal of Botany*, 80(10), 1121-1125 (1993).

n/a He CX, Li JY, Zhou P, Guo M, Zheng Q-S. Changes of leaf morphological, anatomical structure and carbon isotope ratio with the height of the Wanglan Tree (*Parashorea chinensis*) in Xiuhuangbanna, China. *Journal of Integrative Plant Biology* 50:168-173 (2008).

n/a Hemming D, Yarek D, Amba P, Auer M, Bessan C, Black K, Gross P. Pan European δ¹³C values of air and organic matter from forest ecosystems. *Global Change Biology*, 11(7), 1065-1093 (2005).

n/a Holtum AM, Wierke K. Carbon isotope composition of canopy leaves in a tropical forest in Panama throughout a seasonal cycle. *Trees Struct Funct* 19:545-551 (2005).

n/a Hux R, Ferhi A, Guehl JM. Pioneer and late stage tropical rainforest tree species (French Guiana) growing under common conditions differ in leaf gas exchange regulation, carbon isotope discrimination and leaf water potential. *Oecologia*, 99(3-4), 297-305 (1994).

n/a Hutchie KR, Marshall JD. Altitude trends in conifer leaf morphology and stable carbon isotope composition. *Oecologia* 123:32-40 (2000).

n/a Inagaki Y, Mitsu S, Kohzu A. Effects of forest type and stand age on litterfall quality and soil N dynamics in Shikoku district, southern Japan. *For Ecol Manag* 202:107-117 (2004).

n/a Ismail AM, Hall AE. Inheritance of carbon isotope discrimination and water use efficiency in corn. *Crop Science*, 33(3), 498-503 (1993).

n/a Ismail AM, Hall AE, Bray EA. Drought and soil size effects on transpiration efficiency and carbon isotope discrimination of cowpea accessions and hybrids. *Functional Plant Biology*, 21(1), 23-35 (1994).

n/a Johnson RC, Tieszen LL. Carbon isotope discrimination, water relations, and gas exchange in stable isotopes and plant carbon-water relations (pp. 281-296). Academic Press (1993).

n/a Klepper BD, Gower ST, Trechelt MW, Kharuk S. Foliar carbon isotope discrimination in Larix species and sympatric evergreen conifers: a global comparison. *Oecologia* 114:153-159 (1998).

n/a Körner C, Fink D, Amba P, Auer M, Bessan C, Black K, Gross P. Pan European δ¹³C values of air and organic matter from forest ecosystems. *Global Change Biology*, 14(4), 623-632 (1988).

n/a Kohrm LU, Goldstein G, Rundel PW. Morphological and isotopic indicators of growth environment - variability in delta-C-13 in *Silvestra chinensis*, a dioecious desert shrub. *J Exp Bot* 45:1817-1822 (1994).

n/a Lefler AJ, Enquist BJ. Carbon isotope composition of tree leaves from Guanacaste, Costa Rica: comparison across tropical forests and tree life history. *J Trop Ecol* 18:151-159 (2002).

n/a Li ZH, Lewall SW, Mora C, Liu RM. Influence of earlywood-latewood size and isotopic differences on long-term tree-ring δ¹³C trends. *Chem Geol* 216:191-201 (2005).

n/a Lockhead MJ, Van Buren PF. Variability in the stable carbon isotope compositions of individual lipids from the leaves of modern gymnosperms: implications for the study of higher land plant-derived sedimentary organic matter. *Org Geochem* 26:137-153 (1997).

n/a Marshall JD, Zhang J. Carbon isotope discrimination and water-use efficiency in native plants of the north-central Rockies. *Ecology* 75:1887-1895 (1994).

n/a Martin B, Thorntonsen YR. Stable carbon isotope composition (δ¹³C), water use efficiency, and biomass productivity of *Lycopodium esculentum*, *Lycopodium pennellii*, and the F1 hybrid. *Plant Physiology*, 88(1), 213-217 (1988).

n/a Martin B, Bytnerowicz A, Thorntonsen YR. Effects of air pollutants on the composition of stable carbon isotopes, δ¹³C, of leaves and wood, and on leaf injury. *Plant Physiology*, 88(1), 218-223 (1988).

n/a Mayland HF, Johnson DA, Asay KH, Read JJ. Ash, carbon isotope discrimination, and silicon as estimators of transpiration efficiency in crested wheatgrass. *Functional Plant Biology*, 20(3), 361-369 (1993).

n/a McArthur JV, Moohavee KK. Characterization of riparian species and stream detritus using multiple stable isotopes. *Oecologia* 107:232-238 (1996).

n/a Mervenne C. *Isotope ecology of temperate conifers* (Masters' Thesis) (2015).

n/a Mole S, Joem A. Feeding behavior of gaminivorous grasshoppers in response to host-plant extracts, alkaloids, and tannins. *Journal of chemical ecology*, 20(12), 3097-3109 (1994).

n/a Mooney HA, Bullock SH, Ehleringer JR. Carbon isotope ratios of plants of a tropical dry forest in Mexico. *Funct Ecol* 3:137-142 (1989).

n/a Morgan JA, LeCain DR, McCaig TN, Quirk JS. Gas exchange, carbon isotope discrimination, and productivity in winter wheat. *Crop Science*, 33(1), 178-186 (1993).

n/a Rao RN, Williams JH, Wadia KDR, Hultak KT, Farquhar GD. Crop growth, water use efficiency and carbon isotope discrimination in groundnut (*Arachis hypogaea* L.) genotypes under end of season drought conditions. *Annals of applied Biology*, 122(2), 357-367 (1995).

n/a Nagy L, Proctor J. Leaf δ¹³C signatures in heath and lowland evergreen rain forest species from Borneo. *J Trop Ecol* 16:757-761 (2000).

n/a Osorio J, Pereira JS. Genotypic differences in water use efficiency and δ¹³C discrimination in *Eucalyptus globulus*. *Tree Physiology*, 14(7-8-9), 871-882 (1994).

n/a Párek JA. Correlations between stable carbon-isotope abundance and hydraulic conductivity in Douglas fir across a climate gradient in Oregon, USA. *Tree Physiology*, 16(9), 747-755 (1996).

n/a Pelttunen J, Aalto-Belle J. Changes in leaf δ¹³C of herbium plant species during the last 3 centuries of CO₂ increase. *Plant, Cell & Environment*, 15(4), 485-489 (1992).

n/a Polley HW, Johnson HB, Mayeux HS. Nitrogen and water requirements of C3 plants grown at glacial to present carbon dioxide concentrations. *Functional Ecology*, 8:6-9 (1995).

n/a Proctor MCF, Raven JA, Rice SK (1992) Stable carbon isotope discrimination measurements in Sphagnum and other bryophytes: physiological and ecological implications. *Journal of Bryology*, 17(2), 193-202.

n/a Royles J, Horwath AB, Griffiths H. Interpreting bryophyte stable carbon isotope composition: Plants as temporal and spatial climate recorders. *Geochemistry, Geophysics, Geosystems*, 15(4), 1462-1475 (2014).

n/a Rundel PW, Slichter W, Zander RH, Ziegler H. Carbon and hydrogen isotope ratios of bryophytes from arid and humid regions. *Oecologia*, 44(1), 91-94 (1979).

n/a Sandquist DR, Condit S. Functional diversity of carbon, water-use, and leaf allocation traits in trees of a tree-rich lowland dry forest in Hawaii. *Amer J Bot* 94:1459-1469 (2007).

n/a Schubert BA, Jahren AH. The effect of atmospheric CO₂ concentration on carbon isotope fractionation in C3 land plants. *Geochimica et Cosmochimica Acta*, 66, 29-43 (2012).

n/a Sheldon ND, Smith SY, Stein RA, Ng M. Carbon isotope ecology of gymnosperms and implications for paleoclimatic and paleoecological studies. *Global and Planetary Change*, 103060 (2019).

n/a Simpson DA, Munro AM, Chayamant K, Parnell JA, Suddes S, Wilde BD, Pozna R, Khaosooka carioidea, a new genus and species of Cyperaceae from Thailand. *Botanical Journal of the Linnean Society*, 149(3), 357-364 (2005).

n/a Smeley MP, Dawson TE, Donawick JP, Donovan LA, Sherrill E, Cook CS, Ehleringer JR. Seasonal carbon isotope discrimination in a grassland community. *Oecologia*, 85(3), 314-320 (1991).

n/a Sternberg LD, Denno MJ, Johnson HB. Isotope ratios of cellulose from plants having different photosynthetic pathways. *Plant Physiology*, 74(3), 557-561 (1984).

n/a Terwilliger VJ. Changes in the δ¹³C values of trees during a tropical rainy season: some effects in detail on diffusion and carboxylation by Rubisco?. *American Journal of Botany*, 84(12), 1693-1700 (1997).

n/a Toft NL, Anderson JE, Nowak RS. Water use efficiency and carbon isotope composition of plants in a cold desert environment. *Oecologia*, 80(1), 11-18 (1989).

n/a Tu TN, Körner WM, Scholten B, Van Baren PF. Leaf carbon isotope composition of fossil and extant plants grown under differing atmospheric CO₂ levels. *Paleogeography, Paleoclimatology, Paleoecology*, 212(3-4), 199-213 (2004).

n/a Uemura A, Harayama H, Koike N, Ishida A. Coordination of crown structure, leaf plasticity and carbon gain within the crowns of three winter-deciduous mature trees. *Tree Phys* 26:833-841 (2006).

n/a Ueno O, Samejima M, Mitsu S, Miyachi S. Photosynthetic characteristics of an amphibious plant, *Eleocharis vivipara*: expression of C4 and C3 modes in contrasting environments. *Proceedings of the National Academy of Sciences*, 85(18), 6733-6737 (1988).

n/a Valentini R, Anfollio T, Ehleringer JR. Water sources and carbon-isotope composition (delta-C-13) of selected tree species of the Italian Alps. *Canadian J For Res* 24:1575-1579 (1994).

n/a Valentini R, Mugnozza GES, Ehleringer JR. Hydrogen and carbon isotope ratios of selected species of a Mediterranean *Macchia* ecosystem. *Funct Ecol* 6:627-631 (1992).

n/a Van de Water P, Lewis S, Betancourt J. Leaf δ¹³C variability with elevation, slope aspect, and precipitation in the southwest United States. *Oecologia* 132:333-343 (2002).

n/a Van de Water PK, Lewall SW, Betancourt JL. Trends in stomatal density and δ¹³C ratios of *Pinus flexilis* needles during last glacial-interglacial cycle. *Science*, 284(5156), 239-243 (1994).

n/a Welker JM, Wooley PA, Parsons AN, Press MC, Callaghan T, Lee JA. Leaf carbon isotope discrimination and vegetative responses of *Dryas octopetala* to temperature and water manipulations in a High Arctic polar semi-desert. *Svalbard, Oecologia*, 95(4), 463-469 (1993).

n/a White JW, Castillo JA, Ehleringer JR, Garcia JAC, Singh SP. Relations of carbon isotope discrimination and other physiological traits to yield in common bean (*Phaseolus vulgaris*) under rainfed conditions. *The Journal of Agricultural Science*, 122(2), 275-284 (1994).

n/a Williams DG, Ehleringer JR. Carbon isotope discrimination in three semi-arid woodland species along a monsoon gradient. *Oecologia* 100:455-460 (1994).

n/a Williams DG, Ehleringer JR. Carbon isotope discrimination and water relations of oak hybrid populations in southwestern Utah. *West Nor Amer Nat* 60:121-129 (2000).

n/a Wierke K, Troughton JH. Carbon assimilation pathways in *Mesembryanthemum nodiflorum* L. under natural conditions. *Zeitschrift für Pflanzenphysiologie*, 88(2), 153-162 (1978).

n/a Wright GC, Rao RC, Farquhar GD. Water-use efficiency and carbon isotope discrimination in peanut under water deficit conditions. *Crop Science*, 34(1), 90-97 (1994).

n/a Zhang J, Marshall JD, Jaquish BD. Genetic differentiation in carbon isotope discrimination and gas exchange in *Pseudotsuga menziesii*. *Oecologia*, 93(1), 80-87 (1993).

n/a Zhang J, Finn L, Marshall JD. Stable carbon isotope discrimination, photosynthetic gas exchange, and growth differences among western larch families. *Tree Physiology*, 14(5), 531-539 (1994).

n/a Zibulski, R, Wesener F, Wilkes H, Plesken B, Pestayakova LA, Heitzschuh, U. C/N ratio, stable isotope (δ¹³C, δ¹⁵N), and n-alkane patterns of brown mosses along hydrological gradients of low-centred polygons of the Siberian Arctic (2019).

Table B2 Range of climate variables included in the historical portion of this study, as collected from PRISM Climate Group (2004), White et al. (2015), and Eggleston (2016).

Climate, Atmospheric or Temporal Variable	Minimum	Maximum	Mean
Time (Year)	1804	2019	1971
[CO ₂] (ppm)	283	411	351
δ ¹³ C _{CO₂} (‰)	-8.7	-6.4	-7.6
Latitude (°N)	9.9	68.2	42.5
Longitude (°E)	-152.3	139.9	-86.7
Mean Annual Precipitation (mm yr ⁻¹)	193	4368	999
Mean Annual Temperature (°C)	-5.6	25.0	8.0
Maximum Summer Temperature (°C)	13.3	35.9	26.2
Elevation (m)	4	2766	967
Annual Minimum Vapor Pressure Deficit (hPa)	0.18	6.32	1.23
Annual Maximum Vapor Pressure Deficit (hPa)	0.63	21.87	10.58

Table B3 Results from t-tests (assuming unequal variances) comparing the means and ranges of *Arabidopsis* (a) and *Raphanus* (b) and families highly sampled from the literature dataset. N/a denotes that the comparison to the model species is not applicable (in the cases that it would involve comparing the model species to itself).

Taxon	Mean	Standard Deviation	Sample Size	t-Stat	p(T<=t) two-tail value
<i>Arabidopsis</i>	22.66	10.65	22	n/a	n/a
Asteraceae	18.76	1.78	68	5.44	4.14 x 10 ⁻⁵
Other Brassicaceae	20.37	0.93	5	2.80	0.02
Cupressaceae	19.28	3.49	584	4.83	7.72 x 10 ⁻⁵
Cyperaceae	20.78	11.01	212	2.58	3.39 x 10 ⁻³
Fabaceae	20.61	2.80	134	2.89	7.76 x 10 ⁻³
Fagaceae	20.34	1.97	54	3.22	4.25 x 10 ⁻³
Ginkgoaceae	19.93	2.21	221	3.89	7.88 x 10 ⁻⁴
Pinaceae	20.24	3.45	356	3.45	2.28 x 10 ⁻³
Poaceae	18.88	4.20	119	5.25	3.79 x 10 ⁻⁵
Salicaceae	19.77	2.60	261	4.12	4.48 x 10 ⁻⁴
Taxon	Mean	Standard Deviation	Sample Size	t-Stat	p(T<=t) two-tail value
<i>Raphanus</i>	24.47	8.16	23	n/a	n/a
Asteraceae	18.76	1.78	68	9.23	2.37 x 10 ⁻⁹
Other Brassicaceae	20.37	0.93	5	5.33	1.37 x 10 ⁻⁴
Cupressaceae	19.28	3.49	584	8.64	1.07 x 10 ⁻⁸
Cyperaceae	20.78	11.01	212	5.80	1.23 x 10 ⁻⁵
Fabaceae	20.61	2.80	134	6.30	1.25 x 10 ⁻⁶
Fagaceae	20.34	1.97	54	6.61	5.34 x 10 ⁻⁷
Ginkgoaceae	19.93	2.21	221	7.52	1.21 x 10 ⁻⁷
Pinaceae	20.24	3.45	356	7.01	3.79 x 10 ⁻⁷
Poaceae	18.88	4.20	119	8.95	2.60 x 10 ⁻⁹
Salicaceae	19.77	2.60	261	7.79	6.69 x 10 ⁻⁸

Table B4 Results showing the relationship between $\delta^{13}\text{C}_{\text{CO}_2}$ and $\delta^{13}\text{C}_{\text{plant}}$ for each species studied over Industrialization. The first row shows the universal relationship proposed by Arens et al. (2000), and the second shows a generalized relationship that incorporates all 8 of the species we tested. Specimens sampled post-2017 were excluded to focus on the historical portion of this study.

Measurement	Slope	Intercept
Arens et al. (2000)	1.05	-18.72
Total Historical Dataset (pre-2017)	1.22	-17.10
<i>Pinus strobus</i>	1.58	-15.54
<i>Platycladus orientalis</i>	1.47	-15.72
<i>Populus tremuloides</i>	1.08	-18.77
<i>Thuja koraiensis</i>	0.36	-22.84
<i>Thuja occidentalis</i>	1.31	-15.66
<i>Thuja plicata</i>	0.95	-18.53
<i>Thuja standishii</i>	2.46	-6.77
<i>Thuja sutchuenensis</i>	6.42	27.19

Table B5 Sensitivity (S given as ‰ ppm⁻¹) for eight species with long historical record. S is compiled for the entire range of [CO₂] values spanning the collection, and as pre-1960 (acceleration; Keeling et al. 2001) and post-1960 ranges. Expected sensitivity is calculated using the best-fit function, $S (\text{‰ ppm}^{-1}) = 0.21(28.26)^2 / [28.26 + 0.21(\text{CO}_2 + 25)]^2$ from Schubert & Jahren's (2012) study using data from both *Arabidopsis thaliana* and *Raphanus sativus* growth chamber experiments. S-column cells highlighted in blue indicate actual sensitivities far more negative than expected. S-column cells in red indicate sensitivities far more positive than expected, and S-column cells in white indicate sensitivities matching what is expected. N/a is used when there are no samples collected of the species during the specified time period.

Genus	Species	Age (Range in [CO ₂])	S (‰/ppm)	Standard Deviation (‰/ppm)
<i>Pinus</i>	<i>strobus</i>	Total (286-395)	-0.0117	3.019
		<1960 (286-320)	-0.0421	n=51
		>1960 (320-395)	0.0014	
<i>Platycladus</i>	<i>orientalis</i>	Total (290-408)	0.0077	1.642
		<1960 (290-320)	-0.0045	n=12
		>1960 (320-408)	0.0346	
<i>Populus</i>	<i>tremuloides</i>	Total (288-411)	0.0078	9.078
		<1960 (288-320)	-0.0441	n=79
		>1960 (320-411)	-0.0011	
<i>Thuja</i>	<i>koraiensis</i>	Total (311-408)	-0.0411	0.536
		<1960 (311-320)	-0.4977	n=6
		>1960 (320-408)	0.0495	
<i>Thuja</i>	<i>occidentalis</i>	Total (283-408)	0.0128	4.497
		<1960 (283-320)	0.0417	n=85
		>1960 (320-408)	-0.0012	
<i>Thuja</i>	<i>plicata</i>	Total (289-411)	0.0161	4.164
		<1960 (289-320)	-0.0085	n=163
		>1960 (320-411)	0.0338	
<i>Thuja</i>	<i>standishii</i>	Total (292-408)	0.0333	1.583
		<1960 (292-320)	0.0592	n=15
		>1960 (320-408)	0.0474	
<i>Thuja</i>	<i>sutchuenensis</i>	Total (366-408)	0.0851	0.203
		<1960 (n/a)	n/a	n=4
		>1960 (366-408)	0.0851	
Expected Sensitivity		<1960 (280-320)	0.0181	
		>1960 (320-408)	0.0139	

Table B6 Results showing the statistical relationship between carbon isotope discrimination and non-[CO₂] climate variables for each species studied over Industrialization for each species studied over Industrialization. Specimens collected in modern times were included. N/a denotes when climate variables were not accessible for the specified species.

a						
R ² value						
Species	Mean Annual Precipitation (mm yr ⁻¹)	Mean Annual Temperature (°C)	Maximum Summer Temperature (°C)	Elevation (m)	Latitude (°N)	
<i>Pinus strobus</i>	4.00 x 10 ⁻³	0.01	0.01	0.06	0.06	
<i>Platycladus orientalis</i>	7.00 x 10 ⁻⁴	0.01	0.74	0.10	3.47 x 10 ⁻⁶	
<i>Populus tremuloides</i>	0.05	0.01	3.00 x 10 ⁻³	0.08	0.15	
<i>Thuja occidentalis</i>	1.00 x 10 ⁻³	0.01	4.00 x 10 ⁻³	1.00 x 10 ⁻³	0.01	
<i>Thuja koraiensis</i>	0.15	0.76	0.32	0.10	0.37	
<i>Thuja plicata</i>	0.06	0.02	0.07	0.04	0.05	
<i>Thuja standishii</i>	0.55	0.34	n/a	0.03	0.25	
<i>Thuja sutchuenensis</i>	0.03	0.06	n/a	0.44	0.01	
Overall historical study	0.02	0.01	0.01	0.00	4.00 x 10 ⁻³	
b						
p-value						
Species	Mean Annual Precipitation (mm yr ⁻¹)	Mean Annual Temperature (°C)	Maximum Summer Temperature (°C)	Elevation (m)	Latitude (°N)	
<i>Pinus strobus</i>	0.62	0.33	0.43	0.04	0.03	
<i>Platycladus orientalis</i>	0.93	0.77	0.00	0.27	0.99	
<i>Populus tremuloides</i>	1.00 x 10 ⁻³	0.20	0.50	7.88 x 10 ⁻⁶	8.87 x 10 ⁻¹⁰	
<i>Thuja occidentalis</i>	0.72	0.30	0.47	0.66	0.23	
<i>Thuja koraiensis</i>	0.52	0.05	0.43	0.53	0.08	
<i>Thuja plicata</i>	2.00 x 10 ⁻³	0.09	3.00 x 10 ⁻³	8.00 x 10 ⁻³	0.01	
<i>Thuja standishii</i>	0.09	0.22	n/a	0.58	0.06	
<i>Thuja sutchuenensis</i>	0.56	0.46	n/a	0.02	0.75	
Overall historical study	4.00 x 10 ⁻³	0.65	0.24	0.88	0.01	

B. References

- Araus, J. L., Reynolds, M. P., & Acevedo, E. (1993). Leaf posture, grain yield, growth, leaf structure, and carbon isotope discrimination in wheat. *Crop Science*, 33(6), 1273-1279.
- Arens N. C., Jahren A. H. (2000). Carbon isotope excursion in atmospheric CO₂ at the Cretaceous-Tertiary boundary: evidence from terrestrial sediments. *Palaios*, 15(4), 314-322.
- Bai E., Boutton T., Liu F., Wu X., Archer S. (2008). Variation in woody plant δ¹³C along a topographic gradient in a subtropical savanna parkland. *Oecologia*, 156:479-489.
- Beerling D. J., Woodward F. I. (1995). Stomatal responses of variegated leaves to CO₂ enrichment. *Annals of Botany*, 75(5), 507-511.

- Beerling D. J. (1996). ^{13}C discrimination by fossil leaves during the late-glacial climate oscillation 12-10 ka BP: measurements and physiological controls. *Oecologia*, *108*(1), 29-37.
- Bonal D., Sabatier D., Montpied P., Tremeaux D., & Guehl J. M. (2000). Interspecific variability of $\delta^{13}\text{C}$ among trees in rainforests of French Guiana: functional groups and canopy integration. *Oecologia*, *124*, 454-468.
- Brooks J. R., Flanagan L. B., Buchmann N., & Ehleringer J. R. (1997). Carbon isotope composition of boreal plants: functional grouping of life forms. *Oecologia*, *110*:301-311.
- Broadmeadow M. S. J., Griffiths H., Maxwell C., & Borland A. M. (1992). The carbon isotope ratio of plant organic material reflects temporal and spatial variations in CO_2 within tropical forest formations in Trinidad. *Oecologia*, *89*(3), 435-441.
- Bruhl J. J., & Wilson K. L. (2007). Towards a comprehensive survey of C_3 and C_4 photosynthetic pathways in Cyperaceae. *Aliso: A Journal of Systematic and Evolutionary Botany*, *23*(1), 99-148.
- Buchmann N., Guehl J. M., Barigah T. S., & Ehleringer J. R. (1997). Interseasonal comparison of CO_2 concentrations, isotopic composition, and carbon dynamics in an Amazonian rainforest (French Guiana). *Oecologia*, *110*, 120-131.
- Chevillat V. S., Siegwolf R. T. W., Pepin S., & Körner C. (2005). Tissue-specific variation of $\delta^{13}\text{C}$ in mature canopy trees in a temperate forest in central Europe. *Basic and applied ecology*, *6*, 519-534.
- Collister J. W., Rieley G., Stern B., Eglinton G., & Fry B. (1994). Compound-specific $\delta^{13}\text{C}$ analyses of leaf lipids from plants with differing carbon dioxide metabolisms. *Organic Geochemistry*, *21*, 619-627.
- Condon A. G., Richards R. A., & Farquhar G. D. (1993). Relationships between carbon isotope discrimination, water use efficiency and transpiration efficiency for dryland wheat. *Australian Journal of Agricultural Research*, *44*(8), 1693-1711.
- Dawson T. E., Ehleringer J. R. (1993). Isotopic enrichment of water in the “woody” tissues of plants: implications for plant water source, water uptake, and other studies which use the stable isotopic composition of cellulose. *Geochimica et Cosmochimica Acta*, *57*(14), 3487-3492.
- De Lillis M., Matteucci G., & Valentini R. (2004). Carbon assimilation, nitrogen, and photochemical efficiency of different Himalayan tree species along an altitudinal gradient. *Photosynthetica*, *42*, 597-605.
- DeLucia E. H., & Schlesinger W. H. (1991). Resource-use efficiency and drought tolerance in adjacent Great Basin and Sierran plants. *Ecology*, *72*, 51-58.

- Diefendorf, A. F., Mueller, K. E., Wing, S. L., Koch, P. L., & Freeman, K. H. (2010). Global patterns in leaf ^{13}C discrimination and implications for studies of past and future climate. *Proceedings of the National Academy of Sciences*, *107*(13), 5738-5743.
- Dodd M. B., Lauenroth W. K., & Welker J. M. (1998). Differential water resource use by herbaceous and woody plant life-forms in a shortgrass steppe community. *Oecologia*, *117*, 504-512.
- Donovan L. A., Ehleringer J. R., (1991). Ecophysiological differences among juvenile and reproductive plants of several woody species. *Oecologia*, *86*, 594-597.
- Dungait J. A. J., Docherty G., Straker V., & Evershed R. P. (2008). Interspecific variation in bulk tissue, fatty acid and monosaccharide $\delta^{13}\text{C}$ values of leaves from a mesotrophic grassland plant community. *Phytochemistry*, *69*, 2041-2051.
- Dupouey J. L., Leavitt S., Choisnel E., & Jourdain S., (1993). Modelling carbon isotope fractionation in tree rings based on effective evapotranspiration and soil water status. *Plant, Cell & Environment*, *16*(8), 939-947.
- Eggleston, S., Schmitt, J., Bereiter, B., Schneider, R., & Fischer, H. (2016). Evolution of the stable carbon isotope composition of atmospheric CO_2 over the last glacial cycle. *Paleoceanography*, *31*(3), 434-452.
- Ehleringer J. R., & Cerling T. E. (1995). Atmospheric CO_2 and the ratio of intercellular to ambient CO_2 concentrations in plants. *Tree physiology*, *15*(2), 105-111.
- Ehleringer J. R., Lin Z. F., Field C. B., Sun G. C., Kuo C. Y. (1987). Leaf carbon isotope ratios of plants from a subtropical monsoon forest. *Oecologia*, *72*, 109-114.
- Ehleringer J. R., Phillips S. L., Schuster W. S., & Sandquist D. R. (1991). Differential utilization of summer rains by desert plants. *Oecologia*, *88*(3), 430-434.
- Ehleringer J. R., Phillips S. L., & Comstock J. P. (1992). Seasonal variation in the carbon isotopic composition of desert plants. *Functional Ecology*, *6*, 396-404.
- Ehleringer J. R., Hall A. E., Farquhar G. D. (Eds.). (1993). Stable isotopes and plant carbon-water relations (Vol. 109129). San Diego: Academic Press.
- Escudero A., Mediavilla S., Heilmeyer H. (2008). Leaf longevity and drought: avoidance of the costs and risks of early leaf abscission as inferred from the leaf carbon isotopic composition. *Functional Plant Biology*, *35*, 705-713.
- Etheridge, D. M., Steele, L. P., Langenfelds, R. L., Francey, R. J., Barnola, J. M., & Morgan, V. I. (1998). Historical CO_2 records from the Law Dome DE08, DE08-2, and DSS ice cores. *Trends: a compendium of data on global change*, 351-364.
- Franco A. C., Duarte H. M., Geßler A., de Mattos E. A., Nahm M., Rennenberg H., Lüttge U. (2005). In situ measurements of carbon and nitrogen distribution and composition,

- photochemical efficiency and stable isotope ratios in *Araucaria angustifolia*. *Trees*, 19(4), 422-430.
- Friend A. D., Woodward F. I., & Switsur V. R. (1989). Field measurements of photosynthesis, stomatal conductance, leaf nitrogen and $\delta^{13}\text{C}$ along altitudinal gradients in Scotland. *Functional Ecology*, 117-122.
- Garten C. T., & Taylor G. E. (1992). Foliar $\delta^{13}\text{C}$ within a temperate deciduous forest: spatial, temporal, and species sources of variation. *Oecologia*, 90, 1-7.
- Gerdol R., Iacumin P., Marchesini R., & Bragazza L. (2000). Water- and nutrient-use efficiency of a deciduous species, *Vaccinium myrtillus*, and an evergreen species, *V. vitis-idaea*, in a subalpine dwarf shrub heath in the southern Alps, Italy. *Oikos* 88(1), 19-32.
- Gutierrez M. V., & Meinzer F. C. (1994). Carbon isotope discrimination and photosynthetic gas exchange in coffee hedgerows during canopy development. *Functional Plant Biology*, 21(2), 207-219.
- Guy R. D., & Reid D. M. (1986). Photosynthesis and the influence of CO_2 -enrichment on $\delta^{13}\text{C}$ values in a C_3 halophyte. *Plant, Cell & Environment*, 9(1), 65-72.
- Hall A. E., Richards R. A., Condon A. G., Wright G. C., & Farquhar G. D. (1994). Carbon isotope discrimination and plant breeding. *Plant breeding reviews*, 12(81), 113.
- Hansen D., & Steig E. (1993). Comparison of water-use efficiency and internal leaf carbon dioxide concentration in juvenile leaves and phyllodes of *Acacia koa* (leguminosae) from Hawaii, estimated by two methods. *American Journal of Botany*, 80(10), 1121-1125.
- He C.-X., Li J.-Y., Zhou P., Guo M., & Zheng Q.-S. (2008). Changes of leaf morphological, anatomical structure and carbon isotope ratio with the height of the Wangtian Tree (*Parashorea chinensis*) in Xishuangbanna, China. *Journal of Integrative Plant Biology* 50(2), 168-173.
- Hemming D., Yakir D., Ambus P., Aurela M., Besson C., Black K., Gross, P. (2005). Pan-European $\delta^{13}\text{C}$ values of air and organic matter from forest ecosystems. *Global Change Biology*, 11(7), 1065-1093.
- Holtum J. A. M., & Winter K. (2005). Carbon isotope composition of canopy leaves in a tropical forest in Panama throughout a seasonal cycle. *Trees*, 19(5), 545-551.
- Huc R., Ferhi A., & Guehl J. M. (1994). Pioneer and late stage tropical rainforest tree species (French Guiana) growing under common conditions differ in leaf gas exchange regulation, carbon isotope discrimination and leaf water potential. *Oecologia*, 99(3-4), 297-305.
- Hultine K. R., & Marshall J. D. (2000). Altitude trends in conifer leaf morphology and stable carbon isotope composition. *Oecologia*, 123(1), 32-40.

- Inagaki Y., Miura S., & Kohzu A. (2004). Effects of forest type and stand age on litterfall quality and soil N dynamics in Shikoku district, southern Japan. *Forest Ecology and Management*, 202(1-3), 107-117.
- Ismail A. M., & Hall, A. E. (1993). Inheritance of carbon isotope discrimination and water-use efficiency in cowpea. *Crop Science*, 33(3), 498-503.
- Ismail A. M., Hall A. E., & Bray E. A. (1994). Drought and pot size effects on transpiration efficiency and carbon isotope discrimination of cowpea accessions and hybrids. *Functional Plant Biology*, 21(1), 23-35.
- Johnson R. C., & Tieszen L. L. (1993). Carbon isotope discrimination, water relations, and gas exchange in temperate grass species and accessions. In *Stable isotopes and plant carbon-water relations* (pp. 281-296). Academic Press.
- Keeling, C. D., Piper, S. C., Bacastow, R. B., Wahlen, M., Whorf, T. P., Heimann, M., & Meijer, H. A. (2005). Atmospheric CO₂ and ¹³CO₂ exchange with the terrestrial biosphere and oceans from 1978 to 2000: Observations and carbon cycle implications. In *A history of atmospheric CO₂ and its effects on plants, animals, and ecosystems* (pp. 83-113). Springer, New York, NY.
- Keeling, C. D., Piper, S. C., Bacastow, R. B., Wahlen, M., Whorf, T. P., Heimann, M., & Meijer, H. A. (2005). Terrestrial biosphere and oceans from 1978 to 2000: observations and carbon cycle implications. *A History of Atmospheric CO₂ and Its Effects on Plants, Animals and Ecosystems*, 2, 83-113.
- Kloppel B. D., Gower S. T., Treichel I. W., & Kharuk S. (1998). Foliar carbon isotope discrimination in *Larix* species and sympatric evergreen conifers: a global comparison. *Oecologia*, 114(2), 153-159.
- Körner C., Farquhar G. D., Roksandic Z. (1988). A global survey of carbon isotope discrimination in plants from high altitude. *Oecologia*, 74(4), 623-632.
- Kohorn L. U., Goldstein G., & Rundel P. W. (1994). Morphological and isotopic indicators of growth environment - variability in $\delta^{13}\text{C}$ in *Simmondsia chinensis*, a dioecious desert shrub. *Journal of Experimental Botany*, 45(12), 1817-1822.
- Leffler A. J., & Enquist B. J. (2002). Carbon isotope composition of tree leaves from Guanacaste, Costa Rica: comparison across tropical forests and tree life history. *Journal of Tropical Ecology*, 18(1), 151-159.
- Li Z.-H., Leavitt S. W., Mora C. I., & Liu R.-M., (2005). Influence of earlywood-latewood size and isotope differences on long-term tree-ring $\delta^{13}\text{C}$ trends. *Chemical Geology*, 216(3-4), 191-201.
- Lockheart M. J., Van Bergen P. F., & Evershed R. P. (1997). Variations in the stable carbon isotope compositions of individual lipids from the leaves of modern angiosperms:

- implications for the study of higher land plant-derived sedimentary organic matter. *Organic Geochemistry*, 26(1-2), 137-153.
- Marshall J. D., & Zhang J. (1994). Carbon isotope discrimination and water-use efficiency in native plants of the north-central Rockies. *Ecology*, 75(7), 1887-1895.
- Martin B., & Thorstenson Y. R. (1988). Stable carbon isotope composition ($\delta^{13}\text{C}$), water use efficiency, and biomass productivity of *Lycopersicon esculentum*, *Lycopersicon pennellii*, and the F1 hybrid. *Plant Physiology*, 88(1), 213-217.
- Martin B., Bytnerowicz A., & Thorstenson Y. R. (1988). Effects of air pollutants on the composition of stable carbon isotopes, $\delta^{13}\text{C}$, of leaves and wood, and on leaf injury. *Plant Physiology*, 88(1), 218-223.
- Mayland H. F., Johnson D. A., Asay K. H., & Read J. J. (1993). Ash, carbon isotope discrimination, and silicon as estimators of transpiration efficiency in crested wheatgrass. *Functional Plant Biology*, 20(3), 361-369.
- McArthur J. V., & Moorhead K. K. (1996). Characterization of riparian species and stream detritus using multiple stable isotopes. *Oecologia* 107(2), 32-238.
- Merven C. (2015). Isotope ecology of temperate conifers (Masters' Thesis, University of Michigan, Ann Arbor, MI, United States of America).
- Mole S., Joern A. (1994). Feeding behavior of graminivorous grasshoppers in response to host-plant extracts, alkaloids, and tannins. *Journal of chemical ecology*, 20(12), 3097-3109.
- Mooney H. A., Bullock S. H., & Ehleringer J. R. (1989). Carbon isotope ratios of plants of a tropical dry forest in Mexico. *Functional Ecology*, 3, 137-142.
- Morgan J. A., LeCain D. R., McCaig T. N., & Quick J. S. (1993). Gas exchange, carbon isotope discrimination, and productivity in winter wheat. *Crop Science*, 33(1), 178-186.
- PRISM Climate Group, Oregon State University. (2004). <http://prism.oregonstate.edu>, created 4 Feb 2004.
- Rubino, M., Etheridge, D. M., Trudinger, C. M., Allison, C. E., Battle, M. O., Langenfelds, R. L., Steele, L. P., Curran, M., Bender, M., White, J. W. C. & Jenk, T. M. (2013). A revised 1000 year atmospheric $\delta^{13}\text{C}$ -CO₂ record from Law Dome and South Pole, Antarctica. *Journal of Geophysical Research: Atmospheres*, 118(15), 8482-8499.
- Rao R. N., Williams J. H., Wadia K. D. R., Hubick K. T., & Farquhar G. D. (1993). Crop growth, water-use efficiency and carbon isotope discrimination in groundnut (*Arachis hypogaea* L.) genotypes under end-of season drought conditions. *Annals of applied Biology*, 122(2), 357-367.
- Nagy L., & Proctor J. (2000). Leaf $\delta^{13}\text{C}$ signatures in heath and lowland evergreen rain forest species from Borneo. *Journal of Tropical Ecology*, 16, 757-761.

- Osorio J., & Pereira J. S. (1994). Genotypic differences in water use efficiency and ^{13}C discrimination in *Eucalyptus globulus*. *Tree Physiology*, 14(7-8-9), 871-882.
- Panek J. A. (1996). Correlations between stable carbon-isotope abundance and hydraulic conductivity in Douglas-fir across a climate gradient in Oregon, USA. *Tree Physiology*, 16(9), 747-755.
- Peñuelas J., & Azcón-Bieto J. (1992). Changes in leaf $\Delta^{13}\text{C}$ of herbarium plant species during the last 3 centuries of CO_2 increase. *Plant, Cell & Environment*, 15(4), 485-489.
- Polley H. W., Johnson H. B., & Mayeux H. S. (1995). Nitrogen and water requirements of C_3 plants grown at glacial to present carbon dioxide concentrations. *Functional Ecology*, 86-96.
- Royles J., Horwath A. B., & Griffiths H. (2014). Interpreting bryophyte stable carbon isotope composition: Plants as temporal and spatial climate recorders. *Geochemistry, Geophysics, Geosystems*, 15(4), 1462-1475.
- Rundel P. W., Stichler W., Zander R. H., & Ziegler H. (1979). Carbon and hydrogen isotope ratios of bryophytes from arid and humid regions. *Oecologia*, 44(1), 91-94.
- Sandquist D. R., & Cordell S. (2007). Functional diversity of carbon-gain, water-use, and leaf-allocation traits in trees of a threatened lowland dry forest in Hawaii. *American Journal of Botany*, 94(9), 1459-1469.
- Schubert B. A., & Jahren A. H. (2012). The effect of atmospheric CO_2 concentration on carbon isotope fractionation in C_3 land plants. *Geochimica et Cosmochimica Acta*, 96, 29-43.
- Sheldon N. D., Smith SY, Stein R. A., & Ng M. (2020). Carbon isotope ecology of gymnosperms and implications for paleoclimatic and paleoecological studies. *Global and Planetary Change*, 184, 103060, 1-17.
- Simpson D. A., Muasya A. M., Chayamarit K., Parnell J. A., Suddee S., Wilde B. D., & Pooma R. (2005). *Khaosokia caricoides*, a new genus and species of Cyperaceae from Thailand. *Botanical Journal of the Linnean Society*, 149(3), 357-364.
- Smedley M. P., Dawson T. E., Comstock J. P., Donovan L. A., Sherrill E., Cook C. S., & Ehleringer J. R. (1991). Seasonal carbon isotope discrimination in a grassland community. *Oecologia*, 85(3), 314-320.
- Sternberg L. O., Deniro M. J., & Johnson H. B. (1984). Isotope ratios of cellulose from plants having different photosynthetic pathways. *Plant Physiology*, 74(3), 557-561.
- Terwilliger V. J. (1997). Changes in the $\delta^{13}\text{C}$ values of trees during a tropical rainy season: some effects in addition to diffusion and carboxylation by Rubisco? *American Journal of Botany*, 84(12), 1693-1700.

- Toft N. L., Anderson J. E., & Nowak R. S. (1989). Water use efficiency and carbon isotope composition of plants in a cold desert environment. *Oecologia*, 80(1), 11-18.
- Tu T. T. N., Kürschner W. M., Schouten S., & Van Bergen P. F. (2004). Leaf carbon isotope composition of fossil and extant oaks grown under differing atmospheric CO₂ levels. *Palaeogeography, Palaeoclimatology, Palaeoecology*, 212(3-4), 199-213.
- Uemura A., Harayama H., Koike N., & Ishida A. (2006). Coordination of crown structure, leaf plasticity and carbon gain within the crowns of three winter-deciduous mature trees. *Tree Physiology*, 26(5), 633-641.
- Ueno O., Samejima M., Muto S., & Miyachi S. (1988). Photosynthetic characteristics of an amphibious plant, *Eleocharis vivipara*: expression of C₄ and C₃ modes in contrasting environments. *Proceedings of the National Academy of Sciences*, 85(18), 6733-6737.
- Valentini R., Anfodillo T., & Ehleringer J. R. (1994). Water sources and carbon-isotope composition ($\delta^{13}\text{C}$) of selected tree species of the Italian Alps. *Canadian Journal of Forest Research*, 24(8), 1575-1579.
- Valentini R., Mugnozza G. E. S., & Ehleringer J. R. (1992). Hydrogen and carbon isotope ratios of selected species of a Mediterranean Macchia ecosystem. *Functional Ecology*, 627-631.
- Van de Water P., Leavitt S., & Betancourt J. (2002). Leaf $\delta^{13}\text{C}$ variability with elevation, slope aspect, and precipitation in the southwest United States. *Oecologia*, 132(3), 332-343.
- Van de Water P. K., Leavitt S. W., & Betancourt J. L. (1994). Trends in stomatal density and $^{13}\text{C}/^{12}\text{C}$ ratios of *Pinus flexilis* needles during last glacial-interglacial cycle. *Science*, 264(5156), 239-243.
- Welker J. M., Wookey P. A., Parsons A. N., Press M. C., Callaghan T. V., & Lee J. A. (1993). Leaf carbon isotope discrimination and vegetative responses of *Dryas octopetala* to temperature and water manipulations in a High Arctic polar semi-desert, Svalbard. *Oecologia*, 95(4), 463-469.
- White J. W., Castillo J. A., Ehleringer J. R., Garcia J. A. C., & Singh S. P. (1994). Relations of carbon isotope discrimination and other physiological traits to yield in common bean (*Phaseolus vulgaris*) under rainfed conditions. *The Journal of Agricultural Science*, 122(2), 275-284.
- White, J.W.C., Vaughn, B.H., Michel, S.E. (2015). University of Colorado, Institute of Arctic and 720 Alpine Research (INSTAAR), Stable Isotopic Composition of Atmospheric Carbon Dioxide (^{13}C and ^{18}O) from the NOAA ESRL Carbon Cycle Cooperative Global Air Sampling Network, 722 1990-2014, Version: 2015-10-26.
- Williams D. G., & Ehleringer J. R. (1996). Carbon isotope discrimination in three semi-arid woodland species along a monsoon gradient. *Oecologia*, 106(4), 455-460.

- Williams D. G., & Ehleringer J. R. (2000). Carbon isotope discrimination and water relations of oak hybrid populations in southwestern Utah. *Western North American Naturalist*, 121-129.
- Winter K., Troughton J. H. (1978). Carbon assimilation pathways in *Mesembryanthemum nodiflorum* L. under natural conditions. *Zeitschrift für Pflanzenphysiologie*, 88(2), 153-162.
- Wright G. C., Rao R. C., & Farquhar G. D. (1994). Water-use efficiency and carbon isotope discrimination in peanut under water deficit conditions. *Crop Science*, 34(1), 92-97 (1994).
- Zhang J., Marshall J. D., & Jaquish B. D. (1993). Genetic differentiation in carbon isotope discrimination and gas exchange in *Pseudotsuga menziesii*. *Oecologia*, 93(1), 80-87.
- Zhang J., Fins L., & Marshall J. D. (1994). Stable carbon isotope discrimination, photosynthetic gas exchange, and growth differences among western larch families. *Tree Physiology*, 14(5), 531-539.
- Zibulski, R., Wesener F., Wilkes H., Plessen B., Pestryakova L. A., & Herzschuh, U. (2019). C/N ratio, stable isotope ($\delta^{13}\text{C}$, $\delta^{15}\text{N}$), and n-alkane patterns of brown mosses along hydrological gradients of low-centred polygons of the Siberian Arctic. *Biogeosciences*, 14(6), 1617-1630.

APPENDIX C

Supplemental Figures, Tables and References for Chapter IV

Table C1 Range of conditions for which soils are tested.

Variable	Unit	Minimum	Maximum
Time	Year	1900	2017
$\delta^{13}\text{C}_{\text{atm}}$	‰	-8.59	-6.50
$p\text{CO}_2$	ppm	295.3	411.75
Latitude	°N	-78.03	54.65
Longitude	°E	-155.73	175.36
Mean Annual Precipitation	mm yr ⁻¹	100	3350
Mean Annual Temperature	°C	2.5	23.4
Elevation	m	1.0	2854.6
Growing Season Precipitation	mm / season	22.5	1777.2
Vapor Pressure Deficit (Minimum)	hPa	0.00	7.04
Vapor Pressure Deficit (Maximum)	hPa	7.45	32.11

Table C2 Multivariate relationships including coefficients of determination (R^2) and significance (p-value column). Error for coefficients is shown in parentheses in each equation. The comparative single variable relationship between MAP and carbon isotope values in soil is provided in the box below.

Equation	R^2	p - value
$\Delta_{SOM} = 5.24(\pm 0.57) \cdot \log_{10}MAP - 0.01(\pm 0.01) \cdot (\sqrt{\text{Elevation}}) + 4.70(\pm 1.77)$	0.62	<0.001
$\Delta_{SOM} = 0.002(\pm 0.00) \cdot (MAP) - 0.01(\pm 0.01) \cdot (\sqrt{\text{Elevation}}) + 18.03(\pm 0.43)$	0.58	<0.001
$\Delta_{SOM} = 5.25(\pm 0.56) \cdot (\log_{10}MAP) - 0.00(\pm 0.00) \cdot (\text{Elevation}) + 4.54(\pm 1.70)$	0.62	<0.001
$\Delta_{SOM} = 0.002(\pm 0.00) \cdot (MAP) - 0.00(\pm 0.00) \cdot (\text{Elevation}) + 17.80(\pm 0.36)$	0.58	<0.001
$\Delta_{SOM} = 4.83(\pm 0.36) \cdot (\log_{10}MAP) + 0.00(\pm 0.00) \cdot (\text{Longitude}) + 5.69(\pm 1.08)$	0.64	<0.001
$\Delta_{SOM} = 0.00(\pm 0.00) \cdot (MAP) + 0.00(\pm 0.00) \cdot (\text{Longitude}) + 17.76(\pm 0.23)$	0.59	<0.001
$\Delta_{SOM} = 0.01(\pm 0.01) \cdot (\text{Latitude}) + 5.07(\pm 0.35) \cdot (\log_{10}MAP) + 4.74(\pm 1.17)$	0.63	<0.001
$\Delta_{SOM} = 0.02(\pm 0.01) \cdot (\text{Latitude}) + 0.002(\pm 0.00) \cdot (MAP) + 16.76(\pm 0.49)$	0.59	<0.001
$\Delta_{SOM} = 4.69(\pm 0.48) \cdot (\log_{10}MAP) + 0.01(\pm 0.06) \cdot (\text{VPD Min}) + 6.00(\pm 1.39)$	0.37	<0.001
$\Delta_{SOM} = 0.00(\pm 0.00) \cdot (MAP) - 0.31(\pm 0.06) \cdot (\text{VPD Min}) + 18.45(\pm 0.16)$	0.33	<0.001
$\Delta_{SOM} = 2.14 \text{LN}(MAP) + 5.37$	0.64	<0.001
$\delta^{13}\text{C}_{SOM} = -2.04 \text{LN}(MAP) - 11.99$	0.68	<0.001

Table C3 All soil, paleosol, and reference data for modern and ancient samples included in this study. For soil carbon isotope data taken from literature, there is an accompanying reference to the published journal article.

labor et al. 2017	Upper Permian	Maradi, Niger	-6.0	-2.0	-23.8	-25.8	Presence of carbonates	862.47898	13.51	7.09	400.418						
labor et al. 2017	Upper Permian	Maradi, Niger	-6.0	-2.0	-24.2	-26.2	Presence of carbonates	1039.3464	13.51	7.09	400.418						
labor et al. 2017	Upper Permian	Maradi, Niger	-6.0	-2.0	-25.8	-27.8	Presence of carbonates	2191.8336	13.51	7.09	400.418						
labor et al. 2017	Upper Permian	Maradi, Niger	-6.0	-2.0	-26.8	-28.8	Presence of carbonates	3494.1142	13.51	7.09	400.418						
labor et al. 2017	Upper Permian	Maradi, Niger	-6.0	-2.0	-21.6	-23.6	Presence of carbonates	309.16019	13.51	7.09	400.418						
labor et al. 2017	Upper Permian	Maradi, Niger	-6.0	-2.0	-22.5	-24.5	Presence of carbonates	470.39223	13.51	7.09	400.418						
labor et al. 2017	Upper Permian	Maradi, Niger	-6.0	-2.0	-25.5	-27.5	Presence of carbonates	1905.6745	13.51	7.09	400.418						
labor et al. 2017	Upper Permian	Maradi, Niger	-6.0	-2.0	-24.7	-26.7	Presence of carbonates	1312.2757	13.51	7.09	400.418						
labor et al. 2017	Upper Permian	Maradi, Niger	-6.0	-2.0	-25.8	-27.8	Presence of carbonates	2191.8336	13.51	7.09	400.418						
labor et al. 2017	Upper Permian	Maradi, Niger	-6.0	-2.0	-24.2	-26.2	Presence of carbonates	1039.3464	13.51	7.09	400.418						
labor et al. 2017	Upper Permian	Maradi, Niger	-6.0	-2.0	-26.2	-28.2	Presence of carbonates	2641.3101	13.51	7.09	400.418						
labor et al. 2017	Upper Permian	Maradi, Niger	-6.0	-2.0	-26.6	-28.6	Presence of carbonates	3182.9601	13.51	7.09	400.418						
labor et al. 2017	Upper Permian	Maradi, Niger	-6.0	-2.0	-24.8	-26.8	Presence of carbonates	1374.922	13.51	7.09	400.418						
labor et al. 2017	Upper Permian	Maradi, Niger	-6.0	-2.0	-29.3	-31.3	Presence of carbonates	11211.428	13.51	7.09	400.418						
labor et al. 2017	Upper Permian	Maradi, Niger	-6.0	-2.0	-24.1	-26.1	Presence of carbonates	991.99019	13.51	7.09	400.418						
labor et al. 2017	Upper Permian	Maradi, Niger	-6.0	-2.0	-25.9	-27.9	Presence of carbonates	2296.4687	13.51	7.09	400.418						
labor et al. 2017	Upper Permian	Maradi, Niger	-6.0	-2.0	-23.6	-25.6	Presence of carbonates	785.67442	13.51	7.09	400.418						
labor et al. 2017	Upper Permian	Maradi, Niger	-6.0	-2.0	-24.5	-26.5	Presence of carbonates	1195.4163	13.51	7.09	400.418						
labor et al. 2017	Upper Permian	Maradi, Niger	-6.0	-2.0	-24.4	-26.4	Presence of carbonates	1140.949	13.51	7.09	400.418						
labor et al. 2017	Upper Permian	Maradi, Niger	-6.0	-2.0	-21.9	-23.9	Presence of carbonates	355.56417	13.51	7.09	400.418						
labor et al. 2017	Upper Permian	Maradi, Niger	-6.0	-2.0	-22.7	-24.7	Presence of carbonates	516.37599	13.51	7.09	400.418						
labor et al. 2017	Lower Triassic	Teloua, Niger	-6.0	-2.0	-20.9	-22.9	Presence of carbonates	223.05548	17.31	8.19	400.418						
labor et al. 2017	Lower Triassic	Teloua, Niger	-6.0	-2.0	-20.8	-22.8	Presence of carbonates	212.89229	17.31	8.19	400.418						
labor et al. 2017	Lower Triassic	Teloua, Niger	-6.0	-2.0	-22.1	-24.1	Presence of carbonates	390.34474	17.31	8.19	400.418						
labor et al. 2017	Lower Triassic	Teloua, Niger	-6.0	-2.0	-20.7	-22.7	Presence of carbonates	203.19218	17.31	8.19	400.418						
labor et al. 2017	Lower Triassic	Teloua, Niger	-6.0	-2.0	-21.7	-23.7	Presence of carbonates	323.91907	17.31	8.19	400.418						
labor et al. 2017	Middle Triassic	Manda, Tanzania	-6.0	-2.0	-25.4	-27.4	Presence of carbonates	1818.8453	-8.51	32.71	400.418						
labor et al. 2017	Middle Triassic	Manda, Tanzania	-6.0	-2.0	-24.8	-26.8	Presence of carbonates	1374.922	-8.51	32.71	400.418						
labor et al. 2017	Middle Triassic	Manda, Tanzania	-6.0	-2.0	-27.5	-29.5	Presence of carbonates	4842.9253	-8.51	32.71	400.418						
labor et al. 2017	Middle Triassic	Manda, Tanzania	-6.0	-2.0	-24.1	-26.1	Presence of carbonates	991.99019	-8.51	32.71	400.418						
labor et al. 2017	Middle Triassic	Manda, Tanzania	-6.0	-2.0	-24.4	-26.4	Presence of carbonates	1140.949	-8.51	32.71	400.418						
labor et al. 2017	Middle Triassic	Manda, Tanzania	-6.0	-2.0	-25.0	-27.0	Presence of carbonates	1509.3291	-8.51	32.71	400.418						
labor et al. 2017	Middle Triassic	Manda, Tanzania	-6.0	-2.0	-24.7	-26.7	Presence of carbonates	1312.2757	-8.51	32.71	400.418						
labor et al. 2017	Middle Triassic	Manda, Tanzania	-6.0	-2.0	-26.9	-28.9	Presence of carbonates	3860.9184	-8.51	32.71	400.418						
labor et al. 2017	Middle Triassic	Manda, Tanzania	-6.0	-2.0	-24.5	-26.5	Presence of carbonates	1195.4163	-8.51	32.71	400.418						
labor et al. 2017	Middle Triassic	Manda, Tanzania	-6.0	-2.0	-24.7	-26.7	Presence of carbonates	1312.2757	-8.51	32.71	400.418						
labor et al. 2017	Middle Triassic	Manda, Tanzania	-6.0	-2.0	-24.6	-26.6	Presence of carbonates	1252.4839	-8.51	32.71	400.418						
labor et al. 2017	Middle Triassic	Manda, Tanzania	-6.0	-2.0	-26.7	-28.7	Presence of carbonates	3334.9102	-8.51	32.71	400.418						
labor et al. 2017	Middle Triassic	Manda, Tanzania	-6.0	-2.0	-25.4	-27.4	Presence of carbonates	1818.8453	-8.51	32.71	400.418						
labor et al. 2017	Middle Triassic	Manda, Tanzania	-6.0	-2.0	-24.3	-26.3	Presence of carbonates	1088.9634	-8.51	32.71	400.418						
labor et al. 2017	Middle Triassic	Manda, Tanzania	-6.0	-2.0	-24.8	-26.8	Presence of carbonates	1374.922	-8.51	32.71	400.418						
labor et al. 2017	Middle Triassic	Manda, Tanzania	-6.0	-2.0	-23.5	-25.5	Presence of carbonates	749.87636	-8.51	32.71	400.418						
labor et al. 2017	Middle Triassic	Manda, Tanzania	-6.0	-2.0	-24.3	-26.3	Presence of carbonates	1088.9634	-8.51	32.71	400.418						
labor et al. 2017	Upper Permian	Madumabisa, Zambia	-6.0	-2.0	-21.5	-23.5	Presence of carbonates	295.07377			400.418						
labor et al. 2017	Upper Permian	Madumabisa, Zambia	-6.0	-2.0	-20.7	-22.7	Presence of carbonates	203.19218			400.418						
labor et al. 2017	Upper Permian	Madumabisa, Zambia	-6.0	-2.0	-21.7	-23.7	Presence of carbonates	323.91907			400.418						
labor et al. 2017	Upper Permian	Madumabisa, Zambia	-6.0	-2.0	-21.1	-23.1	Presence of carbonates	244.86054			400.418						
labor et al. 2017	Upper Permian	Madumabisa, Zambia	-6.0	-2.0	-24.0	-26.0	Presence of carbonates	946.79167			400.418						
labor et al. 2017	Upper Permian	Madumabisa, Zambia	-6.0	-2.0	-21.3	-23.3	Presence of carbonates	268.79718			400.418						
labor et al. 2017	Upper Permian	Madumabisa, Zambia	-6.0	-2.0	-21.0	-23.0	Presence of carbonates	233.70384			400.418						
labor et al. 2017	Upper Permian	Madumabisa, Zambia	-6.0	-2.0	-21.0	-23.0	Presence of carbonates	233.70384			400.418						
labor et al. 2017	Upper Permian	Madumabisa, Zambia	-6.0	-2.0	-21.0	-23.0	Presence of carbonates	233.70384			400.418						
labor et al. 2017	Upper Permian	Madumabisa, Zambia	-6.0	-2.0	-20.8	-22.8	Presence of carbonates	212.89229			400.418						
labor et al. 2017	Upper Permian	Madumabisa, Zambia	-6.0	-2.0	-21.1	-23.1	Presence of carbonates	244.86054			400.418						
labor et al. 2017	Upper Permian	Madumabisa, Zambia	-6.0	-2.0	-21.2	-23.2	Presence of carbonates	256.54984			400.418						
labor et al. 2017	Upper Permian	Madumabisa, Zambia	-6.0	-2.0	-23.9	-25.9	Presence of carbonates	903.62524			400.418						
labor et al. 2017	Upper Permian	Madumabisa, Zambia	-6.0	-2.0	-22.6	-24.6	Presence of carbonates	492.8481			400.418						
labor et al. 2017	Upper Permian	Madumabisa, Zambia	-6.0	-2.0	-22.4	-24.4	Presence of carbonates	448.95952			400.418						
labor et al. 2017	Upper Permian	Madumabisa, Zambia	-6.0	-2.0	-20.5	-22.5	Presence of carbonates	185.09773			400.418						
labor et al. 2017	Upper Permian	Madumabisa, Zambia	-6.0	-2.0	-19.5	-21.5	Presence of carbonates	116.11052			400.418						
labor et al. 2017	Upper Permian	Madumabisa, Zambia	-6.0	-2.0	-23.7	-25.7	Presence of carbonates	823.16144			400.418						
labor et al. 2017	Upper Permian	Ikakern, Morocco	-6.0	-2.0	-25.4	-27.4	Presence of carbonates	1818.8453	30.82	-8.99	400.418						
labor et al. 2017	Upper Permian	Ikakern, Morocco	-6.0	-2.0	-24.7	-26.7	Presence of carbonates	1312.2757	30.82	-8.99	400.418						
labor et al. 2017	Upper Permian	Ikakern, Morocco	-6.0	-2.0	-24.8	-26.8	Presence of carbonates	1374.922	30.82	-8.99	400.418						
labor et al. 2017	Upper Permian	Ikakern, Morocco	-6.0	-2.0	-24.8	-26.8	Presence of carbonates	1374.922	30.82	-8.99	400.418						
labor et al. 2017	Upper Permian	Ikakern, Morocco	-6.0	-2.0	-24.1	-26.1	Presence of carbonates	991.99019	30.82	-8.99	400.418						
labor et al. 2017	Upper Permian	Ikakern, Morocco	-6.0	-2.0	-24.4	-26.4	Presence of carbonates	1140.949	30.82	-8.99	400.418						
labor et al. 2017	Upper Permian	Ikakern, Morocco	-6.0	-2.0	-23.5	-25.5	Presence of carbonates	749.87636	30.82	-8.99	400.418						
labor et al. 2017	Upper Permian	Ikakern, Morocco	-6.0	-2.0	-23.2	-25.2	Presence of carbonates	651.97479	30.82	-8.99	400.418						
labor et al. 2017	Upper Permian	Ikakern, Morocco	-6.0	-2.0	-23.3	-25.3	Presence of carbonates	683.09917	30.82	-8.99	400.418						
labor et al. 2017	Upper Permian	Ikakern, Morocco	-6.0	-2.0	-23.9	-25.9	Presence of carbonates	903.62524	30.82	-8.99	400.418						
labor et al. 2017	Upper Permian	Balfour, South Africa	-6.0	-2.0	-26.1	-28.1	Presence of carbonates	2520.9628	-26.67	28.56	400.418						
labor et al. 2017	Upper Permian	Balfour, South Africa	-6.0	-2.0	-25.8	-27.8	Presence of carbonates	2191.8336	-26.67	28.56	400.418						
labor et al. 2017	Upper Permian	Balfour, South Africa	-6.0	-2.0	-25.9	-27.9	Presence of carbonates	2296.4687	-26.67	28.56	400.418						
labor et al. 2017	Upper Permian	Balfour, South Africa	-6.0	-2.0	-26.6	-28.6	Presence of carbonates	3182.9601	-26.67	28.56	400.418						
Pustovoytov & Teyhorst 2004	Quaternary	Wurm, Schattenhausen	-6.5	-1.5	-25.4	-26.9		200	851	543.02083	1420.5454	509.20207	1649.1667	1079.1844			
Pustovoytov & Teyhorst 2004	Quaternary	Wurm, Schattenhausen	-6.5	-1.5	-23.3	-24.8		548.64936							49.35	8.72	400.418
Pustovoytov & Teyhorst 2004	Quaternary	Wurm, Schattenhausen	-6.5	-1.5	-24.2	-25.7		807.96842							49.35	8.72	400.418
Pustovoytov & Teyhorst 2004	Quaternary	Wurm, Schattenhausen	-6.5	-1.5	-24.6	-26.1		996.52706							49.35	8.72	400.418
Pustovoytov & Teyhorst 2004	Quaternary	Wurm, Schattenhausen	-6.5	-1.5	-23.2	-24.7		509.20207							49.35	8.72	400.418
Pustovoytov & Teyhorst 2004	Quaternary	Wurm, Schattenhausen	-6.5	-1.5	-24.2	-25.7		834.77888							49.35	8.72	400.418
Pustovoytov & Teyhorst 2004	Quaternary	Wurm, Schattenhausen	-6.5	-1.5	-24.7	-26.2		1053.9893							49.35	8.72	400.418
Pustovoytov & Teyhorst 2004	Quaternary	Wurm, Schattenhausen	-6.5	-1.5	-24.0	-25.5		763.99558							49.35	8.72	400.418
Pustovoytov & Teyhorst 2004	Quaternary	Riss, Schattenhausen	-6.5	-1.5	-24.5	-26.0		960.1306							49.35	8.72	400.418
Pustovoytov & Teyhorst 2004	Quaternary	Riss, Schattenhausen	-6.5	-1.5	-24.4	-25.9		916.38371							49.35	8.72	400.418
Pustovoytov & Teyhorst 2004	Quaternary	Riss, Schattenhausen	-6.5	-1.5	-24.0	-25.5		753.38151							49.35	8.72	400.418
Pustovoytov & Teyhorst 2004	Quaternary	Riss, Schattenhausen	-6.5	-1.5	-24.0	-25.5		736.01808							49.35	8.72	400.418
Pustovoytov & Teyhorst 2004	Quaternary	Riss, Schattenhausen	-6.5	-1.5	-24.8	-26.3		1078.854							49.35	8.72	400.418
Pustovoytov & Teyhorst 2004	Quaternary	Riss, Schattenhausen	-6.5	-1.5	-24.6	-26.1		1001.2856							49.35	8.72	400.418
Pustovoytov & Teyhorst 2004	Quaternary	Riss, Schattenhausen	-6.5	-1.5	-24.9	-26.4		1146.2822							49.35	8.72	400.418

Pustovoytov & Tehorst 2004	Quaternary	Riss, Schattenuhausen	-6.5	-1.5	-25.7	-27.2			1649.1667			49.35	8.72	400.418				
Hatte et al. 2001	Nussloch	-7.0	-1.0	-24.7	-25.7	Pollen	315	315	315	823.18144	823.18144	823.18144	823.18144	16000	49.35	8.72	400.418	180
Hatte et al. 2001	Nussloch	-6.9	-1.1	-24.9	-26.0	Pollen	402	402	402	946.79167	946.79167	946.79167	946.79167	17000	49.35	8.72	400.418	180
Hatte et al. 2001	Nussloch	-6.9	-1.1	-24.9	-26.0	Pollen	495	495	495	946.79167	946.79167	946.79167	946.79167	18000	49.35	8.72	400.418	180
Hatte et al. 2001	Nussloch	-6.5	-1.5	-25.0	-26.5	Pollen	597	597	597	1195.4163	1195.4163	1195.4163	1195.4163	19000	49.35	8.72	400.418	180
Hatte et al. 2001	Nussloch	-6.5	-1.5	-24.8	-26.3	Pollen	621	621	621	1088.9634	1088.9634	1088.9634	1088.9634	20000	49.35	8.72	400.418	180
Hatte et al. 2001	Nussloch	-6.5	-1.5	-24.3	-25.8	Pollen	551	551	551	862.47898	862.47898	862.47898	862.47898	21000	49.35	8.72	400.418	180
Hatte et al. 2001	Nussloch	-6.5	-1.5	-24.2	-25.7	Pollen	570	570	570	823.18144	823.18144	823.18144	823.18144	22000	49.35	8.72	400.418	180
Hatte et al. 2001	Nussloch	-6.5	-1.5	-24.2	-25.7	Pollen	532	532	532	823.18144	823.18144	823.18144	823.18144	23000	49.35	8.72	400.418	180
Hatte et al. 2001	Nussloch	-6.5	-1.5	-24.0	-25.5	Pollen	527	527	527	749.87636	749.87636	749.87636	749.87636	24000	49.35	8.72	400.418	180
Hatte et al. 2001	Nussloch	-6.5	-1.5	-24.1	-25.6	Pollen	612	612	612	785.67442	785.67442	785.67442	785.67442	25000	49.35	8.72	400.418	180
Hatte et al. 2001	Nussloch	-6.5	-1.5	-24.1	-25.6	Pollen	575	575	575	785.67442	785.67442	785.67442	785.67442	26000	49.35	8.72	400.418	180
Hatte et al. 2001	Nussloch	-6.5	-1.5	-24.1	-25.6	Pollen	550	550	550	785.67442	785.67442	785.67442	785.67442	27000	49.35	8.72	400.418	180
Hatte et al. 2001	Nussloch	-6.5	-1.5	-24.1	-25.6	Pollen	474	474	474	785.67442	785.67442	785.67442	785.67442	28000	49.35	8.72	400.418	180
Hatte et al. 2001	Nussloch	-6.5	-1.5	-24.2	-25.7	Pollen	545	545	545	823.18144	823.18144	823.18144	823.18144	29000	49.35	8.72	400.418	180
Hatte et al. 2001	Nussloch	-6.5	-1.5	-24.2	-25.7	Pollen	617	617	617	823.18144	823.18144	823.18144	823.18144	30000	49.35	8.72	400.418	180
Hatte et al. 2001	Nussloch	-6.5	-1.5	-24.2	-25.7	Pollen	591	591	591	823.18144	823.18144	823.18144	823.18144	31000	49.35	8.72	400.418	180
Hatte et al. 2001	Nussloch	-6.5	-1.5	-24.7	-26.2	Pollen	691	691	691	1039.3464	1039.3464	1039.3464	1039.3464	32000	49.35	8.72	400.418	180
Hatte et al. 2001	Nussloch	-6.5	-1.5	-24.5	-26.0	Pollen	581	581	581	946.79167	946.79167	946.79167	946.79167	33000	49.35	8.72	400.418	180
Hatte et al. 2001	Nussloch	-6.5	-1.5	-24.4	-25.9	Pollen	512	512	512	903.65254	903.65254	903.65254	903.65254	34000	49.35	8.72	400.418	180
Hatte et al. 2001	Nussloch	-6.5	-1.5	-24.3	-25.8	Pollen	490	490	490	862.47898	862.47898	862.47898	862.47898	44000	49.35	8.72	400.418	180
Hatte et al. 2001	Nussloch	-6.5	-1.5	-24.4	-25.9	Pollen	569	569	569	903.65254	903.65254	903.65254	903.65254	45000	49.35	8.72	400.418	180
Hatte et al. 2001	Nussloch	-6.5	-1.5	-24.6	-26.1	Pollen	672	672	672	991.99019	991.99019	991.99019	991.99019	46000	49.35	8.72	400.418	180
Hatte et al. 2001	Nussloch	-6.5	-1.5	-24.6	-26.1	Pollen	727	727	727	991.99019	991.99019	991.99019	991.99019	47000	49.35	8.72	400.418	180
Hatte et al. 2001	Nussloch	-6.5	-1.5	-24.7	-26.2	Pollen	745	745	745	1039.3464	1039.3464	1039.3464	1039.3464	48000	49.35	8.72	400.418	180
Hatte et al. 2001	Nussloch	-6.5	-1.5	-24.7	-26.2	Pollen	699	699	699	1039.3464	1039.3464	1039.3464	1039.3464	49000	49.35	8.72	400.418	180
Hatte et al. 2001	Nussloch	-6.5	-1.5	-24.5	-26.0	Pollen	579	579	579	946.79167	946.79167	946.79167	946.79167	50000	49.35	8.72	400.418	180
Hatte et al. 2001	Nussloch	-6.5	-1.5	-24.1	-25.6	Pollen	462	462	462	785.67442	785.67442	785.67442	785.67442	51000	49.35	8.72	400.418	180
Hatte et al. 2001	Nussloch	-6.5	-1.5	-23.9	-25.4	Pollen	379	379	379	715.70938	715.70938	715.70938	715.70938	52000	49.35	8.72	400.418	180
Hatte et al. 2001	Nussloch	-6.5	-1.5	-23.8	-25.3	Pollen	342	342	342	683.09917	683.09917	683.09917	683.09917	53000	49.35	8.72	400.418	180
Hatte et al. 2001	Nussloch	-6.5	-1.5	-24.0	-25.5	Pollen	412	412	412	749.87636	749.87636	749.87636	749.87636	54000	49.35	8.72	400.418	180
Hatte et al. 2001	Nussloch	-6.5	-1.5	-24.0	-25.5	Pollen	408	408	408	749.87636	749.87636	749.87636	749.87636	55000	49.35	8.72	400.418	180
Hatte et al. 2001	Nussloch	-6.5	-1.5	-23.8	-25.3	Pollen	366	366	366	683.09917	683.09917	683.09917	683.09917	56000	49.35	8.72	400.418	180
Hatte et al. 2001	Nussloch	-6.5	-1.5	-23.8	-25.3	Pollen	373	373	373	683.09917	683.09917	683.09917	683.09917	57000	49.35	8.72	400.418	180
Hatte et al. 2001	Nussloch	-6.5	-1.5	-23.7	-25.2	Pollen	343	343	343	651.97479	651.97479	651.97479	651.97479	58000	49.35	8.72	400.418	180
Hatte et al. 2001	Nussloch	-6.5	-1.5	-23.7	-25.2	Pollen	277	277	277	651.97479	651.97479	651.97479	651.97479	59000	49.35	8.72	400.418	180
Hatte et al. 2001	Nussloch	-6.5	-1.5	-23.6	-25.1	Pollen	200	200	200	622.26855	622.26855	622.26855	622.26855	60000	49.35	8.72	400.418	180
Hatte et al. 2001	Nussloch	-6.5	-1.5	-23.9	-25.4	Pollen	295	295	295	715.70938	715.70938	715.70938	715.70938	61000	49.35	8.72	400.418	180
Hatte et al. 2001	Nussloch	-6.5	-1.5	-24.7	-26.2	Pollen	542	542	542	1039.3464	1039.3464	1039.3464	1039.3464	62000	49.35	8.72	400.418	180
Hatte et al. 2001	Nussloch	-6.5	-1.5	-24.6	-26.1	Pollen	533	533	533	991.99019	991.99019	991.99019	991.99019	63000	49.35	8.72	400.418	180
Hatte et al. 2001	Nussloch	-6.5	-1.5	-24.5	-26.0	Pollen	530	530	530	946.79167	946.79167	946.79167	946.79167	64000	49.35	8.72	400.418	180
Hatte et al. 2001	Nussloch	-6.5	-1.5	-24.6	-26.1	Pollen	570	570	570	991.99019	991.99019	991.99019	991.99019	65000	49.35	8.72	400.418	180
Hatte et al. 2001	Nussloch	-6.5	-1.5	-24.8	-26.3	Pollen	652	652	652	1088.9634	1088.9634	1088.9634	1088.9634	66000	49.35	8.72	400.418	180
Hatte et al. 2001	Nussloch	-6.5	-1.5	-24.9	-26.4	Pollen	694	694	694	1140.949	1140.949	1140.949	1140.949	67000	49.35	8.72	400.418	180
Hatte et al. 2001	Nussloch	-6.5	-1.5	-25.0	-26.5	Pollen	750	750	750	1195.4163	1195.4163	1195.4163	1195.4163	68000	49.35	8.72	400.418	180
Hatte et al. 2001	Nussloch	-6.5	-1.5	-24.7	-26.2	Pollen	698	698	698	1039.3464	1039.3464	1039.3464	1039.3464	69000	49.35	8.72	400.418	180
Hatte et al. 2001	Nussloch	-6.5	-1.5	-24.8	-26.3	Pollen	722	722	722	1088.9634	1088.9634	1088.9634	1088.9634	70000	49.35	8.72	400.418	180
Hatte et al. 2001	Nussloch	-6.5	-1.5	-25.2	-26.7	Pollen	851	851	851	1312.2757	1312.2757	1312.2757	1312.2757	71000	49.35	8.72	400.418	180
Hatte et al. 2001	Nussloch	-6.5	-1.5	-25.2	-26.7	Pollen	827	827	827	1312.2757	1312.2757	1312.2757	1312.2757	72000	49.35	8.72	400.418	180

Figure C1 $\delta^{13}\text{C}_{\text{SOM}}$ and Δ_{SOM} versus climate variables (a-b) elevation, (c-d) mean annual temperature, (e-f) Vapor Pressure Deficit Maximums, (g-h) Vapor Pressure Deficit Minimums.

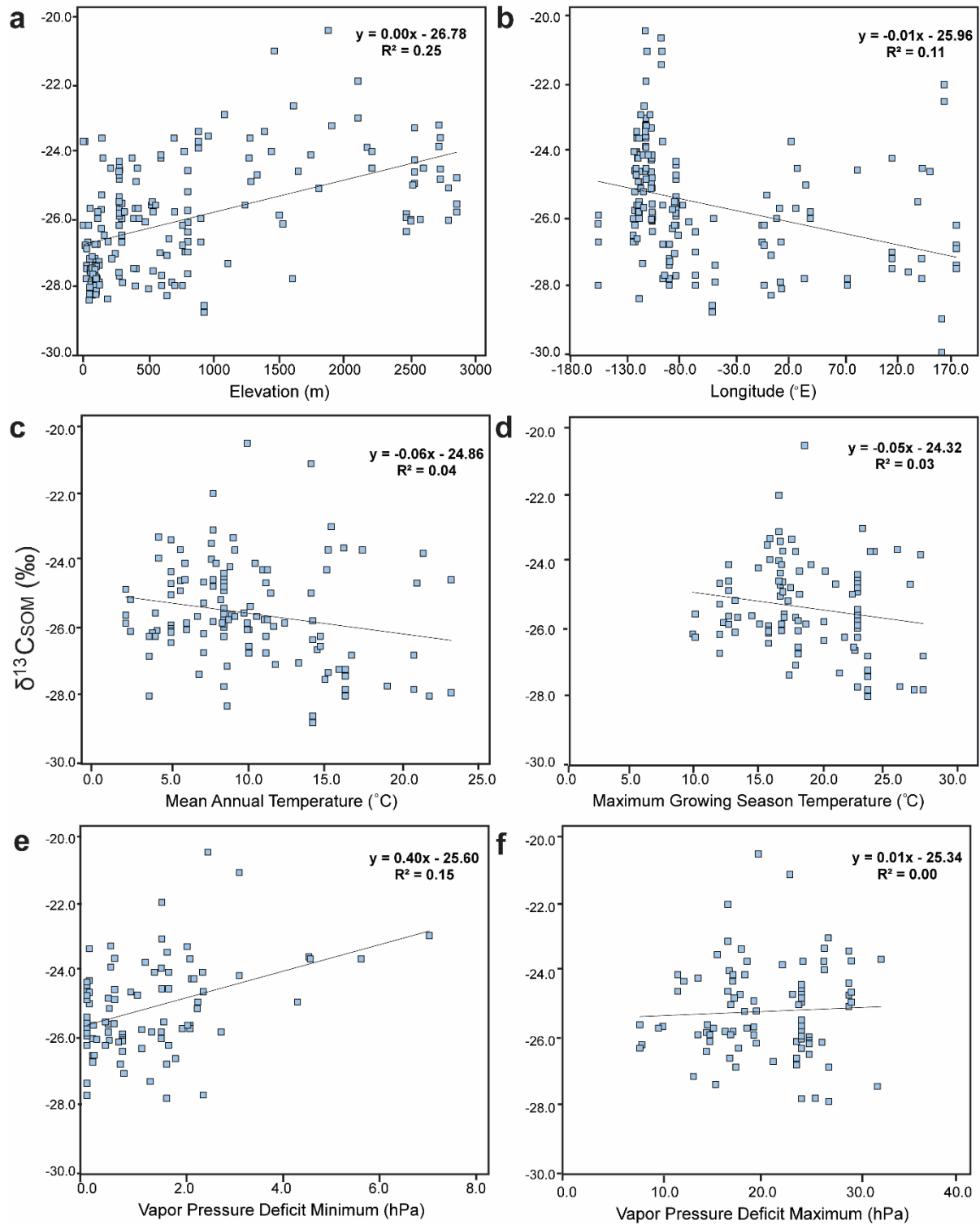


Figure C2 (a) $\delta^{13}\text{C}_{\text{SOM}}$ values compared to growing season precipitation for modern soils (mm yr^{-1}). All soils for which growing season precipitation was available are shown in light blue squares. The best fit logarithmic trend line had an equation of $\delta^{13}\text{C}_{\text{SOM}} = -0.99\ln(\text{GSP}) - 19.65$ and $R^2 = 0.27$. (b) Shows the relationship between mean annual precipitation and growing season precipitation.

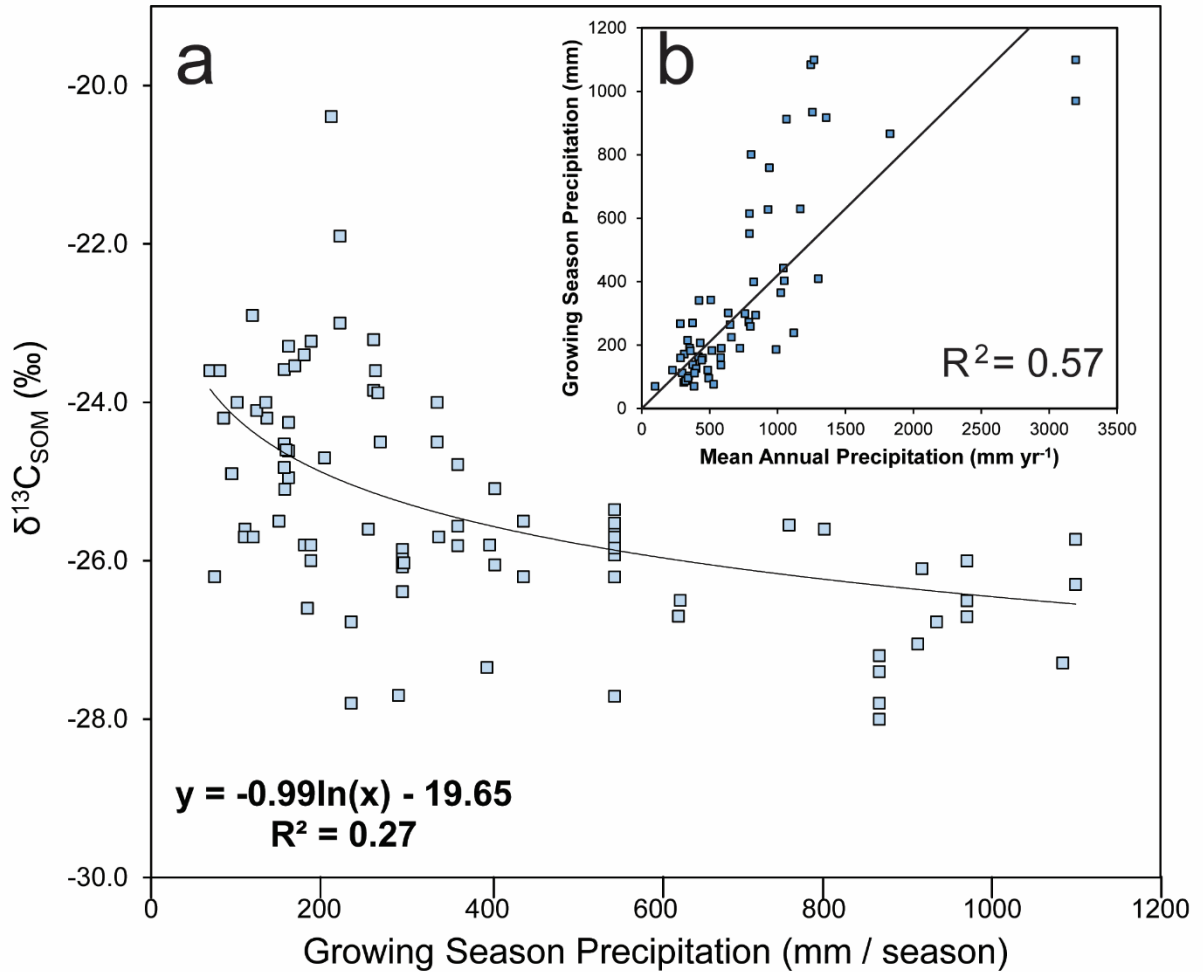


Figure C3 Actual mean annual precipitation values (in mm yr⁻¹) as collected from PRISM and extra-contiguous United States data sources as compared to reconstructed mean annual precipitation values (in mm yr⁻¹) using Equation 4.1. Data from this study are shown in yellow squares, soils from literature data are shown in blue squares, and outliers from our dataset (MAP = 3350 mm yr⁻¹) are shown in yellow circles ($y = 1.02x + 44.85$; $R^2 = 0.68$, $p\text{-value} < 0.001$).

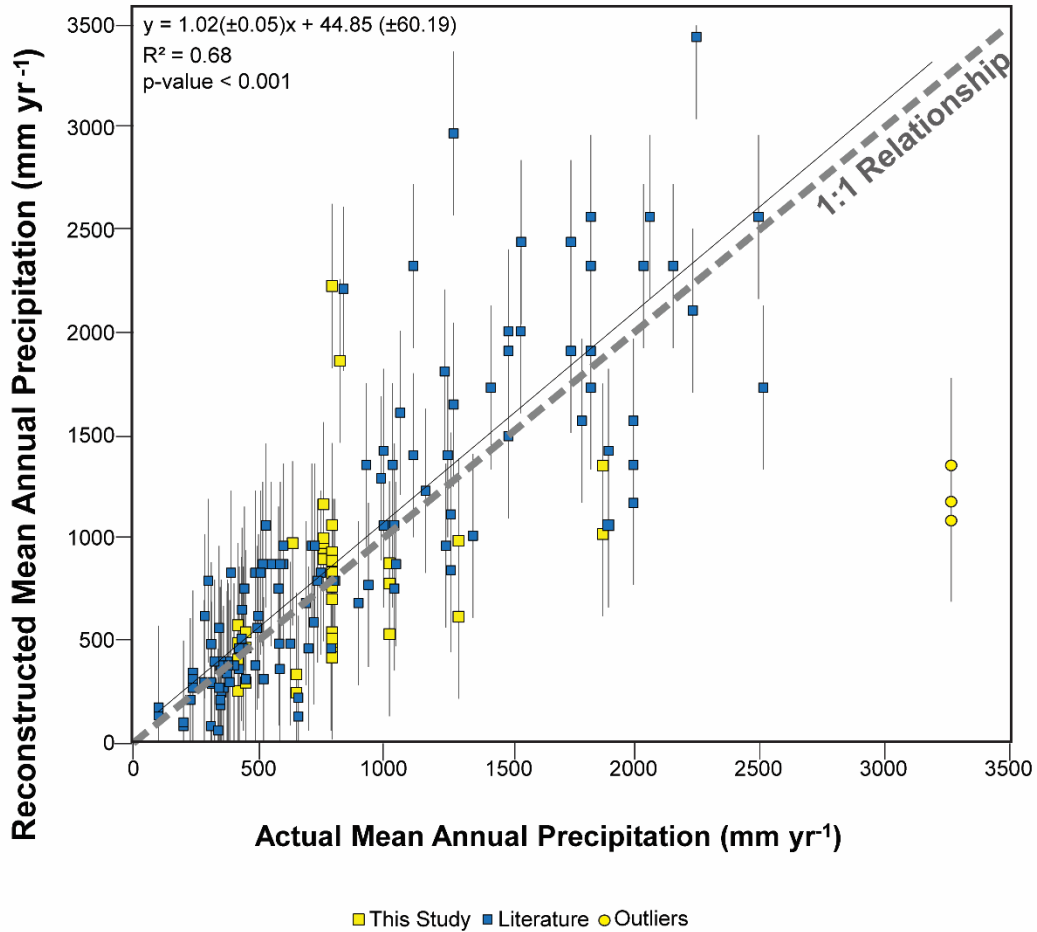


Figure C4 (a) $\delta^{13}\text{C}_{\text{SOM}}$ values compared to mean annual precipitation (mm yr^{-1}) for modern soils divided by soil order. (b) Actual mean annual precipitation compared to reconstructed mean annual precipitation using the logarithmic relationship modeled divided by soil order (Equation 4.5). The 1:1 relationship is shown by the dashed line. This supplements Figure 2 and Supplemental Figure 3 with more information on soil order.

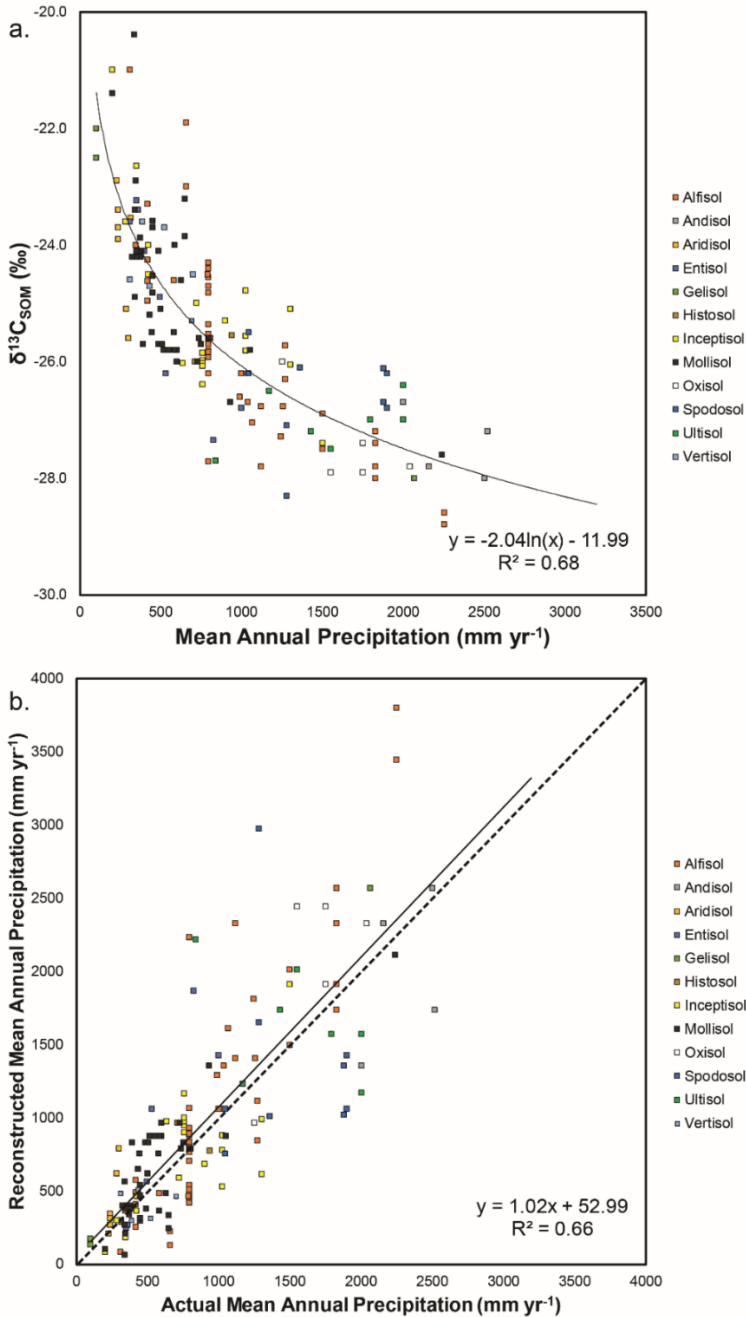


Figure C5 Map of paleosol sites. Red squares represent soils from the Paleozoic, orange squares represent soils from the Mesozoic, and yellow soils represent soils from the early Cenozoic (Paleocene) through the Quaternary (but not modern).

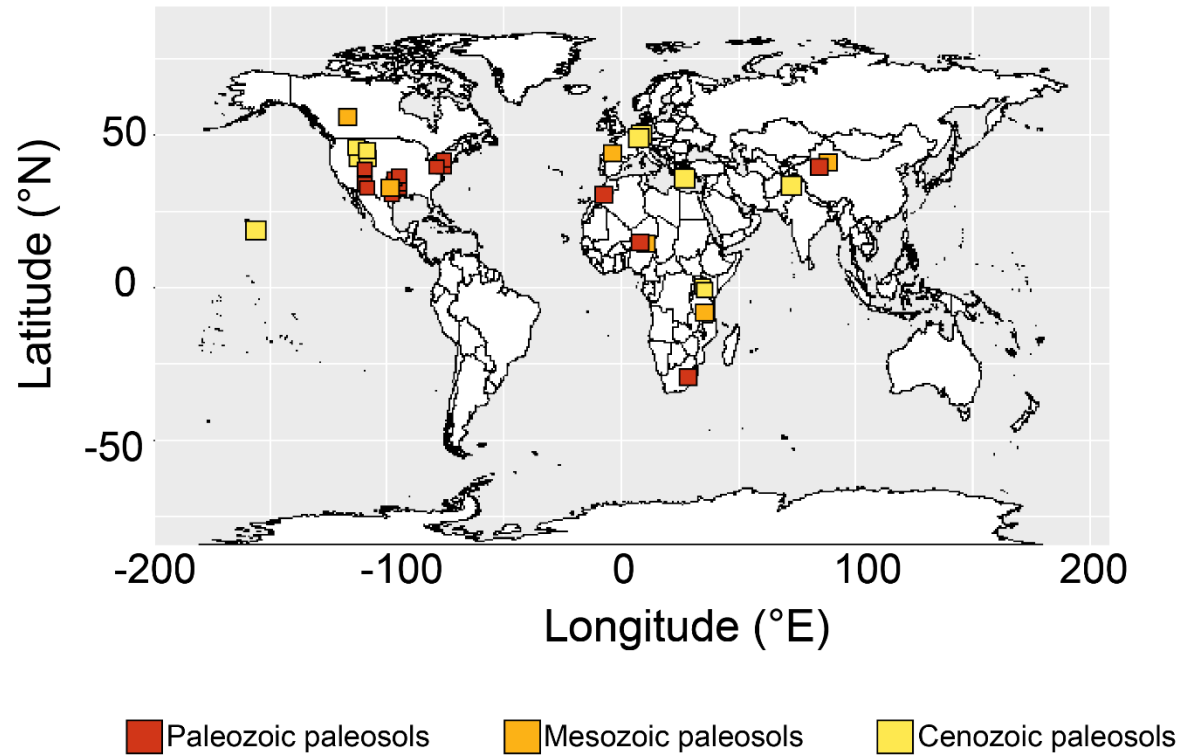


Figure C6 Violin plots showing the distribution of $\delta^{13}\text{C}_{\text{SOM}}$ values in angiosperm- and gymnosperm- dominated ecosystems. The mean $\delta^{13}\text{C}_{\text{SOM}}$ value for angiosperm dominated ecosystems was -25.68% , and the mean $\delta^{13}\text{C}_{\text{SOM}}$ value for gymnosperm dominated ecosystems was -25.52% and are not statistically different (p -value = 0.27).

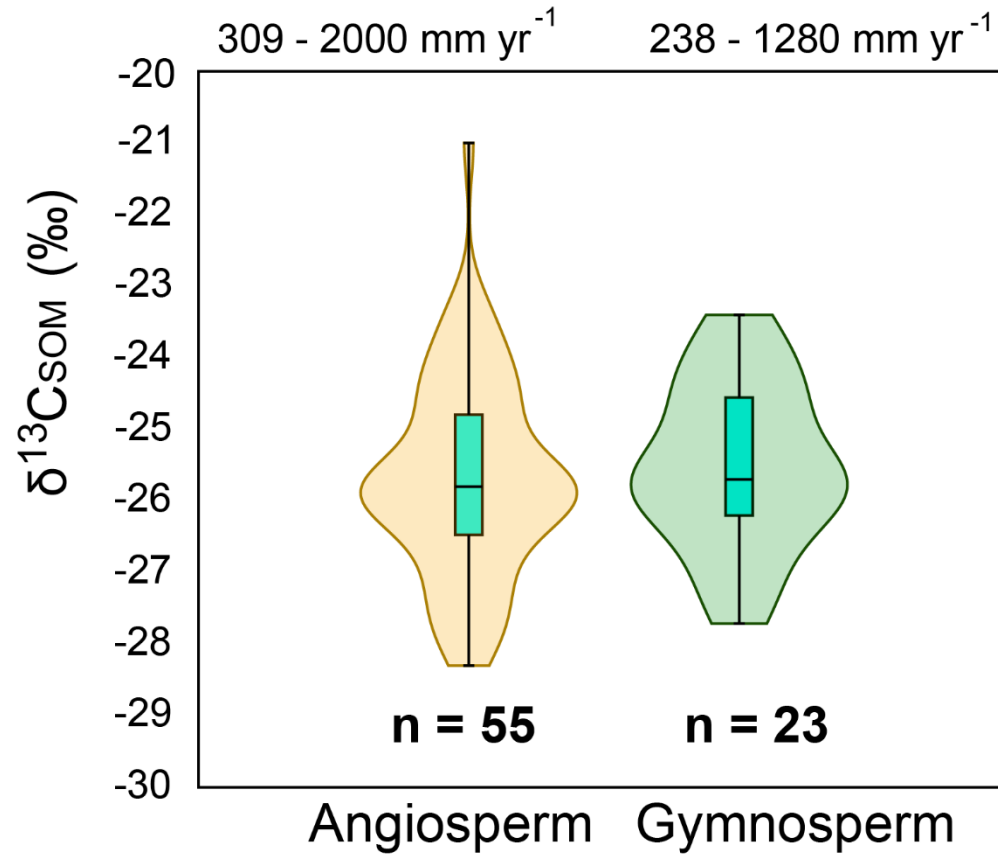
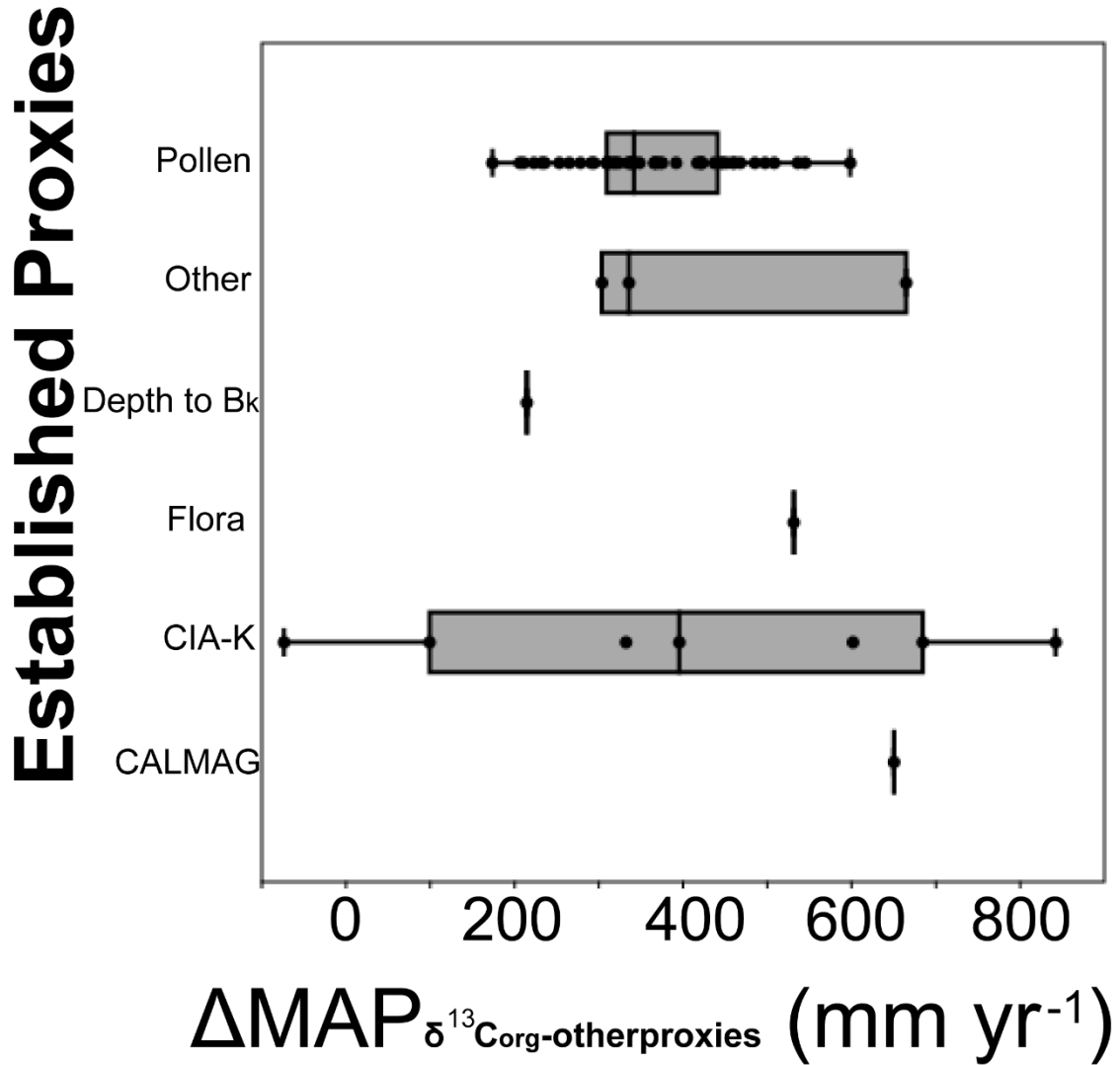


Figure C7 Box plots showing the range of residual values between precipitation reconstructed using the $\delta^{13}\text{C}_{\text{SOM}}$ -paleoprecipitation proxy in this study, and other established proxies, divided by proxy. The whiskers show standard error and points show actual residual values as calculated by subtracting $\text{MAP}_{\delta^{13}\text{CSOM}} - \text{MAP}_{\text{other}}$.



APPENDIX D

Supplemental Table, Figures, and Methods for Chapter V

Table D1: Paleosol features, including color, evidence of disturbance, texture and depth.

Sample ID	Paleosol #	Depth (cm)	Horizon	Root traces, rhizoliths	Redox Haloes	Burrows	Peds	Color (descriptive + Munsell)	Texture
19BRWY1UA	1	0	A	Yes				5Y 6/1	
19BRWY1LA	1	-12	A	Yes			Yes	2.5Y 6/1	silt sandstone
19BRWY1LC	1	-18	C					dark brown, 10YR 5/2	silt sandstone, no bedding, not laminated
19BRWY2UA	2	0 to -5	A	Yes	Yes			green grey, 2.5Y 7/3	
19BRWY2UB	2	-25	B			Yes, up to 1 cm		5Y 7/2	
19BRWY2MB	2	-50	B			Yes, up to 1 cm		olive, 5Y 7/2	mudstone
19BRWY2LB	2	-75	B					2.5YR 7/3	
19BRWY2C	2	-85	C	Yes, very fine				dark grey, GLEY1 7/10Y	clay-silt to silty clay, laminated
19BRWY3UA	3	0	A	Yes				brown green, 5Y 7/2	
19BRWY3UB	3	-35	B					grey-brown, 5Y 8/1	silty mudstone
19BRWY3MB	3	-45	B					10YR 7/1	
19BRWY3C	3	-75	C					dark grey, 5Y 7/1	mudstone
19BRWY4UB1	4	0	B	Yes	Yes			10YR 7/2	sandy
19BRWY4UB2	4	-15	B					GLEY1 7/10Y	sandy mudstone
19BRWY4LB	4	-30	B					2.5Y 6/2	shale, mudstone
19BRWY4C	4	-60	C					5Y 8/1	shale, mudstone
19BRWY5UA	5	0	A	Yes				dark grey, green	silty mudstone
19BRWY5UB	5	-20	B	Yes				5Y 7/1	siltstone
19BRWY5MB	5	-35	B					5Y 7/2	
19BRWY5C	5	-80	C					dark grey, 5Y 6/1	massive fine sand mudstone
19BRWY6UA	6	0	A					10YR 7/1	
19BRWY6UB	6	-42	B					5Y 7/1	
19BRWY6MB	6	-72	B					5Y 7/2	shale, mudstone
19BRWY6C	6	-112	C					2.5Y 5/1	shale, mudstone

Table D2: All bulk geochemical and carbon isotope data from the Blue Rim escarpment. Includes climate reconstructions for the stratigraphic sections and paleosols, as well as $\delta^{13}\text{C}_{\text{atm}}$ values reconstructed from $\delta^{13}\text{C}_{\text{fossil}}$ values.

Strat	Colun	Paleosols	CIA	CIA-K	MAP mm	yi	PWI	Temperatur	SAL	T from	Sal	Provenance	Provenance	Hydrolysis	Leaching	Parent Matr	Parent Matr	Leaching	
Sample ID#	Height (m)	Depth (cm)	Molar Ratio	Molar Ratio	from CIA-K	Gallagher &	from PWI	(Na+K/Al)	(T = -18.5S+Ti/Al)	Zr/Al	Bases / Al	Bases/Ti	La/Ce	U/Th	Ba/Sr				
19BRWY1																			
UA	1	0	74.944715	89.514881	n/a	n/a	n/a	0.2717351	n/a	0.0268739	3.31516E-05	0.6026127	11.214908	0.5168947	0.1720291	1.1913594			
19BRWY1																			
LA	1	-12	73.545233	88.663408	n/a	n/a	n/a	0.2863974	n/a	0.0264247	2.92719E-05	0.6604345	12.499913	0.5007958	0.1629943	1.1714			
19BRWY1																			
LC	1	-18	72.689671	89.62809	n/a	n/a	n/a	0.3235925	n/a	0.0234199	3.39765E-05	0.7796215	16.648938	0.4267995	0.1678518	1.9688065			
19BRWY2																			
UA	1	0	68.83903	83.54252	n/a	n/a	n/a	0.3128456	n/a	0.0239924	2.90733E-05	0.8340616	17.386475	0.4691002	0.1798582	1.3870416			
19BRWY2																			
UB	1	-25	28.035873	30.050058	n/a	n/a	n/a	0.3007465	n/a	0.024065	3.02431E-05	3.0954478	64.331599	0.47987	0.249272	1.1000675			
19BRWY2																			
MB	1	-50	13.473773	13.911244	n/a	n/a	n/a	0.3168156	n/a	0.0237629	3.30279E-05	7.0366995	148.10088	0.4834596	0.5903706	0.852679			
19BRWY2																			
LB	1	-75	36.009847	39.651465	n/a	n/a	n/a	0.4179855	n/a	0.0262274	2.83449E-05	2.3351605	44.529641	0.459205	0.3557779	2.146309			
19BRWY2																			
C	1	-85	73.754133	88.09115	n/a	n/a	n/a	0.2852716	n/a	0.0291812	2.96744E-05	0.6962869	11.933631	0.4800297	0.2261609	0.3052819			
19BRWY3																			
UA	1	0	72.03009	88.215427	n/a	29.692129	12.098983	0.3434965	n/a	0.0262651	3.06959E-05	0.7208159	13.725622	0.4215358	0.1707734	2.311736			
19BRWY3																			
UB	1	-35	71.701149	87.879767	1174.1863	30.105263	12.061122	0.3550163	10.732198	0.0257806	3.06319E-05	0.7595271	14.734585	0.4094801	0.1911434	2.5626162			
19BRWY3																			
MB	1	-45	71.097649	87.302013	1161.3673	30.749262	12.003127	0.364243	10.561504	0.0258389	3.23167E-05	0.7933737	15.356466	0.4285178	0.1715703	2.7304731			
19BRWY3																			
C	1	-75	55.081669	63.991448	n/a	50.017213	10.670114	0.3481233	n/a	0.0256444	2.76112E-05	1.5795586	30.805667	0.4451566	0.1900393	1.9661629			
19BRWY4																			
UB1	1	0	73.131081	89.817636	1218.225	36.125421	11.561629	0.3228134	11.327951	0.0234806	3.09336E-05	0.7887974	16.801355	0.4655718	0.1551635	2.45225			
19BRWY4																			
UB2	1	-15	23.757925	25.243978	357.18386	102.5982	8.7015521	0.3139351	11.492201	0.024477	3.22941E-05	5.753632	117.56314	0.4305623	0.4964419	0.4678087			
19BRWY4																			
LB	1	-30	77.651518	89.591345	1212.9985	24.140455	12.666144	0.2032231	13.540372	0.0273167	2.55578E-05	0.5411209	9.9072712	0.5461501	0.3030023	1.1783606			
19BRWY4																			
C	1	-60	76.87393	87.837298	n/a	25.231752	12.544997	0.1968809	n/a	0.0272168	2.77287E-05	0.5538542	10.177622	0.4965455	0.3263034	1.3161345			
19BRWY5																			
UA	1	0	71.837944	82.701962	n/a	29.893183	12.080493	0.2254047	n/a	0.0260701	2.67674E-05	0.691732	13.27037	0.5216227	0.2455131	1.6257728			
19BRWY5																			
UB	1	-20	52.992616	60.670873	700.19697	48.389334	10.760774	0.590718	6.3717168	0.0238237	4.81161E-05	1.3579801	28.508344	0.4911445	0.2293721	1.3904			
19BRWY5																			
MB	1	-35	41.120416	44.670208	516.64141	61.910922	10.085591	0.5773161	6.6196519	0.0223927	4.08319E-05	1.8677869	41.716618	0.5030624	0.2448007	1.4390269			
19BRWY5																			
C	1	-80	49.872015	55.494064	n/a	52.329203	10.5463	0.5842541	n/a	0.0224102	4.29072E-05	1.4464522	32.280863	0.5053748	0.295931	1.5993514			
19BR6UA																			
19BRWY6																			
UB	1	0	47.885415	51.938899	n/a	59.476114	10.195525	0.6103829	n/a	0.0398623	4.55506E-05	1.5176145	19.04088	0.5126085	0.2358463	0.9380055			
19BRWY6																			
UB	1	-42	49.829928	56.438166	646.09092	53.043886	10.509132	0.6147305	5.927486	0.0251006	4.43431E-05	1.4549457	28.990157	0.484733	0.2898728	1.4002216			
19BRWY6																			
MB	1	-72	53.468079	61.355767	709.36816	48.634582	10.746923	0.577853	6.6097188	0.0237801	4.78319E-05	1.3385716	28.152355	0.5163448	0.2023235	1.3965663			
19BRWY6																			
C	1	-112	51.629703	56.837489	n/a	52.912362	10.515935	0.5905966	n/a	0.0213809	3.7184E-05	1.3611078	31.838658	0.4947117	0.2824278	1.3778666			
BR919-01M	n/a	n/a	51.122884	58.947968	564.34657	n/a	9.2190337	0.5152491	7.767892	0.0263884	4.92954E-05	1.4757329	27.969285	0.5024389	0.2527341	1.1689267			
BR919-02	n/a	n/a	57.476911	72.776515	777.81666	n/a	9.1599577	0.5485369	7.1520668	0.0256427	5.17198E-05	0.9915587	19.339365	0.5019571	0.2485626	1.5831046			
BR919-03	n/a	n/a	3.4822558	3.5275605	156.00922	n/a	7.8571539	0.9050397	0.5667648	0.0242964	5.27801E-05	28.559114	587.88129	0.4731836	0.5269359	2.3926467			
BR919-06b	n/a	n/a	0.2681462	0.2682455	144.64739	n/a	9.561629	4.3630544	-63.41651	0.0563677	0.000804501	n/a	n/a	0.5598327	14.622471	0.0406078			
BR919-07	n/a	n/a	29.23949	31.90147	301.32511	n/a	8.3766988	0.5603004	6.9344421	0.0234941	4.80212E-05	2.8934567	61.594913	0.5400563	0.3198266	0.8926694			
BR919-08	7.25	n/a	9.821433	10.092542	181.6756	n/a	8.1406807	0.5893187	6.3976043	0.0262366	4.82916E-05	10.029478	191.18683	0.4969452		0.4666256			
BR919-09	6.25	n/a	50.228922	57.567183	546.55467	n/a	8.9202509	0.6675846	4.9496848	0.0239006	4.44108E-05	1.4834848	31.042859	0.5075097	0.2208681	1.2760783			
BR919-10	0	n/a	50.378228	57.43433	544.87268	n/a	8.9860767	0.6883919	4.5647507	0.0238513	4.23737E-05	1.505699	31.572807	0.5103976	0.196841	1.4351032			
BR919-11	31	n/a	63.186606	73.351122	788.25506	n/a	10.041457	0.3176305	11.423837	0.0257103	2.53294E-05	1.0136388	19.718046	0.4625749	0.8712556	2.5449876			
BR919-12	31.5	n/a	73.052136	86.500601	1069.4391	n/a	10.180345	0.2810418	12.100727	0.0252083	2.37179E-05	0.8007858	15.887644	0.4676676	0.2137331	1.8918602			
BR919-14	31	n/a	74.231894	88.823612	1128.6568	n/a	10.1686669	0.2865816	11.998241	0.0263494	2.48169E-05	0.7753807	14.717415	0.4405231	0.2159236	1.743479			
BR919-15	31.25	n/a	76.103485	89.936178	1158.1683	n/a	10.33017	0.2637262	12.421065	0.022626	2.51596E-05	0.7388452	16.331751	0.4828643	0.1519218	1.909777			
BR919-16	51.5	n/a	76.607963	90.095746	1162.4638	n/a	10.421217	0.2547188	12.587702	0.0233817	2.8048E-05	0.7305788	15.627117	0.4955513	0.1603836	1.9489195			
BR919-18	12.5	n/a	75.20017	88.378526	1117.0622	n/a	10.276945	0.2616903	12.458729	0.0237781	2.66535E-05	0.7584881	15.953607	0.4583329	0.1592546	2.111589			
BR919-18t	13.25	n/a	74.689862	88.103242	1109.9507	n/a	10.352595	0.2720387	12.267284	0.0225198	2.74646E-05	0.760845	16.897375	0.495091	0.1746808	1.099143			
BR919-20	26	n/a	74.494275	88.020358	1107.8184	n/a	10.305389	0.2681987	12.338323	0.0216748	2.68033E-05	0.7379902	17.028747	0.5562288	0.2490059	1.6790503			
BR919-21	28.25	n/a	73.71939	87.523047	1095.1103	n/a	10.394726	0.2914847	11.907533	0.0235641	2.91263E-05	0.740142	15.709082	0.5213361	0.255313	1.5862851			
BR919-22	29	n/a	69.046192	83.003952	986.10945	n/a	10.474094	0.3648246	10.550745	0.0270637	3.34331E-05	0.8824378	16.307401	0.4621461	0.2426966	2.4183741			
BR919-23	30.5	n/a	46.325704	51.915852	479.3943	n/a	9.7317256	0.3224421	11.334821	0.026531	2.84653E-05	1.5625821	29.456223	0.4971917	0.2280738	1.4247476			
BR919-24	32	n/a	40.082811	44.491501	403.54116	n/a	9.6785718	0.3615154	10.611964	0.0280368	3.22006E-05	1.9272667	34.379579	0.4550024	0.2518314	1.6548565			
BR919-25	33.5	n/a	49.537574	56.368521	531.56494	n/a	9.975311												

ALS Barcode	Sample ID	Depth cm	ENPP kJ m yr ⁻¹	EPPT kJ m yr ⁻¹	DT	dT x 4.18	Peff	ET cm	ET/MAP n/a	Source for climate data
Y995876	19BRWY2UB	-25	36739.85	9625.8407	11.536902	48.224252	15.861734	25.201334	0.6137226	
Y995877	19BRWY2MB	-50	32739.896	8577.8526	10.745266	44.91521	5.3784304	24.132788	0.8177496	
Y995878	19BRWY2LB	-75	38530.547	10095.003	12.331621	51.546174	23.781642	26.008597	0.5223634	
AVERAGE 2B			9432.8989					25.11424	0.6512785	
Y995881	19BRWY3UB	-35	43482.535	11392.424	13.514406	56.490216	95.249239	33.293173	0.2590054	
Y995882	19BRWY3MB	-45	43437.824	11380.71	13.477087	56.334225	93.92485	33.15818	0.2609175	
AVERAGE 3B			11386.567					33.225677	0.2599614	
Y995884	19BRWY4UB1	0	43584.584	11419.161	13.054671	54.568524	99.91481	33.768727	0.252602	
Y995885	19BRWY4UB2	-15	35659.591	9342.8128	11.222093	46.90835	12.387616	24.847223	0.6673111	
Y995886	19BRWY4LB	-30	43857.343	11490.624	14.137247	59.093693	99.699533	33.746784	0.2528866	
AVERAGE 4B			10750.866					30.787578	0.3909332	
B0173201	19BRWY5UB	-20	41468.114	10864.646	12.575261	52.564589	46.754295	28.350162	0.3774764	
B0173202	19BRWY5MB	-35	39523.248	10355.091	12.078631	50.488677	28.35858	26.475117	0.4828257	
AVERAGE 5B			10609.868					27.41264	0.4301511	
B0173205	19BRWY6UB	-42	40999.535	10741.878	12.348014	51.614699	41.308812	27.795113	0.4022219	
B0173206	19BRWY6MB	-72	41536.889	10882.665	12.551417	52.464925	47.7003	28.446587	0.3735752	
AVERAGE 6B			10812.272					28.12085	0.3878985	
		Present	16679.919	833.99595	6.3333	26.473194	3.485785	18.129215	0.8387331	PRISM Climate Group 2004
		PETM	60062.895	15736.479	19.5	81.51	107.367	29.633	0.2162993	Wing et al. 2005
		Early Eocen	58749.252	15392.304	12.8	53.504	74.6574	26.9426	0.2651831	Wing & Currano 2013
		Mid Eocene	57449.812	15051.851	14	58.52	62.9226	25.9774	0.2922092	Leopold & MacGinitie 1972, Roehler 1993
		Allen 2017	59887.454	15690.513	16.54	69.1372	128.02764	31.33236	0.1966137	Allen 2017

Sample ID	$\delta^{13}\text{C}$ (‰)		Taxon-specific	Generalized
	VPDB)	Notes, Identification	$\delta^{13}\text{C}_{\text{atm}}$ (‰)	$\delta^{13}\text{C}_{\text{atm}}$ (‰)
006_001	-23.93	<i>Lygodium</i> , 26m in column	-3.94	-4.78
006_002	-23.90	<i>Lygodium</i> , 26m in column	-3.91	-4.75
006_003	-24.04	<i>Lygodium</i>	-4.05	-4.88
006_004	-23.82	<i>Lygodium</i> , leaf mat	-3.83	-4.68
006_005	-24.68	<i>Lygodium</i> , 26m in column	-4.69	-5.47
009_001	-24.40	plant mat	n/a	-5.21
009_002	-23.59	Sept 2019 roots and stems	n/a	-4.47
009_003	-24.82	Bag 4, charcoal wood and st	n/a	-5.59
009_005SP	-24.64	Sporangia	n/a	-5.43
009_005DI	-24.77	<i>Acer</i>	-5.40	-5.55
009_006	-24.55	Wood, leaf hash/plant mat	n/a	-5.35
009_017	-24.48	charcoalified wood	n/a	n/a
009_016	-22.81	charcoalified wood	n/a	n/a
009_015	-23.32	plant mat	n/a	-4.23
009_010	-23.87	plant mat	n/a	-4.73
009_011	-24.28	plant mat	n/a	-5.10
919-6B	-24.95	charcoalified wood	n/a	-5.71
009_014	-24.56	plant hash/mat	n/a	-5.35
006_007	-24.72	Leaf mat, 26m	n/a	-5.50
006_008	-25.24	Leaf mat, 26m	n/a	-5.97
006_009	-25.47	Dicots (<i>Acer</i>), 26m	-6.10	-6.19
006_010	-25.22	Dicot (<i>Acer</i>), <i>Lygodium</i> , leaf	-5.85	-5.95
006_011	-23.29	Dicots (<i>unspecified</i>), 26m	n/a	-4.20
006_012	-24.93	Leaf mat, 26m	n/a	-5.69
006_013	-23.90	Leaf mat, 26m	n/a	-4.75
006_014	-23.13	Leaf mat, 26m	n/a	-4.06
006_015	-22.79	Leaf mat, 26m	n/a	-3.75
009_012	-25.00	Wood, leaf hash/plant mat	n/a	-5.76
009_013	-24.01	Stems	n/a	-4.85
009_009	-26.17	charcoalified wood, bag 6	n/a	-6.82
009_007	-25.03	Leaf mat	n/a	-5.78
009_004DI	-24.94	Angiosperms	-5.57	-5.70
009_008	-24.43	Angiosperms	n/a	-5.24
009_004SP	-24.89	sporangia	n/a	-5.65

Sample ID	Profile #	Depth (cm)	C _{jw}		C _{jw}		C _{jw}		C _{jw}		C _{jw}		C _{jw}		C _{jw}		C _{jw}			
			Epsilon	Al %	Al tau	Na %	Na tau	Ca %	Ca tau	K %	K tau	Fe %	Fe tau	Zr ppm	Zr tau	Rb ppm	Rb tau			
19BRWY1LA	1	-12	0.353	0.64193	0.64	7.53	-0.28	0.35	-0.38	0.41	0.02	2.53	-0.35	4.42	-0.29	84.4	-0.18	148	-0.27	
19BRWY1LC	1	-18	0.322	0.8	0.80	7.75	-0.18	0.42	-0.18	0.3	-0.18	2.92	-0.18	4.66	-0.18	76.7	-0.18	152	-0.18	
19BRWY1UA	1	0	0.359	0.61448	0.61	7.53	-0.29	0.35	-0.39	0.35	-0.15	2.37	-0.41	3.87	-0.39	86.5	-0.17	124	-0.40	
19BRWY2C	2	-85	0.395	0.8	0.80	7.63	-0.18	0.42	-0.18	0.4	-0.18	2.44	-0.18	3.84	-0.18	75	-0.18	141	-0.18	
19BRWY2LB	2	-75	0.248	1.86694	1.87	5.33	-0.09	0.74	1.30	5.38	16.55	1.97	0.05	1.82	-0.38	54.5	-0.05	86.6	-0.20	
19BRWY2MB	2	-50	0.172	3.13372	3.10	4.08	0.00	0.29	0.29	18.5	85.19	1.38	0.05	1.96	-0.19	39.1	-0.03	65.7	-0.13	
19BRWY2UA	2	0	0.332	1.14157	1.10	7.8	-0.02	0.38	-0.14	0.81	0.93	2.89	0.13	4.8	0.19	87.1	0.11	152	0.03	
19BRWY2UB	2	-25	0.26	1.73462	1.70	6.09	-0.02	0.32	-0.06	10.3	30.45	2.11	0.06	3.5	0.12	61.1	0.00	106	-0.08	
19BRWY3UA	3	0	0.308	0.8	0.80	6.61	-0.20	0.5	-0.26	0.22	-0.92	2.44	-0.20	4.03	-0.20	88.6	-0.11	131	-0.18	
19BRWY3UB	3	-35	0.295	0.87932	0.88	6.45	-0.19	0.54	-0.16	0.19	-0.93	2.4	-0.17	4.62	-0.05	66.8	-0.10	132	-0.14	
19BRWY3MB	3	-45	0.292	0.89863	0.90	6.37	-0.19	0.56	-0.12	0.2	-0.93	2.41	-0.16	4.55	-0.05	69.6	-0.05	124.5	-0.18	
19BRWY3C	3	-75	0.308	0.8	0.80	6.77	-0.18	0.55	-0.18	2.35	-0.18	2.48	-0.18	4.14	-0.18	63.2	-0.18	131.5	-0.18	
19BRWY4UB	1	4	0	0.327	1.16881	1.20	7.85	-0.04	0.46	0.92	0.26	-0.59	2.89	0.51	4.94	0.42	82.1	0.07	149	0.07
19BRWY4UB	2	4	-15	0.208	2.40962	2.40	4.79	-0.09	0.27	0.74	10.3	24.27	1.72	0.38	2.67	0.19	52.3	0.06	87.8	-0.02
19BRWY4LB	4	-30	0.378	0.87619	0.88	7.8	-0.18	0.21	-0.25	0.49	-0.34	1.94	-0.14	3.53	-0.13	67.4	-0.25	136	-0.16	
19BRWY4C	4	-60	0.394	0.8	0.80	8.16	-0.18	0.24	-0.18	0.63	-0.18	1.92	-0.18	3.47	-0.18	76.5	-0.18	139	-0.18	
19BRWY5UA	5	0	0.37	0.27459	0.27	8	-0.30	0.29	-0.92	0.99	-0.72	2.12	-0.37	3.89	-0.11	72.4	-0.56	133	-0.16	
19BRWY5UB	5	-20	0.265	0.77962	0.78	6.27	-0.23	1.88	-0.29	1.38	-0.46	2.17	-0.09	2.54	-0.18	102	-0.14	117	0.04	
19BRWY5MB	5	-35	0.261	0.80969	0.81	6.57	-0.18	2.15	-0.17	4.17	0.67	1.84	-0.22	2.31	-0.25	90.7	-0.22	84.9	-0.24	
19BRWY5C	5	-80	0.262	0.8	0.80	6.59	-0.18	2.14	-0.18	2.06	-0.18	1.94	-0.18	2.52	-0.18	95.6	-0.18	91.4	-0.18	
19BRW6UA	6	0	0.512	-0.0719	-0.70	7.24	-0.86	2.76	-0.85	2.67	-0.80	1.71	-0.87	3.69	-0.79	111.5	-0.83	67.9	-0.89	
19BRWY6UB	6	-42	0.289	0.64429	0.64	6.49	-0.30	2.1	-0.36	1.89	-0.21	2.21	-0.08	2.59	-0.21	97.3	-0.17	101	-0.14	
19BRWY6MB	6	-72	0.27	0.76	0.76	6.4	-0.26	1.84	-0.40	1.39	-0.38	2.23	0.00	2.56	-0.16	103.5	-0.05	121.5	0.11	
19BRWY6C	6	-112	0.264	0.8	0.80	6.96	-0.18	2.45	-0.18	1.79	-0.18	1.79	-0.18	2.45	-0.18	87.5	-0.18	87.8	-0.18	
"parent"				0.263																

Variables		
rho w	1.5	Density of weathered material (paleosol)
C _{jw}		Weight % of element j (Al) in weathered material
rho p	3.3	Density of parent material (sand)
C _{jp} (TI)	0.263	Weight % of element j (TI) in parent material (avg)
Ep		Solve for separately; assume tau is 0, bypassing volume

* Values are actually. Using rho=2.7

C _p - C _{wp}	
Al	6.775
Na	2.295
Ca	1.925
K	1.865
Fe	2.485
Zr	91.55
Rb	89.6

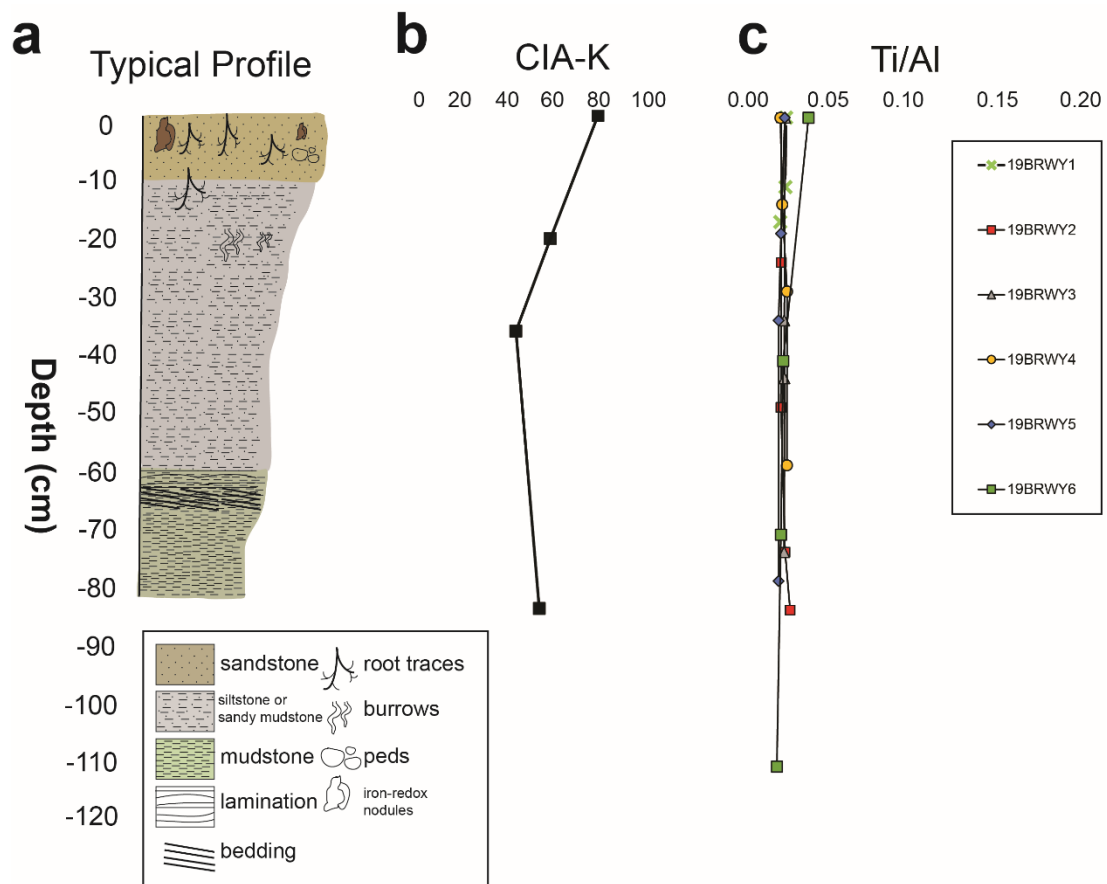


Figure D1 Geochemistry and features of a typical paleosol profile at Blue Rim escarpment. (a) Average paleosol profile at Blue Rim escarpment, (b) typical CIA-K over profile, (b) Ti/Al ratio (molar) for all paleosol profiles.

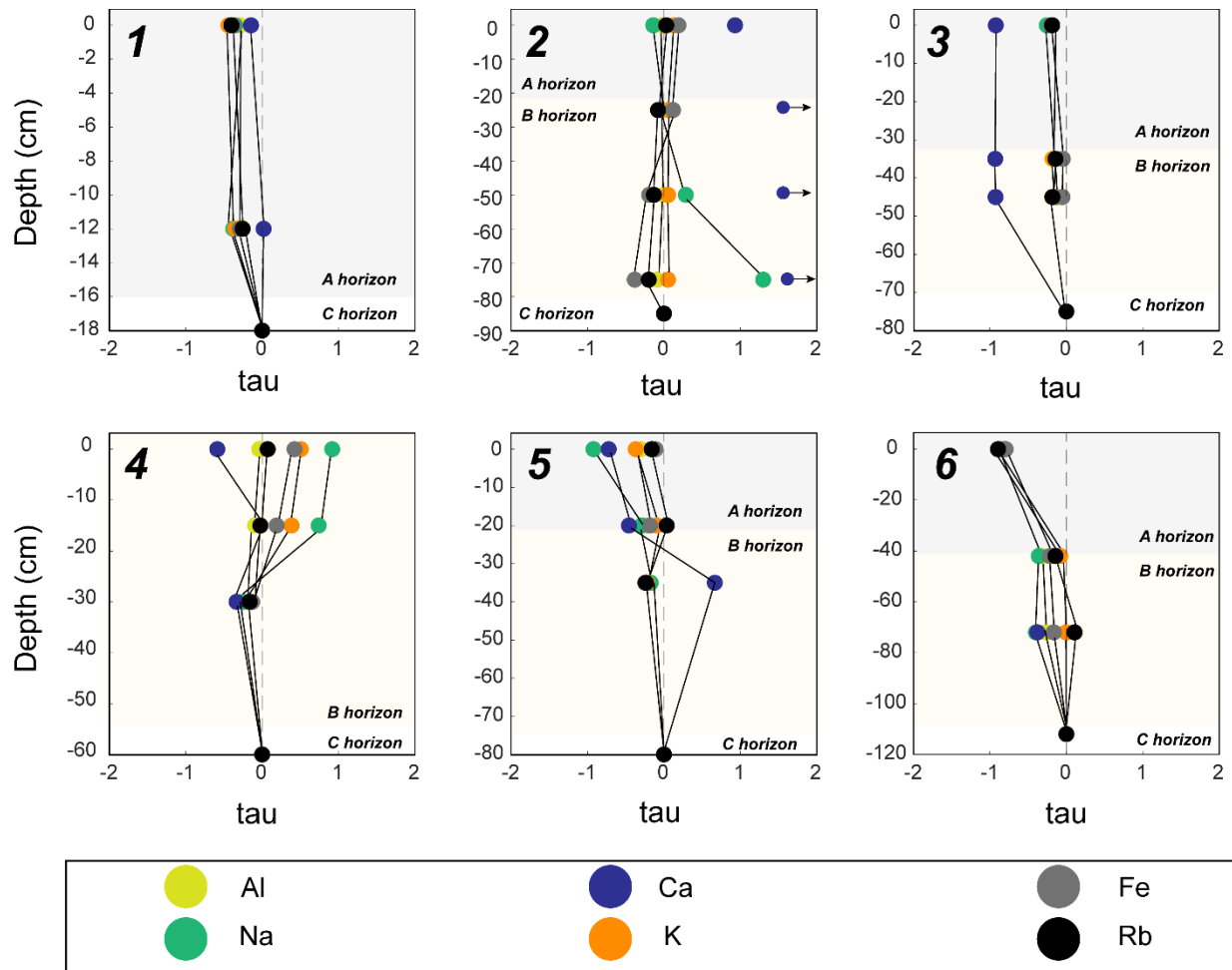


Figure D2 Paleosol profile changes in mobile element transport calculations. Up profile changes in tau (mobile element transport, see equations 5.2 and 5.3, per Chadwick et al. 1990) for Paleosols #1 through #6.

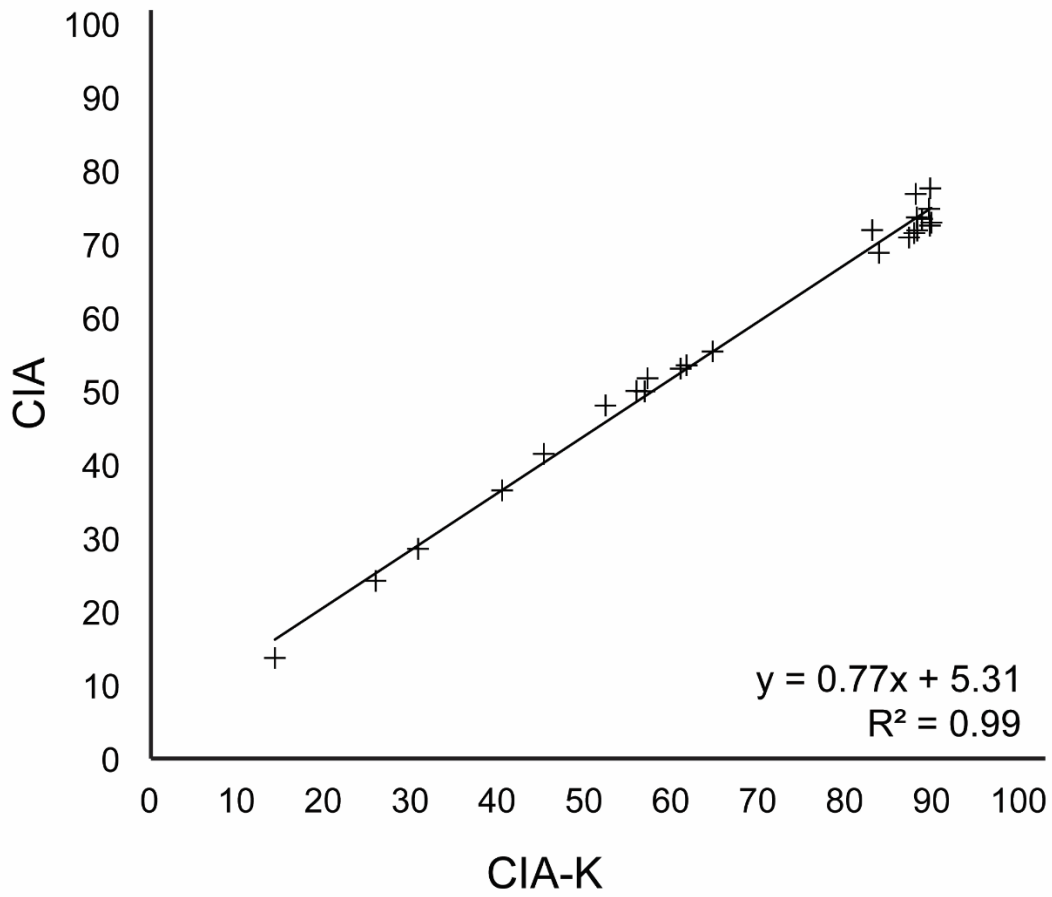


Figure D3 Relationship between CIA-K and CIA for all paleosol bulk geochemistry data, measured by ALS Laboratories.

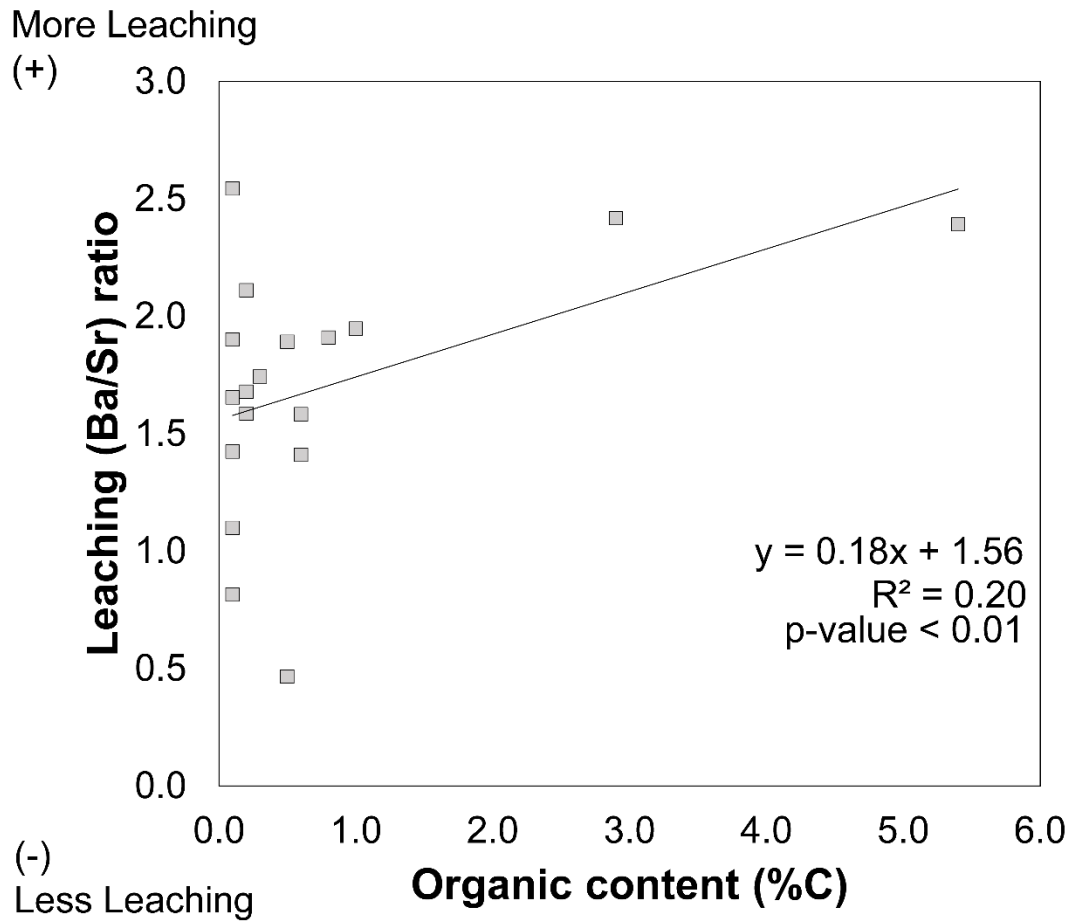


Figure D4 Comparison between organic content in stratigraphic units (%C) and leaching (Ba/Sr ratio).

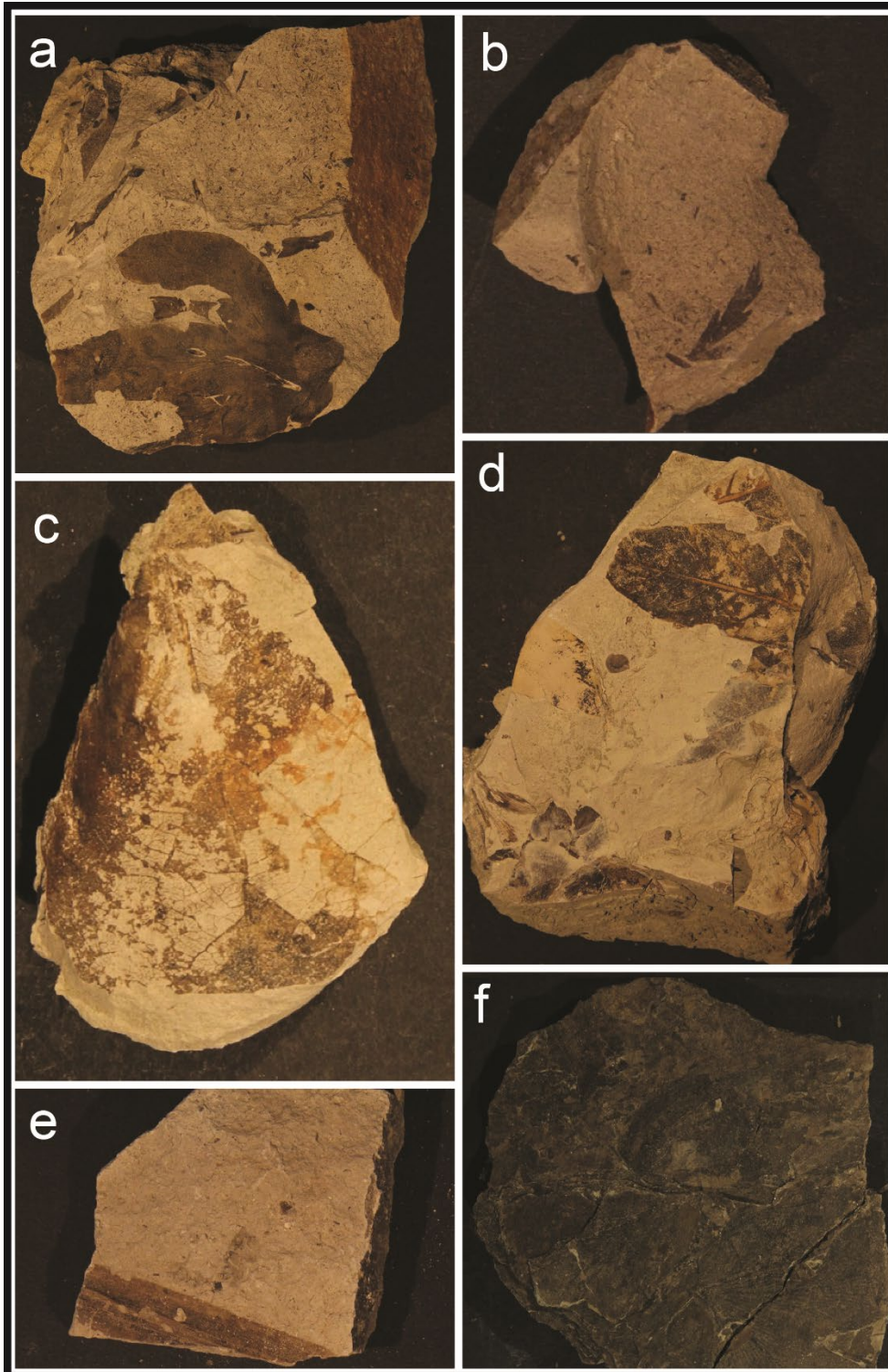


Figure D5 Common fossil formats and taxa found at Blue Rim Escarpment (2019): (a) *Lygodium kaulfussi*, (b) *Asplenium sp.* (c) *Populus cinnamomoides*, (d) *Cedrella sp.* (e) unidentified monocot, (f) unidentified organ carbon-rich leaf mat

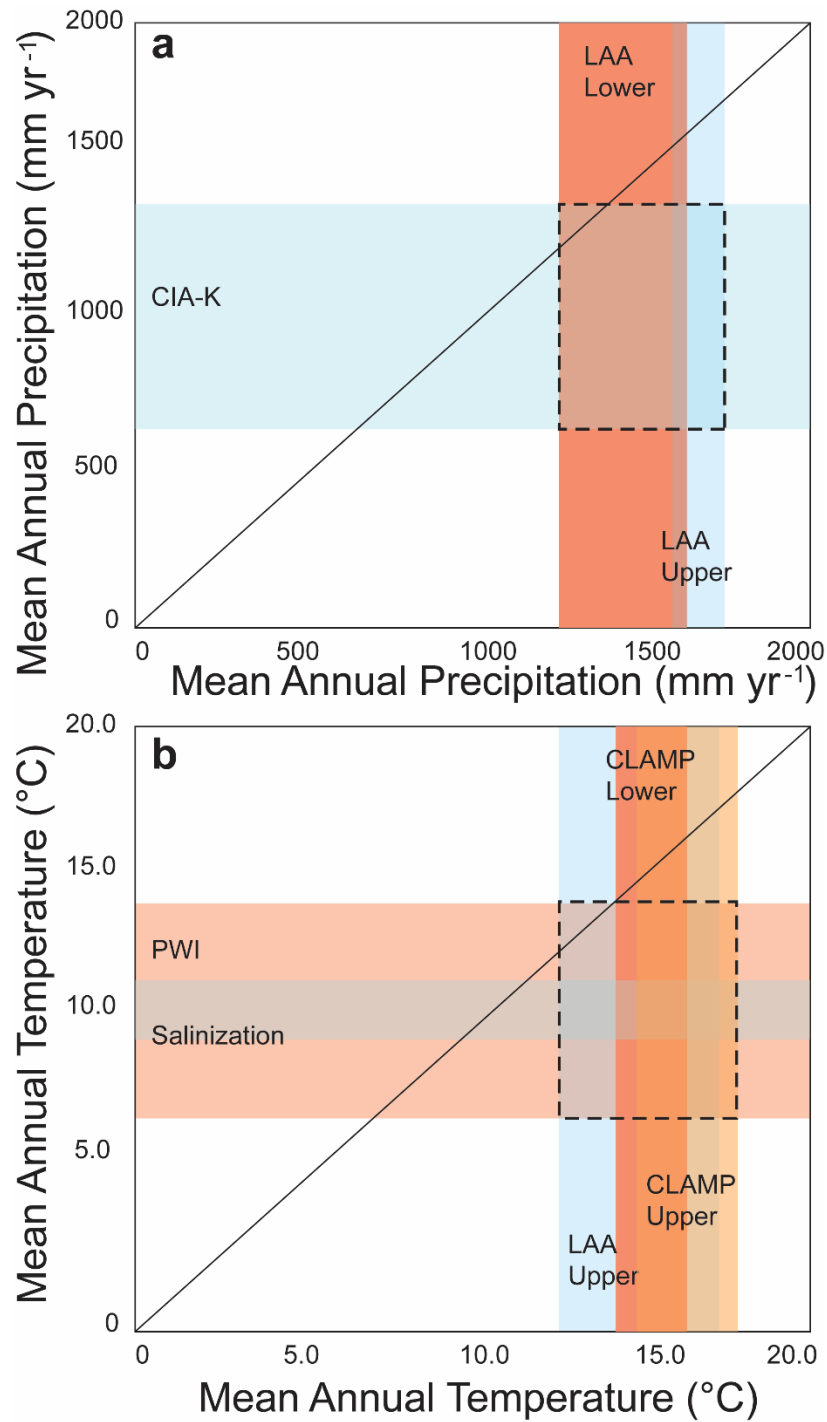


Figure D6 Comparisons of climate reconstructed using multiple proxies. Regression comparing climate values (a) precipitation and (b) temperature, with previous reconstructions on the x-axis and reconstructions in this study on the y-axis). Error is shown for both x and y-values, and the 1:1 relationship is shown with a dashed line. The range represented by both prior estimates and this study is shown in the overlapping boxes, outlined in dashed lines.

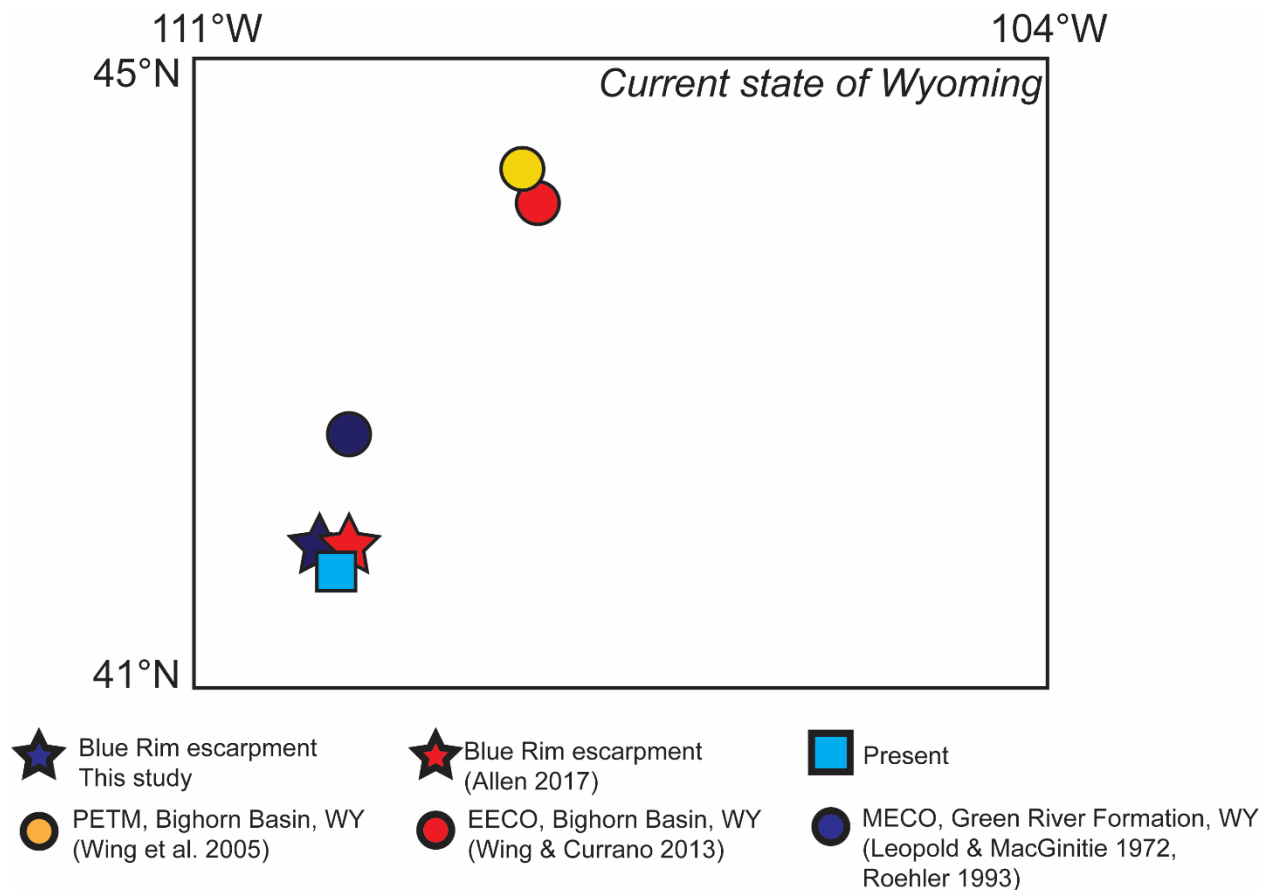


Figure D7 Current boundaries of Wyoming, USA with paleoenvironments plotted. Blue Rim escarpment is plotted in stars (blue for this study, red for Allen 2017). The Paleocene-Eocene Thermal Maximum record from Bighorn Basin is plotted in a yellow circle, while the EECO record from the Bighorn Basin is plotted in a red circle. The MECO is plotted in a blue circle.

Supplemental Methods:

Calculation of MAP

Mean annual precipitation was reconstructed using chemical index of alteration minus potassium (CIA-K).

$$CIA - K = \left(\frac{Al_2O_3}{Al_2O_3 + CaO + Na_2O} \right) * 100 \text{ (Equation 5.4)}$$

$$MAP \text{ (mm yr}^{-1}\text{)} = 221.1e^{0.0197(CIA-K)} \text{ (Equation 5.5)}$$

Calculation of MAT

$$PWI = [(4.20 \times Na) + (1.66 \times Mg) + (5.54 \times K) + (2.05 \times Ca)] * 100 \text{ (Equation 5.2)}$$

$$MAT \text{ (}^\circ\text{C)} = -2.74 \times \ln(PWI) + 21.39 \text{ (Equation 5.6)}$$

Floral humidity province

To contextualize climate variables (temperature, precipitation) to ecoregion and humidity, Gulbranson et al. (2011) developed a life-zone proxy based on Rasmussen et al. (2005) and Rasmussen and Tabor's (2007) pedogenic energy model. This energy quantifies energy influxes due to solar radiation (and subsequent net primary productivity: NPP) and precipitation. The total energy input into a soil (E_{in}) is related to energy supplied by NPP (E_{NPP}) and precipitation (E_{PPT}). E_{PPT} and E_{NPP} are calculated using weathering indices (CIA). E_{PPT} is plotted against evapotranspiration (ET) and divided into humidity zones using Equation 5.9:

$$ET = MAP - E_{PPT} [4.18(\Delta T)]^{-1} \text{ (Equation 5.9)}$$

Where ΔT is the temperature difference between 273.16°K and mean annual temperature.

Mean annual precipitation calculated using the relationship between CIA-K and precipitation was used in this relationship (Equation 5.5).

In modern environments, effective precipitation (P_{eff}) is a linear function of MAP and ET (Equation 5.10):

$$P_{eff} = MAP - ET \text{ (Equation 5.10)}$$

And P_{eff} can be calculated using Equation 5.11.

$$P_{eff} = 0.9075(MAP) - 21.403 \text{ (Equation 5.11)}$$

Paleolatitude has been described as anywhere between 35°N and 44°N (Allen 2017), but temperature was consistently been described as 17-20°C during this time, so we use Equation 5.12 determined by ranges of MAT in Gulbranson et al. (2011), which corresponds to 33°N at present, and latitudinal temperature gradients ranging from 17-20°C.

$$E_{NPP} = -1.943(CIA)^2 + 352.41(CIA) + 28197 \text{ (Equation 5.12)}$$

For reconstructed MAT and MAP values from alternate proxy data (non-paleosol estimates), CIA was back calculated estimating CIA-K using given precipitation values and Equation 5.5, then translated into CIA values using Equation 5.13.

This relationship was calculated using the relationship between CIA and CIA-K for all paleosol bulk geochemistry measurements at this site (Supplemental Fig. D1; $R^2 = 0.99$)

$$CIA = 0.78(CIA - K) + 5.23 \text{ (Equation 5.13)}$$

Holdridge Life Zones

The Holdridge Life Zone classification system (Holdridge 1947) matches climate with vegetation. Higher precipitation adds energy to a soil system, which mobilizes elements and weathers the soil.

Evapotranspiration, represented on the other axis of the Holdridge biome diagram (Fig. 7b) represents energy loss from the soil profile. These two plotted together can then be divided into biome space, allowing for estimation of climate and vegetation through the same diagram.